Identification of a novel ATP binding site and demonstration of ATP hydrolysis by mammalian 14-3-3 isoforms

By

Manoj Pralhadrao Ramteke
[LIFE09200604001]

Tata Memorial Centre
Mumbai

A thesis submitted to the

Board of Studies in Life Sciences

In partial fulfillment of requirements

For the Degree of

DOCTOR OF PHILOSOPHY

Of

HOMI BHABHA NATIONAL INSTITUTE

September, 2014
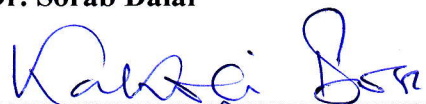
Homi Bhabha National Institute
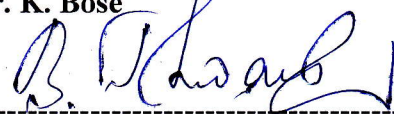
Recommendations of the Viva Voce Board

As members of the Viva Voce Board, we certify that we have read the dissertation prepared by Manoj P. Ramteke entitled **"Identification of a novel ATP binding site and demonstration of ATP hydrolysis by mammalian 14-3-3 isoforms"** and recommend that it may be accepted as fulfilling the dissertation requirement for the Degree of Doctor of Philosophy.

-- Date: 5.9.14.
Chairman - Dr. R. Mulherkar

-- Date: 5.9.14.
Guide / Convener - Dr. Prasanna Venkatraman

-- Date: 5/9/14
Member 1 – Dr. Sorab Dalal

-- Date: 5/9/14
Member 2 – Dr. K. Bose

-- Date: 6/9/14
Member 3 – Prof. B. J. Rao, TIFR

-- Date: 5/9/14
External Examiner – Prof. Raghavan Varadarajan, IISc

Final approval and acceptance of this dissertation is contingent upon the candidate's submission of the final copies of the dissertation to HBNI.

I hereby certify that I have read this dissertation prepared under my direction and recommend that it may be accepted as fulfilling the dissertation requirement.

Date: 5th Sept. 2014
Place: ACTREC, Kharghar

Dr. Prasanna Venkatraman
(Guide)

i

STATEMENT BY AUTHOR

This dissertation has been submitted in partial fulfillment of requirements for an advanced degree at Homi Bhabha National Institute (HBNI) and is deposited in the Library to be made available to borrowers under rules of the HBNI.

Brief quotations from this dissertation are allowable without special permission, provided that accurate acknowledgement of source is made. Requests for permission for extended quotation from or reproduction of this manuscript in whole or in part may be granted by the Competent Authority of HBNI when in his or her judgment the proposed use of the material is in the interests of scholarship. In all other instances, however, permission must be obtained from the author.

M. P. Ramteke

Manoj P. Ramteke

DECLARATION

I, hereby declare that the investigation presented in the thesis has been carried out by me. The work is original and has not been submitted earlier as a whole or in part for a degree / diploma at this or any other Institution / University.

M. P. Ramteke

Manoj P. Ramteke

List of Publications arising from the thesis

Journal:

1. Identification of a novel ATPase activity in 14-3-3 proteins – Evidence from enzyme kinetics, structure guided modeling and mutagenesis studies, **Manoj P. Ramteke**, Pradnya Shelke, Vidhya Ramamoorthy, Arun Kumar Somavarapu, Amit Kumar Singh Gautam, Padma P. Nanaware, Sudheer Karanam, Sami Mukhopadhyay, Prasanna Venkatraman, *FEBS Letters*, 2014, 588, 71–78.

Conferences:

1. Selected for oral presentation at XXXIV All India Cell Biology Conference – December 2010.

2. Best oral presentation award at International Symposium on Conceptual Advances in Cellular homeostasis Regulated by Proteases and Chaperones - the Present, the Future and Impact on Human Diseases – December 2013.

M. P. Ramteke

Manoj P. Ramteke

CONTENTS

Homi Bhabha National Institute

Ph. D. PROGRAMME

1. **Name of the Student:** Manoj Pralhadrao Ramteke

2. **Name of the Constituent Institution:** Tata Memorial Centre (TMC), Advanced Centre for Treatment, Research and Education in Cancer (ACTREC)

3. **Enrolment No. :** LIFE09200604001

4. **Title of the Thesis:** Identification of a novel ATP binding site and demonstration of ATP hydrolysis by mammalian 14-3-3 isoforms

5. **Board of Studies:** Life Sciences (LS)

Introduction:

14-3-3 proteins are a family of highly conserved, acidic, proteins with a subunit molecular weight of 28-30 kDa (Aitken, 2006). In mammals, this family is represented by seven isoforms, namely - β, γ, ε, ζ, η, σ and τ/θ and most of them function both as homo and heterodimeric proteins (Aitken, 2006; Aitken et al., 1995). These proteins bind with the target sequences in a phosphospecific manner by recognizing any of the three consensus motifs defined as mode I, (RSXpSXP) , mode II (RXY/FXpSXP) and mode III pS/pT (X1–2)-COOH, where pS and pT represents phosphoserine and phosphothreonine residues respectively (Ganguly et al., 2005; Muslin et al., 1996; Yaffe et al., 1997). Depending on the target proteins that they bind to, 14-3-3 isoforms control many important cellular processes like apoptosis, metabolism, signal transduction, cell cycle control, protein localization, transcription and stress response (Brunet et al., 1999; Dalal et al., 2004; Datta et al., 2000; Donzelli and Draetta, 2003; Fu et al., 2000; Hosing et al., 2008; Telles et al., 2009). 14-3-3 proteins are also involved in malignant transformation (Hermeking, 2003).

Besides their scaffold or adaptor like functions in recruiting target proteins, 14-3-3 proteins are also recognized for their molecular chaperon like functions. Yano et al., have shown that *Drosophila* 14-3-3ζ, functions as a heat shock protein. In heat shocked *Drosophila* cells, ζ interacts with the aggregated apocytochrome *c* and converts it into a soluble form (Yano et al., 2006). Further studies on protein disaggregation by Danielle et al., showed that human 14-3-3ζ even in the absence of ATP can prevent aggregation of α-lactalbumin, alcohol dehydrogenase, insulin and lysozyme *in vitro* (Danielle et al., 2011). This feature of ATP independent chaperon/disaggregation activity is very similar to that observed in small Heat Shock

Proteins (sHSPs). Furthermore, like the sHSPs, a flexible loop present in the C-terminus of these proteins helps in their stability (Danielle et al., 2011).

In mammalian cells 14-3-3 is also associated with protein aggregation but whether they promote or prevent aggregation remains unclear. Omi et al., showed that in rat N2a neuroblastoma cells, 14-3-3ζ is indispensible for the formation of aggregates of mutant huntingtin (Htt) (Omi et al., 2008) involved in neurodegenerative disorders. When 14-3-3ζ was downregulated using specific siRNA, Htt failed to aggregate and remained in a soluble form in the cytoplasm. 14-3-3ζ also seems to be involved in the pathway that affect the aggregation of proteins like tau, an abundant protein in Alhzeimer's disease (AD) (Berg et al., 2003; Sluchanko and Gusev, 2011).

In addition to the well-recognized scaffold like functions and less well characterized role as chaperones, many enzymatic functions have been ascribed to 14-3-3 family of proteins (Aitken, 2006). Early research on rat liver cytosolic fractions showed that a mitochondrial import stimulation factor (MSF) which is involved in the mitochondrial localization of precursor proteins was a heterodimer of 14-3-3 and this function seem to depend on ATPase activity (Hachiya et al., 1993). Yano et al., reported that 14-3-3τ from human lymphoblastoma cell line and its recombinant form exhibit an intrinsic nucleotide diphosphate (NDP) kinase-like activity and ATP/ADP exchange activity (Yano et al., 1997). Since no further studies have substantiated these observations, any such enzymatic activity associated with 14-3-3 has not been taken seriously. Even the recent reports on the *Drosophila* 14-3-3ζ did not provide any evidence of ATP hydrolysis although a weak disaggregating function was found to be ATP and Hsp 70 dependent (Yano et al., 2006).

Based on this background we were interested in finding out if any of the mammalian 14-3-3 proteins was capable of hydrolyzing ATP and if so what are the residues involves in this intrinsic enzyme activity. These studies would mark a major step in our understanding of the role of these proteins in their chaperone like functions and are likely to provide a new direction in clarifying their role in promoting or dissolving neuronal inclusions. So far only Hsp104 protein from yeast, an ATP dependent chaperone is known for its ability to dissolve preformed aggregates (Bösl et al., 2006).

Therefore we defined following three objectives for the thesis

1. To verify whether the mammalian 14-3-3ζ has an ATPase activity and provide unequivocal evidence for ATP hydrolysis using purified recombinant 14-3-3ζ.

2. To identify the ATP binding pocket of 14-3-3ζ and the catalytic residues involved in hydrolysis.

3. To identify if this activity was structurally and functionally conserved in other 14-3-3 isoforms.

Results and Discussions

1. Identification of Intrinsic ATPase Activity in 14-3-3ζ WT

In order to verify whether human 14-3-3ζ WT has any intrinsic ATPase activity, recombinant form of the protein was expressed in *E.coli* and purified Ni-NTA affinity chromatography (Invitrogen). The infusion His tag was removed and the protein was further purified over a Sephadex G-75 gel filtration column. The identity of the isoform was confirmed by western blotting and mass spectrometry. Using a calorimetric assay and radioactive ATP we show that the pure recombinant homodimeric 14-3-3ζ from human has a detectable ATPase activity which is linear with time. Any non-specific nucleotidase or apyrase activity was ruled out using two non-hydrolysable ATP analogues – ATP-γ-S and AMP-PCP (Sigma). Individual fractions eluting from the gel filtration column were assayed for ATPase activity and the activity was found to be coincident with the elution peak confirming that the 14-3-3ζ has intrinsic ATPase activity.

2. *In silico* Analysis for the Prediction of Putative Residues Involved in ATP Binding/Hydrolysis in 14-3-3ζ and Identification of Gain and Loss of Function Proteins by Mutagenesis

Typical ATPases possess signature sequences or structures by which they can be easily identified, such as the presence of Walker A motif (P-loop), Walker B motif, β sheeted structures and are rich in proline and glycine residues. But unfortunately 14-3-3ζ does not possess any such distinct characteristics. Therefore we performed docking of 14-3-3ζ with that of ATP using Glide application from Schrödinger (in collaboration with Arun Kumar). Two binding pockets were selected based on volume and binding scores. Pocket one lies near the phosphopeptide binding pocket at the

amphipathic groove and second pocket is located at the dimer interface. Residues within 5Å of the bound ATP that are likely to participate in the ATPase activity of 14-3-3ζ were converted into Ala. All mutations were confirmed by sequencing. Among the many mutations screened R55A mutation at the interface resulted in loss of ATPase activity and D124A mutation in the amphipathic groove resulted in gain of ATPase activity. Hsp104 a disaggregating chaperone possesses a sensor motif called GAR and RR (Bösl et al., 2006). R55A in 14-3-3ζ is part of a sequence $G_{53}A_{54}R_{55}R_{56}$. It is possible that R_{55} here is acting as an ATP sensor and hence R55A mutation results in loss of ATPase activity. In order to further investigate the importance of R55 residue, we created double mutant (DR mutant) by mutating R55A in D124A background. Compared to the D124A mutant, the double mutant showed loss of ATPase activity indicating that R55 is an important residue for the ATPase activity of 14-3-3ζ. All other mutation (E17A, R18A, D20A, C25S, V51G, S57A, S58A, E89A, D92G, C94S and D96V) near the dimer interface and at phosphopeptide binding amphipathic pocket (N42A, K49A, R56A, D120A, Y149A, F174A, C189S and S190A) did not alter the ATPase activity of 14-3-3ζ. Kinetic parameters for ATP hydrolysis were determined for the 14-3-3ζ WT and the mutant proteins (Zegzouti et al., 2009). The rate of hydrolysis of ATP by 14-3-3ζ WT (k_{cat} = 0.0087 min^{-1}) was slower than that of Hsp 70 (k_{cat} = 0.16 min^{-1}) used as a positive control here but comparable to the values reported from another classical chaperone Hsp 90. Mutation of D124A increases the k_{cat} of the enzyme (k_{cat} = 0.28 min^{-1}) and the activity of the mutant was closer to that of Hsp 70 (k_{cat} = 0.16 min^{-1}).

The ATPase activity of human 14-3-3ζ WT, R55A and D124A mutant remain unaltered in the presence of phosphopeptides (P1-RLYHpSLP, P2-QSYpTV, P3-ARKpTG). Binding of phosphopeptides was not affected by mutations. These results

again seem to suggest that the pocket near the interface may be the site to which ATP binds.

3. Conservation of ATPase Activity in Other 14-3-3 Isoforms

Structure of 14-3-3 isoforms is highly conserved. While these proteins preserve their fold that helps them to recognize phosphorylated sequences in proteins, they differ in their ability to bind to cellular proteins (Aitken, 2006). To see if the ATPase activity found in 14-3-3ζ was conserved in other isoforms we expressed and purified 14-3-3γ, ε, τ and σ. To see if the activity was conserved across species, *Drosophila* 14-3-3ζ was also expressed and purified. Human 14-3-3γ, ε and τ isoforms and 14-3-3ζ from *Drosophila* showed the similar ATPase activity and K_m and k_{cat} values were comparable to that of human 14-3-3ζ WT. Human 14-3-3σ did not show the detectable ATPase activity. This is typical this isoform and compared to others it is less well conserved in terms of structure and function (Li et al., 2009). Sigma 14-3-3 notably lacks the ATP sensor RR found in other active forms. While one may expect this to be the reason for the lack of ATPase activity of sigma, we were surprised to find that mutation of R55 in another active isoform, gamma (γR56A) did not affect its ATPase activity. Therefore the exact contribution of R to ATP binding or hydrolysis or lack of R in the sensor sequence remains unclear. In contrast, mutation of D124 to Ala in the gamma isoform (γD129A) results in gain of function similar to that seen in the zeta mutant. It is clear that many more mutations and structural evaluation of the ATP bound form will be necessary to resolve these complex issues.

4. ATP binding to 14-3-3

To provide direct evidence for ATP binding uncoupled from hydrolysis which is a kinetic event, a filter trap and gel filtration assays were performed using (γ-^{32}P). All 14-3-3 isoforms except 14-3-3σ could bind to ATP. No radioactivity was retained on the nitrocellulose filter with the R55A mutant. Gel filtration using a spin column showed that about 7% of the total hot ATP was bound by 14-3-3 active isoforms while binding was significantly reduced (1.84% only) in 14-3-3σ . It is possible that sigma which is catalytically inactive can still bind ATP albeit with very less affinity or this amount of binding reflects non-specific interaction. About 2.66% binding was seen in the loss of function mutant R55A mutant (binding attenuated by 50%), ~12% binding (twice more than the ζWT) was seen in the D124A mutant and about 12.47% was seen in γD129A mutant (corresponding Asp mutant in 14-3-3γ isoform). ~13% of hot ATP was bound to Hsp 70 under the same conditions. These results provide additional evidence for the ability of 14-3-3 to specifically bind and hydrolyze ATP.

5. Computational Analysis of Binding Energy and Experimental Constraints Converge on One Putative Binding Site

In the absence of high resolution structural information of bound ATP, it is difficult to explain why other amino acid substitutions in the vicinity of bound ATP in either binding pockets failed to show any effect. It is possible that ATP may bind in different orientations or binding may be accompanied by conformational changes that are not captured by docking algorithms. It is also intriguing that mutation in one pocket (amphipathic pocket) resulted in enhancement of activity of 14-3-3ζ and in the other (dimer interface) a partial loss. This was reemphasized by the double mutant the activity of which was reduced to 40% compared to the hyper active D124A mutant.

By imposing constraints that would mimic these experimental observations in analyzing docking results (collaboration with Vlife Science Technologies, Pune) we could reconcile with these seemingly opposing results and identify the dimer interface as the most likely binding pocket that could account for a) better binding of ATP in D124A mutant (BE -0.77 kcal/mol vs 4.04 kcal/mol for the WT protein) and b) weaker binding in R55A mutant (BE 9.34 kcal/mol). Detailed analysis of this pose indicates that ATP forms two hydrogen bonds with Arg55 in the B chain and also makes charged interactions with Arg55 in the A chain. In addition, Arg55 makes numerous van der waal (vdW) interactions at the dimer interface. Mutation of this residue to Ala would therefore result in loss of hydrogen bond interactions as well as the charge interaction between the positively charged guanidine group of arginine and negatively charged phosphate group of ATP, adversely affecting binding energy and therefore catalysis. Increased rate of hydrolysis of D124A is reflected in better binding energy of ATP in this mutant. This could be due to favorable steric interactions between ATP and the mutated protein mediated by an increase in the vdW component of the overall binding energy.

These results *in toto* seem to define the pocket near the interface as the most likely binding site for ATP at least in 14-3-3ζ. Nevertheless it is possible that there are indeed two binding pockets for ATP. It is also possible that these mutations have a long range effect on a binding site located elsewhere in the protein or they affect equilibrium distribution between active and inactive conformers.

Summary:

Our findings for the first time provide a direct and unequivocal evidence for the ability of human 14-3-3ζ to hydrolyze ATP and its conservation in 14-3-3

isoforms (γ, ε and τ) as well as in the zeta isoform of *Drosophila*. 14-3-3σ similar to its other unique properties, did not show any detectable ATPase activity. We have identified GARR a short sequence motif as a probable ATP sensor sequence in 14-3-3ζ. D124A mutant binds ATP with higher affinity which may explain the enhanced activity observed in this mutant. Mutation may prevent faster dissociation of the complex back to enzyme and substrate which is probably the case with the WT protein.

Future Prospective:

This is the first report which proves that 14-3-3 proteins have ATPase activity. Our findings will open up new areas of investigation on 14-3-3 proteins which for decades are well known for their adaptor functions. It will be interesting to find out how this activity would influence other known and as yet unknown functions of 14-3-3.

It is possible that interactions with other proteins in the cellular environment may stimulate ATPase activity of 14-3-3 proteins similar to that observed in D124A mutant. This may assist in the functions of 14-3-3 proteins. Solving the crystal structure of ATP bound to 14-3-3 will definitely provide the ultra-structural details of the binding pocket and clearly mark the catalytic residues. This will also help us to better understand the subtle similarities and differences about the role of conserved residues in the isoforms involved in ATP binding and hydrolysis. Based on the present study, 14-3-3 proteins may fall under the category of small heat shock proteins (sHSPs) and non-typical ATPases.

References:

Aitken, A. (2006). 14-3-3 proteins: a historic overview. Seminars in cancer biology *16*, 162-172.

Aitken, A., Howell, S., Jones, D., Madrazo, J., and Patel, Y. (1995). 14-3-3 alpha and delta are the phosphorylated forms of raf-activating 14-3-3 beta and zeta. In vivo stoichiometric phosphorylation in brain at a Ser-Pro-Glu-Lys MOTIF. J Biol Chem *270*, 5706-5709.

Berg, D., Holzmann, C., and Riess, O. (2003). 14-3-3 proteins in the nervous system. Nature reviews neuroscience *4*, 752-762.

Bösl, B., Grimminger, V., and Walter, S. (2006). The molecular chaperone Hsp104--a molecular machine for protein disaggregation. Journal of structural biology *156*, 139-148.

Brunet, A., Bonni, A., Zigmond, M.J., Lin, M.Z., Juo, P., Hu, L.S., Anderson, M.J., Arden, K.C., Blenis, J., and Greenberg, M.E. (1999). Akt promotes cell survival by phosphorylating and inhibiting a Forkhead transcription factor. Cell *96*, 857-868.

Dalal, S.N., Yaffe, M.B., and DeCaprio, J.A. (2004). 14-3-3 family members act coordinately to regulate mitotic progression. Cell cycle *3*, 672-677.

Danielle, M.W., Heath, E., Katy, L.G., Huanqin, D., Haian, F., Joanna, M.W., Lixin, Z., and John, A.C. (2011). NMR spectroscopy of 14-3-3zeta reveals a flexible C-terminal extension: differentiation of the chaperone and phosphoserine-binding activities of 14-3-3zeta. Biochemical Journal *437*, 493-503.

Datta, S.R., Katsov, A., Hu, L., Petros, A., Fesik, S.W., Yaffe, M.B., and Greenberg, M.E. (2000). 14-3-3 proteins and survival kinases cooperate to inactivate BAD by BH3 domain phosphorylation. Mol Cell *6*, 41-51.

Donzelli, M., and Draetta, G.F. (2003). Regulating mammalian checkpoints through Cdc25 inactivation. EMBO reports *4*, 671-677.

Fu, H., Subramanian, R.R., and Masters, S.C. (2000). 14-3-3 proteins: structure, function, and regulation. Science Signalling *40*, 617-647.

Ganguly, S., Weller, J.L., Ho, A., Chemineau, P., Malpaux, B., and Klein, D.C. (2005). Melatonin synthesis: 14-3-3-dependent activation and inhibition of arylalkylamine N-acetyltransferase mediated by phosphoserine-205. Proceedings of the National Academy of Sciences of the United States of America *102*, 1222-1227.

Hachiya, N., Alam, R., Sakasegawa, Y., Sakaguchi, M., Mihara, K., and Omura, T. (1993). A mitochondrial import factor purified from rat liver cytosol is an ATP-dependent conformational modulator for precursor proteins. The EMBO journal *12*, 1579.

Hermeking, H. (2003). The 14-3-3 cancer connection. Nature Reviews Cancer *3*, 931-943.

Hosing, A.S., Kundu, S.T., and Dalal, S.N. (2008). 14-3-3 Gamma is required to enforce both the incomplete S phase and G2 DNA damage checkpoints. Cell Cycle *7*, 3171-3179.

Li, Z., Liu, J.-Y., and Zhang, J.-T. (2009). 14-3-3σ, the double-edged sword of human cancers. American journal of translational research *1*, 326.

Muslin, A.J., Tanner, J.W., Allen, P.M., and Shaw, A.S. (1996). Interaction of 14-3-3 with signaling proteins is mediated by the recognition of phosphoserine. Cell *84*, 889-897.

Omi, K., Hachiya, N.S., Tanaka, M., Tokunaga, K., and Kaneko, K. (2008). 14-3-3zeta is indispensable for aggregate formation of polyglutamine-expanded huntingtin protein. Neuroscience letters *431*, 45-50.

Sluchanko, N.N., and Gusev, N.B. (2011). Probable participation of 14-3-3 in tau protein oligomerization and aggregation. Journal of Alzheimer's Disease *27*, 467-476.

Telles, E., Hosing, A.S., Kundu, S.T., Venkatraman, P., and Dalal, S.N. (2009). A novel pocket in 14-3-3ε is required to mediate specific complex formation with cdc25C and to inhibit cell cycle progression upon activation of checkpoint pathways. Experimental cell research *315*, 1448-1457.

Yaffe, M.B., Rittinger, K., Volinia, S., Caron, P.R., Aitken, A., Leffers, H., Gamblin, S.J., Smerdon, S.J., and Cantley, L.C. (1997). The structural basis for 14-3-3: phosphopeptide binding specificity. Cell *91*, 961-971.

Yano, M., Mori, S., Niwa, Y., Inoue, M., and Kido, H. (1997). Intrinsic nucleoside diphosphate kinase-like activity as a novel function of 14-3-3 proteins. FEBS letters *419*, 244-248.

Yano, M., Nakamuta, S., Wu, X., Okumura, Y., and Kido, H. (2006). A novel function of 14-3-3 protein: 14-3-3ζ is a heat-shock–related molecular chaperone that dissolves thermal-aggregated proteins. Molecular biology of the cell *17*, 4769-4779.

Zegzouti, H., Zdanovskaia, M., Hsiao, K., and Goueli, S.A. (2009). ADP-Glo: a bioluminescent and homogeneous ADP monitoring assay for kinases. Assay and drug development technologies 7, 560-572.

Publications:

a. <u>Published:</u>

b. <u>Accepted:</u>

c. <u>Communicated:</u>
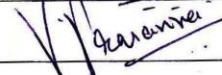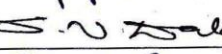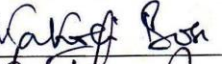
Manoj Ramteke; Pradnya Shelke; Vidhya Ramamoorthy; Arun K Somavarappu; Amit Kumar S Gautam; Padma Nanaware; Sudheer Karanam; Sami Mukhopadhyay; Prasanna Venkatraman (2013). Identification of Intrinsic ATPase Activity in 14-3-3 zeta- Evidence from Structure Guided Modeling and Mutagenesis Studies. *FEBS Letters*; Manuscript No. FEBSLETTERS-D-13-01334.

Padma Nanaware, **Manoj Ramteke**, Arun K Somaravarappu and Prasanna Venkatraman (2013). Discovery of Multiple Interacting Partners of Gankyrin, a Proteasomal Chaperone and an Oncoprotein – Evidence for a Common Hot spot site at the Interface. *PROTEINS: Structure, Function and Bioinformatics*; Manuscript No. Prot-00245-2013.

Signature of Student: M. P. Ramteke

Date: 19th August 2013

Doctoral Committee:

S. No.	Name	Designation	Signature	Date
1.	Dr. R. Mulherkar	Chairman		19·08·03
2.	Dr. Prasanna Venkatraman	Convener		19/Ag2013
3.	Dr. Sorab Dalal	Member		19/8/2013
4.	Dr. Kakoli Bose	Member		19/8/2013
5.	Prof. B. J. Rao (TIFR)	Invitee		19/8/2013

Forwarded through:

Dr. S. Chiplunkar

(Chairperson, Academic and
Training programme, ACTREC)

Dr. S. Chiplunkar

(Dy. Director, ACTREC)

Dr. Rajiv Sarin

(Director, ACTREC)

Dr. K. S. Sharma,

(Director, Academics, TMC)

15

LIST OF FIGURES

LIST OF ABBREVIATIONS

AANAT   Arylalkylamine *N*-acetyltransferase

μCi   Microcurie

ADP   Adenosine5'-diphosphate

AMP-PCP   Adenylylmethylenediphosphonate

ATP   Adenosine5'-triphosphate

ATP-γ-S   Adenosine 5′-(3-thiotriphosphate)

BME   β- Mercaptoethanol

BSA   Bovine Serum Albumin

cDNA   complimentary Deoxyribonucleic acid

DNA   Deoxyribonucleic acid

CSF   Cerebrospinal fluid

DTT   Dithiothreitol

FD   Fast digest

HB   Hydrogen bonds

HEPES   N-(2-Hydroxyethyl)piperazine-N'-2(2-ethanesulphonic acid)

IR   Ionizing radiation

kDa   Kilodalton

M   Molar

mM   Millimolar

MALDI   Matrix assisted laser desorption ionization

MS   Mass spectrometery

MQ   Milli Q (water)

NCBI   National Centre for Biotechnology Information

Ni-NTA   Nickel-nitriloacetic acid

PAGE	Poly acrylamide gel electrophoresis
PD	Parkinson's disease
PCR	Polymerase chain reaction
PDB	Protein Data Bank
Pi	Inorganic phosphate
PLP	Piecewise Linear Pairwise Potential
RMSD	Root mean-square deviation
SDS	Sodium dodecyl sulphate
TEMED	N,N,N',N' Tetramethyl ethylene diamine
TBST	Tris buffered saline with 0.1% Tween-20
vdW	Van der waal
WHO	World health organization
WT	Wild-type

CHAPTER 1.

INTRODUCTION

Identification of a novel ATP binding site and demonstration of ATP hydrolysis by mammalian 14-3-3 isoforms

CHAPTER 1. INTRODUCTION:

The 14-3-3 protein family represent a group of highly conserved, acidic, dimeric proteins of about 20-30 kDa (Aitken, 2006). In mammals, this family is represented by seven highly conserved isoforms - β, γ, ε, ζ, η, σ and τ/θ. 14-3-3α and δ are the phosphoforms of β and ζ respectively (Aitken et al., 1995). All these proteins are expressed in a wide range of organs and tissues. Two other isoforms τ and σ are expressed in T cells and epithelial cells, respectively. 14-3-3 proteins account for ~1% of the total soluble brain protein (Fu et al., 2000). The following table summarizes some of the general properties of human 14-3-3 isoforms.

Table T1.1 General properties of human 14-3-3 isoforms

Sr. No.	Gene Name	Official Symbol	Other Aliases/ Designations	Chromosomal Location	(PI)	Length (Amino Acids)	MW (kDa)
1.	14-3-3ζ	YWHAZ	14-3-3-zeta, KCIP-1, YWHAD, delta polypeptide, zeta polypeptide	8q23.1	4.73	245	27.61
2.	14-3-3γ	YWHAG	14-3-3 gamma	7q11.23	4.8	247	28.12
3.	14-3-3τ/θ	YWHAQ	1C5, HS1, 14-3-3 protein T-cell	2p25.1	4.68	245	27.63

4.	14-3-3ε	YWHAE	14-3-3E, MDCR, MDS, epsilon polypeptide	17p13.3	4.63	255	29.03
5.	24-3-3σ	SFN/ YWHAS	epithelial cell marker protein 1, 14-3-3 sigma	1p36.11	4.68	248	27.64
6.	14-3-3β	YWHAB	RP1-148E22.1, GW128, HS1, YWHAA, beta polypeptide, alpha polypeptide	20q13.1	4.76	246	27.95
7.	14-3-3η	YWHAH	LL22NC03- 44A4.1, YWHA1, 14-3-3 eta	22q12.3	4.76	246	28.09

X-ray crystallographic studies have shown that each 14-3-3 monomer consists of a bundle of nine α-helices organized in an antiparallel fashion, forming a central amphipathic binding groove which is highly conserved across the 14-3-3 isoforms (Fu et al., 2000; Liu et al., 1995). The hydrophobic surface of this groove is formed from helices 7 and 9, with the opposing polar face consisting of basic and polar side chains of helices 3 and 5 (Danielle et al., 2011). The homo and hetero-dimerization of 14-3-3 isomers occurs through N-terminal interactions of the monomers resulting in two amphipathic grooves in each dimer to form a 40 Å wide channel at the center (Danielle et al., 2011). The amino acid sequences throughout the seven human 14-3-3 isoforms are highly conserved and maximum sequence diversity is found in their

extreme C-termini (Fig. 1.1). Despite this diversity, the C-termini of all 14-3-3 isoforms share the amino acid residues with characteristics of acidic are disorder in nature. In the case of 14-3-3 isoform, the majority of its ligands interact with the binding groove via a conserved basic cluster (Lys and Arg) at the ligand binding amphipathic pocket.
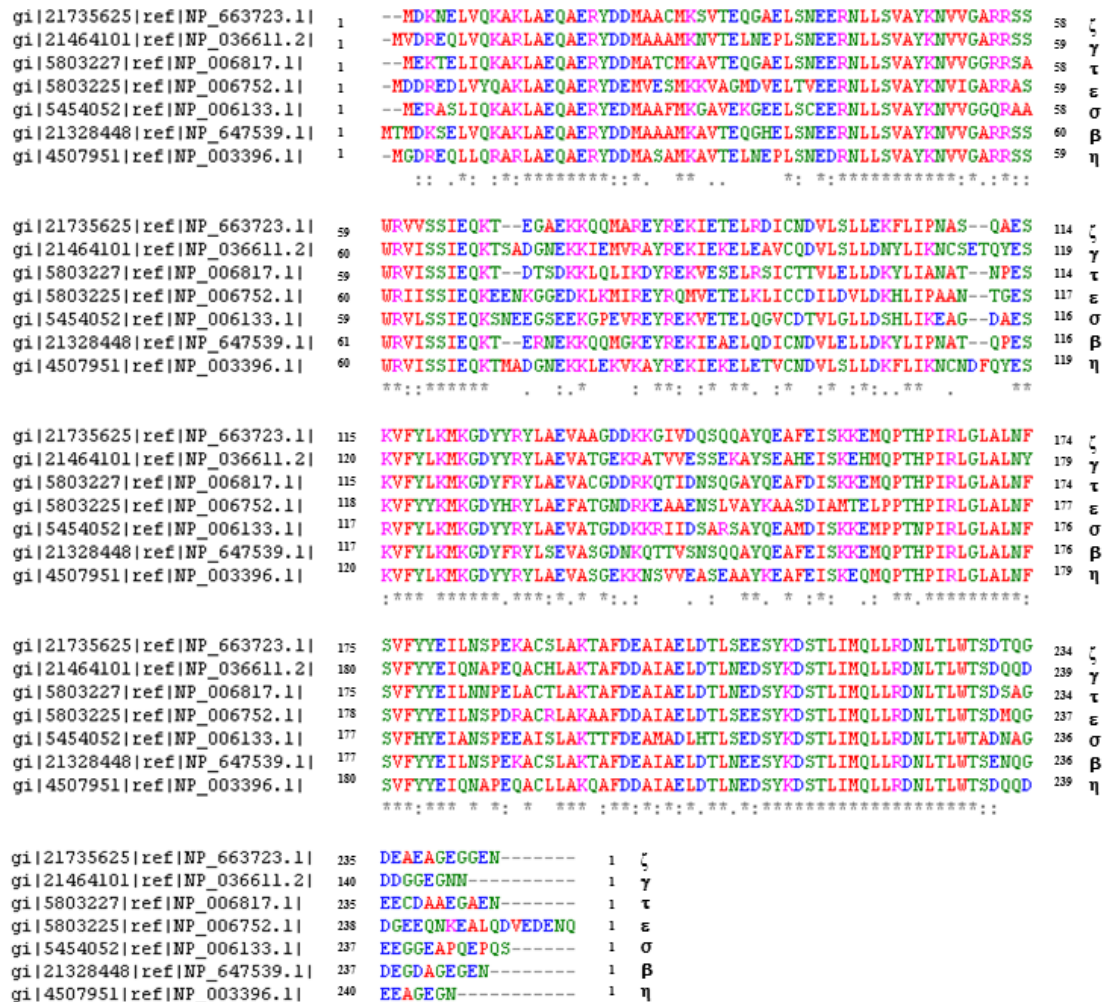
Fig. 1.1 Multiple sequence alignment of human 14-3-3 isoforms

Multiple sequence alignment was performed using clustal omega (http://www.ebi.ac.uk/Tools/msa/clustalo/). Figure shows the conserved residues in human 14-3-3 isoforms and variable residues in flexible c-terminal end.

Different 14-3-3 isoforms form homo- and/or hetero-dimers and bind to client proteins containing phosphoserine or phosphothreonine residues within specific sequence motifs (Muslin et al., 1996). So far three major consensus phospho motifs have been identified on 14-3-3 target proteins. These are RSXpSXP (mode I), RXY/FXpSXP (mode II) and pS/pT (X1–2)-COOH (mode III), where pS and pT represents phosphoserine and phosphothreonine respectively (Ganguly et al., 2005). Interaction between 14-3-3 and client protein affects multiple signaling pathways which determine cell fate and organ development. To date, more than 200 target proteins have been identified for 14-3-3 (Rubio et al., 2004). Through these highly regulated interactions, 14-3-3 proteins govern diverse physiological processes and cellular status like apoptosis, metabolism, signal transduction, cell cycle control, protein localization and stress responses. These proteins are also involved in malignant transformation (Fu et al., 2000; Hermeking and Benzinger, 2006; Hosing et al., 2008; Telles et al., 2009; Yu et al., 2013).

14-3-3 proteins have also been implicated in numerous neurodegenerative diseases such as Alzheimer's disease (Fountoulakis et al., 1999; Hernández et al., 2004; Layfield et al., 1996; Umahara et al., 2004), Parkinson's disease (Kawamoto et al., 2002; Li et al., 2011; Nichols et al., 2010; Sato et al., 2005; Yacoubian et al., 2010) and ataxia (Berg et al., 2003; Chen et al., 2003; Umahara and Uchihara, 2010; Waterman et al., 1998). Various 14-3-3 isoforms are found within intracellular deposits of neurons in the brains of patients with neurodegenerative diseases like Parkinson's disease and huntingtin (Steinacker et al., 2011). Because of their presumed interaction with proteins like α synuclein (in Parkinson's disease) and poly Q repeats in Huntingtin protein (in Huntington's disease) 14-3-3 proteins have been implicated in the pathology of these diseases (Kawamoto et al., 2002; Mackie and

Aitken, 2005; Omi et al., 2008; Rong et al., 2007). Researchers have also studied and correlated the presence of various 14-3-3 isoforms in cerebrospinal fluid (CSF) of patients with different neuropathological disorders (Beaudry et al., 1999; Boston et al., 2006; Burkhard et al., 2001; Green et al., 2001; Hsich et al., 1996; Wiltfang et al., 1999; Zerr et al., 2004). However the exact mechanism of 14-3-3 involvement is not very well understood.

Besides the well known function as adaptor proteins that regulate various cellular activates like cell cycle, cell signaling and apoptosis, 14-3-3 isoforms have also been assigned enzymatic activities. Such activities however are considered ambiguous. The first function ascribed to this family of proteins was activation of tyrosine and tryptophan hydroxylases, the rate limiting enzymes involved in catecholamine and serotonin biosynthesis, essential for the synthesis of dopamine and other neurotransmitters (Ichimura et al., 1987). Hence this protein is also described as tyrosine 3-monooxygenase/tryptophan 5-monooxygenase activation protein. Further 14-3-3 was shown to regulate the activity of protein kinase C (Toker et al., 1990).

In the present thesis the focus is on the unexplored ATPase activity of 14-3-3 isoforms and characterization of its kinetic properties like V_{max}, k_{cat}, K_m and k_{cat}/K_m. Residues that influence this activity have been identified.

CHAPTER 2.

REVIEW OF LITERATURE

CHAPTER 2. REVIEW OF LITERATURE:

This chapter summarizes the known properties and functions of 14-3-3 isoforms. It deals with the nomenclature, expression, distribution and binding specificity of 14-3-3 proteins. It also elaborates on the known target proteins, interactions and summarizes functions of 14-3-3 proteins in normal physiological condition and diseases like cancer and neuropathological disorders. Current literature on the isolated reports on the ATP/ADP exchange reactions seen with some 14-3-3 isoforms is covered. In this context a brief summary on some of the well known ATPase and chaperons is covered with a highlight on small heat shock proteins (sHSPs).

2.1 Nomenclature of 14-3- 3 proteins:

Many names have been given to 14-3-3 proteins by various discoverers depending the particular role, properties or functions performed by the protein (Aitken, 2006). The name 14-3-3 was given first because of its characteristic elution and migration pattern on two-dimensional DEAE-cellulose chromatography and starch gel electrophoresis. The 14-3-3 proteins elute in the 14th fraction of bovine brain homogenate from the DEAE cellulose column and fractions 3.3 in the next step (Moore et al., 1967).

2.2 Expression and distribution of 14-3-3 proteins:

14-3-3 proteins are conserved from yeast to *Drosophila*, to humans and also in plants. 14-3-3 proteins are expressed in almost all tissue type in humans. However each isoform shows specific expression pattern and unique function(s). For example, 14-3-3γ shows relatively strong expression in brain, skeletal muscle and heart, but

weak in peripheral blood leukocytes (Horie et al., 1999). The 14-3-3θ, also named as 14-3-3 tau (14-3-3τ), was shown to be specifically expressed in murine testis and brain (Chaudhary and Skinner, 2000). 14-3-3τ is widely expressed in multiple cells and tissues particularly in T cell (Reuther and Pendergast, 1996). The expression of 4-3-3ε is abundant in epithelial cells. 14-3-3σ, also known as human mammary epithelial marker 1 (HME1) or stratifin, is expressed in normal mammary cells but is found at reduced levels in human mammary carcinoma cell lines (Prasad et al., 1992; Vercoutter-Edouart et al., 2001). 14-3-3 proteins are also present in other organisms and are involved in variety of cellular functions. Table T2.2.1 summarizes the role of 14-3-3 proteins in different organisms.

Table T2.2.1 role of 14-3-3 proteins in different organisms

Sr. No.	Organism	14-3-3 isoform	Function	Reference
1.	*Saccharomyces cerevisiae* (Yeast, Two isoforms)	1. Bmh1 2. Bmh2	Sequestration of transcription factors Msn2p and Msn4p into cytoplasm, control cell cycle progression	Ford et al., 1994; Beck and Hall, 1999
2.	*Schizosaccharomyces pombe*	*1. Rad24* *2. Rad25*	Sequestration of DNA binding	van Heusden and Yde

			Ste11protein into cytoplasm , cell cycle progression, nuclear localization of Chk1 protein	Steensma, 2006; Qin et al., 2003; (Dunaway et al., 2005)
	(Yeast, Two isoforms)			
3.	*Drosophila melanogaster* (Fruit fly, Two isoforms)	1. 14-3-3ε	Differentiation in the adult eye, in innate immunity,	Li et al., 1997; Shandala et al., 2011
		2. 14-3-3ζ	Embryo differentiation, chromosome separation, phagocytosis and microbial resistance	Li et al., 1997; Su et al., 2001; Ulvila et al., 2011
4.	*Arabidopsis thaliana* (Plant)	About 13 isoforms	Phosphorylation dependent binding is not a strict rule, ion and nutrient transport	Ferl, 2004; (Shin et al., 2011)

5.	Gossypium herbaceum (Cotton plant, about six isoforms)	1. Gh14-3-3a 2. Gh14-3-3e 3. Gh14-3-3f 4. Gh14-3-3g 5. Gh14-3-3h 6. Gh14-3-3L	regulation of fiber cell elongation	(Zhang et al., 2010b)

2.3 14-3-3 Binding specificity:

14-3-3 family of proteins is well known for its binding specificity with the client proteins though consensus pS/pT residues (Aitken, 2006). Muslin et al., for the first time defined 14-3-3 proteins as phosphor-serine binding proteins, which bind to the consensus motif RSXpSXP, where X represents any amino acid and pS represents phosphoserine (Muslin et al., 1996). Since the binding is dependent on the phosphorylation of the serine residue, this allows conditional association of 14-3-3 proteins with protein ligands that contain such motif, e.g. RAF1 (Muslin et al., 1996). Yaffe et al., further refined the 14-3-3-binding motif by screening phosphopeptide libraries and identified two different binding motifs as RSXpSXP (mode I) and RXY/ FXpSXP (mode II) that are present in almost all 14-3-3-binding proteins (Yaffe et al., 1997a). Using a panel of five phosphoserine-oriented degenerate peptide libraries, Yaffe et al., have discovered mode I and mode II, two alternative consensus binding sequences for 14-3-3. In contrast to these peptide library experiments, a variety of intracellular signaling proteins seem to demonstrate preferred or specific interactions with particular 14-3-3 isoform. These include preferential interactions between PKCθ and Cbl with 14-3-3τ in T-cells (Liu et al., 1997; Meller et al., 1999), IGF1-receptor

and IRS1 with 14-3-3ε (Craparo et al., 1997), the apoptosis inhibitor A20 with 14-3-3β (Vincenz and Dixit 1996) and the glucocorticoid receptor with 14-3-3η (Wakui et al., 1997). Furthermore, the cooperative nature of the binding can allow proteins containing tandem sequences to bind in cases where neither sequence alone is sufficient. This appears to be the case with Cbl, where neither of the two motifs implicated in 14-3-3 binding, NRHpSLP and RLGpSTF, individually can interact with 14-3-3, but the presence of both motifs confers stable binding (Liu et al., 1997).

The third binding motif, mode III was recognized as pS/pT (X_{1-2})-COOH in arylalkylamine *N*-acetyltransferase (AANAT) (Ganguly et al., 2005). T31 residue in AANAT is phosphorylated by cyclic AMP-dependent protein kinase. Phosphorylation of T31 promotes binding of AANAT to the dimeric 14-3-3 protein, which activates AANAT by increasing arylalkylamine affinity.

Apart from the mode I, II and III sequences, additional binding sites that do not involve phosphorylated S or T residue have also been seen. For example Raf kinase have been shown to have additional binding sites for 14-3-3 on their cysteine rich regions. Breakpoint cluster region protein (Bcr) binds via a serine rich region (Aitken, 2006). Along with several other 14-3-3 binding proteins, Exoenzyme S (ExoS), the ADP-ribosyltransferase toxin secreted by the bacterium *Pseudomonas aeruginosa*, interact with 14-3-3 in a phosphorylation independent manner (Henriksson et al., 2002). The DALDL sequence in ExoS, comprising of residues 424–428 at the C-terminus is essential for interaction with 14-3-3. The same sequence is seen in the unphosphorylated peptide R18 (as LDL sequence). This R18 peptide is a high affinity 14-3-3 binding peptide discovered by Fu and co-workers using phage display (Wang et al., 1999). Other post translational modifications like acylation of

proteins can also regulate interaction with 14-3-3 (Macdonald et al., 2005; Winter et al., 2008).

2.4 Functions of 14-3-3 proteins:

Thus 14-3-3 proteins act as scaffolding molecules which bind with the target protein to either sequester the target protein in the specific compartment of the cell or bring about the favorable conformational changes in the protein. Depending on the target partner, 14-3-3 participates in the regulation of various cellular functions to regulate the homeostasis (Fig. 2.4.1). Furthermore, The 14-3-3 proteins are an important family of protein involved in various processes such as, cell cycle checkpoint (Fig. 2.4.2), signal transduction, apoptosis (Fig. 2.4.3), migration (Aitken, 2006; Hermeking, 2003; Hermeking and Benzinger, 2006; Hosing et al., 2008; Telles et al., 2009). These are briefly summarized in the following figures.
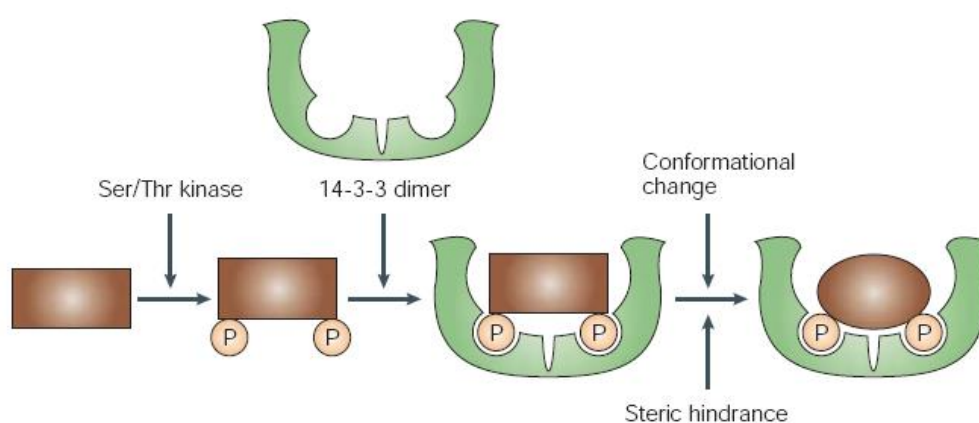
Fig. 2.4.1 Binding of 14-3-3 dimer to its target partners

Figure shows schematic representation of binding of 14-3-3 dimer to the target protein. Dimeric 14-3-3 protein binds to the target protein and sequesters them in the specific cellular compartment or brings about the conformational changes in the target protein (Hermeking, 2003).
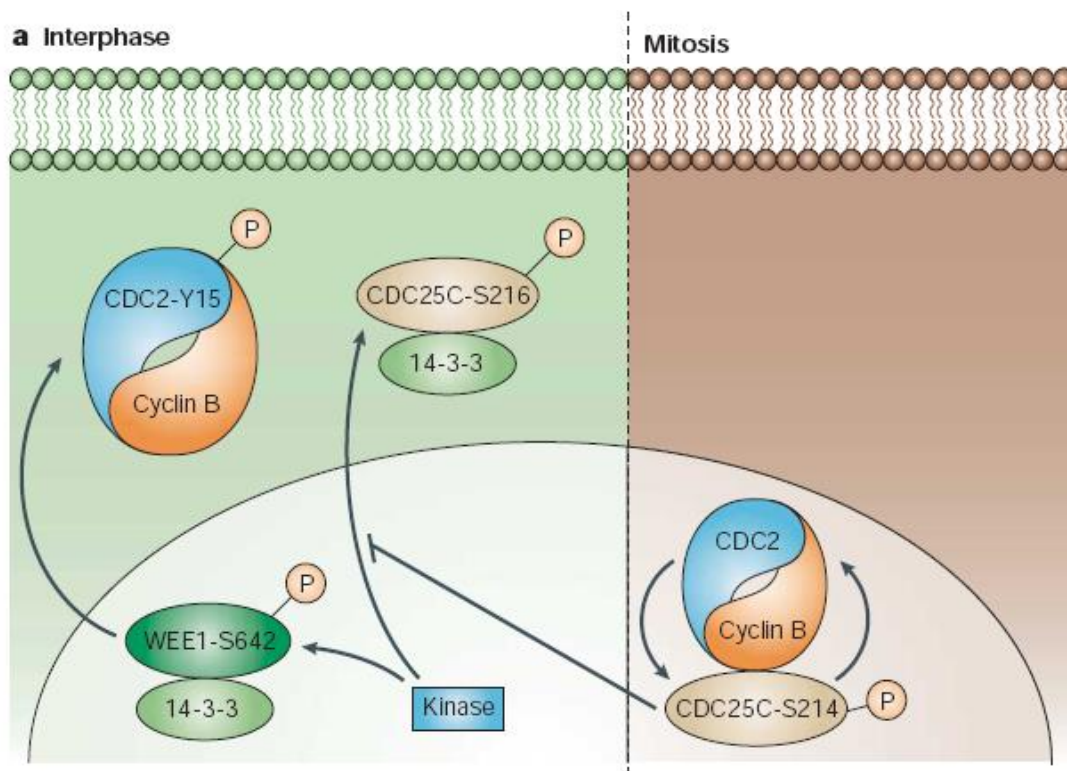
Fig. 2.4.2 Roles of 14-3-3 proteins in cell-cycle regulation

Several mechanisms involving 14-3-3–ligand association are implemented to ensure that mitosis/M-phase is not prematurely activated before the completion of DNA replication in interphase. The tyrosine kinase WEE1 is activated by phosphorylation during interphase; this involves association with 14-3-3 proteins after phosphorylation of Ser642. Active WEE1 inhibits CDC2 by Tyr15 phosphorylation. In parallel, CDC25C - the main inducer of CDC2 - is kept in an inactive state by phosphorylation at Ser216 by TAK1, which results in cytoplasmic sequestration by 14-3-3 proteins. Once mitosis is activated, cytoplasmic sequestration of CDC25C is inhibited by a CDC2-mediated phosphorylation of CDC25C at Ser214, which prevents phosphorylation at Ser216 and, thereby, 14-3-3 association of CDC25C. WEE1 activation leads to inhibitory CDC2 phosphorylation and cytoplasmic sequestration of CDC25C (Hermeking, 2003).
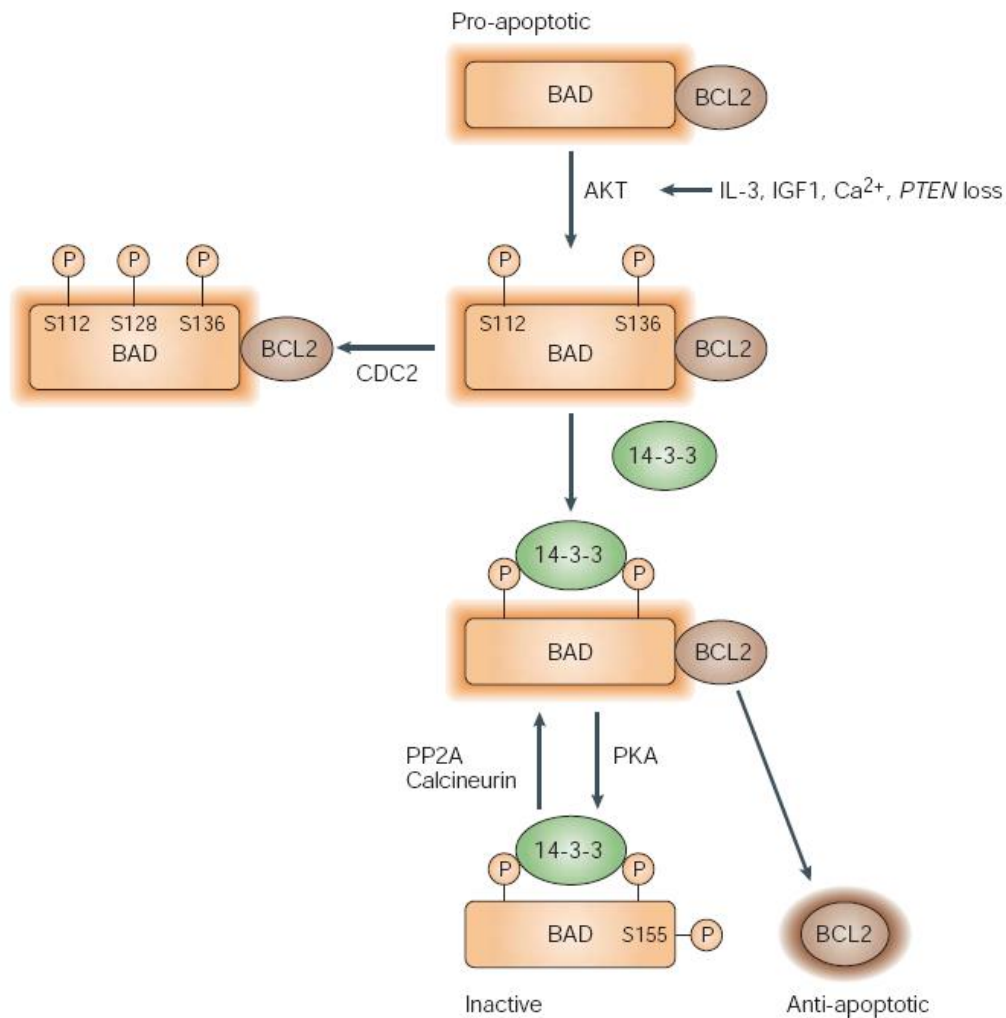
Fig. 2.4.3 Role of 14-3-3 proteins in the regulation of apoptosis

Activation of the AKT protein kinase by survival signals leads to phosphorylation of BAD, which allows its association with 14-3-3 proteins. On 14-3-3 binding, Ser155 becomes accessible for phosphorylation by protein kinase A (PKA). This residue is located within the BH3 domain of BAD, which mediates BCL2 binding, and its phosphorylation leads to the release of BCL2. Removal of the Ser155 phosphate group by the phosphatases protein phosphatase 2A (PP2A) or calcineurin leads to reconstitution of the pro-apoptotic state of BAD–BCL2 dimerization. This applies to other BCL2-like proteins, such as BCL-XL. Active CDC2 might block the association of 14-3-3 proteins with BAD by phosphorylating Ser128 (Hermeking, 2003).

2.5 14-3-3 in Cancer:

Among all the 14-3-3 genes, 14-3-3σ is considered to be tumor suppressor while all other isoforms show oncogenic properties. 14-3-3σ show reduced or loss of expression while other 14-3-3 isoforms show higher expression in cancers. Specifically 14-3-3σ shows reduced expression in human prostate cancer (Cheng et al., 2004). This loss of expression is thought to cause a G2 checkpoint defect, resulting in chromosomal aberrations. More recently, the 14-3-3σ gene was shown to be hypermethylated and silenced in both small cell lung cancer (SCLC) and large cell lung cancer (Hermeking and Benzinger, 2006).

Overexpression of 14-3-3ζ has been observed in esophageal, lung, prostate, pancreatic and breast cancers (Fan et al., 2007; Meehan and Sadar, 2004; Neal et al., 2009). The gene encoding 14-3-3ζ maps to the chromosome region 8q23, which is frequently amplified in metastatic cancer (Tada et al., 2000). The increased expressions of 14-3-3ζ transcripts in oral squamous cell carcinoma in comparison with normal oral epithelium has been verified using differential display (Arora et al., 2005; Matta et al., 2007). Recently, 14-3-3ζ has been proposed as a potential oncogene involved in the development of head and neck cancer (Lin et al., 2009). 14-3-3ζ overexpression increased Akt phosphorylation in human mammary epithelial cells. 14-3-3ζ overexpression was associated with increased Akt phosphorylation in human breast tumors (Neal et al., 2011). Additionally, 14-3-3ζ overexpression combined with strong Akt phosphorylation was associated with increased cancer recurrence in patients. 14-3-3ζ is also overexpressed in gastric cancer and has a pivotal role in tumor cell proliferation through its overexpression highlight its

2.6 Detection of 14-3-3 in neuropathological disorder:

The 14-3-3 proteins are detectable in the cerebrospinal fluid (CSF) of patients with Cretzfeldt-Jakob disease (CJD), a neurodegenerative disorder (Hsich et al., 1996; Zerr et al., 1998; Zerr et al., 2000). It was further determined that only certain 14-3-3 isoforms (β, γ, ε and η) are present in the CSF of CJD patients (Satoh et al., 2010; Wiltfang et al., 1999). Thus WHO included the detection of 14-3-3 CSF proteins in the diagnostic criteria for sporadic CJD (Weber et al., 1997). Recently Fujii et al., reported for the first time that 14-3-3 protein could be detected in the CSF of patients with cerebellar involvement, suggesting a novel role of 14-3-3 proteins as a pathogenic biomarker of the cerebellum (Fujii et al., 2012).

Meningioma is a tumor of meninges, the protective membranes around the brain and spinal cord. Meningioma can originate in any part of the brain or spinal cord, but the most common sites are the cerebral hemispheres. The positive immunohistological reactions of 14-3-3ε, ζ and θ proteins were observed in patients with meningioma (Liu et al., 2010). But there was no expression of 14-3-3 in normal meninges. The expressions of 14-3-3ε, ζ and θ proteins were not related with the patient's sex and age. The expression of 14-3-3ε, ζ and θ increased gradually with the increase of pathological grade of meningioma. Notably, the expression of 14-3-3β, η, γ and σ was not found in three grade meningiomas and normal meninges (Liu et al., 2010).

Parkinson's disease (PD) is considered as a related neurodegenerative disease characterized by the presence of Lewy bodies and the loss of dopaminergic neurons.

14-3-3 proteins have been associated with PD based on their localization, binding partners and neuroprotective function. Lewy bodies are abnormal protein aggregates developed inside nerve cells in cortical and subcortical regions of PD brains. Several immunohistochemical studies have identified that four of the seven 14-3-3 isoforms (ε, γ, σ, and ζ) are also present in Lewy bodies (Kawamoto et al., 2002; Ubl et al., 2002). Interestingly, α-synuclein and 14-3-3 proteins share a substantial sequence homology and may interact with each other. In transgenic mice overexpressing human wild-type α-synuclein, several 14-3-3 isoforms (γ, τ, ε, and σ) were found to have reduced gene expression (Yacoubian et al., 2010).

Alzheimer's disease (AD) is a neurodegenerative disease with dementia and is characterized by two pathological hallmarks: amyloid plaques and neurofibrillary tangles (NFTs) (Greicius et al., 2004; Lee, 1995). Amyloid plaques are the extracellular deposits of amyloid-beta fibrils which are considered to be neurotoxic and result in neuronal dysfunction (Götz et al., 2011). NFTs are mostly composed of paired helical filaments formed by aggregation of the abnormally hyper-phosphorylated tau proteins (Goedert, 1996). Several studies have implicated a role of 14-3-3 proteins in the neuropathology of AD based on their colocalization with NFTs, interactions with AD-associated proteins and their potential utility as an AD biomarker (Blennow, 2004; Dougherty and Morrison, 2004).

Schizophrenia is neuropsychiatric disorder that is among the leading causes of disease related disabilities in the world (Couture et al., 2006; Varga et al., 2007). Schizophrenia is characterized by a combination of positive, negative and cognitive symptoms which vary in severity. Diagnosis is based on the presence of hallucinations, delusions and disorganized thoughts and behavior. In particular, reality distortion is thought to mark the actual onset of schizophrenia. Although the precise

cause of schizophrenia is not fully understood. Genetic analyses have suggested a linkage between schizophrenia and the chromosomal region 22q12-13, in which 14-3-3η gene *YWHAH* is located (Bell et al., 2000; Muratake et al., 1996). A significant association between single nucleotide polymorphisms (SNP) of the 14-3-3η gene and schizophrenia has been established in a majority of studies using human samples from different ethnic groups (Toyooka et al., 1999; Wong et al., 2003). In addition, genetic and post-mortem mRNA analyses have identified other 14-3-3 isoforms as potential susceptibility genes for schizophrenia, including the genes encoding 14-3-3ε and ζ(Horváth et al., 2011; Jia et al., 2004; Wong et al., 2005).

Bipolar disorder also known as manic depression causes serious shifts in mood, thinking and behavior. The cycles of bipolar disorder last for days, weeks or months (Rush, 2003; Tsuang, 2002; Winokur et al., 1995). 14-3-3η and other 14-3-3 isoforms have been implicated in bipolar disorder (Higgs et al., 2006; Liu et al., 2010). YWHAZ gene is located on chromosome 8q23.1, which is close to a probable bipolar disorder susceptibility locus 8q24 (Cichon et al., 2001). Several microarray studies have identified decreased mRNA expression levels of 14-3-3ε, σ and ζ in brain samples from bipolar patients (Higgs et al., 2006; Wong et al., 2005).

2.7 Role of 14-3-3 as a molecular chaperon

In 2006, Yano et al., have shown that 14-3-3 protein is behaving similar to that of heat heat-shock protein (Hsp) and protects cells against physiological stress. They have observed that in *Drosophila* cells, the 14-3-3ζ but not 14-3-3ε is upregulated under heat stress conditions. This upregulation process is mediated by a heat shock transcription factor. As the biological action in response to heat stress, 14-3-3ζ interacted with apocytochrome *c*, a mitochondrial precursor protein of cytochrome *c*

(Yano et al., 2006). On the other hand the suppression of 14-3-3ζ expression by RNA interference resulted in the formation of significant amounts of aggregated apocytochrome *c* in the cytosol. The aggregated apocytochrome *c* was converted to a soluble form by the addition of 14-3-3ζ protein in an ATP dependent manner *in vitro*. Furthermore, 14-3-3ζ also resolubilized heat-aggregated citrate synthase (CS) and facilitated its reactivation in co-operation with Hsp70 or Hsp40 *in vitro* (Yano et al., 2006). These observations provide the first direct evidence that a 14-3-3 protein functions as a stress induced molecular chaperone that dissolves and renaturalizes thermal aggregated proteins.

However the fundamental mechanism behind the resolubilization of insoluble proteins by 14-3-3ζ is unknown. Glover and Lindquist have proposed that Hsp104 solubilizes the aggregates by pulling apart the oligomeric assemblages of heat damaged proteins (Glover and Lindquist, 1998). The observation of an increase in the susceptibility to proteinase K digestion of the heat aggregated apocytochrome *c* by 14-3-3ζ supplementation suggests that like Hsp104, 14-3-3ζ may drive the aggregated apocytochrome *c* into a relaxed state. The above possibility is supported by the observation that the 14-3-3ζ mediated resolubilization of heat-aggregated CS allows the subsequent refolding of CS by Hsp70/Hsp40 *in vitro*. Further, neither 14-3-3ζ nor Hsp70/Hsp40 alone reactivated heat-aggregated CS. The 14-3-3ζ mediated refolding of aggregated CS that occurs only in conjunction with other chaperones (Yano et al., 2006). Suggesting that 14-3-3ζ alone cannot work as an effective manner and always require the help of other chaperons. One possible explanation explained by the researchers is the breaking of large aggregates by 14-3-3ζ, which sequestrate the hydrophobic surfaces of substrate, into smaller species that are more accessible to other chaperones, thus facilitating protein refolding. The unique characteristics of the

14-3-3ζ protein that has been identified may establish its position as a stress tolerance factor that promotes the refolding of heat aggregated proteins in the chaperone machinery forming a bichaperone network. Thus 14-3-3ζ isoform is a molecular chaperone, preventing the stress induced aggregation of target proteins in a manner comparable with that of the unrelated sHSPs (small heat-shock proteins).

^{1}H-NMR spectroscopy revealed the presence of a flexible and unstructured C-terminal extension, 12 amino acids in length, which protrudes from the domain core of 14-3-3ζ and is similar in structure and length to the C-terminal extension of mammalian sHSPs (Danielle et al., 2011). The extension stabilizes 14-3-3ζ, but has no direct role in chaperone function. Lys49 is an important functional residue within the ligand-binding groove of 14-3-3ζ with K49E 14-3-3ζ exhibiting markedly reduced binding to phosphorylated and non-phosphorylated ligands (Fu et al., 2000; Yaffe et al., 1997a). The R18 peptide binds to the binding groove of 14-3-3ζ with high affinity and also reduces the interaction of 14-3-3ζ ligands. However, neither the K49E mutation nor the presence of the R18 peptide affected the chaperone activity of 14-3-3ζ, implying that the C-terminal extension and binding groove of 14-3-3ζ do not mediate interaction with target proteins during chaperone action (Danielle et al., 2011). This proves that the chaperone and phosphoserine binding activities of 14-3-3ζ are structurally and functionally separated.

Both the above studies suggest that 14-3-3ζ functions as a molecular chaperon that dissolves the aggregated proteins. On the other hand studies by Omi et al., showed the exact opposite role for 14-3-3ζ. According to their research, 14-3-3ζ is indispensable for aggregate formation of polyglutamine-expanded huntingtin (Htt) protein (Omi et al., 2008). Omi et al., proposed that 14-3-3ζ might act as a sweeper of

misfolded proteins by facilitating the formation of aggregates possibly for neuroprotection, these aggregates are referred to as inclusion bodies. They used N2a cells, mouse neuroblastoma cell line as a model system to study the aggregates of poly Q expanded huntingtin. When Htt86Q-EGFP was expressed in N2a cells, Htt86Q-EGFP aggregated which was distinctly visible as GFP dots which were further confirmed as aggregates in stacking part of gel by western blotting using GFP antibody. Immunoprecipitation of HttQ86-EGFP with anti GFP antibody showed that out of six 14-3-3 isoforms (ζ, γ, ε, η, σ and β) tested only four (β, γ, ζ and η) interact with Htt aggregate. This indicates that Htt interacts with 14-3-3 in an isoform specific manner. Out of four isoform that interacts with Htt, only when 14-3-3ζ was knockdown using siRNA, showed uniform localization of Htt86Q-EGFP. This proves that the 14-3-3ζ is required for the formation of Htt aggregates (Omi et al., 2008). However the researchers did not test the 14-3-3γ using siRNA. Further, it still needs to be determined how 14-3-3ζ recognizes and binds other aggregation-prone, non-native proteins and mediates the formation of these nonnative protein aggregates. It is likely that 14-3-3ζ is recruited to form deposits of protein aggregates with non-native, misfolded proteins in order to protect the cell against toxicity, when the abnormal processing of misfolded proteins take over the quality control systems of the cell.

2.8 Non classical ATP dependent functions of 14-3-3 family members

14-3-3 family members are classically known to function as an adaptor protein. Apart from its role as an adapter protein, 14-3-3 family members are known to exhibit ATP dependent functions. Many of these functions show enzymatic characteristics, but none of these functions were controversial. Some of the ATP dependent functions of 14-3-3 family members are described below.

Hachiya et al., have characterized rat liver cytosolic protein that contained an activity to stimulate the import of wheat germ lysate-synthesized precursor proteins into mitochondria. The activity was purified 10,000 fold from the cytosol as a homogeneous heterodimeric protein (Hachiya et al., 1993). This protein was termed as mitochondrial import stimulation factor or MSF that stimulated the binding and import of mitochondrial precursor proteins. MSF was also found to recognize the presequence portion of mitochondrial precursors and catalyze the depolymerization and unfolding of *in vitro* synthesized mitochondrial precursor proteins in an ATP-dependent manner. In this connection, MSF exhibited ATPase activity depending on the import-incompetent mitochondrial precursor protein. Based on this observation it can be concluded that MSF is a multifunctional cytoplasmic chaperone specific for mitochondrial protein import. MSF was also found to possess ATPase activity. The specific activity of MSF was shown to be roughly 0.7 µmol/min/mg protein which was stimulated by about 230 fold in the presence of import incompetent mitochondrial precursoe pAd (Hachiya et al., 1993).

Further Alam et al., showed that MSF heterodimer consists of 32-kDa (MSFL) and 30-kDa (MSFS) polypeptides as assessed by SDS-PAGE (Alam et al., 1994). MSF recognized the presequence portion of mitochondrial precursor proteins and catalyzed the depolymerization and unfolding of *in vitro* synthesized mitochondrial precursor proteins in an ATP-dependent manner. Microsequencing of MSFL and MSFS showed that they belonged to a highly conserved, widely distributed eukaryotic protein family, collectively designated as 14-3-3 proteins (Alam et al., 1994). They cloned the cDNA of MSFL and that of one component of MSFS (MSFSl) from a rat liver cDNA library. The cloned cDNAs were separately expressed in *Escherichia coli* and the expressed proteins were purified to homogeneity. The purified recombinant

MSFL and MSFSl stimulated mitochondrial import of adrenodoxin precursor (pAd) synthesized *in vitro* with wheat germ lysate translation system. Recombinant MSFL or MSFSl had the ability to bind with denatured pAd and they kept the precursor in an import-competent state (Alam et al., 1994). Identification of MSF as 14-3-3 proteins establishes a novel function for this family of proteins and indicates their role as cytosolic chaperones to aid many important cellular events. Now MSFL and MSFS1 represent rat 14-3-3ε and 14-3-3ζ isoform respectively.

Komiya et al., as a step toward understanding the specificity of substrate recognition by MSF, examined various synthetic peptides for their ability to induce MSF ATPase activity (Komiya et al., 1994). The peptides corresponding to various mitochondria targeting signal sequences elicited significant ATPase activity. MSF bound the synthetic mitochondrial signal peptides and ATP hydrolysis caused dissociation of the peptides from MSF. Basic amino acid residues in the signal peptides seemed to be essential for recognition.

Yano et al., have shown that 14-3-3 purified from a human lymphoblastoma and also its recombinant human 14-3-3τ isoform exhibited intrinsic nucleoside diphosphate (NDP) kinase like activity (Yano et al., 1997). 14-3-3 proteins preferentially catalyzed the transfer of the γ-phosphate group from ATP, dATP or dGTP to all nucleoside diphosphates and this transfer involved acid labile phosphor-enzyme intermediates. They also simultaneously catalyzed the reverse reaction of ATP hydrolysis (Yano et al., 1997). However the residues involved in this function have not been characterized.

All the above characteristics of 14-3-3 proteins especially their role as chaperones, their association with neurodegenerative diseases that are characterized by protein aggregates, their ability at least in the *Drosophila* to dissolve preformed

aggregates of proteins in association with Hsp70 and isolated evidence about their role on nucleotide binding and exchange strongly imply a role for 14-3-3 proteins as small heat shock proteins. With this circumstantial evidence and keeping in view of the objectives of the thesis we summarize some of the properties of heat shock proteins, associated ATPase activity, structure and function.

2.9 Small heat shock proteins (sHSPs):

Small heat shock proteins (sHSPs) are relatively low molecular weight proteins with the molecular weight ranging from 10-42 kDa. They regulate a large number of fundamental cellular processes and are involved in many pathological diseases. They share complex oligomerization and phosphorylation properties allowing them to interact and modulate the activity of many target proteins. Notably sHsps are ATP-independent molecular chaperones. A majority of sHSPs form large oligomers, a property that has been linked to their effective chaperone action. All small heat shock proteins play important housekeeping roles and regulate many vital processes and therefore they are considered as attractive therapeutic targets.

sHSPs were originally discovered in different *Drosophila* tissues during recovery following a transiently and sublethal increase of normal body temperature (Tissiéres et al., 1974). Synthesis of these proteins was accompanied by the increased tolerance not only to heat shock, but also to many other unfavorable conditions such as hypoxia, ischemia, and stress factors like endotoxins, heavy metals, organic solvents and reactive oxygen species.

All proteins of sHSP family contain the α-crystallin domain, a region of about 90 residues that is homologous to the corresponding region in the primary structure of the main eye lens proteins αA- and αB-crystallin. This domain is considered as an

important hallmark of small heat shock protein (Kappé et al., 2010). The classification

and function of sHSPs (HSPB) is summarized as follows (Mymrikov et al., 2011):

Table T2.9.1 classification and function of small heat shock proteins (sHSPs)

Name	Synonyms	Chromosome Location	Residues (aa)	Function / Diseases
HspB1	Hsp25, Hsp27, Hsp28	7q11.23	205	Control of protein folding; when mutated, plays a significant role in the development of certain neurodegenerative disorders, regulation of apoptosis, protects the cell against oxidative stress, involved in the regulation of the cytoskeleton.
HspB2	MKBP, myotonic dystrophy protein kinase binding protein	11q22-q23	182	Myotonic dystrophy, different forms of neuropathology
HspB3		5q11.2	150	Motor neuropathy
HspB4	αA-Crystallin	21q22.3	173	Cataract

HspB5	αB-Crystallin	11q22.3-q23.1	175	Cataract, desmin-related and myofibrillar myopathy
HspB6	Hsp20, p20	19q13.12	157	Possesses chaperone-like activity, involved in regulation of smooth muscle contraction, has cardioprotective activity,
HspB7	cvHsp, cardiovascular heat shock protein	1p36.23-p34.3	170	Upregulated in muscular dystrophy
HspB8	Hsp22, H11 protein kinase, product of E2IG1 gene	12q24.23	196	Prevents accumulation of aggregated proteins in the cell and participates in the regulation of proteolysis of unfolded proteins, regulation of apoptosis and carcinogenesis; Charcot-Marie-Tooth disease type 2, distal hereditary motor neuropathy
HspB9		17q21.2	159	Upregulated in certain tumors

HspB10	ODF1, outer dense fiber proteins	8q22.3	250	Not reported

The small heat shock proteins tend to form highly mobile oligomers, starting from easily dissociating dimers (HSPB8) to multimers of more than 20 subunits (HSPB1, HSPB5), of different size and composition and this significantly complicates structural investigations. Human small heat shock proteins have very flexible quaternary structure. Depending on intracellular conditions and posttranslational modifications, they can undergo structural changes leading reversible cycles of dissociation and association (Benesch et al., 2008; Mchaourab et al., 2009). Having similar primary structure and being presented in a rather high concentration in the cell, different small heat shock proteins can interact with each other to generate hetero-oligomers of various sizes and compositions (Benndorf et al., 2001; MacRae, 2000; Sugiyama et al., 2000). This ability to form oligomers highly heterogeneous in size and composition (Haslbeck et al., 2005; Mymrikov et al., 2011).

Although all sHSPs protect the cell under unfavorable conditions and therefore seem to show similar effects but the mechanism of action of different members of this protein family can be different. For instance, HSPB1 and HSPB5 predominantly address unfolded proteins to ATP-dependent chaperones and thereby provide for their refolding. If refolding is impossible, then HSPB1 promotes proteasomal degradation of unfolded client proteins (Bryantsev et al., 2007; Zhang et al., 2010).

2.10 ATPases and Molecular Chaperons:

2.10.1 ATPases – General structure, active site and kinetics

ATPases are the class of enzymes that catalyze the breakdown of ATP to ADP and inorganic phosphate (Pi). ATPases are multisubunits complex and have evolved over time to meet specific demands of cells. These ATPases have been classified as F, V, A, P and E-ATPases based on functional differences. The driving force for the synthesis of ATP is the H^+ gradient, while during ATP hydrolysis the energy from breaking the ATP phosphodiester bond is the driving force for creating an ion gradient.

The F-ATPases (F stands for phosphorylation factor) are also known as H^+-transporting ATPases or F_0F_1-ATPases. These are the main enzymes used for ATP synthesis and are conserved throughout evolution. F_0F_1-ATPases performs the function of ATP break down in bacteria when metabolic conditions require doing so. They are found in the plasma membranes of bacteria, thylakoid membranes of chloroplasts and inner membranes of mitochondria. The yeast mitochondrial F_0F_1-ATPase is a large 600 kDa complex. These membrane proteins can synthesize ATP using H^+ gradient and work in the reverse to create H^+ gradient using the energy gained from the hydrolysis of ATP. The *E. coli* F_0F_1-ATPase has been extensively used to investigate the mechanism of ATPase action. The F-ATPase is formed from two sub-complexes, the catalytic F_1 complex and the trans-membrane proton translocation F_0 complex. There are five different subunits in F_1 ($\alpha_3\beta_3\gamma\delta\epsilon$) and three different subunits in the F_0 (ab_2c_{10}). X-ray crystal analysis of *E. coli* F_0F_1-ATPase shows that there are three different catalytic sites at F_1 subunit (Bianchet et al., 1998; Orriss et al., 1998) between α and β subunits. The three catalytic sites are structurally asymmetric when binding with Mg-ATP. The binding affinities are of the order of 1

nmol l^{-1}, 1 μmol l^{-1} and 100 μmol l^{-1} for the catalytic sites 1, 2 and 3 respectively (Löbau et al., 1997). In addition to three catalytic sites, F1 also contains three non-catalytic Mg-ATP binding sites. These binding sites play no direct or regulatory role in ATP hydrolysis. The first single site of ATP catalysis has the hydrolysis rate of 0.001 Sec^{-1} (Penefsky and Cross, 1991). However for the enzyme to reach to its V_{max} (approximately 100 Sec^{-1}) all the sites must be saturated with Mg-ATP.

Critical residues in the F-ATPase catalytic sites are βLys155, βThr156, βGlu181 and βArg182 (*E. coli* numbering, Fig. 2.11.1.2) (Nakanishi-Matsui et al., 2010). βLys155 and βArg182 are required for the binding of the ATP γ-phosphate and βThr156 is essential for coordinating the Mg^{2+} ion (Futai et al., 2012; Ida et al., 1991; Omote et al., 1995; Omote et al., 1992).
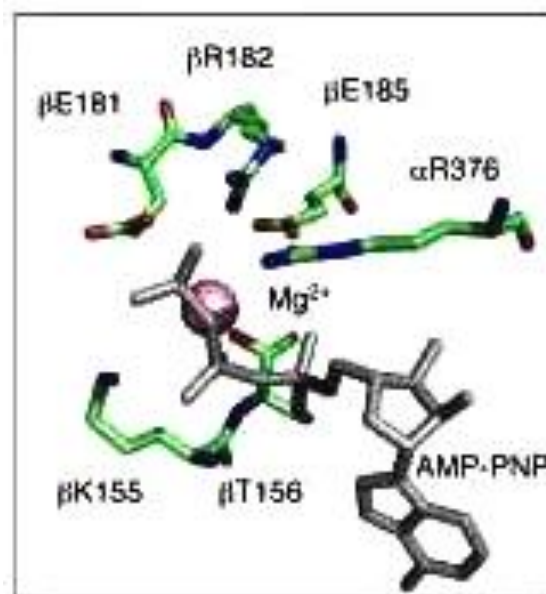
Fig. 2.10.1.1 Catalytic site of the F-ATPase

*The positions of critical amino acid residues in the three catalytic site $β_{TP}$, $β_{DP}$ and $β_E$ (*E. coli *numbering) of F-ATPase (Futai M. et al., 2012).*

The V_{max} and K_m for bovine heart mitochondrial F_0F_1 ATPase is 0.9 µmol/min/mg protein and 100 nM respectively (Johnson et al., 2005) whereas F_1F_0 ATPase from *Clostridium thermoaceticum* shows the V_{max} of 6.7 µmol/min/mg protein and K_m values of 0.43 mM (for ATP) (Ivey and Ljungdahl, 1986). Rate acceleration of ATP hydrolysis in F_0F_1 ATPase is regulated by various factors.

The basic structure of the V-ATPase is reminiscent of the F-ATPase with the V_1 and V_0 sectors corresponding to F_1 and F_0. It is likely that the V-ATPase has a similar catalytic site and mechanism because the residues of the F-ATPase involved in the ATPase activity βLys155, βThr156, βGlu181, βArg182 and βGlu186 are conserved in the V-ATPase catalytic subunit. These residues are part of the consensus "P-loop" sequence Gly-X-X-X-X-Gly-<u>Lys</u>-<u>Thr</u> and the Gly-<u>Glu</u>-<u>Arg</u>-X-X-<u>Glu</u> sequence (the catalytically important residues conserved in the F and V-ATPases are underlined) (Beyenbach and Wieczorek, 2006; Hirata et al., 2003).

A-ATPases (A stand for Archaea) are found exclusively in Archaea and have a similar function to F-ATPases. It is well known that Archaea faces extreme environmental conditions and hence it is believed that A-ATPases may have arisen as an adaptation to the different cellular needs faced by Archaeal species.

P-type ATPases belongs to a large superfamily of cation and lipid pumps. They are simple with only a single catalytic subunit and carry out large domain motions during transport. P-type ATPases contain five functional and structurally distinct domains as three cytoplasmic domains (A, actuator; N, nucleotide binding; P, phosphorylation) and two membrane-embedded domains (T, transport; S, class specific support domain).

E-ATPases (E stand for Extracellular) are membrane-bound cell surface enzymes that have broad substrate specificity. E-ATPases are abundant on cell

surfaces and their catalytic site faces the extracellular milieu (Wink et al., 2006). These ecto-enzymes constitute a highly organized enzymatic cascade in the regulation of nucleotide-mediated signaling, controlling the rate, amount and timing of nucleotide degradation and ultimately the nucleoside formation. Extracellular nucleotides/nucleosides are known to regulate several physiological responses including vascular tone, cardiac function and haemostasis (Kunapuli and Daniel, 1998; Ralevic and Burnstock, 2003).

2.10.2 Molecular Chaperons - General structure, active site and kinetics

Molecular Chaperons were originally defined as a group of proteins that mediate the correct assembly of other proteins, but are not themselves components of the final functional structure (Ellis, 2006). To counteract mis-folding and the appearance of toxic protein aggregates, molecular chaperones play a crucial role. Chaperones also assist nascent polypeptides in de novo folding and unfold them for degradation by proteolytic machines. They even regulate the conformation of certain natively folded proteins (Picard, 2002; Rodriguez et al., 2008). Molecular chaperons can be ATP independent like sHSPs and ATP dependent like Hsp 60, Hsp 70, Hsp 90 and Hsp 100 families.

Heat shock proteins vary in their ATPase kinetics. Table T2.11.2.1 summarizes the ATPase kinetics for HSPs.

Table T2.10.2.1 ATPase kinetics for HSPs

Sr. No.	Protein	K_m (µM)	k_{cat} (min^{-1})	Reference
1.	Hsp 60/Hsp10	0.43	0.63	(Tanabe et al., 2012)
2.	GroEL/GroES	3.03	1.32	(Tanabe et al., 2012)
3.	Hsp 70 (Human)	85	0.05 – 1	(Bimston et al., 1998; Jaiswal et al., 2011; Olson et al., 1994)
4.	Hsp 90 (Human)	320 – 890	0.015 – 0.086	(McLaughlin et al., 2002; Owen et al., 2002)
5.	Hsp 104 (*S. cerevisiae*)	11000	70	(Grimminger et al., 2004)

Hsp 60s are also called chaperonins are large cylindrical oligomers consisting of two rings arranged back to back. Hsp 60 forms homo-oligomeric protein composed of 14 subunits that are arranged in two-stacked heptameric rings, thereby forming the barrel-like structure. Each ring contains a central cavity in which non-native proteins are encapsulated in an ATP-dependent manner for folding into the native state (Horwich et al., 2007). Chaperonins are divided into two groups. Group I chaperonins are mostly found in prokaryotes, mitochondria and plastids (e.g. *E. coli* GroEL) and group II chaperons are found in Archaea and eukaryotic cytosol (Mayer, 2010; Spiess et al., 2004). The *E. coli* GroEL chaperonin has been studied extensively. From the biochemical analysis it is clear that the ATP binding and hydrolysis affects the functional state of GroEL complex. The complexes have high affinity for their protein

substrate in the absence of nucleotide and in the presence of ADP but low affinity in the presence of ATP (Yifrach and Horovitz, 1995). Fig 2.10.2.1 explains the GroEL structure with ATP bound subunit.
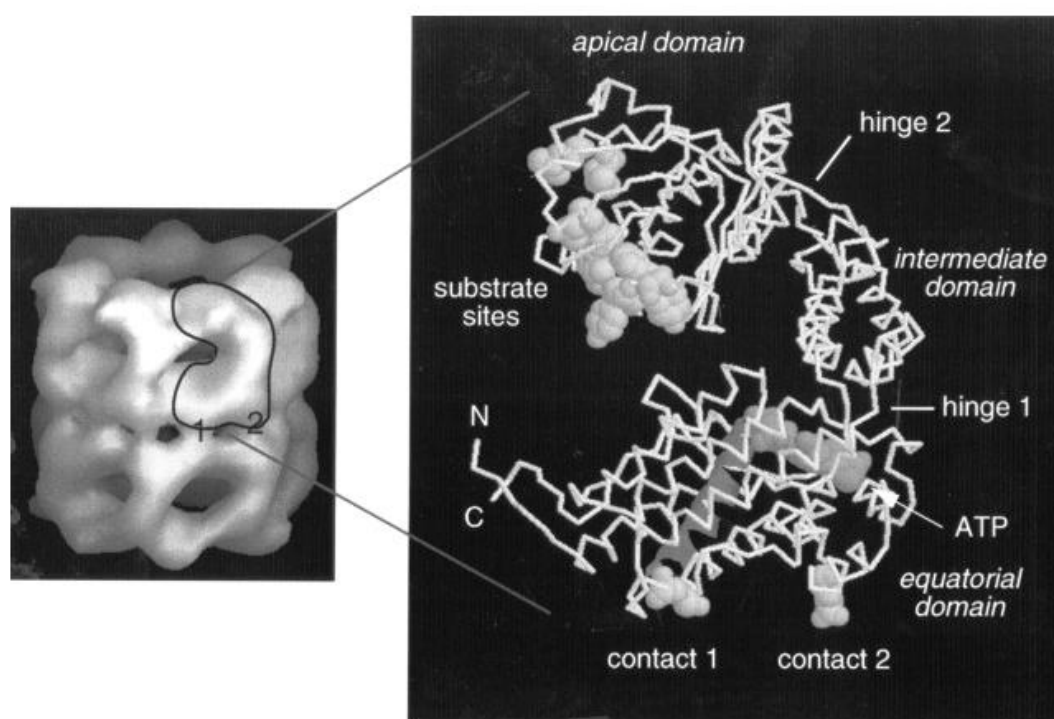
Fig. 2.10.2.1 GroEL Structure

Structure of the GroEL 14 mer with one subunit outlined (left) and expanded to show the polypeptide backbone (right) from the X-ray crystallographic results. The oligomer structure on the left was produced from the atomic structure, filtered to 25 Å resolution, and shown as a rendered surface. Two bridges of density, numbered 1 and 2, link each subunit to two others on the opposite heptameric ring. Right, each subunit contains three domains: equatorial, intermediate, and apical. The equatorial domain contains the interring contacts and the ATP binding site. A helical segment running between contact 1 and the ATP phosphates is shown as a ribbon. An exposed region of antiparallel polypeptide chains (hinge 1) forms the junction between equatorial

and intermediate domains. The small intermediate domain consists mainly of antiparallel α-helices coiled around each other and joins to the apical domain via a second exposed region (hinge 2). The apical domain contains the substrate-binding sites (shown in space-filling form), which coincide with most of the GroES binding sites (Roseman et al., 1996).

Residues 89-91 and Tyr 477 of GroES are ATP interacting residues and Glu 461 is important for maintaining contact with GroES. Mutation of Glu 461 interfere with GroES binding and also block polypeptide release (Fenton et al., 1994; Roseman et al., 1996).

Hsp70 chaperones are essential in all eukaryotes and assist a large number of protein folding processes, including *de novo* folding of polypeptides, refolding of misfolded proteins and solubilization of protein aggregates. These are also involved in the translocation of proteins across membranes, assembly and disassembly of oligomeric complexes. Hsp 70 also play an important role in regulation of stability and activity of certain natively folded proteins (Mayer and Bukau, 2005). Several new findings provide insights into the mechanistic diversity by which cofactors regulate Hsp70 functions. Nucleotide exchange factors (NEFs) are critical for the functional cycle of Hsp70s because they promote the release of ADP and rebinding of ATP that triggers unloading of bound substrate. Well-known NEFs are GrpE, which facilitates nucleotide dissociation from DnaK (Harrison et al., 1997; Sondermann et al., 2001). Hsp 70 consist of 44 kDa N-terminal ATPase domain (aa residue 1-386) consisting four domains forming two lobes with deep cleft between, middle 18 kDa peptide binding domain (aa residue 386-543) consisting of two antiparallel β sheets and a single α helix and C-terminal 10 kDa (aa residue 543-640) containing conserved

EEVD domain (Kiang and Tsokos, 1998). Isolated Hsp70 nucleotide binding domains and substrate-free Hsp70s exhibit low basal ATPase rates. Binding of protein substrate to the substrate binding stimulates this constitutively low ATPase rate several fold (Szabo et al., 1994). Intrinsic ATPase activity (V_{max}) of Hsp 70 is about 3 pmol/min/μg protein (Sadis and Hightower, 1992). C-terminal EEVD domain play an important role in regulating the ATPase activity of Hsp 70. Alteration or deletion of conserved EEVD domain of Hsp 70 affects its ATPase activity. Complete deletion of EEVD or complete (AAAA) or partial alanine substitution (AAVD) of these residue leads to severe loss in substrate binding but an enhanced ATPase activity. Effect of EEVD mutation on substrate reduced carboxymethylated lactalbumin (RCMLA) binding and ATPase activity is summarized in the following table (Freeman et al., 1995).

Table T2.10.2.2 Effect of EEVD mutation on substrate binding and ATPase activity of Hsp 70

Protein	% RCMLA bound	ATPase rate (pmol/min/μg)	
		Alone	+RCMLA
WT Hsp70	44 ± 4	2.94 ± 0.25	4.20 ± 0.16
ΔEEVD	3 ± 1	4.45 ± −0.36	7.29 ± 0.33
AEVD	32 ± 4	3.08 ± 0.12	4.77 ± 0.39
EEKD	33 ± 3	2.78 ± 0.23	3.92 ± 0.22
EAVD	24+ ±	2.74 ± 0.15	3.74 ± 0.22
EEAA	34 ± 3	1.93 ± 0.18	2.87 ± 0.26
AEVA	28 ± 3	2.31 ± 0.20	4.20 ± 0.57
AAVD	2 ± 1	7.53 ± 0.36	11.45 ± 0.92
AAAA	3 ± 1	7.21 ± 0.64	10.63 ± 0.84

Like Hsp 60s and Hsp 70s, Hsp 90s can bind to misfolded proteins and prevent their aggregation. Hsp90 proteins consist of three functional domains as the N-terminal NBD, the middle domain (MD), which is involved in ATP hydrolysis and

and co-chaperone binding and a C-terminal dimerization domain (DD). Hsp 90 is predominantly localized in the cytoplasm as a homodimer. Dimerization of Hsp 90 is essential for ATP hydrolysis (Richter et al., 2001). ATP hydrolysis and N-terminal dimerization are essential *in vivo* and were shown to accelerate client release (Young and Hartl, 2000). N-terminal NBD of Hsp 90 contains unusual adenine nucleotide binding pocket also known as Bergerat fold. This structural fold belongs to a GHKL superfamily and has no similarity with ATP binding domain found in kinases or chaperon Hsp 70. In eukaryote, a highly flexible, charged linker sequence connects N-terminal domain with that of middle domain. The structure of middle domain indicates that it has an important role in modulating ATP hydrolysis by interacting with the γ phosphate of ATP molecule bound to the NBD. Mutagenesis experiments also indicate that middle domain is also important for binding of many client proteins to Hsp 90. Fig. 2.10.2.2 shows the ADP/ATP interacting residues in NBD of Hsp 90.
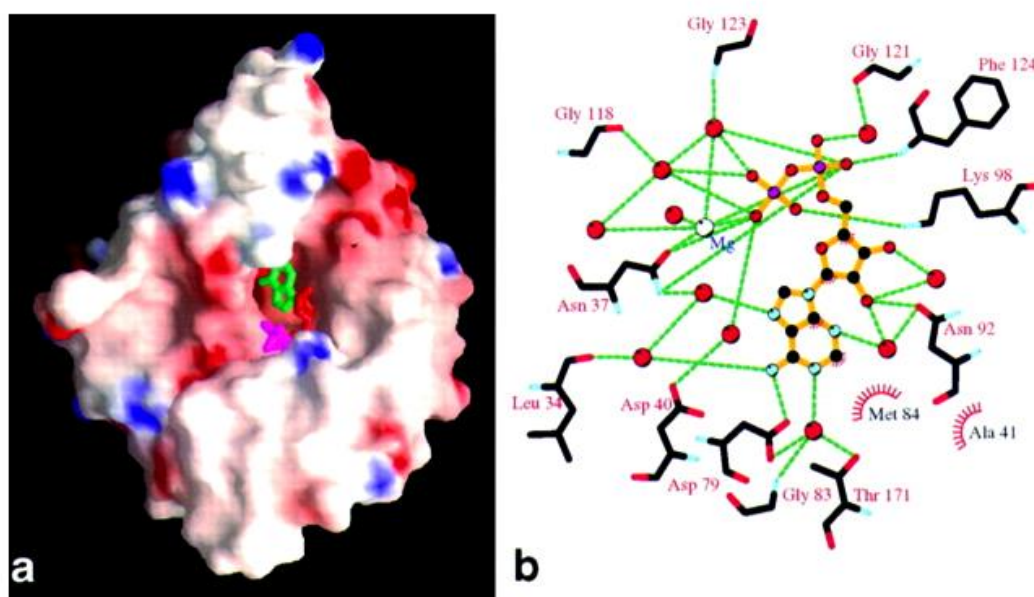
Fig. 2.10.2.2 ADP/ATP interacting residues in NBD of Hsp 90

(a) Overall view of ADP bound in the pocket on the helical face of the Hsp90 N-domain monomer. The solvent accessible protein surface is colored to reflect the electrostatic potential, going from negative (red) to positive (blue). The bound ADP molecule is colored. (b) Schematic diagram of ADP interactions. Hydrogen bonds are shown as dashed lines, van der Waals interactions are indicated by fur (Prodromou et al., 1997).

Hsp100 or Clp family of chaperones belongs to the superfamily of AAA+ domain-containing **A**TPases **a**ssociated with various cellular **a**ctivities. The AAA+ domain is characterized by the Walker A (e.g. 212GEPGIGKT219 in NBD1 and 614GLSGSGKT621 in NBD2 of Hsp 104), Walker B (e.g. 280VLFIDEI285 and 682 VLLFDEV687 of Hsp 104), sensor 1(e.g. T317 and N728 of Hsp 104) and sensor 2 (e.g. 824GAR826 of Hsp 104) sequence motifs (Bösl et al., 2006b). Most AAA+ proteins form oligomers with ATP bound close to the interface between subunits, and the neighboring subunit contributes the so-called arginine finger for ATP hydrolysis (Mayer, 2010). The first NBD is preceded by ~ 160 N-terminal residues which in *E. coli* has been reported to assist in substrate binding. Downstream of second NBD domain there is a short stretch of acidic residue which is missing in bacterial and mitochondrial homologue of Hsp 104. C-terminal residue of NBD2 and acidic residue take part in substrate binding. Poly L lysine stretch which is shown to stimulate the ATPase activity of Hsp 90 binds to this region. Hsp 104 assembles into a two tired ring shaped hexamer. Top view of Hsp 104 is ~ 15.5 nm wide and shows a central pore of ~ 2.5 nm diameter (Whitesell and Lindquist, 2005).

The presence of ATP or ADP shifts the oligomeric structure of Hsp 104 to hexameric form. When Lys 218 (Walker A) of NBD1 was mutated to Thr, it barely

affected the oligomerization but the corresponding mutation of Lys 620 to Thr resulted in decreased tendency of Hsp 104 to form hexamer (Schirmer et al., 1998). Lys 218 to Thr mutation inactivates the NBD1 whereas Lys 620 to Thr reduces the ATPase activity of Hsp 104 to ~ 25% compared to WT (Schirmer et al., 2001). It is to be noted that the NBD2 has high affinity for ATP but it accounts for lea that 1% of its ATPase activity. Asymmetric reconstructions of the EM images suggest that ATP binding and hydrolysis occur in a sequential manner in the NBD1 ring. The schematic representation of ATPase activity and chaperon function has been demonstrated in fig. 2.10.2.3.
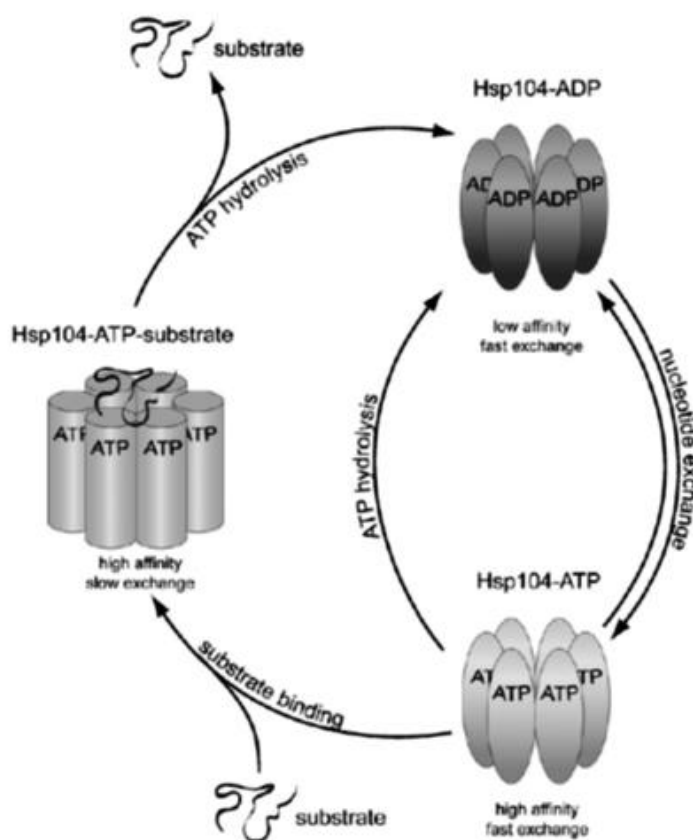
Fig. 2.10.2.3 The coupled substrate/nucleotide cycle of Hsp104

During steady-state ATP hydrolysis the molecular chaperone Hsp104 cycles between different conformational states: an ADP state with low affinity toward polypeptide substrates (top right) and an ATP state with high affinity toward polypeptides (bottom

right). Substrates exclusively bind to the high affinity form of the chaperone thereby generating a ternary Hsp104 ·ATP· substrate complex (left). Reduced nucleotide exchange dynamics of this complex suggests that substrate binding induces a conformational change within Hsp104. As a consequence, the ternary complex is committed to hydrolysis. This lock-in mechanism ensures that the energy provided by ATP hydrolysis can be efficiently used for substrate processing (Bösl et al., 2006).

The sequence analysis, structural and mutagenesis studies have revealed that these chaperons possess the characteristics feature of ATPases like nucleotide binding domain (like Walker A, Walker B). There may be proteins inside the living cell which may have altered nucleotide binding domain that differs from the classical one or they may not at all possess any characteristics of ATPase or chaperon. In the absence of such conserved domain or structure it will be very difficult to prove the role of unknown ATPases as in case of 14-3-3 proteins. In such cases, the molecular docking can be used as an alternative approach to predict the putative ATPase binding domain/residue. We have used the similar approach of molecular docking to predict the putative ATP binding pocket in 14-3-3ζ and verified the pocket by site directed mutagenesis and biochemical approach.

OBJECTIVES

OBJECTIVES:

With the above background, the objectives for the proposed topic are -

1. To verify whether the mammalian 14-3-3ζ has an ATPase activity and provide unequivocal evidence for ATP hydrolysis using purified recombinant 14-3-3ζ.

2. To identify the ATP binding pocket of 14-3-3ζ and the catalytic residues involved in hydrolysis.

3. To identify if this activity was structurally and functionally conserved in other 14-3-3 isoforms.

CHAPTER 3.

MATERIAL AND

METHODS

CHAPTER 3. MATERIAL AND METHODS:

3.1 Buffers and Reagents:

3.1.1 Luria-Bertani (LB) medium (for 1 L)

NaCl   10 g

Tryptone   10 g

Yeast extract   5 g

Deionized water (MQ) was added to a final volume of 1 litre and pH was adjusted to

7.0 with 1 M NaOH and autoclaved.

Or

25 g of LB powder (Merck) was dissolved in 1 L of MQ water and autoclaved.

3.1.2 LB-Ampicillin Agar Plates (for 1 L)

NaCl   10 g

Tryptone   10 g

Yeast extract   5 g

Agar   20 g

1. Deionized water was added to a final volume of 1 litre and pH was adjusted to 7.0
   with 10 N NaOH and autoclaved.

2. It was cooled to about 55 °C and 1 ml of 100 mg/ml ampicillin was added.

3. It was poured into Petri dishes (~25 ml/100 mm plate).

3.1.3 Super Optimal broth with Catabolite repression (SOC) Medium (for 1 L)

NaCl   0.5 g

Tryptone   20 g

Yeast extract   5 g

KCl   186.38 mg (2.5 mM)

      Deionized water was added to a final volume of 1 litre and pH was adjusted to

7.0 with NaOH. 5 ml sterile 2 M $MgCl_2$ (0.952gm, 10 mM) was added before use.

3.1.4 Tris-EDTA (TE) Buffer (for 50 ml)

Tris   60.66 mg (10 mM)

EDTA   14.62 (1 mM)

pH was adjusted to 8.0 with 10 N NaOH and autoclaved.

3.1.5 Ampicillin Stock

Stock concentration   : 100 mg/ml (Filter sterilized using 0.2 μm membrane)

Working concentration: 100 μg/ml

3.1.6 50X TAE Buffer (for 1 L)

Tris base   242 g

Glacial acetic acid   57.1

0.5 M EDTA (pH 8.0)   100 ml

      Prepare 1X TAE buffer for agarose gel electrophoresis.

3.1.7 6X Gel Loading Buffer for DNA (for 100 ml)

Xylene Cyanol FF   0.25 g (migrates at 4160 bp with TAE)

Bromophenol blue   0.25 g (migrates at 370 bp with TAE)

Glycerol   30 ml

3.1.8 Ethidium Bromide (EtBr)

Stock concentration   10 mg/ml (20000X)

Working concentration   0.5 μg/ml

3.1.9 Buffers for Ni NTA Column Purification and Gel Filtration:

3.1.9.1 Ni-NTA Lysis Buffer (for 1 L)

Tris	6.06 g (50 mM, pH 8.0)
NaCl	29.22 g (500 mM)
Imidazole	0.6 g (10 mM, reduces non-specific binding of proteins)
Glycerol	100 ml (10%)
TritonX-100	1 g (0.1%)
Protease inhibitor (10X)	1X
BME (14.3 M)	1.4 ml (20 mM)
Lysozyme	1 g (1 mg/ml)

3.1.9.2 Ni-NTA Binding/Washing Buffer (for 1 L)

Tris	6.06 g (50 mM, pH 8.0)
NaCl	29.22 g (500 mM)
Imidazole	0.6 g (10 mM, reduces non-specific binding of proteins)
Glycerol	100 ml (10%)
TritonX-100	1 g (0.1%)
Protease inhibitor (10X)	1X
BME (14.3 M)	1.4 ml (20 mM)

3.1.9.3 Ni-NTA Elution Buffer (for 1 L)

Tris	6.06 g (50 mM, pH 8.0)
NaCl	29.22 g (500 mM)
Imidazole	30.04 g (500 mM, for elution)
Glycerol	500 ml (10%)
TritonX-100	1 g (0.1%)
Protease inhibitor (10X)	1X
BME (14.3 M)	1.4 ml (20 mM)

3.1.9.4 Running Buffer for Gel Filtration (for 1 L)

Tris	6.06 g (50 mM, pH 7.5) or 25 ml of 2 M Tris pH 7.5
NaCl	17.53 g (300 mM) or 60 ml of 5 M NaCl
BME (14.3 M)	1.4 ml (20 mM)

3.1.10 Buffers and Dye for ATPase Reaction:

3.1.10.1 10X Reaction Buffer (RB) (for 1 ml)

HEPES (1 M, pH 7.5)	500 μl (500 mM)
$MgCl_2$ (1 M)	50 or 250 μl (50 mM or 250 mM)
DTT (1 M)	20 μl (20 mM)
MQ water (autoclaved)	430 or 230 μl

Note: 10X RB with 250 mM $MgCl_2$ was used for ADP Glo^{TM} Max Kinase assay.

3.1.10.2 Malachite Green Dye

A. Malachite Green	0.4 g (0.4%) in 100 ml MQ water
B. Ammonium Molybdate	4.2 g (4.2%) in 5 N 100 ml HCl
C. Poly Venyl Alcohol (PVA)	2 g (2%) in 100 ml water

For the preparation of working dye, add 3 parts of reagent A, 1 part of reagent B and 28 μl/ml (0.056%) of reagent C. Working dye was filtered with 0.45 μm filter membrane (Millipore) the working reagent.

3.1.10.3 TLC Plate Running Buffer (for 1 L)

KH_2PO_4 (Solution, pH 3.5) - 102.06 g (0.75 M, pH 3.5 adjusted with ortho-phosphoric acid).

3.1.10.4 Nitrocellulose Membrane Washing Buffer (for 100 ml)

HEPES (1 M, pH 7.5)   2 ml   (20 mM, pH 7.5)

$MgCl_2$ (1 M)   2.5 ml (25 mM)

MQ Water   95.5 ml

3.1.11 Other Reagents (for 100 ml)

2 M Tris   24.22 g (pH 7.5, adjust pH with concentrated HCl)

1 M HEPES   23.83 g (adjust pH with 1 M NaOH)

1 M $MgCl_2$ 9.52 g

1 M DTT   15.42 g

5 M NaCl   29.22 g

10 M NaOH   58.44 g

All the reagents were filtered with 0.22 μm filter membrane (Millipore).

3.2 Experimental Protocol:

3.2.1 Primer Reconstitution

1. All the primers used were obtained from Sigma.

2. Primers were obtained as a nucleic acid pellets in powder form (not visible with naked eyes).

3. Upon arrival the primer pellet was centrifuged at 10,000 rpm (Eppendorf centrifuge, Model - 5417C) for 1 min.

4. Primers were suspended in 10 mM Tris, pH 8.0 to obtain a stock concentration of 100 μM as per the manufacturer's instruction written on the primer tube.

5. 100 μM stock primers were allowed to suspend in 10 mM Tris, pH 8.0 on ice bath for about 1 hour with intermittent overtaxing after every 15 min.

6. Reconstituted primers were stored at - 20° C.

3.2.2 Determination of Nucleic Acid Concentration

The concentration of the nucleic acid in solution was estimated using a spectrophotometer (NanoDrop, Model - ND 1000). The absorbance of the solution was measured at 260 nm and concentration was calculated using the following formula:

$1 \ OD_{260} = 50$ μg/ml for double stranded DNA

$1 \ OD_{260} = 40$ μg/ml for RNA

3.2.3 PCR amplification

5X – reaction Buffer	10 μl
Template DNA	50 -100 ng
25 mM dNTP Mix	1 μl
MQ Water	Variable
Primer (Forward 10 μM)	1 μl
Primer (Reverse 10 μM)	1 μl
DNA polymerase	1 U
Reaction volume	50 μl

3.2.4 Thermal Cycling Steps

1. 95 °C for denaturation 5 min (for first step) then 1 min subsequent steps

2. 50-55 °C for primer annealing 1 min.

3. 72 °C for PCR extension 1-4 min (depending upon PCR product size)

4. 72 °C for final extension 10 min

5. Store at 4 °C

6. Extension time of 30 sec per Kb of PCR product amplification was used for high fidelity Fusion DNA polymerase (Thermo Scientific).

7. For site directed mutagenesis total 18 cycles were repeated without any final extension.

3.2.5 Restriction Digestion Reaction

10 buffer (Tango/FD/FD Green)	2X
DNA template	250-300 ng
Restriction enzyme	1 unit/ 1µl for FD enzymes
Autoclaved MQ water	variable
Final Reaction Volume	20 µl

Restriction reaction was carried out at 37° C for 1-4 hours.

3.2.6 Agarose Gel Electrophoresis of DNA

1. 0.8 − 1 % agarose in 1X TAE was heated to boil using microwave oven (MS-2342-AE, GE).

2. Agarose solution was allowed to cool to ~50-60 °C (5-10 min) and ethidium bromide (EtBr) was added to a final concentration of 0.5 µg/ml.

3. The solution was mixed thoroughly and poured in a gel casting tray with comb.

4. Gel was allowed to polymerize (20-30 min).

5. The samples were loaded along with the 1X DNA loading buffer.

6. The samples were allowed to run at 120 mA for 30-50 min.

7. The gel was then documented (UVP, Bioimaging Systems) and viewed using LaunchVision Works LS software.

3.2.7 Recovery of DNA from Low Melting Agarose Gel

1. 0.8% low melting agarose gel with ethidium bromide (0.5 μg/ml) was casted using 1X TAE buffer.

2. The samples were loaded with DNA gel loading buffer and allowed to run at 120 mA for 30-50 min.

3. The gel was then viewed under trans-illuminator and the band of interest was excised using a clean scalpel blade.

4. The agarose gel piece containing DNA was allowed to melt at 65°C and DNA was extracted using gel elution columns (Sigma).

5. In final step DNA was eluted in 20 μl of elution buffer.

3.2.8 Ligation/Cloning

2X rapid ligation buffer   - 10 μl

Vector   - 80 ng

Insert   - 30 – 40 ng

Ligase enzyme   - 1 U

Total volume   - 20 μl

Incubation temperature 22 °C 4-16 hours

Ligase enzyme was finally heat inactivated at 65 °C for 10 min.

3.2.9 Transformation

1. The ultra-competent cells were thawed on ice [*E. coli* DH5α or *E. coli* XL1 for mutagenesis and cloning and *E. coli* Bl 21 (DE3) for Protein expression].

2. 10 µl of the Ligation mixture was added to an aliquot of 100 µl ultra-competent cells

3. It was tapped gently and incubated in ice for 30 min.

4. The cells were heat shocked at 42°C for 90 sec and incubated in ice for 2 min.

5. 500 µl of SOC medium was added to the tube and kept for outgrowth at 37°C for 45 min with vigorous shaking (200-250 rpm).

6. The cells were centrifuged at 5000 rpm for 3 min.

7. The cells were suspended in 100 µl of the medium and plated on LB ampicillin (100 µg/ml) plates and incubated overnight (16 hours) at 37 °C.

3.2.10 Plasmid Mini Preparation

1. For the analysis of desired site directed mutagenesis or to select the desired clone, a single colony of bacteria was picked up with the help of autoclaved tooth pick and inoculated in 5 ml of LB medium containing 100 µg/ml of ampicillin.

2. The culture was allowed to grow overnight at 37 °C shaker incubator (Lab companion, Model – SIF6000R).

3. Bacteria were pelleted down by centrifugation at 5000 rpm (Plasto Craft, Model - Rota 4R).

4. Plasmid miniprep was done using miniprep spin columns (Sigma).

3.2.11 Plasmid Construction

1. 14-3-3ζ, γ, ε, and σ WT constructs were obtained as a gift from Dr. Sorab Dalal (ACTREC). *Drosophila* larvae cDNA was obtained from Dr. Girish Ratnaparkhi

2. For bacterial expression of 14-3-3, we cloned 14-3-3 isoforms in pRSET-A vector (Invitrogen) into BamHI – EcoRI sites.

3. 14-3-3τ was PCR amplified from cDNA obtained from HEK 293 RNA, cloned in pRSET-A vector (Invitrogen) into BamHI – EcoRI sites and confirmed by sequencing. The sequencing result matches with NCBI gene ID - 10971, symbol - YWHAQ.

3. In pRSETA-14-3-3ζ constructs, single amino acid mutation of each amino acid E17A, R18A, D20A, C25S, N42A, K49A, V51A, R55A, R56A, S57A, S57D, S57T, S58A, E89A, D92G, C94S, D96V, K120A, D124A, Y149A, F174A, C189S and S190A were created using site directed mutagenesis with the help of high fidelity DNA polymerase (Thermo Scientific).

4. For the generation of DR double mutant pRSET-A-ζD124A plasmid was used as a template and R55 residue was mutated to Ala. All mutations were confirmed by sequencing.

Table T3.2.12 List of Primers used for PCR and Site Directed Mutagenesis (SDM)

Sr. No.	Primers	Sequence 5′ - 3′
1.	D14-3-3ζ WT F	GGATCCATGTCGACAGTCGATAAGGA
2.	D14-3-3ζ WT R	GAATTCTTAGTTGTCGCCGCCCTCCT
3.	14-3-3τ WT F	GGATCCATGGAGAAGACTGAGCTGATC
4.	14-3-3τ WT R	GAATTCTTAGTTTTCAGCCCCTTCTGC
5.	ζE17A F	GAGCAGGCTGCGCGATATGAT
6.	ζE17A R	ATCATATCGCGCAGCCTGCTC
7.	ζR18A F	GAGCAGGCTGAGGCTTATGATGACATGGCAGC
8.	ζR18A R	GCTGCCATGTCATCATAAGCCTCAGCCTGCTC
9.	ζD20A F	GAGCGATATGCTGACATGGCA
10.	ζD20A R	TGCCAATGTCAGCATATCGCTC
11.	ζC25S F	CATGGCAGCCAGCATGAAGTCTGTAAC
12.	ζC25S R	GTTACAGACTTCATGCTGGCTGCCATG
13.	ζN42A F	AATGAGGAGAGGGCTGTTCTCTCAGTT
14.	ζN42A R	AACTGAGAGAACAGCCCTCTCCTCATT
15.	ζK49A F	TCAGTTGCTTATGCTAATGTTGTAGGA
16.	ζK49A R	TCCTACAACATTAGCATAAGCAACTGA
17.	ζV51G F	TATAAAAATGGTGTAGGAGCC
18.	ζV51G R	GGCTCCTACACCATTTTTATA
19.	ζR55A F	GTTGTAGGAGCCGCTAGGTCATCTTGG

76

20.	ζR55A R	CCAAGATGACCTAGCGGCTCCTACAAC
21.	ζR56A F	GGAGCCCGTGCGTCATCTTGG
22.	ζR56A R	CCAAGATGACGCACGGGCTCC
23.	ζS57A F	GCCCGTAGGGCATCTTGGAGG
24.	ζS57A R	CCTCCAAGATGCCCTACGGGC
25.	ζS58A F	CGTAGGTCAGATTGGAGGGTC
26.	ζS58A R	GACCCTCCAATCTGACCTACG
27.	ζE89A F	ATAGAGACCGCGCTAAGAGAT
28.	ζE89A R	ATCTCTTAGCTCGGTCTCTAT
29.	ζD92G F	GAGCTAAGAGGTATCTGCAAT
30.	ζD92G R	ATTGCAGATACCTCTTAGCTC
31.	ζC94S F	GCTAAGAGATATCAGCAATGATGTACTGTC
32.	ζC94S R	GACAGTACATCATTGCTGATATCTCTTAGC
33.	ζD96V F	ATCTGCAATGTTGTACTGTCT
34.	ζD96V R	AGACAGTACAACATTGCAGAT
35.	ζK120A F	GTCTCCTTTCATTGCCAAATAGAAG
36.	ζK120A R	CTTCTATTTGGCAATGAAAGGAGAC
37.	ζD124A F	TTGAAAATGAAAGGAGCCTACTACCGTTACTTG
38.	ζD124A R	CAAGTAACGGTAGTAGGCTCCTTTCATTTTCAA
39.	ζY149A F	CAGCAAGCAGCCCAAGAAGCT
40.	ζY149A R	AGCTTCTTGGGCTGCTTGCTG
41.	ζF174A F	GCCCTTAACGCCTCTGTGTTC
42.	ζF174A R	GAACACAGAGGCGTTAAGGGC

43.	ζC189S F	CTGAGAAAGCCAGCTCTCTTGCAAAG
44.	ζC189S R	CTTTGCAAGAGAGCTGGCTTTCTCAG
45.	ζS190A F	GAAAGCCTGCGCTCTTGCAAAG
46.	ζS190A R	CTTTGCAAGAGCGCAGGCTTTC
47.	γD129A F	GATGAAAGGGGCATACTACCGC
48.	γD129A R	GCGGTAGTATGCCCCTTTCATC

3.2.13 Confirmation of Positive Clones or Mutation

The positive clone or the desired mutation was confirmed by sequencing (3500 Genetic Analyzer, Applied Biosystem).

3.2.14 Preparation of Apocytochrome c

1. About 77 mg of cytochrome c were dissolved in 10 ml of water.

2. Two milliliters of glacial acetic acid and 15 ml of 0.8% silver sulfate solution were added to cytochrome c solution and the mixture was incubated in the dark for 4 hours at 45 °C.

3. The reaction mixture was then dialyzed against 0.2 M acetic acid to remove the excess silver sulfate.

4. The apoprotein was precipitated from the heme by addition of 10 volumes of cold acid acetone (1 ml of 5 N H_2SO_4 and 100 ml of acetone).

5. The precipitate was collected by centrifugation, washed several times with acid acetone, and then suspended in a small volume of about 1 ml of 0.2 M acetic acid.

6. Solid urea was added until a clear solution was obtained.

7. The bound silver was removed by reaction of the apoprotein with a 25 fold molar excess of 2-mercaptoethanol for 20 min at room temperature.

8. The silver free apoprotein solution was clarified by centrifugation and either dialyzed against Tris pH 7.5.

9. Apocytochrome c solution was further centrifuged at 15000 rpm for 30 min and stored at -20 ℃.

10. Aggregation of apocytochrome c was induced by heat treatment at 48 ℃ for 10 min.

3.2.15 Docking of ATP using Schrödinger software and Molecular Dynamic Simulation of the Bound Complex

1. The PDB ID: 2C1J which has no structure breakage in between (1-230) was used for ATP docking.

2. The protein structure was processed with the help of protein preparation wizard from Schrödinger software suite.

3. Bond orders were assigned, hydrogen atoms were added, water and peptide ligand (chains C, D-Histone H3 Acetylphosphopeptide) were removed and finally the structure was minimized using Optimized Potential for Liquid Simulations 2005 (OPLS 2005) forcefield.

4. To predict the binding site of ATP on the dimeric structure of 14-3-3, sitemap application from Schrödinger 2011 software suite, which predicts the protein-ligand, protein-protein interaction sites was used.

5. Top three sites which had high site score, size and volume were considered as binding sites for ATP.

6. Initially ATP was downloaded from pubchem (CID 5957) and different conformations were generated using LigPrep an application in Schrödinger for preparation 3D structures of ligands.

7. Three sitemaps from sitemap results were used to build three grid files and ATP was docked using Glide application.

8. Molecular dynamic simulation was performed using Desmond 2010 software package using standard procedure (Guo et al., 2010; Shivakumar et al., 2010).

9. The protein structure was solvated by using TIP3P water model with periodic boundary conditions in an orthorhombic box covering 10 Å distance from the protein edges.

10. The system was then neutralized by replacing water molecules with sodium and chloride counter ions.

11. Optimized Potentials for Liquid Simulations (OPLS-2001) all-atom force field was used. The particle-mesh Ewald method (PME) was used to calculate long-range electrostatic interactions.

12. Short range electrostatic interactions were handled by Cutoff method at 9.0 Å radius.

13. Nose–Hoover thermostats were used to maintain the constant temperature and the Martina–Tobias–Klein method was used to control the pressure. A time step of 2 femtoseconds was used.

14. The prepared system was equilibrated and simulated with the default protocol provided in Desmond that comprises a series of restrained minimizations and molecular dynamics simulations.

15. Finally 5 nanoseconds NPT production simulation was run at 300 K temperature and 1 atmosphere pressure.

16. We could observe ATP binding in two distinct pockets one at amphipathic groove (phosphopeptide binding pocket) and other at dimer interface.

17. Based on the docking results, we marked the residues within 5 Å range as mentioned below.

Table T3.2.15.1 List of putative ATP binding/hydrolyzing residue near phosphopeptide binding pocket and dimer interface of 14-3-3ζ

Residues at Pocket 1 (Phosphopeptide binding)	Residues at Pocket 2 (Dimer interface)
1. N42	1. E17
2. K49	2. R18
3. R56	3. D20
4. K120	4. D21
5. D124	5. C25
6. Y149	6. V51
7. F174	7. R55
8. C189	8. S57
9. S190	9. S58
	10. E89
	11. D92
	12. C94
	13. D96

3.2.16 Protein Expression

1. All proteins were expressed and purified by using *Escherichia coli* BL21 (DE3) strain.

2. A single, transformed, isolated colony of *E. coli* BL 21 (DE3) was inoculated in 10 ml LB medium and grown overnight at 37° C with vigorous shaking (200-250 rpm).

3. 10 ml inoculum was made in 1000 ml LB broth and allowed to reach 0.8 $O.D._{600}$ (Biophotometer, Eppendorf).

4. Protein was induced with 100 μM isopropyl-D-thiogalactoside (IPTG) and growth was continued at 24°C for 16 hours.

5. Cells were lysed by sonication in lysis buffer (50 mM Tris (pH 7.5), 20 mM β-mercaptoethanol (BME), 500 mM NaCl, 10% glycerol, 0.1% Triton X-100) with protease inhibitor cocktail (Sigma).

6. The culture was transferred into HS50 tubes (Tarson) and centrifuged at 15000 rpm for 30 min at 4° C using SS-34 rotor in Sorvall RC5C Plus centrifuge.

7. Supernatant containing soluble protein was used for further purification.

6. Individual protein was purified by nickel-nitriloacetic acid (Ni-NTA) agarose affinity chromatography (Invitrogen).

3.2.17 Cell Density Measurement

The O.D. was measured at 600 nm with LB medium as blank using with the help of Biophotometer (Eppendorf).

3.2.18 Ni-NTA Agarose Affinity Chromatography

1. 1-2 ml of Ni –NTA agarose beads from Invitrogen was liquated in 1 X 30 cm econo column (Bio-Rad).

2. Beads were washed with 1X washing/equilibration buffer with at least two column volumes under native conditions.

3. Equilibrated Ni-NTA beads were incubated with protein lysate at 4 °C for about 30 min.

4. After incubation unbound lysate (flow through) were collected separately.

5. Beads were washed with washing buffer with 2-3 column volume.

6. 6X His tagged protein was eluted with elution buffer containing imidazole (500 mM).

3.2.19 Cleavage of His Tag

1. Protein eluted from Ni-NTA agarose beads was dialyzed against tris buffer pH 7.5.

2. 6X His tag was cleaved in the presence of 2 mM $CaCl_2$ either with enterokinase (0.02 U/mg protein, Sigma) or with Tev protease (Invitrogen) for overnight at room temperature.

3. After cleavage, 6X his tag was removed by Ni-NTA affinity and the protein fraction was further subjected for gel filtration chromatography.

3.2.20 Gel Filtration Chromatography

1. For the removal of enterokinase or Tev protease and further purification of protein, it was subjected for gel filtration chromatography using sephadex G-75 beads (GE Healthcare Life Sciences).

2. Initially the gel filtration column was equilibrated with gel filtration running buffer with the flow rate of 0.5 ml/min using HPLC system (Bio-Rad).

3. 2 ml of total protein volume injected in the gel filtration column and eluted under native conditions.

4. Peak fraction were collected either separately or pulled together, dialyzed against Tris buffer pH 7.5 and used for further experiments.

5. All the proteins were stored at – 20 °C.

3.2.21 Protein Estimation using Bradford Assay

1. BSA standards (1, 0.5, 0.25, and 0.125 mg/ml) were prepared from 20 mg/ml of BSA stock.

2. Unknowns (protein samples) were taken in various dilutions. 5 μl of the standards and the unknowns were taken in duplicates in a 96-well plate.

3. 200 μl of Bradford reagent (1:4 diluted, Bio-Rad) was added.

4. Readings were taken with ELISA plate reader (Spectra Max 790) at 595 nm using SoftMaxPro 4.6 software.

5. Protein concentration for unknown was determined with the help of standard graph generated with BSA.

3.2.22 SDS PAGE

1. Protein samples were boiled using digital dry bath (JENCON-PLS) at 100 °C with 1X Laemmli buffer for 10 min before loading.

2. The samples were loaded to the gel placed in the tank containing 1X SDS-PAGE running buffer.

3. The gel was run at 120 V for 1:30 hours.

4. The gel was stained with coomassie brilliant blue R (Sigma) for 15-30 min.

5. The gel was then destained overnight in the destainer with 2-3 changes at regular interval.

6. The gel was finally preserved in 10 % acetic acid and documented.

3.2.23 Native PAGE

1. Protein samples were prepared in native PAGE loading dye without detergent or boiling.

2. Samples were loaded in 7.5% native PAGE.

3. The native PAGE was run at 100 V in cold room.

4. Do not allow the front dye to run out. It runs close to 20 kDa.

5. The gel was stained in coomassie brilliant blue and destained as mentioned above.

6. The gel was preserved in 10 % acetic acid and documented.

3.2.24 Preparation of Glycerol Stocks

1. 100 µl of the overnight culture was transferred into a autoclaved 1.7 ml microfuge tube (Axygen).

2. 100 µl of 30% glycerol (autoclaved) was added to the tube and gently mixed.

3. When the solution was homogenous, the samples were snap-freezed in liquid nitrogen.

4. The glycerol stocks were stored at -80°C.

3.2.25 Mass Spectrometry (MS) analysis of 14-3-3ζ WT

1. 14-3-3ζ WT protein was resolved on 12% SDS PAGE.

2. Protein was in gel digested with 10 ng/ml of trypsin (MS grade, Sigma) in 25 mM ammonium bicarbonate in water and peptides were recovered by extraction with 50% acetonitrile (ACN) and 5% trifluoroacetic acid (TFA).

3. Tryptic peptide digests were reconstituted in 0.1% TFA solution containing 10% ACN.

4. Aliquotes were mixed with matrix (alpha-cyano-4-hydroxycinnamic acid, Bruker Daltonics) and spotted on MTP 384 ground steel plate (Bruker Daltonics).

5. Mass spectra were acquired using MALDI-TOF/TOF Ultraflex instrument (Bruker Daltonics, Germany).

6. The resulting MS data was analyzed using Flex analysis 3.0 software (Bruker Daltonics).

7. The MS peak list were searched against SwissProt database version_2010_08.fasta using MASCOT search engine 2.3.01.02 with mass tolerance of 100 ppm with one allowed missed cleavage.

8. MS spectra searches were allowed for carbamidomethylation of cysteine as fixed modification and methionine oxidation as variable modification.

9. The individual spectrum was subjected to the default threshold score of $p < 0.05$.

3.2.26 Nano-LC-MS^E analysis of 14-3-3ζ WT

1. LC-MS^E analysis was performed as described earlier (Silva et al., 2006). 400 ng of trypsin digested peptides after reconstituting in 3% acetonitrile were injected into nano LC-MS/MS system (Synapt-HDMS, Waters Corporation).

2. The peptides were separated by using BEH-C18 reversed phase column (1.7 µm x 75 µm x 250 mm, Waters Corporation).

3. The binary solvent system used comprised 99.9% water and 0.1% formic acid (mobile phase A) and 99.9% acetonitrile and 0.1% formic acid (mobile phase B).

4. Peptides were initially preconcentrated and desalted online at a flow rate of 5 µl/min using a Symmetry C18 trapping column (internal diameter 180 µm, length 20 mm) (Waters Corporation) with a 0.1% B.

5. After each injection, peptides were eluted into the NanoLockSpray ion source at a flow rate of 300 nl/min using a gradient of 2–40% B for 90 min, then the column was washed and equilibrated. All mass spectrometric analysis was performed in a positive V-mode at a resolution of about 10000 full width half maximum (FWHM).

6. The external calibration standard [(GLU1)]-FibrinopeptideB, 50 fmol) was constantly infused by the NanoACQUITY auxiliary pump at a constant flow rate of 250 nl/min at an interval of 20 seconds.

7. The eluted peptide spectra were acquired by Synapt–HDMS (Q-TOF) with the following parameters.

8. Sample was analyzed in a positive V mode in a mass range of 50-2000 m/z with a scan time of 0.7 seconds.

9. The on-line eluted peptides were analyzed at both low collision energy (4 eV) and high collision energy (15-40 eV).

3.2.27 Western blotting

1. For western blotting, purified 14-3-3ζ WT, R55A and D124A mutant proteins (His tag cleaved and uncleaved) were resolved on 12% SDS PAGE.

2. Proteins were transferred on polyvinylidene difluoride (PVDF) membrane (Hybond, GE Healthcare).

3. PVDF membrane was blocked with 3% BSA in TBST at room temperature for 1 hour on rocker.

3. PVDF membrane was incubated with 1:2000 dilution of anti 14-3-3ζ antibody (rabbit polyclonal, Santa Cruz Biotechnology) or anti His antibody (mouse monoclonal, Cell Signaling) for 1 hour at room temperature on rocker. Antibodies were diluted in TBST (TBST - 50 mM Tris, 150 mM NaCl, 0.1% Tween 20) containing 3% BSA.

4. Now, primary antibody was removed and membrane was washed with TBST at least four times, 15 min each time at room temperature on rocker.

5. PVDF membrane was incubated with corresponding secondary antibody (1:5000 dilution; Sigma) at room temperature for 1 hour on rocker.

6. Secondary antibody was removed and membrane was washed with TBST at least four times, 15 min each time on rocker at room temperature.

7. PVDF membrane was incubated with ECL plus reagent (GE Healthcare).

8. Membrane was exposed to X-ray film (Kodak) and was developed using automated developer machine (Optimax 2010, Protec GmBH & Co.).

9. Developed X-rays was analyzed for the corresponding western blotting.

3.2.28 ATPase Assay:

3.2.25.1 ATPase Assay using Malachite Green assay mixture

1. 7 μM of protein (calculated for dimeric protein) was incubated with 1mM of ATP or ATP-γ-S or AMP-PCP (Sigma) at 37°C in reaction buffer (20 mM HEPES buffer pH 7.5, 5 mM $MgCl_2$ and 2 mM DTT)

2. The reaction volume in each case was 50 μl.

3. Release of inorganic phosphate (Pi) was monitored at different time points as described by Ames 1966 with some modifications.

4. 200 μl of assay mixture (3 part of 0.4% malachite green, 1 part 4.2% ammonium molybdate made in 5 N HCl, 0.056% polyvinyl alcohol) was added to 50 μl reaction volume.

5. The mixture was allowed to incubate for 10 min at room temperature and read at 630 nm (Spectra Max 190, Molecular Devices) with appropriate blank.

6. Amount of phosphate formed was estimated with the help of standards generated using KH_2PO_4.

3.2.28.2 ATPase Assay using radiolabeled (γ-^{32}P) ATP (PerkinElmer)

1. ATPase activity using radiolabeled ATP was performed with or without 7 μM of protein using 10 μCi (3000 Ci/mmol) of hot (γ-^{32}P) ATP (PerkinElmer) acting as a tracer in reaction buffer (mentioned above) containing 100 μM of cold ATP (Sigma).

2. Total reaction volume was 25 μl.

3. Reaction mixture was incubated at 37 °C for indicated time points (e.g. 0, 0.25, 0.5, 1, 2, 3 hours).

4. Reaction was stopped by spotting 2 µl of sample on *poly(ethylene)imine cellulose* thin layer chromatographic *(*PEI-TLC) plates (Fluka), which was developed with 0.75 M KH_2PO_4 (pH 3.5).

5. Plate was dried after developing and exposed to X-ray film (Kodak) to monitor inorganic phosphate (Pi) release.

6. The experiment was repeated at least two times with two independent protein preparations.

7. All radioactive experiments were performed according to standard institutional guidelines.

3.2.28.3 ATPase Assay using ADP Glo^TM Max ATPase Assay (Promega)

1. ATPase assay using ADP-Glo^TM max ATPase assay kit (Promega) was performed as per manufacturer's instructions with 5 µl reaction volume.

2. ATPase reaction was performed in reaction buffer as explained above at 37 °C.

3. After ATPase reaction, ADP-Glo^TM reagent was added to terminate the enzymatic reaction and deplete the remaining ATP.

4. The mixture was incubated at room temperature for 40 min.

5. After incubation, ADP-Glo^TM max detection reagent was added to convert ADP to ATP.

6. Again the mixture was incubated at room temperature for 1 hour and luminescence was recorded using multimode microplate reader (Mitras LB 940, Berthold Technologies).

7. Total amount of ATP hydrolyzed was calculated with the help of standard graph generated with ADP standards.

3.2.29 ATP binding assay:

3.2.29.1 Filter Trap ATP Binding Assay

1. 7 μM of protein was incubated with 20 μCi (3000 Ci/mmol) of hot (γ-^{32}P) ATP (PerkinElmer) with appropriate control (without protein) in reaction buffer (mentioned above) at 4 °C for 1 hour.

2. The total reaction volume was 25 μl. After incubation, 2 μl of reaction mixture was spotted on nitrocellulose membrane and allowed to dry for 10-15 minutes.

3. The nitrocellulose membrane was washed with washing buffer (20 mM HEPES, pH 7.5, 5 mM MgCl$_2$) and exposed to X-ray film (Kodak) to monitor binding.

4. Hsp 70 (2.86 μM) was used as a positive control.

5. All radioactive experiments were performed according to standard institutional guidelines.

3.2.29.2 ATP Binding Assay Using Desalting Spin Column

1. 7 μM of protein was incubated with 20 μCi (3000 Ci/mmol) of hot (γ-^{32}P) ATP (PerkinElmer) with appropriate control (without protein) in reaction buffer (mentioned above) at 4 °C for 1 hour.

2. The total reaction volume was 25 μl.

3. After incubation, 2 μl of reaction mixture was mixed in 135 μl of ATP binding buffer (20 mM HEPES pH7.5, 25 mM MgCl$_2$) passed through Zeba^{TM} desalting spin column (Pierce) according to the manufacturer's instruction.

4. ATP bound protein was separated from free ATP using desalting column by centrifugation at 5000 rpm.

5. Radiolabeled (γ-^{32}P) ATP (from control reaction) was eluted from desalting column with ATP binding buffer and the radioactivity was counted using liquid scintillation counter (Tri-Carb$^{®}$ 2810 TR, PerkinElmer).

6. The percentage of ATP bound of the total (γ-^{32}P) ATP is plotted for each protein.

7. All radioactive experiments were performed according to standard institutional guidelines.

3.2.30 ELISA for Peptide Binding

1. ELISA plate (Nunc) was coated with the 100 μl of 14-3-3ζ WT (2 μg/ml).

2. The plates were rinsed with TBST (TBST - 50 mM Tris, 150 mM NaCl, 0.1% Tween 20) and then incubated with blocking solution (3% BSA in TBST) for 60 min at 37 °C followed by incubation with 100 μM biotin conjugated phosphopeptides P1 or P2 or P3 for 60 min at 37 °C in 0.1% BSA in TBST.

3. The wells were rinsed thrice with TBST and then incubated with streptavidin conjugated alkaline phosphatase (Sigma).

4. Plate was incubated at 37 °C for 60 min, wells were rinsed thrice with TBST, pNPP substrate was added (GeNei) according to manufacturer's instruction and finally read at 405 nm.

Note: P1-RLYHpSLP, P2-QSYpTV and P3-ARKpTG where pS and pT represents phospho-serine and phospho-threonine respectively.

3.2.31 Computational Analysis of Binding Energy and Experimental Constraints Converge on One Putative Binding Site

1. ATP was blind docked separately into monomer and dimer structures of 14-3-3ζ (PDB ID: 2C1J) using VlifeMDS software.

2. Top 10 poses based on PLP score were selected for carrying out the binding energy (BE) calculations (mentioned in Table T8.1) (Gehlhaar et al., 1995).

3. The binding energy for each pose is calculated using the following formula:

$$E_{bind} = E_{complex} - (E_{protein} + E_{ligand}).$$

4. This is represented in units of kcal/mole. Specified mutations R55A and D124A were carried out on the protein using VlifeMDS software.

5. After optimization of the mutated proteins, top ten scoring docked poses of ATP were used in the mutant structures for calculating binding energies.

6. These same top ten scoring poses had earlier been used for calculating binding energy in 14-3-3ζ WT protein. The pose that satisfied the experimental observation was selected as the final pose (pose 4 in Table T8.1).

3.2.32 Single turnover ATPase assay

1. Single turnover ATPase assay was performed as previously described (Goswami et al., 2010). Briefly, 100 μg of proteins (14-3-3ζ WT, 14-3-3σ WT, R55A, D124A) were independently incubated with radioactive 50 μCi of hot (γ-^{32}P) ATP [4000 Ci/mmol, Board of radiation and isotope technology (BRIT), India] in RB (100 μl) at 4 °C for 30 min.

2. ATP bound protein complex was separated by 2 ml desalting column (Merck) using cold buffer and snap frozen using liquid nitrogen and stored at -80 °C.

3. Protein bound ATP complex was subjected for the ATPase assay at 37 °C.

4. The reaction was stopped using stop solution (2 M LiCl, 4 M formic acid and 36 μM ATP) and spotted on *poly(ethylene)imine cellulose* thin layer chromatographic *(*PEI-TLC) plates (Macherey-Nagel) and developed with 1:1,v/v mixture of 1 LiCl and 2 M formic acid.

5. Plates were dried, scanned using phosphorimager and quantified using Multi Gauge software 3.0 (FujiFilm). All radioactive experiments were performed according to standard institutional guidelines.

CHAPTER 4.
IDENTIFICATION OF
INTRINSIC ATPase
ACTIVITY IN 14-3-3ζ WT

CHAPTER 4. IDENTIFICATION OF INTRINSIC ATPase ACTIVITY IN 14-3-3ζ WT

4.1 Introduction:

14-3-3 proteins (β, γ, ε, η, σ, τ and ζ isoforms) are an important family of highly conserved dimeric proteins that bind to Ser/Thr phosphorylated proteins through two major consensus motifs, designed as mode I (RSXpSXP) and mode II (RXY/FXpSXP), where pS represents phospho-serine (Gardino and Yaffe, 2011; Yaffe et al., 1997b; Zhao et al., 2011). A third minor binding signature designed as mode III [pS/pT(X 1–2)-COOH] has also been identified, where pT represent phospho-threonine (Ganguly et al., 2005). These proteins are involved in myriad of activities like metabolism, signal transduction, cell cycle control, apoptosis, protein trafficking, transcription and stress response (Aitken, 2011; Dalal et al., 2004; Hosing et al., 2008; Telles et al., 2009). They are also known to be responsible for malignant transformation. These functions have been attributed primarily to their ability to bind to phosphorylated sequences within the client proteins.(Forrest and Gabrielli, 2001; Gardino et al., 2006; Muslin et al., 1996; Obsil et al., 2001) In 1990s, in addition to these well-known adaptor functions, one of the isoforms, 14-3-3τ was shown to possess an ATP/ADP exchange activity (Yano et al., 1997).The mitochondrial import function of rat liver cytosolic 14-3-3 seemed to require energy from ATP hydrolysis (Hachiya et al., 1994; Komiya and Mihara, 1996; Komiya et al., 1996). These observations caught our attention as this activity of 14-3-3 did not seem to be the major focus in research and any enzymatic activity of 14-3-3 has remained controversial (Aitken, 2006). Of late *Drosophila* 14-3-3ζ in conjunction with Hsp70 was shown to solubilize aggregated proteins in an ATP dependent manner although whether this function is dependent on energy from ATP hydrolysis has not been demonstrated so far (Yano et al., 2006). This disaggregating function seems

analogous to yeast Hsp104 which is probably the only other chaperone well known to solubilize preformed aggregates. No such activity has been identified in any mammalian proteins and the role of 14-3-3ζ in the aggregation of proteins like tau and huntingtin is unclear (Berg et al., 2003; Omi et al., 2008; Sluchanko and Gusev, 2011). Besides this the information on the structural basis for this enzymatic activity is unclear.

With this background, we asked if human 14-3-3ζ has any detectable ATPase activity and whether we could identify the residues involved in this process. If so identifying residues involved in ATP binding/hydrolysis is likely to better define the enzymatic property associated with the 14-3-3 protein which is otherwise well known for its scaffold and chaperone-like functions.

There are many established methods to perform ATPase assays. The classical colorimetric ATPase assay using malachite green assay buffer is the oldest one. The Pi released during ATPase reaction react with the malachite green and form co-ordinate colored complex which has the absorption maxima near 600-650 nm (Ames, 1966). This colorimetric assay has many limitations; the first is of sensitivity issue and second is that it doesn't have good control over background coming through ADP or Pi contamination in pure ATP. We can measure the Pi released in the range of 0.5 - 10 nmol. On the other hand radiolabeled ATPase assay which involves the use of α-^{32}P or γ-^{32}p labeled ATP is the most sensitive method. One can measure Pi released in pmol range. The major drawback of this method is that it involves radioactive ATP which is potentially hazardous and mishandling may even cause serious disease like cancer. The highly sensitive and nonhazardous method will be of preference over earlier two discussed methods. Fluorescence and luminescence based ATPase methods are the best suitable as they are time saving and does not involve the use of

any hazardous chemicals. Depending on the need and the compatibility of enzymes (kinases or ATPases) there are various principles are being utilized to monitor the ATP hydrolysis; one of such method measures the decrease in the initial fluorescence polarization due to presence of ADP formed during ATP hydrolysis (Transcreener ADP2 FP assay by BellBrook Labs). The detection mixture added after the ATPase/kinase reaction is over contains 4 nM ADP Alexa633 and ADP^2 antibody (2* EC). More the ADP formed more will be decrease in fluorescence polarization which can be estimated from standards (Fig 4.1)
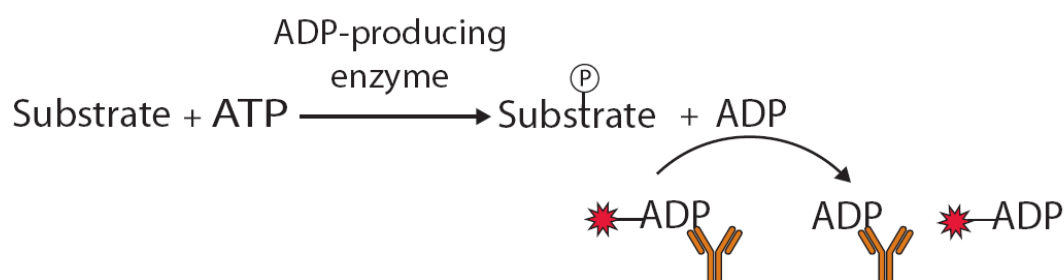
Fig.4.1 Principle of characterization of ATPase assay using transcreener ADP2 FP assay

The ADP-Glo^{TM} max assay (Promega) can be used to monitor the activity of virtually any ADP-generating enzyme (e.g., kinase or ATPase) when higher ATP concentration is required (up to 5mM). The ADP-Glo™ max assay is performed in a multiwell plate and can detect kinase or ATPase activity in a reaction volume as low as 5 µl. The assay is performed in two steps: first, after the completion of the ADP-producing reaction, an equal volume of ADP-Glo™ reagent is added to terminate the reaction and deplete the remaining ATP. Second, the ADP-Glo™ max detection reagent is added to simultaneously convert ADP to ATP, and the latter is converted to light using a luciferase/luciferin reaction (Fig. 4.2).
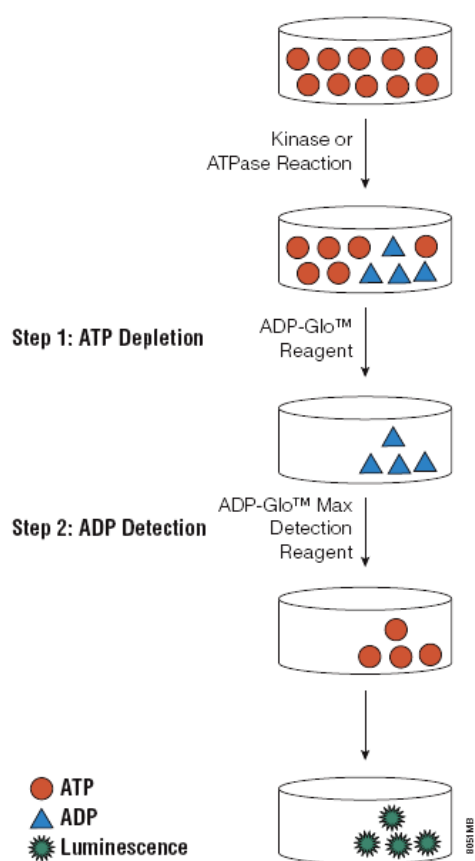
Fig. 4.2. Principle of the ADP-Glo™ max assay

The assay is performed in two steps: 1) after the kinase or ATPase reaction, ADP-Glo™ reagent is added to terminate the enzymatic reaction and to deplete the remaining ATP, and 2) the ADP-Glo™ max detection reagent is added to convert ADP to ATP and allow the newly synthesized ATP to be measured using a luciferase/luciferin reaction.

We have used three different ATPase methods to verify ATPase activity of 14-3-3 proteins viz. colorimetric assay using malachite green, radiolabeled assay using $(\gamma\text{-}^{32}P)$ ATP and ADP-Glo^{TM} max assay (Promega).

4.2 Results and Discussion:

We cloned the 14-3-3ζ WT isoform (a kind gift from Dr. Sorab Dalal, ACTREC) in a 6X His tagged, prokaryotic inducible pRSET-A vector (Invitrogen). The protein was induced in *E. coli* BL 21 (DE3) and purified on Ni-NTA affinity chromatography (Invitrogen). The 6X His tag was removed by the treatment with enterokinase (Sigma) and purified further by gel filtration. Protein identity was confirmed with mass spectrometry (Fig. 4.3 and Table T4.1) and western blotting (Fig. 4.4). Furthermore we performed nano LC-MS^E analysis of purified 14-3-3ζ WT (Table T4.2). Nano LC-MS^E analysis reveals 89.39% sequence coverage with no *E. coli* protein was detected (Table T4.2). Three other identifications also belong to 14-3-3 proteins (Table T4.2). Two other proteins identified are very different from 14-3-3ζ in molecular weight and are undetectable by standard techniques. Considering 14-3-3ζ used here is a recombinant protein with high sequence coverage other identifications are false positive and very low sequence coverage (10-13%), these identifications of two other proteins (TAT_HV1SC; MW 8.3 kDa and ARI4B_Human; MW 137.5 kDa) are clearly false positive identifications.
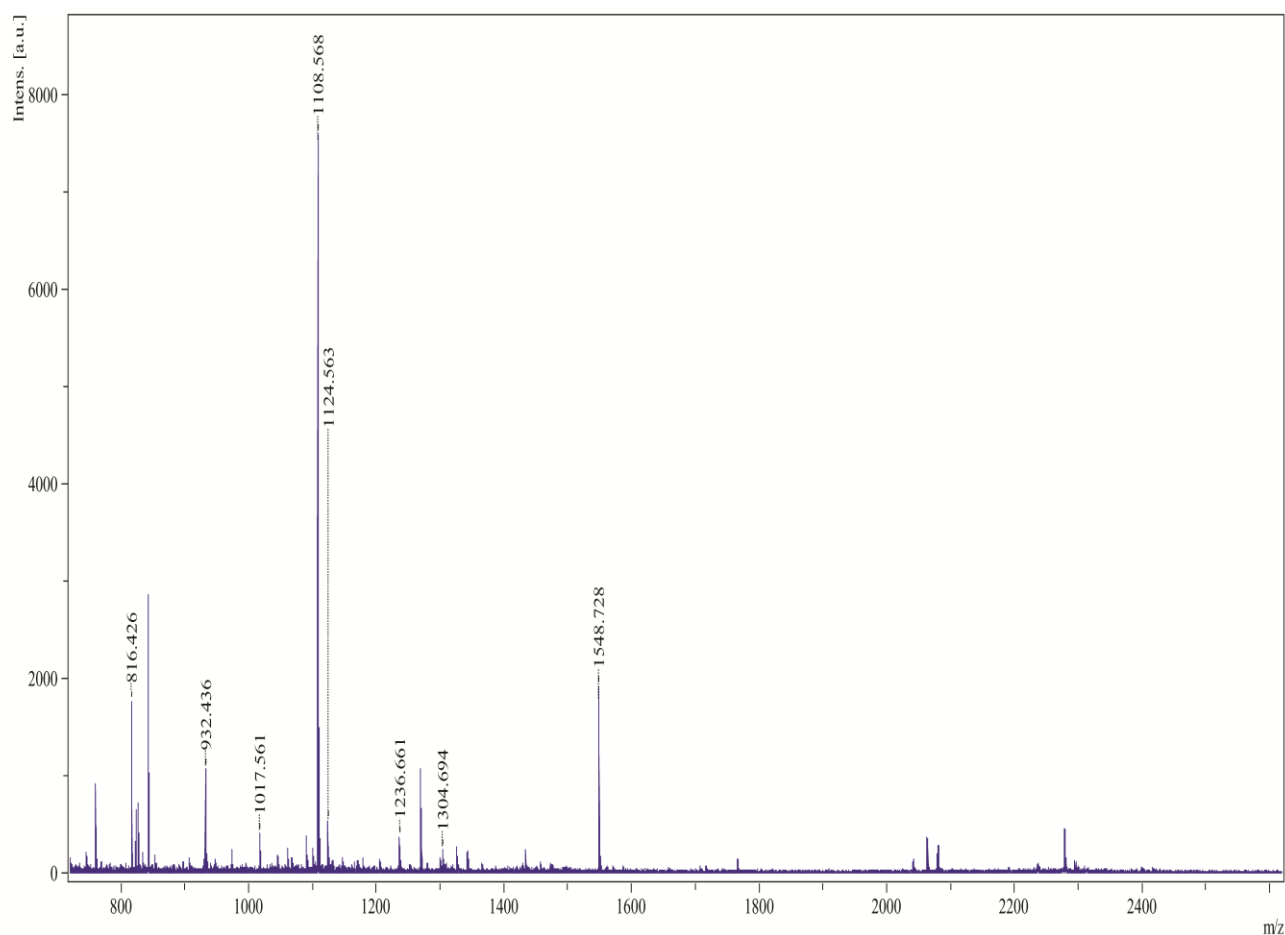
Fig. 4.3 MALDI TOF analysis of 14-3-3ζ WT

14-3-3ζ_HUMAN **Mass:** 27899 **Score: 76 Expect:** 0.00056 **Matches:** 8

14-3-3 protein zeta/delta Organism = Homo sapiens Gene Name = YWHAZ

Number of mass values searched: **17**

Number of mass values matched: **8**

Sequence Coverage: **23%**

Matched peptides in 14-3-3 protein (Total 245 amino acid long) are shown in **Bold:**

1 MDKNELVQKA K**LAEQAER**YD DMAACMK**SVT EQGAELSNEE**

RNLLSVAYKN

51 VVGARRSSWR VVSSIEQKTE GAEKKQQMAR

EYR**EKIETELR**DICNDVLSL

101 LEK**FLIPNAS QAESKVFYLK MKGDYYR**YLA EVAAGDDKKG

IVDQSQQAYQ

151 EAFEISK**KEM QPTHPIR**LGL ALNFSVFYYE ILNSPEKACSLAKTAFDEAI

201 AELDTLSEES YKDSTLIMQL LRDNLTLWTS DTQGDEAEAG EGGEN

Table T4.1 Peptides of 14-3-3ζ identified in MS analysis

Start – End	MW (Da) Observed	MW (Da) (expected)	MW (Da) (calculated)	ppm	Miss	Sequence
12 – 18	816.4257	815.4184	815.4137	6	0	K.LAEQAER.Y
28 – 41	1548.7284	1547.7212	1547.7063	10	0	K.SVTEQGAELSNEER.N
84 – 91	1017.5612	1016.554	1016.5502	4	1	R.EKIETELR.D
104 – 115	1304.694	1303.6867	1303.6772	7	0	K.FLIPNASQAESK.V
121 – 127	932.4362	931.4289	931.4222	7	1	K.MKGDYYR.Y
158 – 167	1236.6608	1235.6535	1235.6445	7	1	K.KEMQPTHPIR.L
159 – 167	1108.5676	1107.5603	1107.5495	10	0	K.EMQPTHPIR.L
159 – 167	1124.5628	1123.5555	1123.5444	10	0	K.EMQPTHPIR.L Oxidation
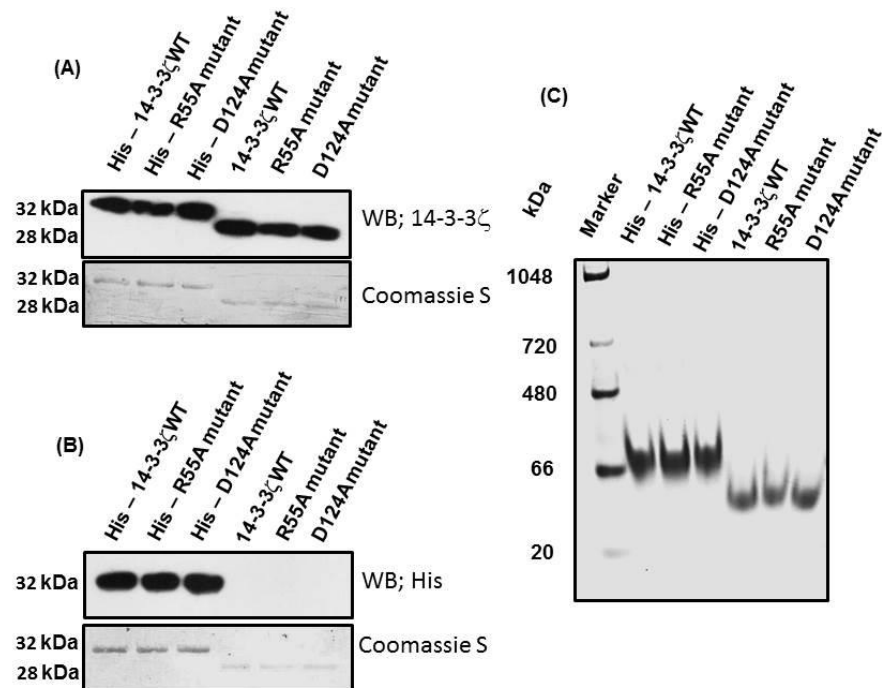
Fig. 4.4 Characterization of 14-3-3ζ WT and mutant protein

(A) All three proteins (14-3-3ζ WT, R55A and D124A mutant proteins) with their fusion His-tag intact and cleaved were subjected to SDS-PAGE and processed for western blotting. Proteins were detected using 14-3-3ζ specific antibody (Santa Cruz Biotechnology). Cleaved proteins run faster than the uncleaved protein. (B) Proteins were detected by anti His antibody (Cell Signaling). There is no reaction in wells carrying the enterokinase treated proteins that no longer carry the His-tag. Proteins were visualized by coomassie staining of the PVDF membrane. WB – western blotting. (C) Native PAGE analysis of all proteins with intact and cleaved His-tag. Note that the disordered extended 3.5 kDa His tag in the uncleaved proteins retards mobility (Ramteke et al., 2014).

Table T4.2 Nano LC-MS^E analysis of purified protein

Accession	Entry	Description	MW (Da)	pI (pH)	PLGS Score	Coverage (%)
P63104	1433Z_HUMAN	14 3 3 protein zeta delta OS Homo sapiens GN YWHAZ PE 1 SV 1	27727	4.53	16830.13	89.39
P31946-2	1433B_HUMAN	Isoform Short of 14 3 3 protein beta alpha OS Homo sapiens GN YWHAB	27832	4.57	2320.79	38.11
Q04917	1433F_HUMAN	14 3 3 protein eta OS Homo sapiens GN YWHAH PE 1 SV 4	28201	4.56	1265.30	36.59
P05906-2	TAT_HV1SC	Isoform Short of Protein Tat OS Human immunodeficiency virus type 1 group M subtype	8285	10.10	711.98	12.5

Q4LE39-2	ARI4B_HUMAN	B isolate SC				
Q4LE39-2	ARI4B_HUMAN	Isoform 2 of AT rich interactive domain containing protein 4B OS Homo sapiens GN ARID4B	137522	5.24	269.88	10.11

This pure protein was used to monitor ATPase activity. Initially we performed the ATPase assay using radiolabelled (γ-^{32}P) ATP (PerkinElmer) which acts as a tracer in a buffer containing 100 μM cold ATP and $MgCl_2$. Inorganic phosphate (Pi) released was monitored using TLC [Fig. 4.5 (A)]. Further Pi released was also monitored using malachite green assay (colorimetric assay). The amount of Pi released was quantitated with the help of standard graph generated using KH_2PO_4. The amount of Pi released was plotted against time [Fig. 4.5 (B)]. From the graph it is very clear that the 14-3-3ζ in fact can hydrolyze the ATP. We asked if this is enzyme mediated is due to gamma phosphate hydrolysis and to verify its specificity we use non hydrolysable analogues (ATP-γ-S and AMP-PCP; Sigma) and GTP. Nucleotide hydrolysis was observed only in the presence of ATP. Non hydrolysable analogues and GTP do not show any detectable Pi release. This nucleotidase activity seems specific to ATP [Fig. 4.5 (B)] indicating that 14-3-3ζ requires gamma phosphate for hydrolysis and thus possess an ATPase activity and not any non-specific nucleotidase or apyrase activity.
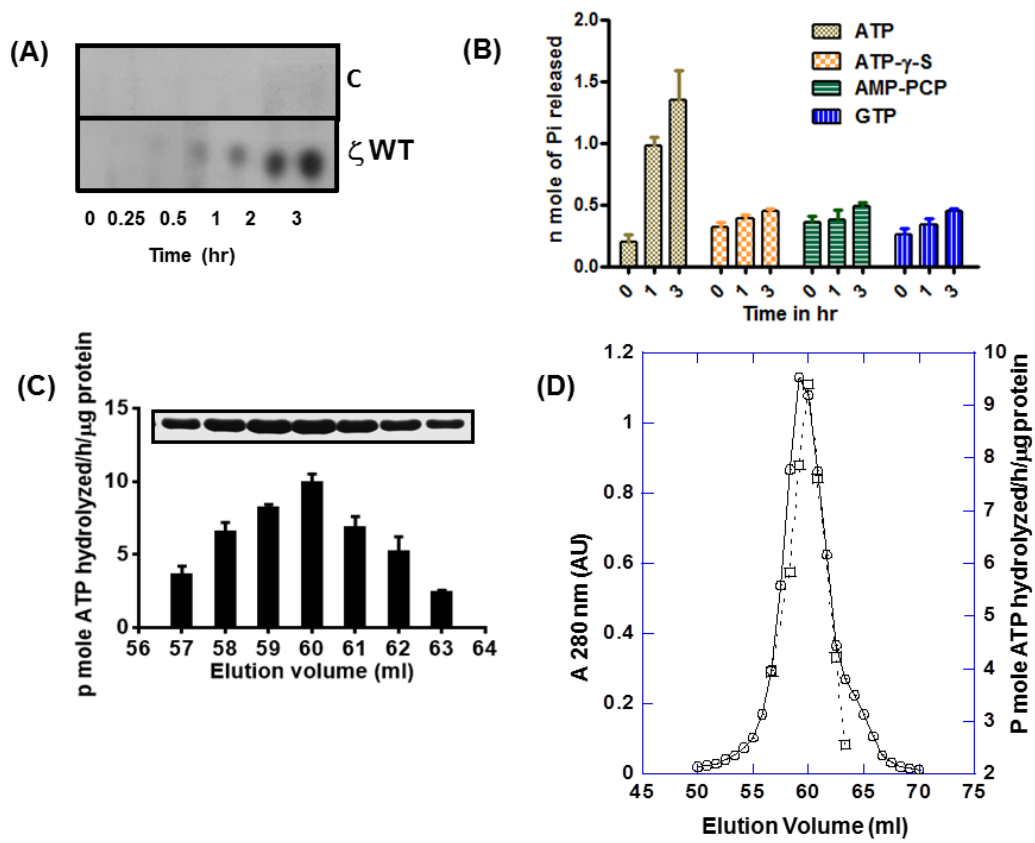
Fig. 4.5 Demonstration of ATPase activity in 14-3-3ζ

(A) Inorganic phosphate (γ-³²Pi) released from (γ-³²P) ATP hydrolysis by 14-3-3ζ WT at different time points was monitored by PEI-TLC. Lane C represents control (γ-³²P) ATP without any protein. (B) Pi release by 14-3-3ζ WT in presence of cold ATP, ATP-γ-S, AMP-PCP or GTP was monitored at different time points using malachite green. Data are represented as mean ± SD (n=3). (C) ATPase activity of each fraction of 14-3-3ζ WT eluted from gel filtration Proteins. Data are represented as mean ± SD (n=3). SD - standard deviation. Proteins from each elution fraction were run on 12% SDS-PAGE (top panel). (D) Correlation between ATPase activity and gel filtration profile of 14-3-3ζ WT. Data represents gel filtration profile of 14-3-3ζ WT (continuous line) and corresponding ATPase activity (dotted line) (Ramteke et al., 2014).

106

To further confirm that the 14-3-3ζ linked ATPase activity, we separately collected the protein fractions eluting from gel filtration column during purification. These individual fractions were dialyzed in Tris buffer pH 7.5 and tested for the ATPase activity using ADP-Glo^{TM} kinase assay (Promega). The ATPase activity from each fraction was correlated with the major peak from gel filtration profile of 14-3-3ζ [Fig. 4.5 (C) and (D)].

From the above graph it is very clear that the ATPase activity of 14-3-3ζ correlates with its gel filtration profile indicating that the ATPase activity is that intrinsic ATPase activity and is not contributed by any contaminating protein.

Our interest in 14-3-3ζ comes from the observation that *Drosophila* 14-3-3ζ isoform can disaggregate the aggregated protein in an ATP dependent manner. Therefore it is like that *Drosophila* 14-3-3ζ may also possess the ATPase activity. Therefore, we amplify *Drosophila* 14-3-3ζ WT from the larvae cDNA (a kind gift from Dr. Girish Ratnaparkhi, IISER, Pune) and cloned it in 6X his tagged, prokaryotic inducible expression pRSET-A vector. The protein was purified, subjected for the ATPase activity and compared with that of human 14-3-3ζ WT with malachite green assay (colorimetric assay). The ATPase activity of *Drosophila* 14-3-3ζ was comparable with that of human 14-3-3ζ [Fig 4.6 (A)]. We further confirmed the ATPase activity of both human and *Drosophila* 14-3-3ζ isoforms with the radiolabelled (γ-^{32}P) ATP. 14-3-3 protein was incubated in the presence of radiolabelled (γ-^{32}P) ATP which acts as a tracer in a buffer containing $MgCl_2$ and 100 μM cold ATP. The ATP hydrolysis was monitored by poly(ethylene)imine cellulose thin layer chromatographic (PEI-TLC) plates (Fluka) [Fig 4.6 (B)]. In order to visualize the product of ATP hydrolysis that is radioactive Pi (γ-^{32}P) released, the

separated product on the PEI-TLC plate was exposed to the X-ray film and autoradiogram was developed.
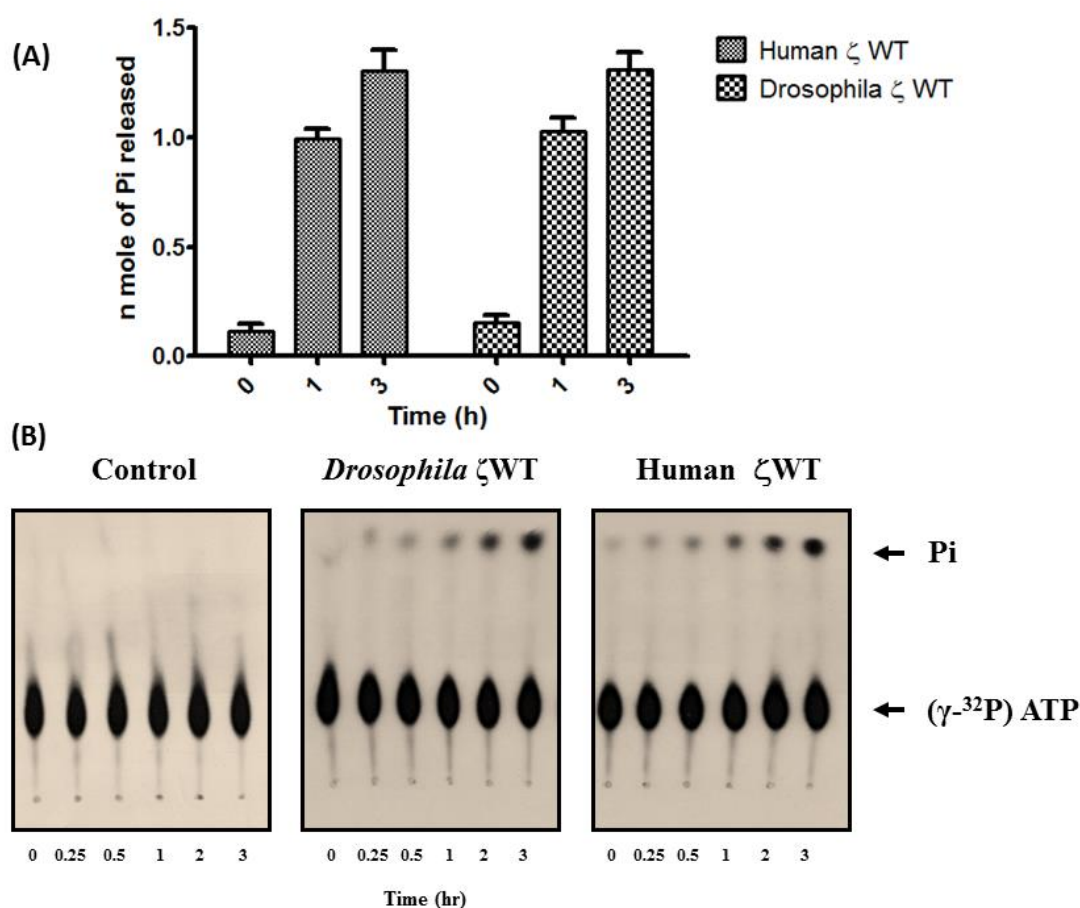
Fig. 4.6 Comparison of ATPase activity of Human and Drosophila 14-3-3ζ isoforms

(A) Human and Drosophila 14-3-3 were incubated with ATP at 37 °C and Pi released was monitored at different time point as mentioned using colorimetric assay. Data are represented as mean ± SEM of three experiments performed in triplicates. SEM – standard error of mean. (B) Drosophila and human 14-3-3ζ WT were incubated with tracer radiolabeled (γ-^{32}P) ATP a buffer containing $MgCl_2$ and 100 μM cold ATP. The ATP hydrolysis was monitored at different time point by poly(ethylene)imine cellulose *thin layer chromatographic (PEI-TLC) plates. Lane 'control' represents ATP alone without any protein.*

The basal ATPase activity of chaperons is known enhance in the presence of their target denatured proteins (Freeman et al., 1995). Studies by Yano et. al., on *Drosophila* 14-3-3ζ has shown that it can disaggregate the aggregated apocytochrome c *in vitro* in an ATP dependent manner (Yano et al., 2006). But they did not establish any ATPase activity in *Drosophila* 14-3-3ζ. Guided by this finding we wanted to check if aggregated apocytochrome c triggers the ATPase activity of *Drosophila* 14-3-3ζ like other HSPS. We tested ATPase activity of *Drosophila* 14-3-3ζ in the presence of aggregated apocytochrome c (Fig. 4.7).
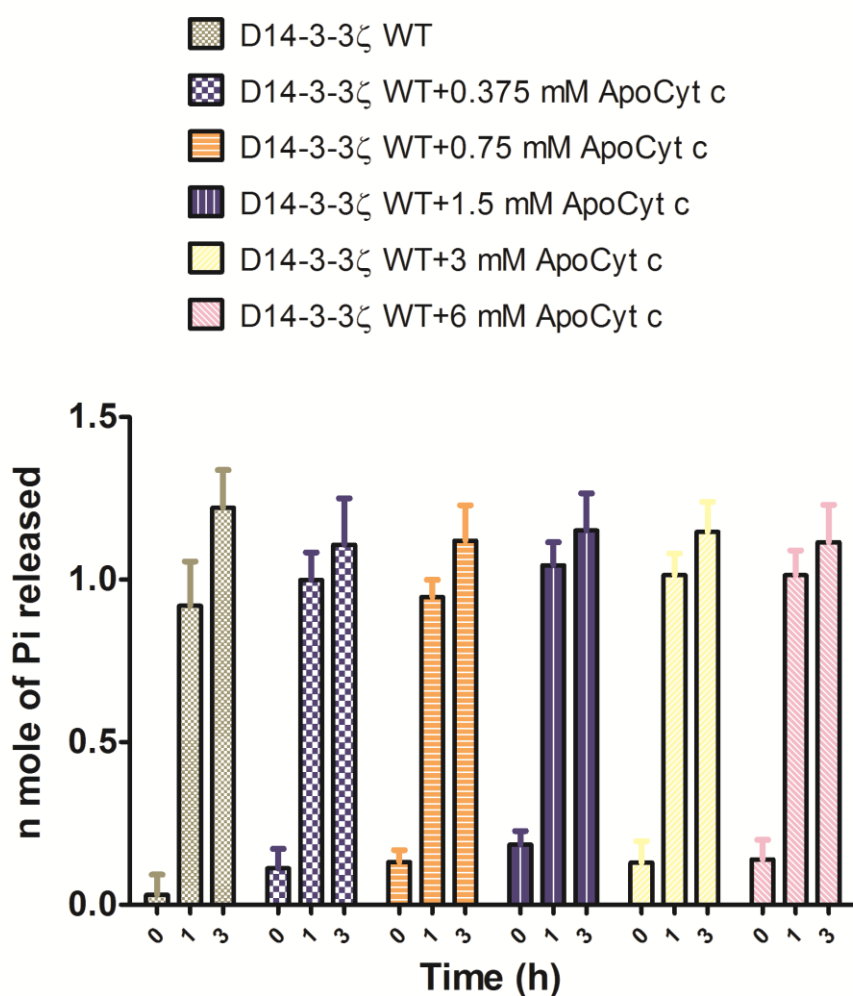
Fig. 4.7 Effect of Apocytochrome c on the ATPase activity of Drosophila 14-3-3ζ

Drosophila 14-3-3ζ WT was incubated with ATP at 37 °C in the presence of different concentrations of aggregated apocytochrome c and the ATPase activity was performed at different time point as indicated above using colorimetric assay. Data are represented as mean ± SEM of three experiments performed in triplicates. SEM – standard error of mean.

From the graph it is clear that the aggregated apocytochrome c does not trigger the ATPase activity of *Drosophila* 14-3-3ζ.

4.3 Summary

Human 14-3-3ζ possesses an intrinsic ATPase activity. The ATPase activity of *Drosophila* 14-3-3ζ isoform is comparable with that of human 14-3-3ζ. Using various biochemical assays and MS analysis we show that ATPase is an intrinsic activity of 14-3-3ζ. Aggregated apocytochrome c dis not trigger the ATPase activity of *Drosophila* 14-3-3ζ.

CHAPTER 5.

In silico Analysis for the Prediction of Putative Residues Involved in ATP Binding / Hydrolysis in 14-3-3ζ and Identification of Gain and Loss of Function Proteins by Mutagenesis

5.1 Introduction

Typical ATPases possess signature sequences or structures by which they can be easily identified such as the presence of Walker A motif (P-loop), Walker B motif, β sheeted structures. They are also rich in proline and glycine residues. To obtain clues towards the structural motif in 14-3-3ζ involved in ATP binding/hydrolysis, we performed BLAST analysis of the protein sequence of 14-3-3ζ (NCBI Reference Sequence: NP_663723.1; YWHAZ) against other ATP binding proteins. There was no significant homology between 14-3-3 and ATP binding proteins. Scan Prosite showed no other signature other than those associated with 14-3-3. 14-3-3ζ does not possess any distinct characteristics signature of ATPase. Primarily 14-3-3 is alpha helical protein with nine antiparallel alpha helices and flexible c-terminal loop. There are no β sheets in the crystal structure of 14-3-3ζ (Liu et al., 1995). Based on these observations we used *in silico* computational approach to predict putative ATP binding residues that might involve in ATP binding/hydrolysis. These probable ATP interacting residues could be verified by site directed mutagenesis. In our approach we used molecular docking to predict the putative residues involved in ATP binding/hydrolysis.

Molecular docking can be defined as the prediction of the structure of receptor-ligand complexes, where the receptor is usually a protein or a protein oligomer and the ligand is either a small molecule or another protein (Brooijmans and Kuntz, 2003). Initially docking studies were done to predict and reproduce the protein-ligand complexes. Since the development of molecular biology, genomics, proteomics and metabolomics along with combinational chemistry, molecular docking is applied to aid in the design of prescreening molecular interactions *in silico*. Molecular docking experiment involves the atomic representations of both the

interacting molecules. The interactions are evaluated by overlap between atoms and the potential to form hydrogen bonds in the complex. The pose score is the measure of fit of a ligand into the active site. Scoring during the posing phase usually involves simple energy calculations (e.g. electrostatic, van der Waals, ligand strains). Further rescoring might attempt to estimate more accurately the free energy of binding (ΔG) perhaps including properties such entropy and solvation. Experimental biochemical data helped filter the highest scoring configurations. The rigid body approximation of protein-ligand interactions has some limitations. It does not account for induced-fit, especially when a cryptic site in the uncomplexed receptor "opens" under the influence of the ligand. To overcome this multiple algorithm has been developed that explore ligand flexibility. Using this approach, HIV-1 protease was studied using *in silico* library screening after the crystal structure was solved and several interesting non-peptide inhibitors were found. The most promising inhibitors were screened experimentally and inhibit the protease selectively (DesJarlais et al., 1990). Molecular docking has promising outputs without actually doing the experimental procedure at the initial stage. In another example the microbes have gained multiple drug resistance (MDR) and are becoming serious threats to the human health. Using molecular docking one can select the inhibitors that can interfere with the biochemical pathways specific to the MDR bacteria. Recently modeling and docking studies were performed to achieve two key objectives that are important for the identification of new selective inhibitors of aspartate semialdehyde dehydrogenases (ASADHs) which produces an early branch point metabolite in a microbial biosynthetic pathway for essential amino acids and for quorum sensing molecules. First, virtual screening of a small library of compounds was used to identify new core structures that could serve as potential inhibitors of the ASADHs. Compounds have been identified from diverse

chemical classes that are predicted to bind to ASADH with high affinity. Next, molecular docking studies were used to prioritize analogs within each class for synthesis and testing against representative bacterial forms of ASADH from *Streptococcus pneumoniae* and *Vibrio cholerae*. These studies have led to new micromolar inhibitors of ASADH, demonstrating the utility of this molecular modeling and docking approach for the identification of new classes of potential enzyme inhibitors (Luniwal et al., 2012). Using similar approaches, molecular docking can be used for identifying the protein-protein or protein-ligand interacting sites that may have great implications in the healthcare.

5.2 Results and Discussion

Since human 14-3-3ζ does not possess any distinct characteristic signature of ATPase, we performed docking of 14-3-3ζ with that of ATP using Glide application from Schrödinger (in collaboration with Arun Kumar). We used the X-ray coordinates of 14-3-3ζ (PDB ID 2C1J) as the template (Macdonald et al., 2005). Site map suite and Glide from Schrödinger were used for pocket identification and docking (Glide). Two binding pockets were selected based on volume and binding scores (Fig. 5.1, and Table T5.1).
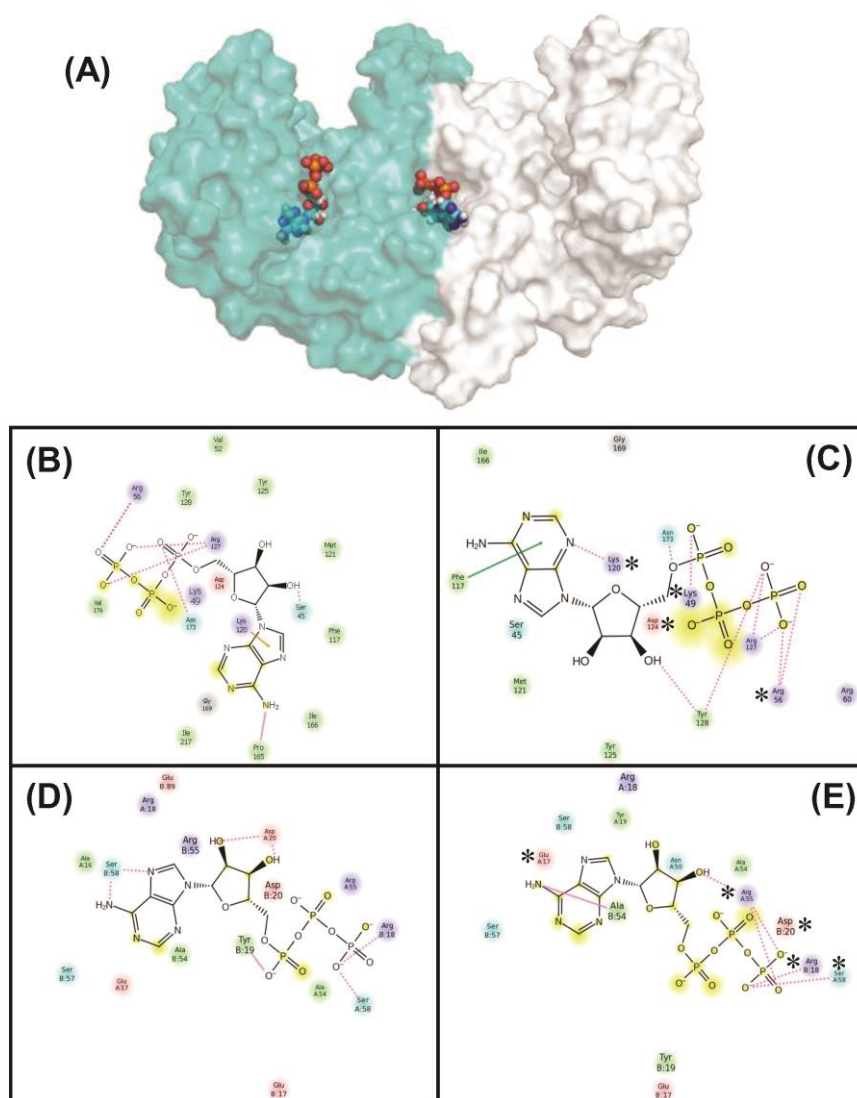
Fig. 5.1 Prediction of putative ATP binding sites in 14-3-3ζ by docking

ATP was docked using Glide application from Schrödinger. (A) ATP was bound both at the amphipathic groove (binding is shown only for one pocket) and at the dimer interface. Interacting residues within 5 Å of bound ATP in each pocket are shown. Fig. 2(B) and 2(C) represent the pre and post simulated complex in the amphipathic pocket. Fig. 2(D) and 2(E) represent the pre and post simulated complex at the dimer interface. *Represents mutated residues (Ramteke et al., 2014).

Table T5.1 Docking Scores for ATP

Sites	Region	Site Score	Size	Volume $(\text{Å})^3$	Glide Score
Site1	Chain B (Amphipathic groove)	1.006	99	416.402	-9.27
Site2	Chain A (Amphipathic groove)	0.933	77	383.817	-10.32
Site3	Dimer Interface	0.931	75	393.421	-9.35

Pocket one lies near the phosphopeptide binding pocket at the amphipathic groove and second pocket is located at the dimer interface [Fig. 5.1 (A)]. The bound complexes were subjected to molecular dynamic simulation and pre and post simulated structures are shown in Fig. 5.1. Residues within 5Å of docked ATP in both pockets are marked in Fig. 5.1 (B, C, D and E). Both pockets harbored residues expected to bind and hydrolyze ATP. Residues within 5 Å of the bound ATP that are likely to participate in the ATPase activity of 14-3-3ζ were converted into Ala. All mutations were confirmed by sequencing. Among the many mutations screened R55A mutation at the dimer interface resulted in loss of ATPase activity and D124A mutation in the amphipathic groove resulted in gain of ATPase activity as tested by colorimetric assay [Fig. 5.2(A)]. Further the ATPase activity of R55A and D124A mutant was also confirmed by radiolabelled (γ-^{32}P) ATP [Fig. 5.2(B)]. Hsp104 a disaggregating chaperone possesses a sensor motif called GAR and RR (Bösl et al., 2006a). R55A in 14-3-3ζ is part of a sequence $G_{53}A_{54}R_{55}R_{56}$. It is possible that R_{55} here is acting as an ATP sensor and hence R55A mutation results in loss of ATPase activity. In order to further investigate the importance of R55 residue, we created

double mutant (DR mutant) by mutating R55A in D124A background. For this we used pRSET-AζD124A as a template and mutated R55A by site directed mutagenesis. Mutation was confirmed by sequencing and DR mutant was generated. Compared to the D124A mutant, the double mutant showed about 40% loss of ATPase activity [Fig. 5.2 (C)] indicating that R55 is an important residue for the ATPase activity of 14-3-3ζ. It is also likely that these mutations may have a long range effect or they may affect equilibrium distribution between active and inactive conformers.
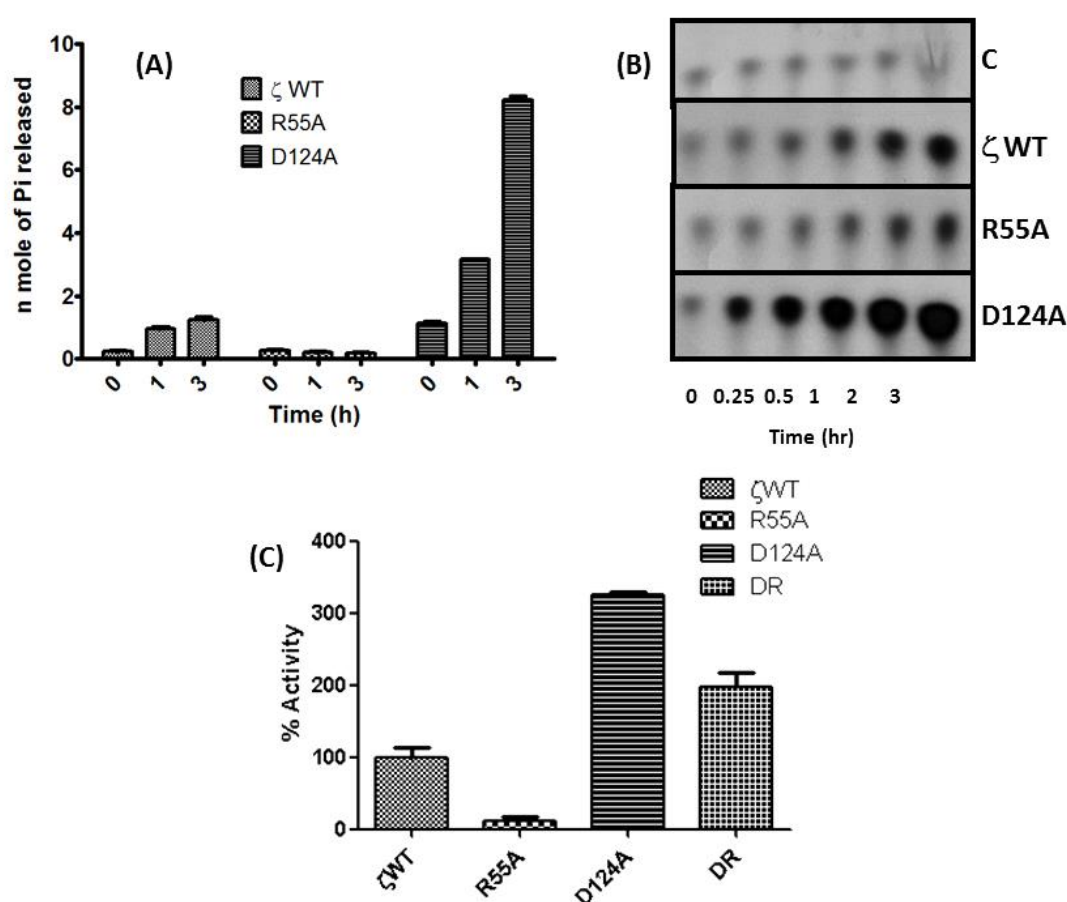
Fig. 5.2 Effect of mutation on the ATPase activity of 14-3-3ζ WT

(A) 14-3-3ζ WT, R55A and D124A mutants were individually incubated with ATP at 37 °C and the Pi released was monitored using malachite green at different time point

as indicated above. Data are represented as mean ± SEM from three experiments performed in triplicates. SEM – standard error of mean. (B) ATPase activity of R55A and D124A mutants was monitored using radiolabeled (γ-^{32}P) ATP and compared with the 14-3-3ζ WT protein. Lane C represents control (γ-^{32}P) ATP without any protein (Ramteke et al., 2014). (C) 14-3-3ζ WT, R55A, D124A and DR (R55A, D124A) double mutant was subjected for ATPase assay in the presence of 1 mM ATP (Sigma). Pi released was monitored using calorimetry assay. R55A mutation in D124A background resulted in reduction of ATPase activity of D124A mutant. Data are represented as mean ± SD (n=3). SD - standard deviation (Ramteke et al., 2014).

All other mutations (E17A, R18A, D20A, C25S, V51G, S57A, S58A, E89A, D92G, C94S and D96V) near the dimer interface or near phosphopeptide binding amphipathic pocket (N42A, K49A, R56A, K120A, Y149A, F174A, C189S and S190A) did not alter the ATPase activity of 14-3-3ζ (Fig. 5.3 and Fig. 5.4).
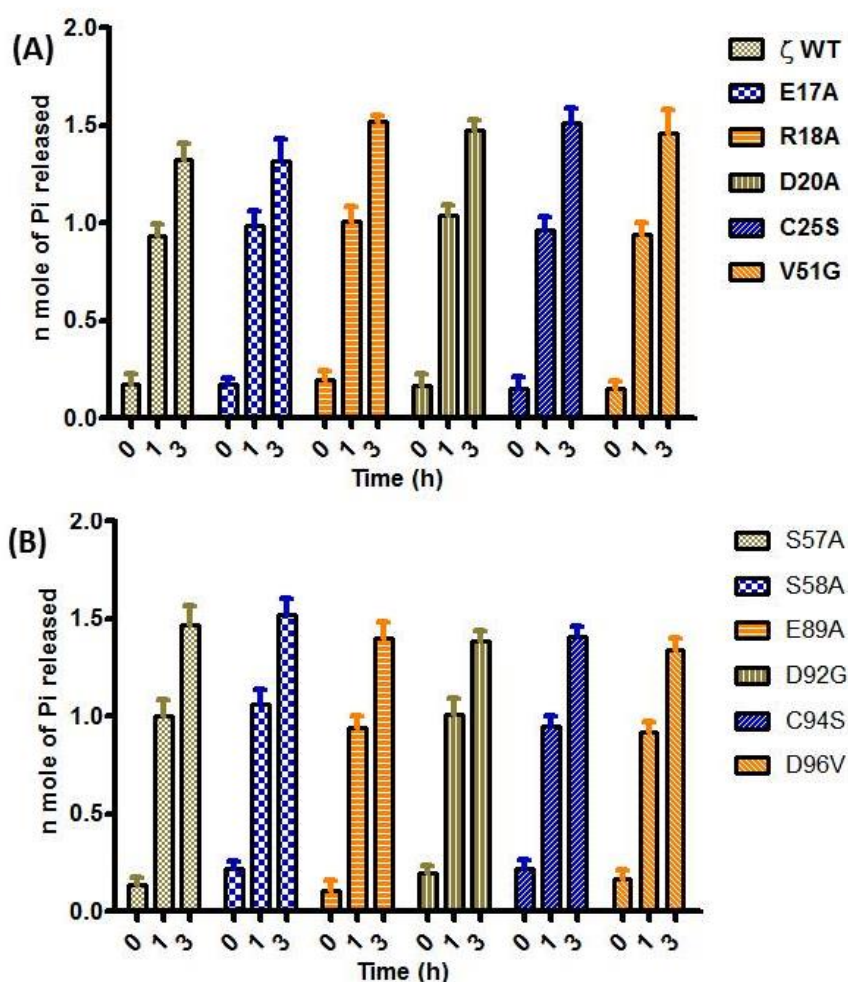
Fig. 5.3 Effect of other mutation near dimer interface in ATPase activity of human

14-3-3ζ WT

Individual mutant protein was tested for the ATPase activity at different time point as indicated above using colorimetric assay. ATPase activity was compared with that of human 14-3-3ζ WT (panel A and B). Data are represented as mean ± SEM from three experiments performed in triplicates. SEM – standard error of mean.
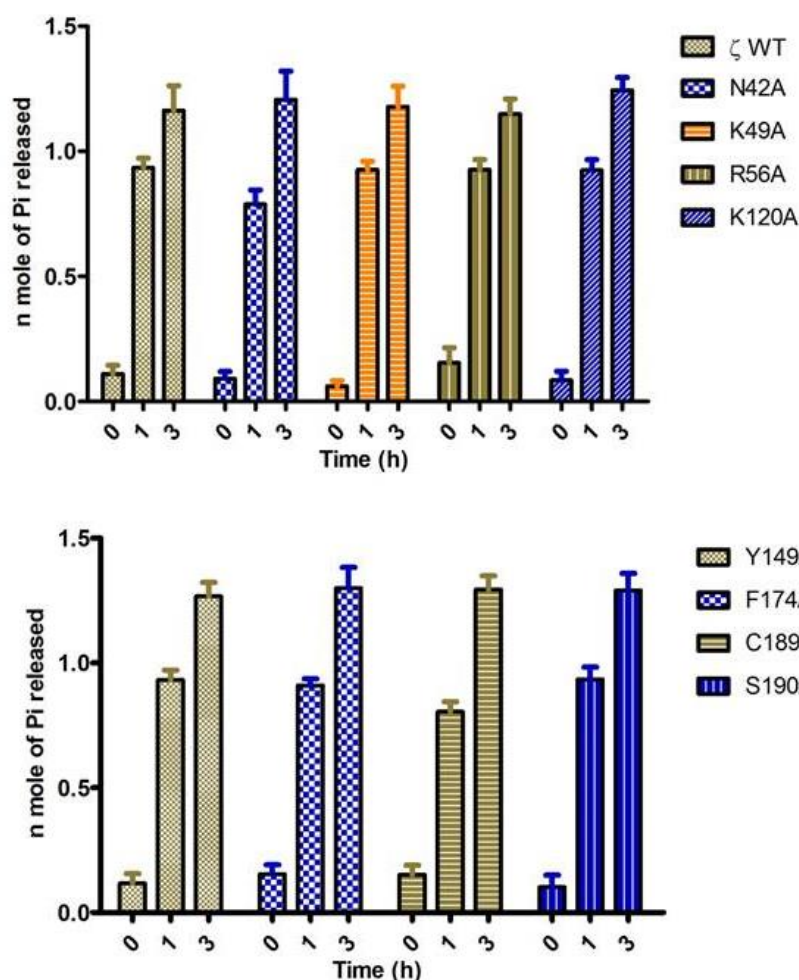
Fig. 5.4 Effect of other mutation near amphipathic pocket in ATPase activity of human 14-3-3ζ WT

Individual mutant protein was tested for the ATPase activity at different time point as indicated above using colorimetric assay. ATPase activity was compared with that of human 14-3-3ζ WT (panel A and B). Data are represented as mean ± SEM from three experiments performed in triplicates. SEM – standard error of mean.

Colorimetric estimation of Pi released during ATP hydrolysis is limited by low signal to noise ratio. We therefore used a more sensitive ADP-Glo[TM] max ATPase assay kit (Promega) particularly suited to eliminate background from ATP. This assay involves two steps. Addition of ADP-Glo[TM] reagent terminates the

enzymatic reaction and depletes all remaining ATP. This step is followed by the addition of ADP-Glo^{TM} max detection reagent which converts all ADP formed upon hydrolysis (by 14-3-3ζ in this case) back to ATP in a quantitative manner. Amount of ATP formed is measured using luciferase/luciferin reaction. Initial standardization was undertaken to obtain the optimum enzyme concentration and time required for reproducible estimation of ATP hydrolyzed. We used 7 μM of protein for the determination of kinetic constants because the ATPase activity of all active 14-3-3 isoforms was in the linear range. It is to be noted that 14-3-3σ does not show any ATPase activity even at higher protein concentration.

Kinetic parameters for ATP hydrolysis were determined for the 14-3-3ζ WT (human and *Drosophila* isoforms) and the mutant proteins (Fig. 5.5) (Zegzouti et al., 2009). 14-3-3ζ WT R55A and D124A mutants were incubated with different concentrations of ATP ranging from 0-500 μM. The reaction was incubated at 37 °C and the amount of ATP hydrolysis was quantitated. The velocity (rate) of ATPase activity was plotted against the ATP (substrate) concentration. The graphs were analyzed, kinetic constants – V_{max}, K_m, k_{cat} and k_{cat}/K_m were calculated with the help of GraphPad Prism 5 and compared with that of Hsp 70 used as a positive control (Table T5.2). Pure recombinant human 14-3-3ζ hydrolyzes ATP with a V_{max} of 152 p moles/min/mg of protein and K_m of 44 μM. The turnover number (k_{cat}) of 14-3-3ζ is 0.0087 min^{-1}. The V_{max}, K_m and k_{cat} values for *Drosophila* 14-3-3ζ WT (D14-3-3ζ WT) are comparable with that of human 14-3-3ζ isoform (Table T5.2). Mutation of D124A in the amphipathic pocket increases K_m (214.5 μM) by about 5 fold and k_{cat} (0.28 min^{-1}) by about 32 fold respectively. Mutation of a critical Arg (R55A) at the dimer interface reduces binding and decreases catalysis. The rate of hydrolysis of

ATP by 14-3-3ζ WT (k_{cat} = 0.0087 min^{-1}) was slower than that of Hsp 70 (k_{cat} = 0.16 min^{-1}) used as a positive control here but comparable to the values reported from another classical chaperone Hsp 90 (k_{cat} = 0.015 min^{-1} to 0.086 min^{-1}) (McLaughlin et al., 2002; Owen et al., 2002). Mutation of D124A increases the k_{cat} of the enzyme (k_{cat} = 0.28 min^{-1}) and the activity of the mutant was closer to that of Hsp 70 (k_{cat} = 0.16 min^{-1}). These kinetic parameters could not be measured for R55A as the activity did not attain saturation [Fig. 5.5 (A)].
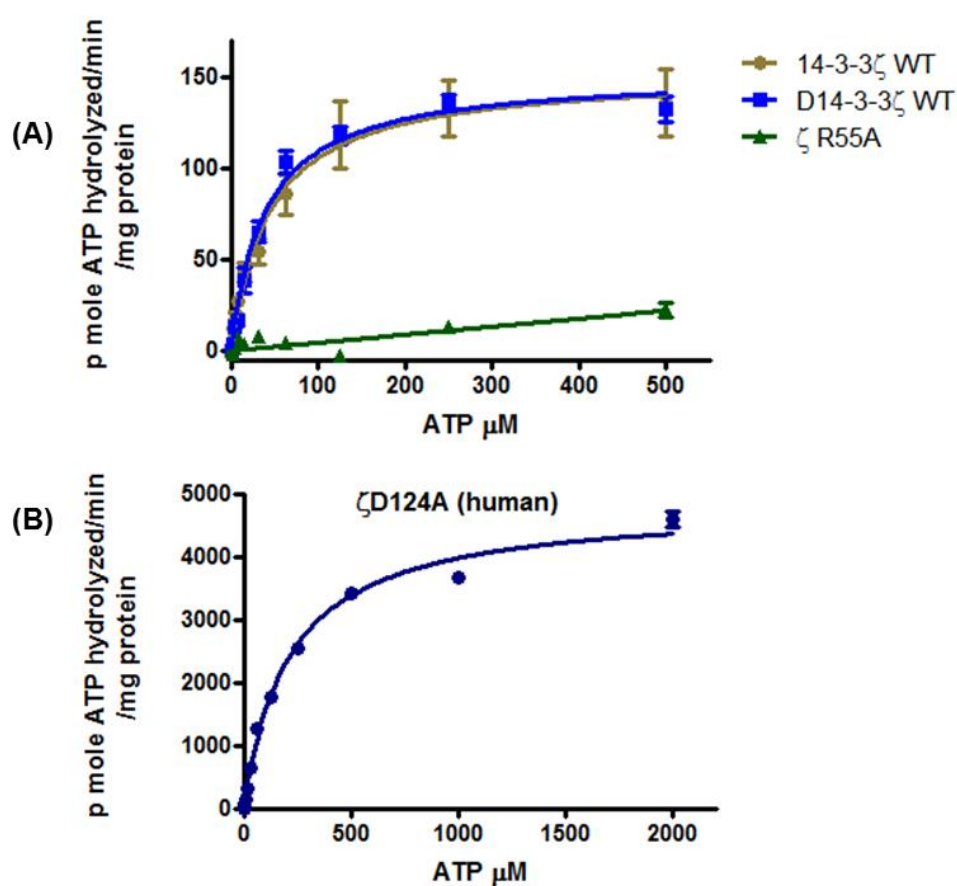
Fig. 5.5 Characterization of ATPase Activity in human 14-3-3ζ WT, R55A and D124A mutant

(A) ATPase activity for 14-3-3ζ WT (human and Drosophila isoforms), R55A (human) and (B) D124A mutant (human) were performed in the presence of 0-500 or 2000 μM

of ATP concentration using Max Glo^{TM} ATPase assay (Promega). Velocity of the

reaction was plotted against ATP concentration to determine the kinetic constants.

Two independent experiments in triplicates were conducted. Data are represented as

mean ± SEM. SEM - standard error of mean. **Note:** *D14-3-3ζ WT represents*

Drosophila isoform.

Table T5.2 Characterization of ATPase activity in 14-3-3ζ WT and D124A mutant

Sr. No.	Protein	V_{max} (p mole ATP hydrolysed/min/ mg protein)	K_m (μM)	k_{cat} (min^{-1})	k_{cat}/K_m (min^{-1} μM^{-1})
1.	14-3-3ζ WT (Human)	152 ± 10.19	44.33 ± 10.05	0.0087 ± 0.00058	0.000196
2.	D14-3-3ζ WT (*Drosophila*)	151.8 ± 4.79	39.64 ± 4.34	0.0087 ± 0.00027	0.000219
3.	D124A mutant (Human)	4830 ± 80.22	214.5 ± 11.53	0.28 ± 0.0046	0.001305
4.	Hsp 70 (Human)	2335 ± 54.22	51.07 ± 4.51	0.16 ± 0.0038	0.003133

For many chaperons, it holds true that presence of denatured proteins or their

binding partners can trigger their ATPase activity (Freeman et al., 1995). Since 14-3-3

proteins bind to their target partners *via* conserved phospho-motifs, we asked if

phosphopeptide binding triggers the ATPase activity of 14-3-3ζ WT. Therefore we

performed an ATPase assay with 14-3-3ζ WT in the presence of 100 μM of

phosphopeptides P1, P2 and P3 (P1-RLYHpSLP, P2-QSYpTV, P3-ARKpTG). The

ATPase activity of human 14-3-3ζ WT mutant remain unaltered in the presence of

phosphopeptides, indicating that the phosphopeptide binding does not alter the

ATPase activity of 14-3-3 [Fig 5.6 (A)]. Binding of phosphopeptides to 14-3-3ζ WT, R55A and D124A mutant was not affected as tested by ELISA [Fig. 5.6 (B)].
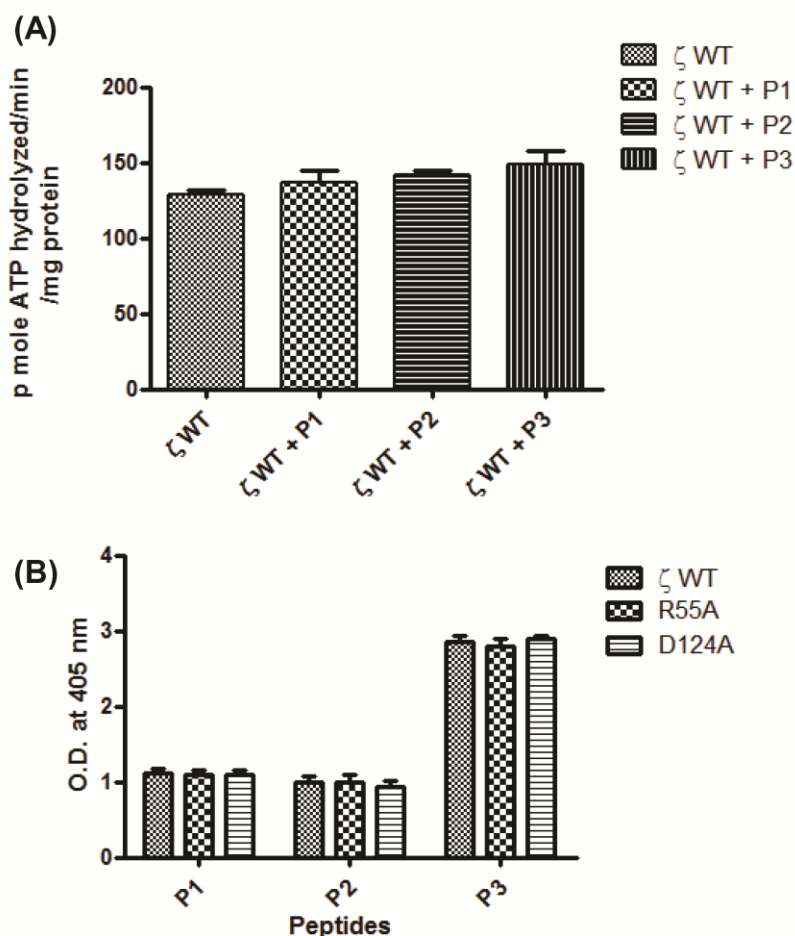
Fig.5.6 Phosphopeptides did not affect the ATPase activity of 14-3-3ζ WT

(A) Purified recombinant 14-3-3ζ WT was incubated with 500 μM of ATP in reaction buffer (RB) (20 mM HEPES buffer pH 7.5, 5 mM $MgCl_2$ and 2 mM 1,4-Dithiothreitol) in the presence or absence of 100 μM phosphopeptides P1, P2 or P3 at 37 °C. ATP hydrolysis was monitored using ADP-Glo^{TM} max ATPase assay (Promega). Data represented as mean ± SD (n=3). SD - standard deviation. P1-RLYHpSLP, P2-QSYpTV and P3-ARKpTG where pS and pT represents phosphoserine and phosphothreonine respectively. (B) Phosphopeptides P1, P2 amd P3 showed

comparable binding with 14-3-3ζ WT, R55A and D124A mutants as tested by ELISA.

Data are represented as mean ± SEM from three experiments performed in

duplicates. SEM – standard error of mean (Ramteke et al., 2014).

5.3 Summary:

Using structural guided molecular docking, we identified R55A and D124A residues that can modulate the ATPase activity of 14-3-3ζ. R55A mutation resulted in loss of ATPase activity while D124A mutation resulted in gain of ATPase function. We have identified $G_{53}A_{54}R_{55}$ as a probable ATP sensor sequence in 14-3-3ζ located near the dimer interface. Kinetic parameters for the ATPase activity of human and *Drosophila* 14-3-3ζ isoform were comparable. Individual mutation (R55A and D124A) in 14-3-3ζ does not result in loss of its dimeric nature and also retain their ability to bind with the phosphopeptides as tested by ELISA. Phosphopeptide binding does not alter the ATPase activity of 14-3-3ζ.

Taken together, these results again seem to suggest that the pocket near the dimer interface may be the site which binds to ATP. Nevertheless, it is quite likely that there could be two binding pockets for ATP in 14-3-3ζ. It is also likely that the effect seen is due to long range effect of these mutations while the actual pocket is elsewhere in the protein. It is likely that there may be regulatory mechanisms inside the cell that mimic the effect of these mutations and regulate the activity in a spatio-temporal manner to influence the functions executed by this protein.

CHAPTER 6.
CONSERVATION OF ATPase ACTIVITY IN OTHER 14-3-3 ISOFORMS

6.1 Introduction

14-3-3 family members are highly conserved in their sequence (Ref. Fig. 1.1 and Fig. 6.1), structure and form homo or heterodimers (Aitken, 2006). 14-3-3 family members shows variable region consisting of many acidic residues in their flexible c-terminal region. Some of the functions of 14-3-3 family proteins, for example binding of consensus phosphorylated residue are common but differ in their cellular function (Aitken, 2006; Cheng et al., 2004; Hermeking and Benzinger, 2006). Since we find that *Drosophila* and human 14-3-3ζ isoforms show similar ATPase activity, we wanted to check if this ATPase activity is conserved among other 14-3-3 isoforms. The presence of GAR motif in 14-3-3ζ which may act as sensor is conserved in many isoforms barring 14-3-3σ. It is interesting to verify whether 14-3-3σ possess any ATPase activity. Therefore we tested 14-3-3γ, ε, τ and σ isoforms for ATPase activity.
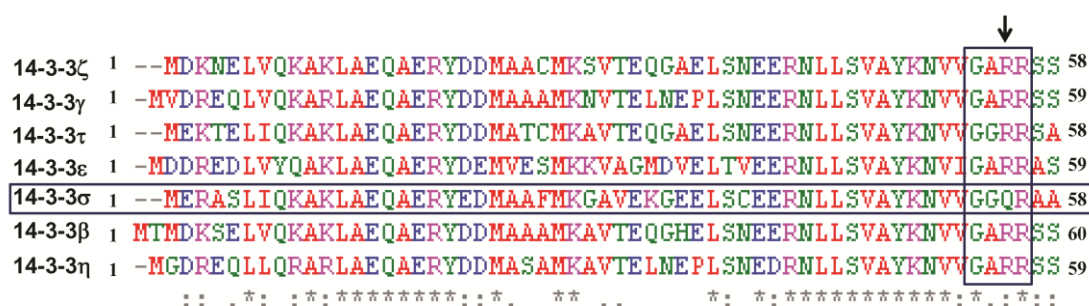
Fig. 6.1 Conservation of 'GAR', an ATP sensor motif in 14-3-3 isoforms

Multiple sequence alignment was performed using clustal omega (website - http://www.ebi.ac.uk) for 14-3-3 isoforms. R55 (as in 14-3-3ζ isoform, arrow mark) is conserved in all 14-3-3 isoforms except 14-3-3σ.

6.2 Results and Discussion

We cloned human 14-3-3γ, ε and σ isoforms (a kind gift from Dr. Sorab Dalal, ACTREC) in pRSET-A vector. 14-3-3τ was PCR amplified from cDNA obtained from HEK 293 RNA, cloned in pRSET-A vector (Invitrogen) into BamHI − EcoRI sites sequence verified. The sequencing result matches with gene ID − 10971 (NCBI), symbol − YWHAQ of 14-3-3τ. Proteins were purified as described above and tested for the ATPase activity with malachite green assay. 14-3-3γ, ε and τ isoforms showed the similar ATPase activity and is comparable with that of 14-3-3ζ (Fig. 6.2). 14-3-3σ did not show the release of Pi with time and hence no ATPase activity was detected.
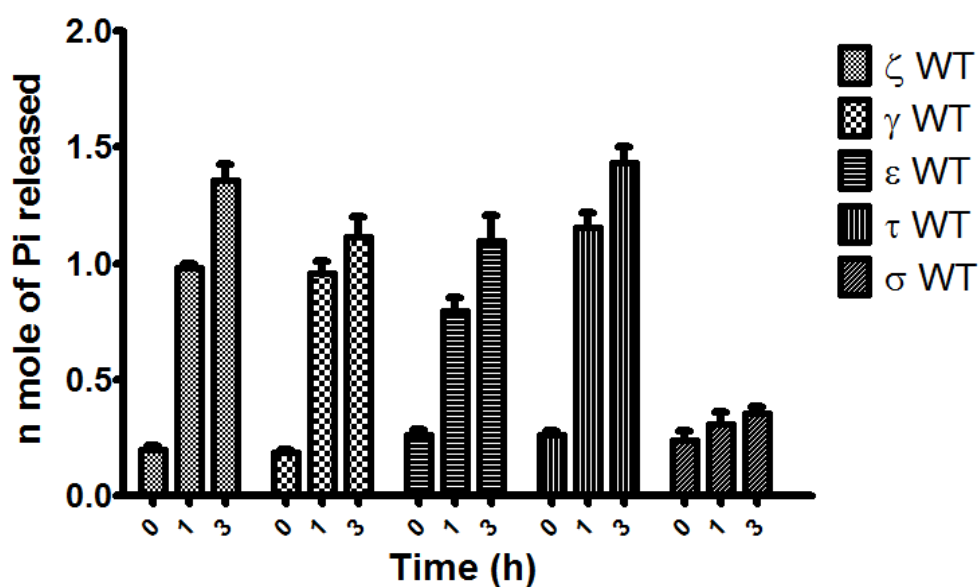
Fig. 6.2 Characterization of ATPase activity in 14-3-3 isoforms

Individual 14-3-3 isoform was incubated with ATP at 37 °C and the ATPase activity was monitored using colorimetric assay at different time point as indicated above. Data are represented as mean ± SEM from three experiments performed in triplicates. SEM − standard error of mean.

We further confirmed the ATPase activity of 14-3-3γ, ε, τ and σ isoforms with radiolabelled (γ-^{32}P) ATP [Fig. 6.3 (A)]. Individual 14-3-3 isoform was incubated in the presence of radiolabelled (γ-^{32}P) ATP which acts as a tracer in a buffer containing $MgCl_2$ and 100 μM cold ATP. The ATP hydrolysis was monitored by poly(ethylene)imine cellulose thin layer chromatographic (PEI-TLC) plates (Fluka) [Fig 6.3 (A)]. In order to visualize the product of ATP hydrolysis that is radioactive Pi (γ-^{32}P) released, the separated product on the PEI-TLC plate was exposed to the X-ray film and autoradiogram was developed. All tested 14-3-3 isoforms showed ATPase activity except 14-3-3σ [Fig. 6.3 (A)]. Following we determine K_m, V_{max} and k_{cat} for all active 14-3-3 isoforms [Fig. 6.3 (B)]. All active isoforms possess similar ATPase activity and is comparable with that of human 14-3-3ζ (Table T6.1). Interestingly all active isoforms also show the presence of conserved GAR motif probably acting as ATP sensor sequence and is responsible for the ATP binding.
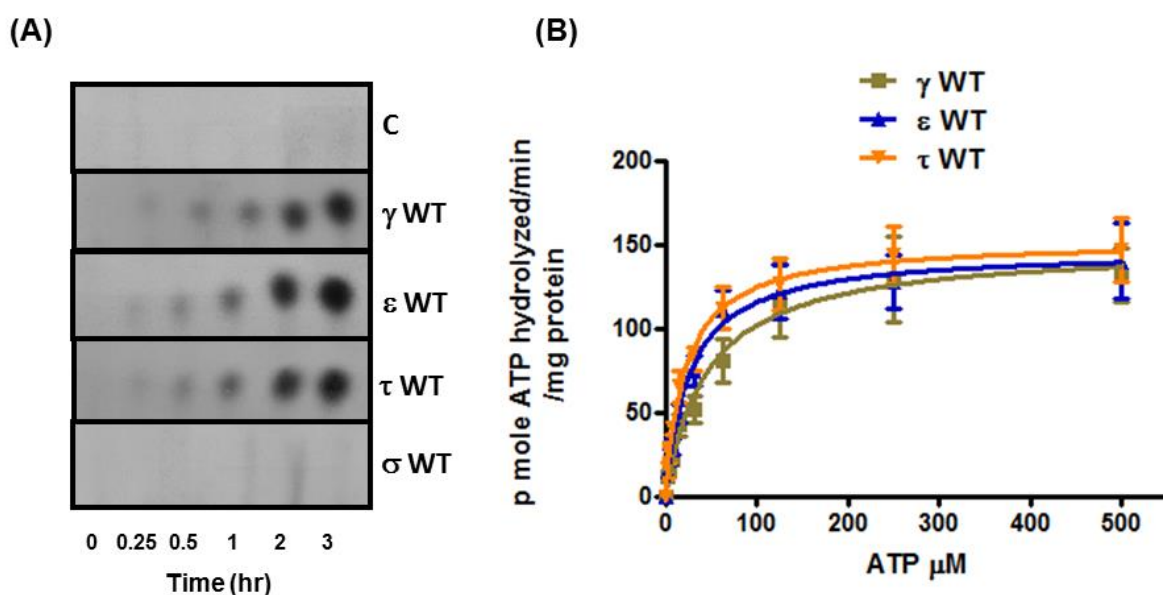
Fig. 6.3 ATPase activity in 14-3-3 isoforms

(A) Inorganic phosphate (γ-^{32}Pi) released from (γ-^{32}P) ATP hydrolysis by 14-3-3 isoforms at different time points was monitored by PEI-TLC. There is no detectable γ-^{32}P in lanes where ATP was incubated with the sigma isoform. Lane C represents control (γ-^{32}P) ATP without any protein. (B) ATP hydrolysis of active human 14-3-3 γ, ε and τ isoforms were monitored by ADP-Glo^{TM} max ATPase assay at different ATP concentrations as indicated above. Rate of the reaction (velocity) was plotted against ATP (substrate) concentration. Two independent experiments in triplicates were conducted. Data are represented as mean ± SEM. SEM - standard error of mean (Ramteke et al., 2014).

Table T6.1. Characterization of ATPase activity in 14-3-3 active isoforms

Sr. No.	Protein	V_{max} (p mole ATP hydrolyzed/min/mg protein)	K_m (µM)	k_{cat} (min^{-1})	k_{cat}/K_m (min^{-1} µM^{-1})
1.	D14-3-3ζ WT	151.8 ± 4.79	39.64 ± 4.34	0.0087 ± 0.00027	0.000219
2.	14-3-3ζ WT	152 ± 10.19	44.33 ± 10.05	0.0087 ± 0.00058	0.000196
3.	14-3-3γ WT	149.3 ± 12.55	46.81 ± 13.15	0.0085 ± 0.00072	0.000182
4.	14-3-3τ WT	152.4 ± 8.18	22.57 ± 4.72	0.0087 ± 0.00047	0.000385
5.	14-3-3ε WT	146.9 ± 8.9	27.31 ± 6.22	0.0084 ± 0.00051	0.000308
6.	Hsp 70	2335 ± 54.22	51.07 ± 4.51	0.16 ± 0.0038	0.003133

6.3 Summary

Human 14-3-3γ, ε and τ isoforms possess similar ATPase activity and is comparable with that of human 14-3-3ζ. Human 14-3-3σ did not show the detectable ATPase activity. Interestingly all active isoforms shows the presence of sensor 'GAR' motif. This ATP sensor is likely to be involved in ATP binding at the dimer interface of ATPase active 14-3-3 isoforms.

CHAPTER 7.

ANALYSIS OF ATP BINDING WITH 14-3-3

7.1 Introduction

It is to be noted that V_{max} of D124A mutant is ~30 times more than the WT protein and the K_m for ATP hydrolysis is approximately four times higher (Table T6.1). While K_m is routinely considered as a measure of binding affinity, the relationship holds true only under specific conditions where substrate is not limiting and reactions follow steady state kinetics. To obtain the measure of direct binding affinity, we report here radioactive ATP based filter trap ATP binding assay. In Michaelis-Menten kinetics, K_m is the substrate concentration when enzyme reaches to its half of the maximum velocity. A more accurate statement in fact may be, for reactions obeying Michaelis-Menten kinetics, K_m is a measure of the substrate concentration required for effective catalysis to occur. Therefore an enzyme with a high K_m requires a higher substrate concentration to achieve a given reaction velocity than an enzyme with a low K_m. In other words, a lower K_m value indicates a higher affinity for the substrate. However it may not hold true in all the cases.

7.2 Results and Discussion

To provide the direct evidence for the ATP binding, filter trap assay was performed. 14-3-3 isoforms (ζ, γ, ϵ, τ and σ) and the mutant proteins (R55A and D124A) were incubated with radiolabelled (γ-^{32}P) ATP on ice and spotted on nitrocellulose membrane. Membrane was allowed to dry and any unbound ATP was washed with washing buffer containing $MgCl_2$. Membrane was allowed to dry and autoradiogram was developed to monitor ATP binding. All 14-3-3 isoforms could bind to ATP except 14-3-3σ. R55A mutation also did not show ATP binding (Fig. 7.1).
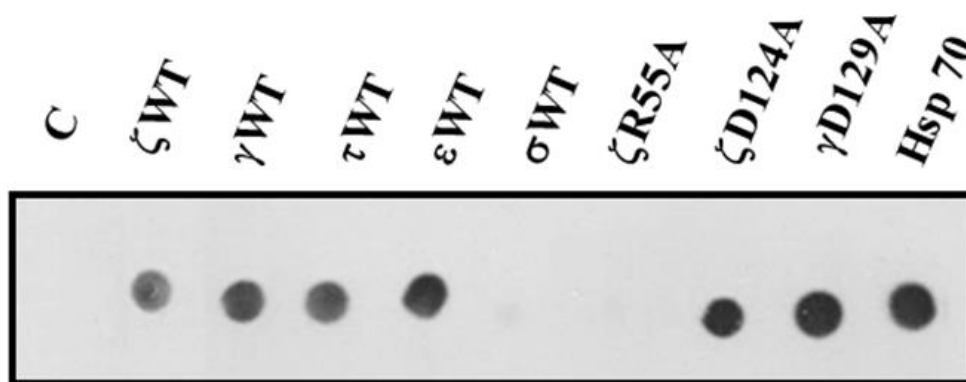
Fig. 7.1 Demonstration of ATP Binding with 14-3-3 and mutant proteins

Individual protein was incubated with 20 μCi of radiolabeled (γ-^{32}P) ATP on ice and spotted on nitrocellulose membrane, allowed to dry and washed with HEPES buffer containing MgCl2. The membrane was exposed to X-ray film and was developed to observe ATP binding to 14-3-3 proeins. HSP 70 was used as a positive control. Lane C represents control radiolabeled (γ-^{32}P) ATP alone without any protein.

Furthermore for quantitative analysis, protein bound radiolabeled (γ-^{32}P) ATP was separated form unbound free ATP using Zeba^{TM} desalt spin column (Pierce) and protein associated radioactivity was counted in a liquid scintillation counter (Fig. 7.2). Amount of ATP bound to 14-3-3 isoforms (ζ, γ, ε and τ) was about 7% of the total hot ATP added whereas 14-3-3σ showed only 1.84% of the ATP binding. About 2.66% binding was seen in R55A mutant (binding attenuated by about 50%), ~12% binding (twice more than the 14-3-3ζ WT) was seen in the D124A mutant and about 12.47% was seen in γD129A mutant (corresponding Asp mutant in 14-3-3γ isoform). About 13% of hot ATP was bound to Hsp 70 analyzed under the same conditions. The direct binding profile supports the energy calculations derived from docking studies.
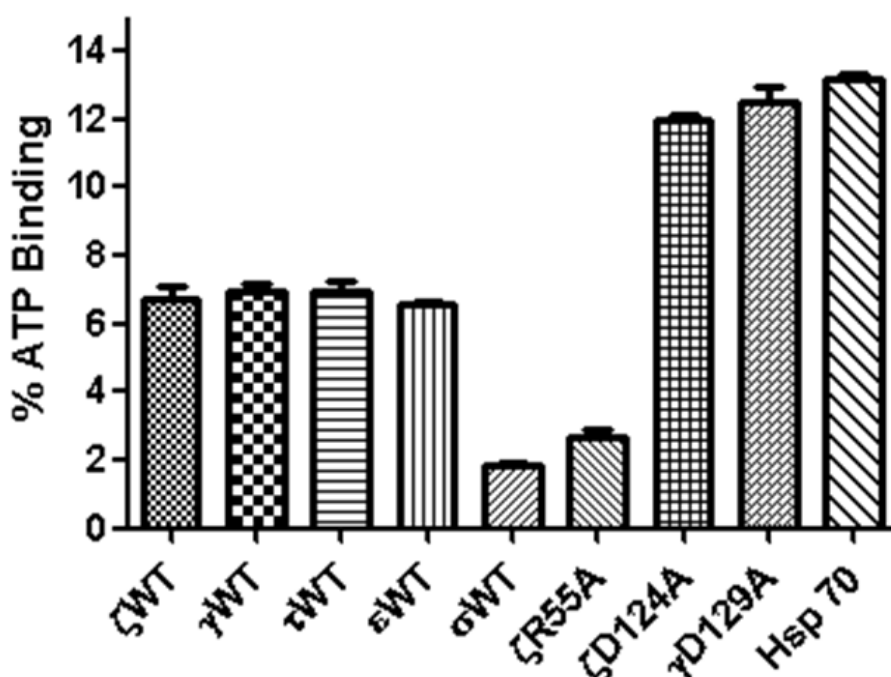
Fig. 7.2 Quantitation of ATP binding with 14-3-3 and mutant proteins

Individual protein was incubated with 20 μCi of radiolabeled (γ-^{32}P) ATP on ice and separated form unbound free ATP using Zeba^{TM} desalt spin column. To obtain the quantity of ATP bound with protein, radioactive counts were measured using liquid scintillation counter. Percentage of ATP binding was calculated by comparing the counts with total 20 μCi ATP used for binding. Data represented as mean $\pm$ SD of three individual experiments. SD – standard deviation.

From the above figure, it is very clear that all 14-3-3 active isoforms bind with ATP. R55A and 14-3-3σ isoform showed about 50% reductions in their ability to bind ATP, whereas hyperactive Asp mutant binds strongly with ATP. These results indicate that the D124A mutant has a better binding affinity for ATP while R55A mutant has less affinity as compared to the WT protein.

It is to be noted that K_m is a measure of substrate concentration required for effective catalysis. K_m is also considered as a measure of binding affinity, when the

k_{cat} is much less than k_{-1} that is rate of dissociation of ES. For enzymatic reaction under steady state kinetics -

$$E + S \underset{K\text{-}1}{\overset{K1}{\longleftrightarrow}} ES \overset{k_{cat}}{\longrightarrow} E + P$$
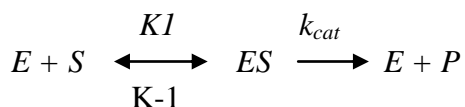
Where,

$K1$ is the forward rate constant for substrate binding.

$K\text{-}1$ is the reverse rate constant for substrate binding.

ES is the enzyme-substrate complex.

k_{cat} is the catalytic rate constant K_m ($K\text{-}1+K2/K1$) is approximates the affinity of enzyme for substrate when $k_{cat} << K\text{-}1$. Under these conditions, k_{cat} can be removed from the equation and $K_m = K_D$.

In case of D124A even though the K_m is higher than WT, the ES complex formed dissociates to form product faster than dissociation into free enzyme and substrate thus increasing the catalytic efficiency. Thus it explains our observation that D124A mutant binds to more ATP that WT protein.

7.3 Summary

All active 14-3-3 isoforms show detectable binding with ATP except sigma isoform. The inactive 14-3-3σ and R55A mutant which reduced ATPase activity showed decrease binding with ATP. R55A mutation at the dimer interface of 14-3-3ζ resulted in the abrogation of ATP binding and hence showed reduced ATPase activity. On the other hand D124A mutation in 14-3-3ζ (and corresponding D129A in 14-3-3γ) resulted in increase in ATP binding as well as hydrolysis. This indicates that D124 may act as an inhibitory loop which restricts the supply of ATP for hydrolysis.

137

However the role of corresponding conserved Arg residue (R55 in case of 14-3-3ζ isoform) in other 14-3-3 isoforms needs to be determined.

We have shown direct physical binding of ATP with protein under these conditions where we observed that R55A and 14-3-3 sigma (having no ATPase activity) bind to less ATP. On the other hand hyperactive D124A mutant (in zeta isoform and corresponding D129A mutation in gamma isoform) bind more ATP. In these cases where the excess substrate has been removed the net result is a reflection of off rate.

CHAPTER 8. COMPUTATIONAL ANALYSIS OF BINDING ENERGY AND EXPERIMENTAL CONSTRAINTS CONVERGE ON ONE PUTATIVE BINDING SITE

8.1 Introduction

Human 14-3-3ζ possesses an intrinsic ATPase activity. R55A mutation at the dimer interface resulted in loss of ATPase activity while D124A mutation near the phospho-peptide binding amphipathic pocket resulted in gain of ATPase activity. In the absence of high resolution structural information of protein bound ATP, it is difficult to explain why other amino acid substitutions in the vicinity of bound ATP in either binding pockets failed to show any effect. It is possible that ATP may bind in different orientations or binding may be accompanied by conformational changes that are not captured by docking algorithms. It is also intriguing that mutation in one pocket (amphipathic pocket) resulted in enhancement of activity of 14-3-3ζ and in the other (dimer interface) a partial loss. This was reemphasized by the double mutant the activity of which was reduced by 40% compared to the hyper active D124A mutant.

8.2 Results and Discussion

In order to reconcile the differential effect of the two mutations located in seemingly different pockets, we used docking algorithms, *in silico* mutagenesis and binding energy calculations using VlifeMDS software to understand the structural basis of the observed ATPase activity. We introduced two experimental constraints in analyzing the docking results. As compared to the wild type protein the docked pose should have more negative energy in D124A and more positive energy in R55A mutant. With this experimentally guided presumption, D124A and R55A mutations were carried out on the WT protein using VlifeMDS software (VLifeMDS). Protein optimization, complex optimization and binding energy calculations were carried out on the monomeric and dimeric forms of 14-3-3ζ WT and the mutant proteins (R55A and D124A). ATP was docked to these proteins and the binding energies for each of

the poses in the mutated proteins were compared with wild type protein (Table T8.1). No pose on the monomer confirmed to the experimental criteria. However a single pose (pose 4 in Table T8.1) at the dimer interface obeyed these experimental constraints. This docking pose clearly explains the importance of Arg55 in binding interactions [Fig. 8.1 (A)]. Detailed analysis of the pose indicates that ATP forms two hydrogen bonds with Arg55B and also makes charged interaction with Arg55A. In addition, Arg55 makes numerous van der waal (vdW) interactions at the dimer interface [Fig. 8.1 (A)]. Mutation of this residue to Ala would result in loss of hydrogen bond interactions as well as the charge interaction between the positively charged guanidine group of arginine and negatively charged phosphate group of ATP, adversely affecting the binding energy (BE of 9.34 kcal/mol for R55A mutant). Increased rate of hydrolysis of D124A is reflected in better binding energy in D124A (BE of - 0.77 kcal/mol; Table T8.1) which could be due to increase in the vdW component of the overall binding energy contributing to favorable steric interactions between ATP and the mutated protein [Fig. 8.1 (B)].
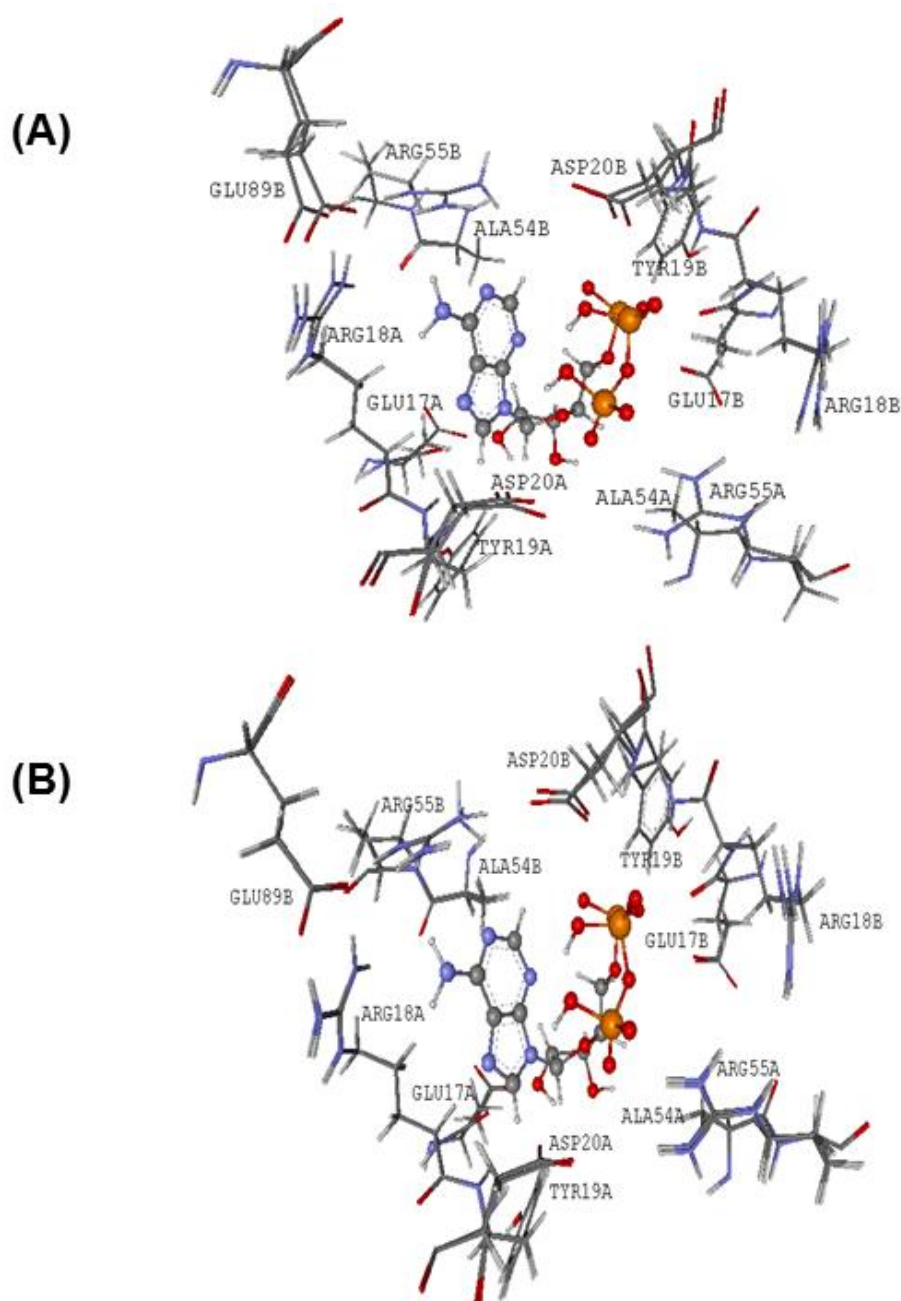
Fig. 8.1 Effect of mutations on ATP binding

(A) An overlay of 14-3-3ζ WT and R55A mutant docked poses and (B) is an overlay of D124A mutant and the 14-3-3ζ WT docked poses (only the ligand and interacting residues are shown). D124 is not in view. Bound ATP is represented as a ball and stick model. Residues within 4 Å from ATP are shown and RMSD of superposition (of backbone atoms) is 0.15 Å (Ramteke et al., 2014).

Table T8.1 Comparison of binding energies for each of the poses in the mutated proteins (R55A and D124A) with 14-3-3ζ WT

Pose	PLP score WT	PLP score D124A	PLP score R55A	BE in WT	BE in D124A (kcal/mole)	BE in R55A (kcal/mole)
1	-7.27	1.46	-14.05	4.96	7.5	-3.04
2	-38.61	-26.76	-33.87	-0.74	15.21	-2.33
3	-48.95	-41.06	-47.53	24.97	53.36	25.76
4*	-46.75	-48.82	-28.14	4.04	-0.77	9.34
5	-57.41	-47.12	-48.07	9.63	10.05	2.22
6	-22.75	-12.91	-19.46	14.39	10.99	6.63
7	-45.2	-47.59	-39.03	6.4	-8.65	-0.66
8	-28.29	-21.17	-19.74	15.45	24.72	14.29
9	-27.37	-22.01	-17.52	5.31	10.41	16.66
10	-48.92	-36.16	-47.96	-6.28	-20.74	-18.74

BE – Binding energy.

* Pose 4 is the one which we have reported as the best pose in accordance with experimental results of mutation.

Note: PLP docked score is an empirical scoring function and is reported in arbitrary energy unit.

8.3 Summary

ATP with better affinity to D124A mutant is reflected in the docking studies. The lower affinity of ATP with 14-3-3ζ WT and even further decrease in case of R55A mutant could be due to overall decrease in vdW components of binding. This result also suggests that ATP binding may be one of the rate limiting steps in case of 14-3-3 protein in ATP hydrolysis.

CHAPTER 9.

SINGLE TURNOVER

ATPASE STUDIES

9.1 Introduction

ATPase assay performed in steady state conditions are performed such that there is no limiting factor for the enzyme to perform catalysis. In steady state kinetics enzyme bind with the substrate to form enzyme substrate (E-S) complex. Enzymes act as catalyst and lower down the energy of activation required for the formation of product. As soon as the product is produced, enzyme is free to bind the next substrate molecule and perform the catalysis. In single turnover enzyme assay, the enzyme bound complex is isolated and is subjected for the catalysis.

9.2 Results and Discussion

To correlate ATP binding and ATP hydrolysis, we performed single turnover ATPase assay. WT 14-3-3ζ, D124A and R55A mutant proteins and 14-3-3σ were independently incubated with radioactive ATP and the bound complex free from ATP was isolated. Protein fraction which has the maximum signal for ATP was chosen and hydrolysis was followed with time (Fig. 9.1).
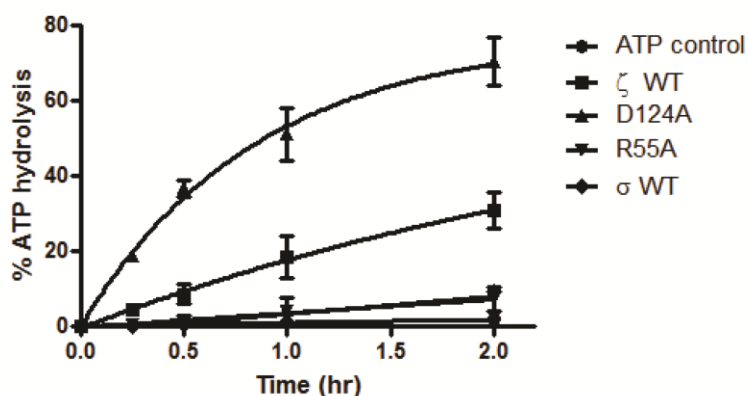
Fig. 9.1 Single turnover ATPase assay

WT 14-3-3ζ, R55A, D124A or WT 14-3-3σ bound-ATP complex was isolated and single turnover ATPase assay was performed. Data represents percentage of ATP hydrolysis with time from two independent experiments. Data are represented as mean ± SD. SD - standard deviation.

The data could be readily fit to a single exponential function and results indicate that 30% of bound ATP is hydrolyzed in 2 hours by 14-3-3ζ while D124A hydrolyzes almost 70% of bound ATP by this time (Rate constant, K = 1.17 ± 0.21). R55A and 14-3-3σ did not show any detectable hydrolysis of ATP under these conditions. Conversion of almost 70% of the bound ATP to product by D124A in a single exponential manner indicates that binding is likely to be stochiometric ruling out the presence of any non-specifically bound ATP that cannot be hydrolyzed. Commensurate with other results 14-3-3ζ WT is slow in hydrolyzing the bound ATP which is very likely due to the faster dissociation of the protein-ATP complex into the free forms.

9.3 Summary:

Single turnover ATPase assay further confirms the intrinsic activity of human 14-3-3ζ. Single turnover ATPase assay using radioactive ATP provide an unequivocal evidence for the loss and gain of ATPase activity in R55A and D124A mutant respectively.

CHAPTER 10.

CONCLUSIONS AND

FUTURE PROSPECTIVES

CHAPTER 10. CONCLUSIONS AND FUTURE PROSPECTIVES

Our study assigns for the first time an ATP hydrolyzing activity to human 14-3-3ζ, γ, ε and τ isoforms. Notably the 14-3-3σ isoform had no detectable ATPase activity. The study reported is based on the integrated knowledge from multiple disciplines like biochemistry, molecular biology, bioinformatics, protein structure and function to demonstrate a new hitherto unreported enzymatic activity in 14-3-3 proteins. This is a first step towards identifying the functions that may be dependent on this activity and discovering regulatory molecules/mechanisms that may enhance or attenuate the activity. Since 14-3-3 family is an important for the regulation of many cellular functions, the reported ATPase activity opens up new avenues for further investigation that how any known or unknown functions of 14-3-3 is dependent on this ATPase activity. We hope that this finding also sets aside the controversy long associated with any enzymatic activity of 14-3-3 proteins providing impetus for further in depth investigations. Our mutagenesis results show that this activity can be altered resulting in gain or loss of function. More importantly the 14-3-3 protein emerges as a new fold in the class of ATP binding proteins/chaperones. While the ultra-structural details of the binding pocket, catalytic residues and more importantly the physiological and functional relevance of this ATP hydrolyzing activity remains to be established, our results are likely to provide the necessary impetus for an in depth investigation of this enzymatic activity and its physiological significance. The ATPase activity in active 14-3-3 isoforms (ζ, γ, ε and τ) seem to stem from an unconventional binding pocket.

Based on our *in vitro* results we believe that these 14-3-3 proteins will exhibit similar ATPase activity within the cellular milieu and some of their known functions and perhaps many unknown functions are likely to depend on this activity. The effect

of *in vitro* mutations may also be mimicked by regulatory mechanisms inside the cell to control the various functions.

REFERCENCES:

Aitken, A. (2006). 14-3-3 proteins: a historic overview. Seminars in cancer biology *16*, 162-172.

Aitken, A. (2011). Post-translational modification of 14-3-3 isoforms and regulation of cellular function. Seminars in Cell & Developmental Biology *22*, 673-680.

Aitken, A., Howell, S., Jones, D., Madrazo, J., and Patel, Y. (1995). 14-3-3 alpha and delta are the phosphorylated forms of raf-activating 14-3-3 beta and zeta. In vivo stoichiometric phosphorylation in brain at a Ser-Pro-Glu-Lys MOTIF. The Journal of biological chemistry *270*, 5706-5709.

Alam, R., Hachiya, N., Sakaguchi, M., Kawabata, S.-i., Iwanaga, S., Kitajima, M., Mihara, K., and Omura, T. (1994). cDN A Cloning and Characterization of Mitochondrial Import Stimulation Factor (MSF) Purified from Rat Liver Cytosol. Journal of biochemistry *116*, 416-425.

Ames, B.N. (1966). Assay of inorganic phosphate, total phosphate and phosphatase. Methods in enzymology *8*, 115-118.

Arora, S., Matta, A., Shukla, N.K., Deo, S., and Ralhan, R. (2005). Identification of differentially expressed genes in oral squamous cell carcinoma. Molecular carcinogenesis *42*, 97-108.

Beaudry, P., Cohen, P., Brandel, J., Delasnerie-Laupretre, N., Richard, S., Launay, J., and Laplanche, J. (1999). 14-3-3 protein, neuron-specific enolase, and S-100 protein in cerebrospinal fluid of patients with Creutzfeldt-Jakob disease. Dementia and geriatric cognitive disorders *10*, 40-46.

Bell, R., Munro, J., Russ, C., Powell, J.F., Bruinvels, A., Kerwin, R.W., and Collier, D.A. (2000). Systematic screening of the 14-3-3 eta (η) chain gene for polymorphic variants and case-control analysis in schizophrenia. American journal of medical genetics *96*, 736-743.

Benesch, J.L., Ayoub, M., Robinson, C.V., and Aquilina, J.A. (2008). Small heat shock protein activity is regulated by variable oligomeric substructure. Journal of Biological Chemistry *283*, 28513-28517.

Benndorf, R., Sun, X., Gilmont, R.R., Biederman, K.J., Molloy, M.P., Goodmurphy, C.W., Cheng, H., Andrews, P.C., and Welsh, M.J. (2001). HSP22, a new member of the small heat shock protein superfamily, interacts with mimic of phosphorylated HSP27 (3DHSP27). Journal of Biological Chemistry *276*, 26753-26761.

Berg, D., Holzmann, C., and Riess, O. (2003). 14-3-3 proteins in the nervous system. Nature Reviews Neuroscience *4*, 752-762.

Beyenbach, K.W., and Wieczorek, H. (2006). The V-type H+ ATPase: molecular structure and function, physiological roles and regulation. Journal of Experimental Biology *209*, 577-589.

Bianchet, M.A., Hullihen, J., Pedersen, P.L., and Amzel, L.M. (1998). The 2.8-Å structure of rat liver F1-ATPase: Configuration of a critical intermediate in ATP synthesis/hydrolysis. Proceedings of the National Academy of Sciences *95*, 11065-11070.

Bimston, D., Song, J., Winchester, D., Takayama, S., Reed, J.C., and Morimoto, R.I. (1998). BAG-1, a negative regulator of Hsp70 chaperone activity, uncouples nucleotide hydrolysis from substrate release. The EMBO journal *17*, 6871-6878.

Blennow, K. (2004). Cerebrospinal fluid protein biomarkers for Alzheimer's disease. NeuroRx *1*, 213-225.

Bösl, B., Grimminger, V., and Walter, S. (2006a). The molecular chaperone Hsp104-- a molecular machine for protein disaggregation. Journal of structural biology *156*, 139-148.

Bösl, B., Grimminger, V., and Walter, S. (2006b). The molecular chaperone Hsp104—a molecular machine for protein disaggregation. Journal of structural biology *156*, 139-148.

Boston, P.F., Jackson, P., and Thompson, R. (2006). Human 14-3-3 Protein: Radioimmunoassay, Tissue Distribution, and Cerebrospinal Fluid Levels in Patients with Neurological Disorders. Journal of neurochemistry *38*, 1475-1482.

Brooijmans, N., and Kuntz, I.D. (2003). Molecular recognition and docking algorithms. Annual review of biophysics and biomolecular structure *32*, 335-373.

Bryantsev, A.L., Kurchashova, S.Y., Golyshev, S.A., Polyakov, V.Y., Wunderink, H.F., Kanon, B., Budagova, K.R., Kabakov, A.E., and Kampinga, H.H. (2007). Regulation of stress-induced intracellular sorting and chaperone function of Hsp27 (HspB1) in mammalian cells. The Biochemical journal *407*, 407.

Burkhard, P.R., Landis, T., and Hochstrasser, D.F. (2001). CSF detection of the 14-3-3 protein in unselected patients with dementia. Neurology *56*, 1528-1533.

Chaudhary, J., and Skinner, M.K. (2000). Characterization of a Novel Transcript of 14–3-3 Theta in Sertoli Cells. Journal of andrology *21*, 730-738.

Chen, H.K., Fernandez-Funez, P., Acevedo, S.F., Lam, Y.C., Kaytor, M.D., Fernandez, M.H., Aitken, A., Skoulakis, E., Orr, H.T., and Botas, J. (2003). Interaction of Akt-phosphorylated ataxin-1 with 14-3-3 mediates neurodegeneration in spinocerebellar ataxia type 1. Cell *113*, 457-468.

Cheng, L., Pan, C.-X., Zhang, J.-T., Zhang, S., Kinch, M.S., Li, L., Baldridge, L.A., Wade, C., Hu, Z., and Koch, M.O. (2004). Loss of 14-3-3σ in prostate cancer and its precursors. Clinical cancer research *10*, 3064-3068.

Cichon, S., Schumacher, J., Müller, D.J., Hürter, M., Windemuth, C., Strauch, K., Hemmer, S., Schulze, T.G., Schmidt-Wolf, G., and Albus, M. (2001). A genome screen for genes predisposing to bipolar affective disorder detects a new susceptibility locus on 8q. Human molecular genetics *10*, 2933-2944.

Couture, S.M., Penn, D.L., and Roberts, D.L. (2006). The functional significance of social cognition in schizophrenia: a review. Schizophrenia bulletin *32*, S44-S63.

Craparo, A., Freund, R., and Gustafson, T.A. (1997). 14-3-3 (ε) interacts with the insulin-like growth factor I receptor and insulin receptor substrate I in a phosphoserine-dependent manner. Journal of Biological Chemistry *272*, 11663-11669.

Dalal, S.N., Yaffe, M.B., and DeCaprio, J.A. (2004). 14-3-3 family members act coordinately to regulate mitotic progression. Cell Cycle *3*, 672-677.

Danielle, M.W., Heath, E., Katy, L.G., Huanqin, D., Haian, F., Joanna, M.W., Lixin, Z., and John, A.C. (2011). NMR spectroscopy of 14-3-3zeta reveals a flexible C-terminal extension: differentiation of the chaperone and phosphoserine-binding activities of 14-3-3zeta. Biochemical Journal *437*, 493-503.

DesJarlais, R., Seibel, G., Kuntz, I., Furth, P., Alvarez, J., De Montellano, P.O., DeCamp, D., Babe, L., and Craik, C. (1990). Structure-based design of nonpeptide inhibitors specific for the human immunodeficiency virus 1 protease. Proceedings of the National Academy of Sciences *87*, 6644-6648.

Dougherty, M.K., and Morrison, D.K. (2004). Unlocking the code of 14-3-3. Journal of cell science *117*, 1875-1884.

Dunaway, S., Liu, H.-Y., and Walworth, N.C. (2005). Interaction of 14-3-3 protein with Chk1 affects localization and checkpoint function. Journal of cell science *118*, 39-50.

Ellis, R.J. (2006). Molecular chaperones: assisting assembly in addition to folding. Trends in biochemical sciences *31*, 395-401.

Fan, T., Li, R., Todd, N.W., Qiu, Q., Fang, H.-B., Wang, H., Shen, J., Zhao, R.Y., Caraway, N.P., and Katz, R.L. (2007). Up-regulation of 14-3-3ζ in lung cancer and its implication as prognostic and therapeutic target. Cancer research *67*, 7901-7906.

Fenton, W.A., Kashi, Y., Furtak, K., and Norwich, A.L. (1994). Residues in chaperonin GroEL required for polypeptide binding and release.

Forrest, A., and Gabrielli, B. (2001). Cdc25B activity is regulated by 14-3-3. Oncogene *20*, 4393-4401.

Fountoulakis, M., Cairns, N., and Lubec, G. (1999). Increased levels of 14-3-3 gamma and epsilon proteins in brain of patients with Alzheimer's disease and Down syndrome. Journal of neural transmission Supplementum *57*, 323-335.

Freeman, B., Myers, M., Schumacher, R., and Morimoto, R. (1995). Identification of a regulatory motif in Hsp70 that affects ATPase activity, substrate binding and interaction with HDJ-1. The EMBO journal *14*, 2281.

Fu, H., Subramanian, R.R., and Masters, S.C. (2000). 14-3-3 proteins: structure, function, and regulation. Science Signalling *40*, 617-647.

.

Fujii, K., Uchikawa, H., Tanabe, Y., Omata, T., Nonaka, I., and Kohno, Y. (2012). 14-3-3 Proteins, particularly of the epsilon isoform, are detectable in cerebrospinal fluids of cerebellar diseases in children. Brain and Development.

Futai, M., Nakanishi-Matsui, M., Okamoto, H., Sekiya, M., and Nakamoto, R.K. (2012). Rotational catalysis in proton pumping ATPases: From< i> E. coli</i> F-ATPase to mammalian V-ATPase. Biochimica et Biophysica Acta (BBA)-Bioenergetics *1817*, 1711-1721.

Ganguly, S., Weller, J.L., Ho, A., Chemineau, P., Malpaux, B., and Klein, D.C. (2005). Melatonin synthesis: 14-3-3-dependent activation and inhibition of arylalkylamine N-acetyltransferase mediated by phosphoserine-205. Proceedings of the National Academy of Sciences of the United States of America *102*, 1222-1227.

Gardino, A.K., Smerdon, S.J., and Yaffe, M.B. (2006). Structural determinants of 14-3-3 binding specificities and regulation of subcellular localization of 14-3-3-ligand complexes: a comparison of the X-ray crystal structures of all human 14-3-3 isoforms. Seminars in cancer biology *16*, 173-182.

Gardino, A.K., and Yaffe, M.B. (2011). 14-3-3 proteins as signaling integration points for cell cycle control and apoptosis. Seminars in Cell & Developmental Biology *22*, 688-695.

Gehlhaar, D.K., Verkhivker, G.M., Rejto, P.A., Sherman, C.J., Fogel, D.R., Fogel, L.J., and Freer, S.T. (1995). Molecular recognition of the inhibitor AG-1343 by HIV-1 protease: conformationally flexible docking by evolutionary programming. Chemistry & biology *2*, 317-324.

Glide, v., Schrödinger, LLC, New York, NY, 2011; http://www.schrodinger.com.

Glover, J.R., and Lindquist, S. (1998). Hsp104, Hsp70, and Hsp40: a novel chaperone system that rescues previously aggregated proteins. Cell *94*, 73-82.

Goedert, M. (1996). Tau protein and the neurofibrillary pathology of Alzheimer's disease. In Apolipoprotein E and Alzheimer's Disease (Springer), pp. 103-125.

Goswami, A.V., Chittoor, B., and D'Silva, P. (2010). Understanding the functional interplay between mammalian mitochondrial Hsp70 chaperone machine components. Journal of Biological Chemistry *285*, 19472-19482.

Götz, J., Eckert, A., Matamales, M., Ittner, L.M., and Liu, X. (2011). Modes of Aβ toxicity in Alzheimer's disease. Cellular and Molecular Life Sciences *68*, 3359-3375.

Green, A., Thompson, E., Stewart, G., Zeidler, M., McKenzie, J., MacLeod, M., Ironside, J., Will, R., and Knight, R. (2001). Use of 14–3–3 and other brain-specific proteins in CSF in the diagnosis of variant Creutzfeldt-Jakob disease. Journal of Neurology, Neurosurgery & Psychiatry *70*, 744-748.

Greicius, M.D., Srivastava, G., Reiss, A.L., and Menon, V. (2004). Default-mode network activity distinguishes Alzheimer's disease from healthy aging: evidence from functional MRI. Proceedings of the National Academy of Sciences of the United States of America *101*, 4637-4642.

Grimminger, V., Richter, K., Imhof, A., Buchner, J., and Walter, S. (2004). The prion curing agent guanidinium chloride specifically inhibits ATP hydrolysis by Hsp104. Journal of Biological Chemistry *279*, 7378-7383.

Guo, Z., Mohanty, U., Noehre, J., Sawyer, T.K., Sherman, W., and Krilov, G. (2010). Probing the α-Helical Structural Stability of Stapled p53 Peptides: Molecular Dynamics Simulations and Analysis. Chemical biology & drug design *75*, 348-359.

Hachiya, N., Alam, R., Sakasegawa, Y., Sakaguchi, M., Mihara, K., and Omura, T. (1993). A mitochondrial import factor purified from rat liver cytosol is an ATP-dependent conformational modulator for precursor proteins. The EMBO journal *12*, 1579.

Hachiya, N., Komiya, T., Alam, R., Iwahashi, J., Sakaguchi, M., Omura, T., and Mihara, K. (1994). MSF, a novel cytoplasmic chaperone which functions in precursor targeting to mitochondria. Embo J *13*, 5146-5154.

Harrison, C.J., Hayer-Hartl, M., Di Liberto, M., Hartl, F.-U., and Kuriyan, J. (1997). Crystal structure of the nucleotide exchange factor GrpE bound to the ATPase domain of the molecular chaperone DnaK. Science *276*, 431-435.

Haslbeck, M., Franzmann, T., Weinfurtner, D., and Buchner, J. (2005). Some like it hot: the structure and function of small heat-shock proteins. Nature structural & molecular biology *12*, 842-846.

Henriksson, M.L., Francis, M.S., Peden, A., Aili, M., Stefansson, K., Palmer, R., Aitken, A., and Hallberg, B. (2002). A nonphosphorylated 14-3-3 binding motif on exoenzyme S that is functional in vivo. European Journal of Biochemistry *269*, 4921-4929.

Hermeking, H. (2003). The 14-3-3 cancer connection. Nature Reviews Cancer *3*, 931-943.

Hermeking, H., and Benzinger, A. (2006). 14-3-3 proteins in cell cycle regulation. Paper presented at: Seminars in cancer biology (Elsevier).

Hernández, F., Cuadros, R., and Avila, J. (2004). Zeta 14-3-3 protein favours the formation of human tau fibrillar polymers. Neuroscience letters *357*, 143-146.

Higgs, B., Elashoff, M., Richman, S., and Barci, B. (2006). An online database for brain disease research. BMC genomics *7*, 70.

Hirata, T., Iwamoto-Kihara, A., Sun-Wada, G.-H., Okajima, T., Wada, Y., and Futai, M. (2003). Subunit rotation of vacuolar-type proton pumping ATPase relative rotation of the G and C subunits. Journal of Biological Chemistry *278*, 23714-23719.

Horie, M., Suzuki, M., Takahashi, E.-i., and Tanigami, A. (1999). Cloning, expression, and chromosomal mapping of the human 14-3-3gamma gene (YWHAG) to 7q11. 23. Genomics *60*, 241.

Horváth, S., Janka, Z., and Mirnics, K. (2011). Analyzing schizophrenia by DNA microarrays. Biological psychiatry *69*, 157-162.

Horwich, A.L., Fenton, W.A., Chapman, E., and Farr, G.W. (2007). Two families of chaperonin: physiology and mechanism. Annu Rev Cell Dev Biol *23*, 115-145.

160

Hosing, A.S., Kundu, S.T., and Dalal, S.N. (2008). 14-3-3 Gamma is required to enforce both the incomplete S phase and G2 DNA damage checkpoints. Cell Cycle *7*, 3171-3179.

Hsich, G., Kenney, K., Gibbs Jr, C.J., Lee, K.H., and Harrington, M.G. (1996). The 14-3-3 brain protein in cerebrospinal fluid as a marker for transmissible spongiform encephalopathies. New England Journal of Medicine *335*, 924-930.

Ichimura, T., Isobe, T., Okuyama, T., Yamauchi, T., and Fujisawa, H. (1987). Brain 14-3-3 protein is an activator protein that activates tryptophan 5-monooxygenase and tyrosine 3-monooxygenase in the presence of Ca^{2+}, calmodulin-dependent protein kinase II. FEBS letters *219*, 79-82.

Ida, K., Noumi, T., Maeda, M., Fukui, T., and Futai, M. (1991). Catalytic site of F1-ATPase of Escherichia coli. Lys-155 and Lys-201 of the beta subunit are located near the gamma-phosphate group of ATP in the presence of Mg2+. Journal of Biological Chemistry *266*, 5424-5429.

Ivey, D.M., and Ljungdahl, L.G. (1986). Purification and characterization of the F1-ATPase from Clostridium thermoaceticum. Journal of bacteriology *165*, 252-257.

Jaiswal, H., Conz, C., Otto, H., Wölfle, T., Fitzke, E., Mayer, M.P., and Rospert, S. (2011). The chaperone network connected to human ribosome-associated complex. Molecular and cellular biology *31*, 1160-1173.

Jia, Y., Yu, X., Zhang, B., Yuan, Y., Xu, Q., Shen, Y., and Shen, Y. (2004). An association study between polymorphisms in three genes of 14-3-3 (tyrosine 3-monooxygenase/tryptophan 5-monooxygenase activation protein) family and paranoid schizophrenia in northern Chinese population. European psychiatry *19*, 377-379.

Johnson, K.M., Chen, X., Boitano, A., Swenson, L., Opipari Jr, A.W., and Glick, G.D. (2005). Identification and Validation of the Mitochondrial F_1F_0-ATPase as the Molecular Target of the Immunomodulatory Benzodiazepine Bz-423. Chemistry & biology *12*, 485-496.

Kappé, G., Boelens, W.C., and de Jong, W.W. (2010). Why proteins without an α-crystallin domain should not be included in the human small heat shock protein family HSPB. Cell Stress and Chaperones *15*, 457-461.

Kawamoto, Y., Akiguchi, I., Nakamura, S., Honjyo, Y., Shibasaki, H., and Budka, H. (2002). 14-3-3 proteins in Lewy bodies in Parkinson disease and diffuse Lewy body disease brains. Journal of Neuropathology & Experimental Neurology *61*, 245-253.

Kiang, J.G., and Tsokos, G.C. (1998). Heat shock protein 70 kDa: molecular biology, biochemistry, and physiology. Pharmacology & therapeutics *80*, 183-201.

Komiya, T., Hachiya, N., Sakaguchi, M., Omura, T., and Mihara, K. (1994). Recognition of mitochondria-targeting signals by a cytosolic import stimulation factor, MSF. Journal of Biological Chemistry *269*, 30893-30897.

Komiya, T., and Mihara, K. (1996). Protein import into mammalian mitochondria. Characterization of the intermediates along the import pathway of the precursor into the matrix. J Biol Chem *271*, 22105-22110.

Komiya, T., Sakaguchi, M., and Mihara, K. (1996). Cytoplasmic chaperones determine the targeting pathway of precursor proteins to mitochondria. Embo J *15*, 399-407.

Kunapuli, S., and Daniel, J. (1998). P2 receptor subtypes in the cardiovascular system. Biochem J *336*, 513-523.

Layfield, R., Fergusson, J., Aitken, A., Lowe, J., Landon, M., and Mayer, R.J. (1996). Neurofibrillary tangles of Alzheimer's disease brains contain 14-3-3 proteins. Neuroscience letters *209*, 57-60.

Lee, V.M. (1995). Disruption of the cytoskeleton in Alzheimer's disease. Current opinion in neurobiology *5*, 663-668.

Li, X., Wang, Q.J., Pan, N., Lee, S., Zhao, Y., Chait, B.T., and Yue, Z. (2011). Phosphorylation-dependent 14-3-3 binding to LRRK2 is impaired by common mutations of familial Parkinson's disease. PLoS One *6*, e17153.

Lim, G., Piske, M., and Johnson, J. (2013). 14-3-3 proteins are essential signalling hubs for beta cell survival. Diabetologia, 1-13.

Lin, M., Morrison, C.D., Jones, S., Mohamed, N., Bacher, J., and Plass, C. (2009). Copy number gain and oncogenic activity of YWHAZ/14-3-3ζ in head and neck squamous cell carcinoma. International journal of cancer *125*, 603-611.

Liu, D., Bienkowska, J., Petosa, C., Collier, R.J., Fu, H., and Liddington, R. (1995). Crystal structure of the zeta isoform of the 14-3-3 protein. Nature *376*, 191-194.

Liu, Y.-C., Liu, Y., Elly, C., Yoshida, H., Lipkowitz, S., and Altman, A. (1997). Serine phosphorylation of Cbl induced by phorbol ester enhances its association with 14-3-3 proteins in T cells via a novel serine-rich 14-3-3-binding motif. Journal of Biological Chemistry *272*, 9979-9985.

Liu, Y., Tian, R.-f., Li, Y.-m., Liu, W.-p., Cao, L., Yang, X.-l., Cao, W.-d., and Zhang, X. (2010). The expression of seven 14-3-3 isoforms in human meningioma. Brain research *1336*, 98-102.

Löbau, S., Weber, J., Wilke-Mounts, S., and Senior, A.E. (1997). F1-ATPase, roles of three catalytic site residues. Journal of Biological Chemistry *272*, 3648-3656.

Luniwal, A., Wang, L., Pavlovsky, A., Erhardt, P.W., and Viola, R.E. (2012). Molecular docking and enzymatic evaluation to identify selective inhibitors of aspartate semialdehyde dehydrogenase. Bioorganic & medicinal chemistry *20*, 2950-2956.

Macdonald, N., Welburn, J.P., Noble, M.E., Nguyen, A., Yaffe, M.B., Clynes, D., Moggs, J.G., Orphanides, G., Thomson, S., and Edmunds, J.W. (2005). Molecular basis for the recognition of phosphorylated and phosphoacetylated histone h3 by 14-3-3. Molecular cell *20*, 199-211.

Mackie, S., and Aitken, A. (2005). Novel brain 14-3-3 interacting proteins involved in neurodegenerative disease. FEBS Journal *272*, 4202-4210.

MacRae, T. (2000). Structure and function of small heat shock/α-crystallin proteins: established concepts and emerging ideas. Cellular and Molecular Life Sciences CMLS *57*, 899-913.

Matta, A., Bahadur, S., Duggal, R., Gupta, S.D., and Ralhan, R. (2007). Over-expression of 14-3-3zeta is an early event in oral cancer. BMC cancer *7*, 169.

Mayer, M., and Bukau, B. (2005). Hsp70 chaperones: cellular functions and molecular mechanism. Cellular and Molecular Life Sciences *62*, 670-684.

Mayer, M.P. (2010). Gymnastics of molecular chaperones. Molecular cell *39*, 321-331.

Mchaourab, H.S., Godar, J.A., and Stewart, P.L. (2009). Structure and mechanism of protein stability sensors: chaperone activity of small heat shock proteins. Biochemistry *48*, 3828-3837.

McLaughlin, S.H., Smith, H.W., and Jackson, S.E. (2002). Stimulation of the weak ATPase activity of human hsp90 by a client protein. Journal of molecular biology *315*, 787-798.

Meehan, K.L., and Sadar, M.D. (2004). Quantitative profiling of LNCaP prostate cancer cells using isotope-coded affinity tags and mass spectrometry. Proteomics *4*, 1116-1134.

Meller, N., Elitzur, Y., and Isakov, N. (1999). Protein kinase C-θ (PKCθ) distribution analysis in hematopoietic cells: proliferating T cells exhibit high proportions of PKCθ in the particulate fraction. Cellular immunology *193*, 185-193.

Moore, B., Perez, V., and Carlson, F. (1967). Physiological and biochemical aspects of nervous integration. Englewood Cliffs, NJ: Prentice-Hall, 343-359.

Muratake, T., Hayashi, S., Ichikawa, T., Kumanishi, T., Ichimura, Y., Kuwano, R., Isobe, T., Wang, Y., Minoshima, S., and Shimizu, N. (1996). Structural organization and chromosomal assignment of the human 14-3-3 η chain gene (YWHAH). Genomics *36*, 63-69.

Muslin, A.J., Tanner, J.W., Allen, P.M., and Shaw, A.S. (1996). Interaction of 14-3-3 with signaling proteins is mediated by the recognition of phosphoserine. Cell *84*, 889-897.

Mymrikov, E.V., Seit-Nebi, A.S., and Gusev, N.B. (2011). Large potentials of small heat shock proteins. Physiological Reviews *91*, 1123-1159.

Nakanishi-Matsui, M., Sekiya, M., Nakamoto, R.K., and Futai, M. (2010). The mechanism of rotating proton pumping ATPases. Biochimica et Biophysica Acta (BBA)-Bioenergetics *1797*, 1343-1352.

Neal, C.L., Xu, J., Li, P., Mori, S., Yang, J., Neal, N.N., Zhou, X., Wyszomierski, S.L., and Yu, D. (2011). Overexpression of 14-3-3ζ in cancer cells activates PI3K via binding the p85 regulatory subunit. Oncogene *31*, 897-906.

Neal, C.L., Yao, J., Yang, W., Zhou, X., Nguyen, N.T., Lu, J., Danes, C.G., Guo, H., Lan, K.-H., and Ensor, J. (2009). 14-3-3ζ overexpression defines high risk for breast cancer recurrence and promotes cancer cell survival. Cancer research *69*, 3425-3432.

Nichols, R.J., Dzamko, N., Morrice, N.A., Campbell, D.G., Deak, M., Ordureau, A., Macartney, T., Tong, Y., Shen, J., and Prescott, A.R. (2010). 14-3-3 binding to LRRK2 is disrupted by multiple Parkinson's disease-associated mutations and regulates cytoplasmic localization. Biochemical Journal *430*, 393-404.

Obsil, T., Ghirlando, R., Klein, D.C., Ganguly, S., and Dyda, F. (2001). Crystal structure of the 14-3-3zeta:serotonin N-acetyltransferase complex. a role for scaffolding in enzyme regulation. Cell *105*, 257-267.

Olson, C.L., Nadeau, K.C., Sullivan, M.A., Winquist, A.G., Donelson, J.E., Walsh, C.T., and Engman, D.M. (1994). Molecular and biochemical comparison of the 70-kDa heat shock proteins of Trypanosoma cruzi. Journal of Biological Chemistry *269*, 3868-3874.

Omi, K., Hachiya, N.S., Tanaka, M., Tokunaga, K., and Kaneko, K. (2008). 14-3-3zeta is indispensable for aggregate formation of polyglutamine-expanded huntingtin protein. Neuroscience letters *431*, 45-50.

Omote, H., Le, N.P., Park, M.-Y., Maeda, M., and Futai, M. (1995). β subunit Glu-185 of Escherichia coli H+-ATPase (ATP synthase) is an essential residue for cooperative catalysis. Journal of Biological Chemistry *270*, 25656-25660.

Omote, H., Maeda, M., and Futai, M. (1992). Effects of mutations of conserved Lys-155 and Thr-156 residues in the phosphate-binding glycine-rich sequence of the F1-ATPase beta subunit of Escherichia coli. Journal of Biological Chemistry *267*, 20571-20576.

Orriss, G.L., Leslie, A.G., Braig, K., and Walker, J.E. (1998). Bovine F< sub> 1</sub>-ATPase covalently inhibited with 4-chloro-7-nitrobenzofurazan: the structure provides further support for a rotary catalytic mechanism. Structure *6*, 831-837.

Owen, B.A., Sullivan, W.P., Felts, S.J., and Toft, D.O. (2002). Regulation of heat shock protein 90 ATPase activity by sequences in the carboxyl terminus. Journal of Biological Chemistry *277*, 7086-7091.

Penefsky, H.S., and Cross, R. (1991). Structure and mechanism of FoF1-type ATP synthases and ATPases. Adv Enzymol Relat Areas Mol Biol *64*, 173-214.

Picard, D. (2002). Heat-shock protein 90, a chaperone for folding and regulation. Cellular and Molecular Life Sciences CMLS *59*, 1640-1648.

Prasad, G., Valverius, E., McDuffie, E., and Cooper, H. (1992). Complementary DNA cloning of a novel epithelial cell marker protein, HME1, that may be down-regulated in neoplastic mammary cells. Cell growth & differentiation: the molecular biology journal of the American Association for Cancer Research *3*, 507.

Prodromou, C., Roe, S.M., O'Brien, R., Ladbury, J.E., Piper, P.W., and Pearl, L.H. (1997). Identification and structural characterization of the ATP/ADP-binding site in the Hsp90 molecular chaperone. Cell *90*, 65-75.

Ralevic, V., and Burnstock, G. (2003). Involvement of purinergic signaling in cardiovascular diseases. Drug News Perspect *16*, 133-140.

Ramteke, M.P., Shelke, P., Ramamoorthy, V., Somavarapu, A.K., Gautam, A.K.S., Nanaware, P.P., Karanam, S., Mukhopadhyay, S., and Venkatraman, P. (2014). Identification of a novel ATPase activity in 14-3-3 proteins–Evidence from enzyme kinetics, structure guided modeling and mutagenesis studies. FEBS letters *588*, 71-78.

Reuther, G.W., and Pendergast, A.M. (1996). The roles of 14-3-3 proteins in signal transduction. Vitamins & Hormones *52*, 149-175.

Richter, K., Muschler, P., Hainzl, O., and Buchner, J. (2001). Coordinated ATP hydrolysis by the Hsp90 dimer. Journal of Biological Chemistry *276*, 33689-33696.

Rodriguez, F., Arsène-Ploetze, F., Rist, W., Rüdiger, S., Schneider-Mergener, J., Mayer, M.P., and Bukau, B. (2008). Molecular Basis for Regulation of the Heat

Shock Transcription Factor σ< sup> 32</sup> by the DnaK and DnaJ Chaperones. Molecular cell *32*, 347-358.

Rong, J., Li, S., Sheng, G., Wu, M., Coblitz, B., Li, M., Fu, H., and Li, X.J. (2007). 14-3-3 protein interacts with Huntingtin-associated protein 1 and regulates its trafficking. Journal of Biological Chemistry *282*, 4748-4756.

Roseman, A.M., Chen, S., White, H., Braig, K., and Saibil, H.R. (1996). The chaperonin ATPase cycle: mechanism of allosteric switching and movements of substrate-binding domains in GroEL. Cell *87*, 241-251.

Rubio, M.P., Geraghty, K.M., Wong, B.H.C., Wood, N.T., Campbell, D.G., Morrice, N., and Mackintosh, C. (2004). 14-3-3-affinity purification of over 200 human phosphoproteins reveals new links to regulation of cellular metabolism, proliferation and trafficking. Biochemical Journal *379*, 395.

Rush, A.J. (2003). Toward an understanding of bipolar disorder and its origin. The Journal of clinical psychiatry Supplement *64*, 4-8.

Sadis, S., and Hightower, L.E. (1992). Unfolded proteins stimulate molecular chaperone Hsc70 ATPase by accelerating ADP/ATP exchange. Biochemistry *31*, 9406-9412.

Sato, S., Chiba, T., Sakata, E., Kato, K., Mizuno, Y., Hattori, N., and Tanaka, K. (2005). 14-3-3η is a novel regulator of parkin ubiquitin ligase. The EMBO journal *25*, 211-221.

Satoh, K., Tobiume, M., Matsui, Y., Mutsukura, K., Nishida, N., Shiga, Y., Eguhchi, K., Shirabe, S., and Sata, T. (2010). Establishment of a standard 14-3-3 protein assay

of cerebrospinal fluid as a diagnostic tool for Creutzfeldt–Jakob disease. Laboratory investigation *90*, 1637-1644.

Schirmer, E.C., Queitsch, C., Kowal, A.S., Parsell, D.A., and Lindquist, S. (1998). The ATPase activity of Hsp104, effects of environmental conditions and mutations. Journal of Biological Chemistry *273*, 15546-15552.

Schirmer, E.C., Ware, D.M., Queitsch, C., Kowal, A.S., and Lindquist, S.L. (2001). Subunit interactions influence the biochemical and biological properties of Hsp104. Proceedings of the National Academy of Sciences *98*, 914-919.

Shin, R., Jez, J.M., Basra, A., Zhang, B., and Schachtman, D.P. (2011). 14-3-3 Proteins fine-tune plant nutrient metabolism. FEBS letters *585*, 143-147.

Shivakumar, D., Williams, J., Wu, Y., Damm, W., Shelley, J., and Sherman, W. (2010). Prediction of absolute solvation free energies using molecular dynamics free energy perturbation and the OPLS force field. Journal of Chemical Theory and Computation *6*, 1509-1519.

Sluchanko, N.N., and Gusev, N.B. (2011). Probable participation of 14-3-3 in tau protein oligomerization and aggregation. J Alzheimers Dis *27*, 467-476.

Sondermann, H., Scheufler, C., Schneider, C., Höhfeld, J., Hartl, F.-U., and Moarefi, I. (2001). Structure of a Bag/Hsc70 complex: convergent functional evolution of Hsp70 nucleotide exchange factors. Science *291*, 1553-1557.

Spiess, C., Meyer, A.S., Reissmann, S., and Frydman, J. (2004). Mechanism of the eukaryotic chaperonin: protein folding in the chamber of secrets. Trends in cell biology *14*, 598-604.

Steinacker, P., Aitken, A., and Otto, M. (2011). 14-3-3 proteins in neurodegeneration. Seminars in cell & developmental biology *22*, 696-704.

Sugiyama, Y., Suzuki, A., Kishikawa, M., Akutsu, R., Hirose, T., Waye, M.M., Tsui, S.K., Yoshida, S., and Ohno, S. (2000). Muscle develops a specific form of small heat shock protein complex composed of MKBP/HSPB2 and HSPB3 during myogenic differentiation. Journal of Biological Chemistry *275*, 1095-1104.

Szabo, A., Langer, T., Schröder, H., Flanagan, J., Bukau, B., and Hartl, F.U. (1994). The ATP hydrolysis-dependent reaction cycle of the Escherichia coli Hsp70 system DnaK, DnaJ, and GrpE. Proceedings of the National Academy of Sciences *91*, 10345-10349.

Tada, K., Oka, M., Tangoku, A., Hayashi, H., Oga, A., and Sasaki, K. (2000). Gains of 8q23-qter and 20q and loss of 11q22-qter in esophageal squamous cell carcinoma associated with lymph node metastasis. Cancer *88*, 268-273.

Tanabe, M., Ishida, R., Izuhara, F., Komatsuda, A., Wakui, H., Sawada, K., Otaka, M., Nakamura, N., and Itoh, H. (2012). The ATPase activity of molecular chaperone HSP60 is inhibited by immunosuppressant mizoribine. American Journal of Molecular Biology *2*, 93-102.

Telles, E., Hosing, A.S., Kundu, S.T., Venkatraman, P., and Dalal, S.N. (2009). A novel pocket in 14-3-3ε is required to mediate specific complex formation with cdc25C and to inhibit cell cycle progression upon activation of checkpoint pathways. Experimental cell research *315*, 1448-1457.

Tissiéres, A., Mitchell, H.K., and Tracy, U.M. (1974). Protein synthesis in salivary glands of< i> Drosophila melanogaster</i>: Relation to chromosome puffs. Journal of molecular biology *84*, 389-398.

Toker, A., ELLIS, C.A., SELLERS, L.A., and AITKEN, A. (1990). Protein kinase C inhibitor proteins. European Journal of Biochemistry *191*, 421-429.

Toyooka, K., Muratake, T., Tanaka, T., Igarashi, S., Watanabe, H., Takeuchi, H., Hayashi, S., Maeda, M., Takahashi, M., and Tsuji, S. (1999). 14-3-3 protein η chain gene (YWHAH) polymorphism and its genetic association with schizophrenia. American journal of medical genetics *88*, 164-167.

Tsuang, M.T. (2002). Family, twin, and adoption studies of bipolar disease. Current psychiatry reports *4*, 130-133.

Ubl, A., Berg, D., Holzmann, C., Krüger, R., Berger, K., Arzberger, T., Bornemann, A., and Riess, O. (2002). 14-3-3 protein is a component of Lewy bodies in Parkinson's disease—Mutation analysis and association studies of< i> 14-3-3 eta</i>. Molecular brain research *108*, 33-39.

Umahara, T., and Uchihara, T. (2010). 14-3-3 proteins and spinocerebellar ataxia type 1: from molecular interaction to human neuropathology. The Cerebellum *9*, 183-189.

Umahara, T., Uchihara, T., Tsuchiya, K., Nakamura, A., Iwamoto, T., Ikeda, K., and Takasaki, M. (2004). 14-3-3 proteins and zeta isoform containing neurofibrillary tangles in patients with Alzheimer's disease. Acta neuropathologica *108*, 279-286.

Varga, M., Magnusson, A., Flekkøy, K., David, A.S., and Opjordsmoen, S. (2007). Clinical and neuropsychological correlates of insight in schizophrenia and bipolar I disorder: does diagnosis matter? Comprehensive psychiatry *48*, 583-591.

Vercoutter-Edouart, A.-S., Lemoine, J., Le Bourhis, X., Louis, H., Boilly, B., Nurcombe, V., Révillion, F., Peyrat, J.-P., and Hondermarck, H. (2001). Proteomic analysis reveals that 14-3-3σ is down-regulated in human breast cancer cells. Cancer research *61*, 76-80.

VLifeMDS, V., VLife Sciences Technologies Pvt. Ltd., Pune, India 2012; http://www.vlifesciences.com.

Wakui, H., Wright, A.P., Gustafsson, J.-Å., and Zilliacus, J. (1997). Interaction of the ligand-activated glucocorticoid receptor with the 14-3-3η protein. Journal of Biological Chemistry *272*, 8153-8156.

Wang, B., Yang, H., Liu, Y.-C., Jelinek, T., Zhang, L., Ruoslahti, E., and Fu, H. (1999). Isolation of high-affinity peptide antagonists of 14-3-3 proteins by phage display. Biochemistry *38*, 12499-12504.

Waterman, M.J.F., Stavridi, E.S., Waterman, J.L.F., and Halazonetis, T.D. (1998). ATM-dependent activation of p53 involves dephosphorylation and association with 14-3-3 proteins. Nature genetics *19*, 175-178.

Weber, T., Otto, M., Bodemer, M., and Zerr, I. (1997). Diagnosis of Creutzfeldt-Jakob disease and related human spongiform encephalopathies. Biomedicine & pharmacotherapy= Biomedecine & pharmacotherapie *51*, 381.

Whitesell, L., and Lindquist, S.L. (2005). HSP90 and the chaperoning of cancer. Nature Reviews Cancer *5*, 761-772.

Wiltfang, J., Otto, M., Baxter, H., Bodemer, M., Steinacker, P., Bahn, E., Zerr, I., Kornhuber, J., Kretzschmar, H., and Poser, S. (1999). Isoform Pattern of 14-3-3 Proteins in the Cerebrospinal Fluid of Patients with Creutzfeldt-Jakob Disease. Journal of neurochemistry *73*, 2485-2490.

Wink, M., Braganhol, E., Tamajusuku, A., Lenz, G., Zerbini, L., Libermann, T., Sevigny, J., Battastini, A., and Robson, S. (2006). Nucleoside triphosphate diphosphohydrolase-2 (NTPDase2/CD39L1) is the dominant ectonucleotidase expressed by rat astrocytes. Neuroscience *138*, 421-432.

Winokur, G., Coryell, W., Keller, M., Endicott, J., and Leon, A. (1995). A family study of manic-depressive (bipolar I) disease: is it a distinct illness separable from primary unipolar depression? Archives of general psychiatry *52*, 367.

Winter, S., Fischle, W., and Seiser, C. (2008). Modulation of 14-3-3 interaction with phosphorylated histone H3 by combinatorial modification patterns. Cell Cycle *7*, 1336-1342.

Wong, A., Macciardi, F., Klempan, T., Kawczynski, W., Barr, C., Lakatoo, S., Wong, M., Buckle, C., Trakalo, J., and Boffa, E. (2003). Identification of candidate genes for psychosis in rat models, and possible association between schizophrenia and the 14-3-3η gene. Molecular psychiatry *8*, 156-166.

Wong, A.H., Likhodi, O., Trakalo, J., Yusuf, M., Sinha, A., Pato, C.N., Pato, M.T., Van Tol, H.H., and Kennedy, J.L. (2005). Genetic and post-mortem mRNA analysis

of the 14-3-3 genes that encode phosphoserine/threonine-binding regulatory proteins in schizophrenia and bipolar disorder. Schizophrenia research *78*, 137-146.

Yacoubian, T.A., Slone, S.R., Harrington, A.J., Hamamichi, S., Schieltz, J.M., Caldwell, K.A., Caldwell, G.A., and Standaert, D.G. (2010). Differential neuroprotective effects of 14-3-3 proteins in models of Parkinson's disease. Cell death & disease *1*, e2.

Yaffe, M.B., Rittinger, K., Volinia, S., Caron, P.R., Aitken, A., Leffers, H., Gamblin, S.J., Smerdon, S.J., and Cantley, L.C. (1997a). The structural basis for 14-3-3: phosphopeptide binding specificity. Cell *91*, 961-971.

Yaffe, M.B., Rittinger, K., Volinia, S., Caron, P.R., Aitken, A., Leffers, H., Gamblin, S.J., Smerdon, S.J., and Cantley, L.C. (1997b). The structural basis for 14-3-3:phosphopeptide binding specificity. Cell *91*, 961-971.

Yano, M., Mori, S., Niwa, Y., Inoue, M., and Kido, H. (1997). Intrinsic nucleoside diphosphate kinase-like activity as a novel function of 14-3-3 proteins. FEBS letters *419*, 244-248.

Yano, M., Nakamuta, S., Wu, X., Okumura, Y., and Kido, H. (2006). A novel function of 14-3-3 protein: 14-3-3ζ is a heat-shock–related molecular chaperone that dissolves thermal-aggregated proteins. Molecular biology of the cell *17*, 4769-4779.

Yifrach, O., and Horovitz, A. (1995). Nested cooperativity in the ATPase activity of the oligomeric chaperonin GroEL. Biochemistry *34*, 5303-5308.

Young, J.C., and Hartl, F.U. (2000). Polypeptide release by Hsp90 involves ATP hydrolysis and is enhanced by the co-chaperone p23. The EMBO journal *19*, 5930-5940.

Yu, M., Guo, H.-X., Wang, X.-H., Li, C.-Y., Zhan, Y.-Q., Ge, C.-H., and Yang, X.-M. (2013). 14-3-3ζ interacts with hepatocyte nuclear factor 1α and enhances its DNA binding and transcriptional activation. Biochimica et Biophysica Acta (BBA)-Gene Regulatory Mechanisms.

Zegzouti, H., Zdanovskaia, M., Hsiao, K., and Goueli, S.A. (2009). ADP-Glo: a bioluminescent and homogeneous ADP monitoring assay for kinases. Assay and drug development technologies *7*, 560-572.

Zerr, I., Bodemer, M., Gefeller, O., Otto, M., Poser, S., Wiltfang, J., Windl, O., Kretzschmar, H.A., and Weber, T. (1998). Detection of 14-3-3 protein in the cerebrospinal fluid supports the diagnosis of Creutzfeldt-Jakob disease. Annals of neurology *43*, 32-40.

Zerr, I., Bodemer, M., Gefeller, O., Otto, M., Poser, S., Wiltfang, J., Windl, O., Kretzschmar, H.A., and Weber, T. (2004). Detection of 14-3-3 protein in the cerebrospinal fluid supports the diagnosis of Creutzfeldt-Jakob disease. Annals of neurology *43*, 32-40.

Zerr, I., Pocchiari, M., Collins, S., Brandel, J., de Pedro Cuesta, J., Knight, R., Bernheimer, H., Cardone, F., Delasnerie-Lauprêtre, N., and Corrales, N.C. (2000). Analysis of EEG and CSF 14-3-3 proteins as aids to the diagnosis of Creutzfeldt–Jakob disease. Neurology *55*, 811-815.

Zhang, H., Rajasekaran, N.S., Orosz, A., Xiao, X., Rechsteiner, M., and Benjamin, I.J. (2010). Selective degradation of aggregate-prone CryAB mutants by HSPB1 is mediated by ubiquitin–proteasome pathways. Journal of molecular and cellular cardiology *49*, 918-930.

Zhao, J., Meyerkord, C.L., Du, Y., Khuri, F.R., and Fu, H. (2011). 14-3-3 proteins as potential therapeutic targets. Seminars in Cell & Developmental Biology *22*, 705-712.

Identification of a novel ATPase activity in 14-3-3 proteins – Evidence from enzyme kinetics, structure guided modeling and mutagenesis studies

Manoj P. Ramteke [a], Pradnya Shelke [a], Vidhya Ramamoorthy [a], Arun Kumar Somavarapu [a], Amit Kumar Singh Gautam [a], Padma P. Nanaware [a], Sudheer Karanam [b], Sami Mukhopadhyay [b], Prasanna Venkatraman [a,*]

[a] *Advanced Centre for Treatment, Research and Education in Cancer (ACTREC), Tata Memorial Centre (TMC), Kharghar, Navi Mumbai 410210, India*
[b] *Vlife Sciences Technologies Pvt. Ltd., 2nd Floor, Plot No-05, Ram Indu Park, Baner Road, Pune 411045, India*

ARTICLE INFO

ABSTRACT

14-3-3 Proteins bind phosphorylated sequences in proteins and regulate multiple cellular functions. For the first time, we show that pure recombinant human 14-3-3 ζ, γ, ε and τ isofoms hydrolyze ATP with similar K_m and k_{cat} values. In sharp contrast the sigma isoform has no detectable activity. Docking studies identify two putative binding pockets in 14-3-3 zeta. Mutation of D124A in the amphipathic pocket enhances binding affinity and catalysis. Mutation of a critical Arg (R55A) at the dimer interface in zeta reduces binding and decreases catalysis. These experimental results coincide with a binding pose at the dimer interface. This newly identified function could be a moon lighting function in some of these isoforms.

© 2013 Federation of European Biochemical Societies. Published by Elsevier B.V. All rights reserved.

1. Introduction

14-3-3 proteins (β, γ, ε, η, σ, τ and ζ isoforms) are an important family of highly conserved dimeric proteins. They bind to Ser/Thr phosphorylated proteins through two major consensus motifs, RSXpSXP (mode I) and RXY/FXpSXP (mode II), where pS represents phosphoserine [1–3] and a third minor binding motif pS/pT(X 1–2)-COOH (mode III) where pT represent phosphothreonine [4]. These proteins are involved in cell metabolism, signal transduction, cell cycle control, apoptosis, protein trafficking, transcription and stress response as well as in malignant transformation [5–9]. These functions have been attributed primarily to their ability to bind to

phosphorylated sequences within the client proteins [10–13]. In addition to these well known adaptor functions, 14-3-3τ was shown to possess an ATP/ADP exchange activity [14]. In rat liver, mitochondrial import function of a cytosolic 14-3-3 seemed to require energy from ATP hydrolysis [15–18]. Of late *Drosophila* 14-3-3ζ in conjunction with Hsp70 was shown to solubilize aggregated proteins in an ATP dependent manner although whether this function is dependent on energy from ATP hydrolysis has not been demonstrated so far [19]. This disaggregating function seems analogous to yeast Hsp104 which is probably the only other chaperone well known to solubilize preformed aggregates. No such activity has been identified in any mammalian proteins but mammalian 14-3-3ζ seems to affect aggregation of tau and huntingtin [20–22].

These observations caught our attention as these ATP dependent activity of 14-3-3 is not a major focus of research and any enzymatic activity of 14-3-3 seems controversial [23]. Prompted, we asked if human 14-3-3ζ has any detectable ATPase activity. If so identifying residues involved in ATP binding/hydrolysis is likely to better define the enzymatic property associated with the 14-3-3 protein which is otherwise well known for its scaffold and chaperone-like functions. Here we report the in vitro characterization of ATPase activity of 14-3-3ζ and identify residues that are important

for binding/hydrolysis. By virtue of residue/structure conservation 14-3-3 γ, ε and τ isoforms also show similar ATPase activity while the sigma isoform which does not carry an ATP sensor sequence lacks any detectable activity.

2. Results and discussion

2.1. ATPase activity of human 14-3-3 zeta

We expressed and purified 14-3-3 by affinity chromatography and gel filtration. Identity of the recombinant protein was confirmed by MALDI-TOF–TOF (data not shown) and by nano LC–MS[E] (Supplementary Table T1) as well as by Western blotting using 14-3-3ζ specific antibody (Supplementary Fig. S1(A)). Mass spectrometric analysis reveals 89.39% sequence coverage with no contaminating proteins from *Escherichia coli* in which the protein was expressed (Supplementary Table T1). Three other identifications also belong to 14-3-3 proteins (Supplementary Table T1). Two other proteins identified are very different from 14-3-3ζ in molecular weight and are undetectable by standard techniques. Considering 14-3-3ζ used here is a recombinant protein, these identifications are clearly false positive identifications.

In fusion His-tag was cleaved and confirmed by western blotting using anti His-antibody (Supplementary Fig. S1(B)). Dimeric nature was confirmed by native PAGE (Supplementary Fig. S1(C)).

Ability of this pure 14-3-3ζ WT to hydrolyze ATP was then tested using γ-^{32}P labeled ATP (Fig. 1(A)). 14-3-3ζ WT hydrolyses ATP and releases inorganic phosphate (Pi) in a time dependent manner. Similar results were obtained with the calorimetric assay (Fig. 1(B)) [24]. Absorbance values in presence of two non-hydrolysable analogs ATP-γ-S and AMP-PCP were not very different in the presence or absence of 14-3-3ζ indicating that the calorimetric reaction is a true reflection of gamma phosphate hydrolysis (Fig. 1(B)). Due to the inherent low signal to noise ratio of the calorimetric assay, we standardized a luminescence based assay called the ADP-Glo™ max from Promega which has higher sensitivity, a large dynamic range and is designed to eliminate background from unhydrolyzed ATP. Using this assay we followed ATP hydrolysis of each fraction of the single peak of 14-3-3ζ that elutes out from the gel filtration column and correlated it with UV absorption (Fig. 1(C and D)). Results show that activity is coincident with the protein fractions confirming that 14-3-3ζ has detectable intrinsic ATPase activity.

2.2. Prediction of putative residues involved in ATP binding/hydrolysis

To obtain clues towards the structural motif in 14-3-3ζ involved in ATP binding/hydrolysis, we performed BLAST search of the protein sequence of 14-3-3ζ (YWHAZ) against other ATP binding proteins (data not shown). No consensus motif such as the AAA
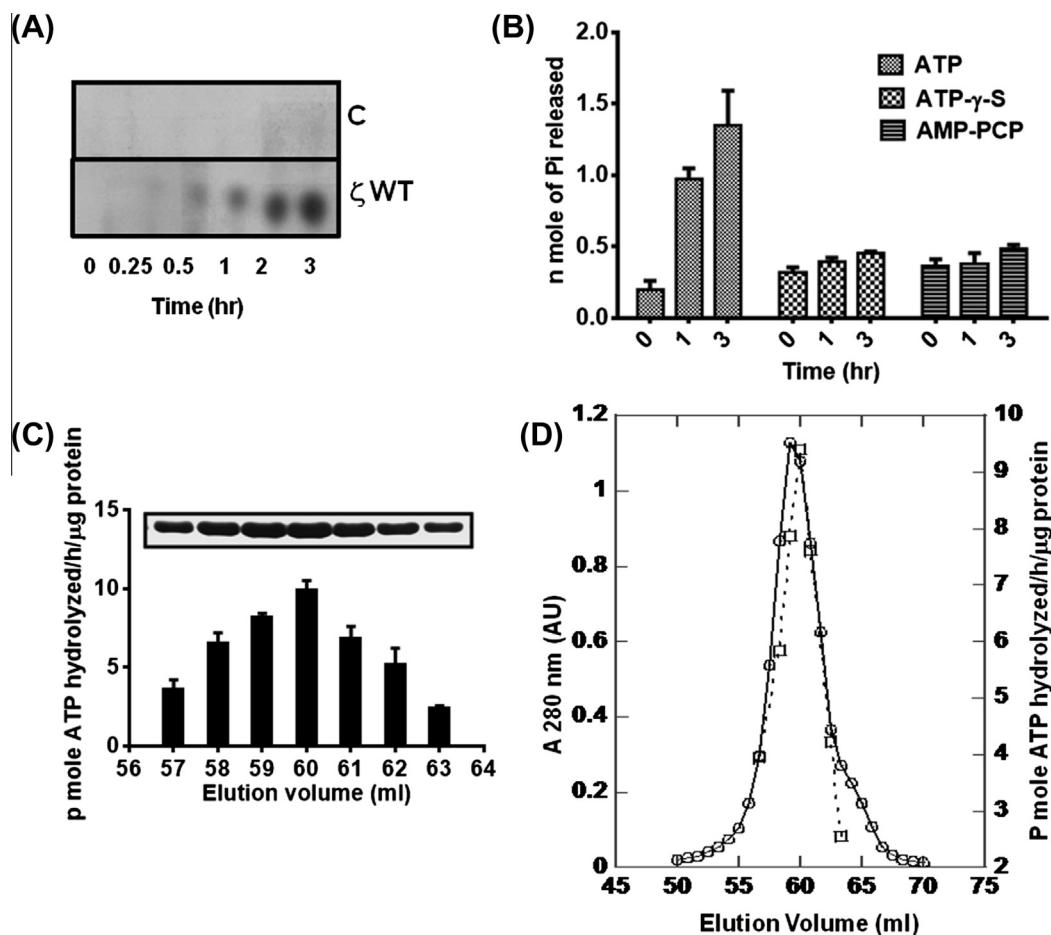
Fig. 1. Demonstration of ATPase activity in 14-3-3ζ (A) Inorganic phosphate (γ-^{32}Pi) released from (γ-^{32}P) ATP hydrolysis by 14-3-3ζ WT at different time points was monitored by PEI-TLC. Lane C represents control (γ-^{32}P) ATP without any protein. (B) Pi release by 14-3-3ζ WT in presence of cold ATP, ATP-γ-S or AMP-PCP was monitored at different time points using malachite green. Data are represented as mean ± S.D. (*n* = 3). (C) ATPase activity of each fraction of 14-3-3ζ WT eluted from gel filtration Proteins. Data are represented as mean ± S.D. (*n* = 3). S.D. – standard deviation. Proteins from each elution fraction were run on 12% SDS–PAGE (top panel). (D) Correlation between ATPase activity and gel filtration profile of 14-3-3ζ WT. Data represents gel filtration profile of 14-3-3ζ WT (continuous line) and corresponding ATPase activity (dotted line).

domain/Walker A domain or glycine rich motif present in other typical ATPases could be identified within 14-3-3ζ. Such ATP binding proteins by and large contain β sheets which act as a base stack for ATP to bind [25] and there are no β sheets in the crystal structure of 14-3-3ζ [26]. In order to identify putative ATP binding pockets we used Schrödinger software (Supplemental method) [27]. Two major binding pockets for ATP seem possible in the crystal structure of 14-3-3ζ (Fig. 2(A)). One of them is located within the amphipathic groove and the other near the dimer interface. Residues within 5 Å of docked ATP in each pocket are marked in Fig. 2(B–E). Both pockets harbored residues expected to bind and hydrolyze ATP. Guided by these results we created many independent single amino acid variants of the protein. There was no change in activity upon K49A, R56A or K120A mutations in the amphipathic pocket (data not shown) but D124A surprisingly showed significant increase in the ATPase activity (Fig. 3(A)). Among the residues E17, R18, D20, R55, and S58 at the interface, R55A mutation alone showed partial reduction in activity (Fig. 3(A)). The dimeric nature of these mutant proteins and the successful removal of His-tag were confirmed by native PAGE and Western blot (Supplementary Fig. S1(B and C)).

2.3. Determination of kinetic constants

ADP-Glo™ max assay was used to determine the kinetic parameters of ATP hydrolysis. D124A mutant shows higher V_{max} (4830 versus 152 pmole/min/mg protein for WT) and higher K_m (214.5 μM) than the WT enzyme (44 μM) (Fig. 3(B and C)). Activity of R55A mutant did not attain saturation and the kinetic parameters could not be measured. The k_{cat} values for 14-3-3ζ WT and the D124A mutant are 0.0087 and 0.28 min[1] respectively (Table 1). k_{cat} value of pure recombinant human Hsp 70, assayed under identical conditions is 0.016 min^{-1} (Table 1). A k_{cat} value between 0.05 and 1 min^{-1} has been reported for human Hsp 70 [28–30]. Another chaperone ATPase, Hsp 90 is reported to have k_{cat} values of 0.015 and 0.086 min^{-1} [31,32]. The K_m value for Hsp 70 is 51 μM (Table 1; reported value 85 μM [30]). K_m values of 320 and 890 μM are reported for Hsp90 [31,32].

Since one of the putative binding pocket is located at the amphipathic groove, we tested the effect of three phosphopeptides on ATPase activity. Peptides did not alter the ATPase activity of 14-3-3ζ WT (Supplementary Fig. S2(A)) or those of the mutants (data not shown). Binding of the peptides was confirmed by ELISA. Muta-
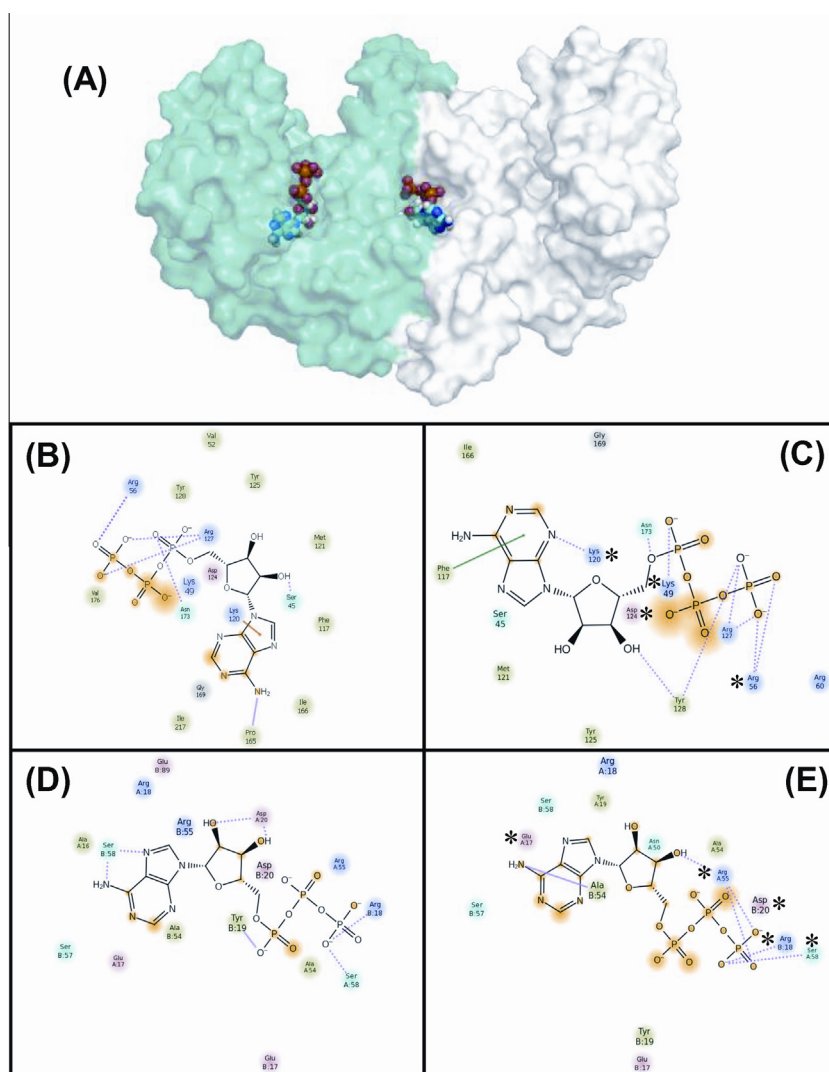
Fig. 2. Prediction of putative ATP binding sites in 14-3-3ζ by docking ATP was docked using Glide application from Schrödinger. (A) ATP was bound both at the amphipathic groove (binding is shown only for one pocket) and at the dimer interface. Interacting residues within 5 Å of bound ATP in each pocket are shown. (B and C) represent the pre and post simulated complex in the amphipathic pocket. (D and E) represent the pre and post simulated complex at the dimer interface. *Represents mutated residues.
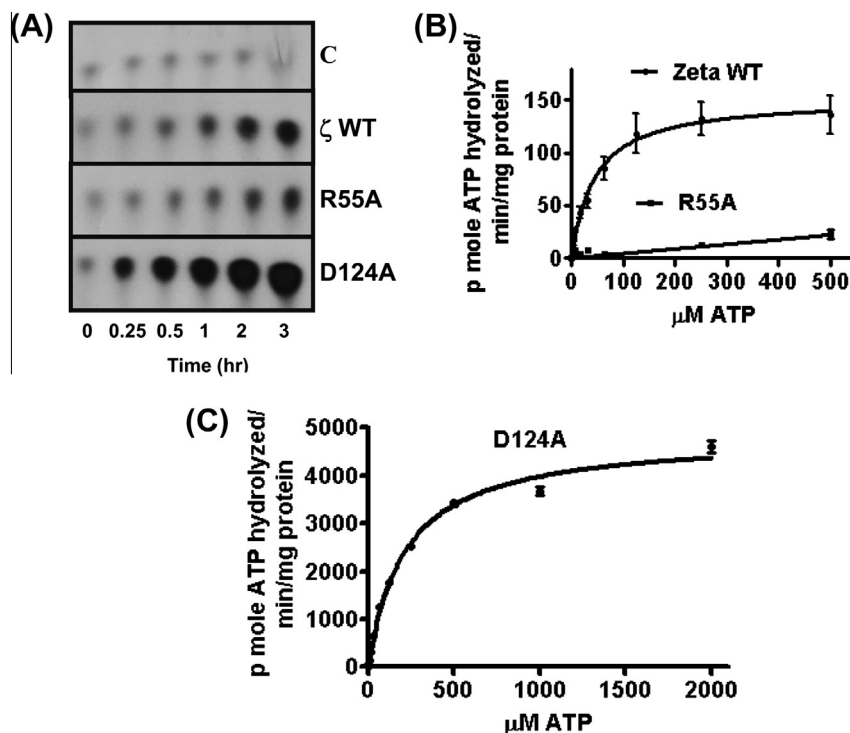
Fig. 3. Mutations enhance or decrease ATPase activity of 14-3-3ζ (A) ATPase activity of R55A and D124A mutants was monitored using radiolabeled (γ-^{32}P) ATP and compared with the WT protein. Lane C represents control (γ-^{32}P) ATP without any protein. (B) ATPase activity of 14-3-3ζ WT, R55A and (C) D124A mutants was measured using ADP-Glo™ max assay. Two independent experiments in triplicates were conducted. Data are represented as mean ± S.E.M. S.E.M. – standard error of mean.

Table 1
V_{max}, K_m and k_{cat} for 14-3-3 active isoforms, D124A mutant and Hsp 70.

Sr. no.	Protein	V_{max} (p mole ATP hydrolyzed/min/mg protein)	K_m (μM)	k_{cat} (min^{-1})
1	14-3-3ζ WT	152 ± 10.19	44.33 ± 10.05	0.0087 ± 0.00058
2	14-3-3γ WT	149.3 ± 12.55	46.81 ± 13.15	0.0085 ± 0.00072
3	14-3-3τ WT	152.4 ± 8.18	22.57 ± 4.72	0.0087 ± 0.00047
4	14-3-3ε WT	146.9 ± 8.9	27.31 ± 6.22	0.0084 ± 0.00051
5	D124A mutant	4830 ± 80.22	214.5 ± 11.53	0.28 ± 0.0046
6	Hsp 70	2335 ± 54.22	51.07 ± 4.51	0.16 ± 0.0038

tions did not affect ability of any of these proteins to bind peptides (Supplementary Fig. S2(B)).

It is to be noted that14-3-3 structure is very different from these chaperones and carries no structural or sequence homology with these or other ATPase family members. The ATPase activity of 14-3-3ζ although slow, is nevertheless close to the classical chaperone Hsp 90 and the activity of D124A mutant (k_{cat} 0.28 min^{-1}) is even better than that of Hsp 70 (k_{cat} 0.16 min^{-1}). This enhancement in activity by single amino acid substitution is rare and provides the strongest support for the intrinsic ATPase activity of 14-3-3ζ. Literature survey suggested that Hsp 104 protein carries RR and GAR motif which act as sensors for ATP [33]. R_{55} at the dimer interface of 14-3-3ζ is part of an identical Short Linear Sequence Motif $G_{53}A_{54}R_{55}R_{56}$. By extrapolation, one may presume that R_{55} in this motif is probably acting as an ATP sensor in 14-3-3ζ.

Prompted by this possibility we looked for the presence of GARR sequence in other 14-3-3 isoforms. We compared the reported structural alignment of 14-3-3 isoforms and found that while D124 is present in all isoforms, R_{55} is conserved in all but the sigma protein (GGQR Supplementary Fig. S3). We expressed and purified 14-3-3 γ, ε, τ and the σ isoform and found that all except sigma show similar ATPase activity measured using radioactive ATP and the ADP-Glo™ assay (Fig. 4(A and B)). The K_m and

k_{cat} values are also similar in the active isoforms (Table 1). Absence of the critical Arg may be the reason for the lack of activity in the sigma isoform. ATPase activity seen in these isoforms could be a moon lighting function. Such a function seems to correlate with the presence of the same ATP sensor sequence motif G(A/G)RR. This however needs to be tested by mutagenesis. Lack of ATPase activity in the sigma isoform which was expressed and purified identical to 14-3-3ζ isoform, further supports our contention that observed ATPase activity in 14-3-3 preparations is intrinsic to the respective isoforms.

2.4. Estimation of binding affinity of ATP to 14-3-3 zeta and the mutants

It is to be noted that V_{max} of D124A mutant is ∼30 times more than the WT protein and the K_m for ATP hydrolysis is approximately four times higher (Table 1). While K_m is routinely considered as a measure of binding affinity, the relationship holds true only under specific conditions. To obtain a measure of binding affinity of WT 14-3-3ζ and two mutant proteins for ATP, we incubated γ-^{32}P radiolabelled ATP with each protein and aliquots were spotted on to nitrocellulose membrane. ATP bound to protein was visualized using autoradiogram. Hsp 70 was used as a control (Fig. 5(A)). Results confirm that these proteins bind to ATP. ATP
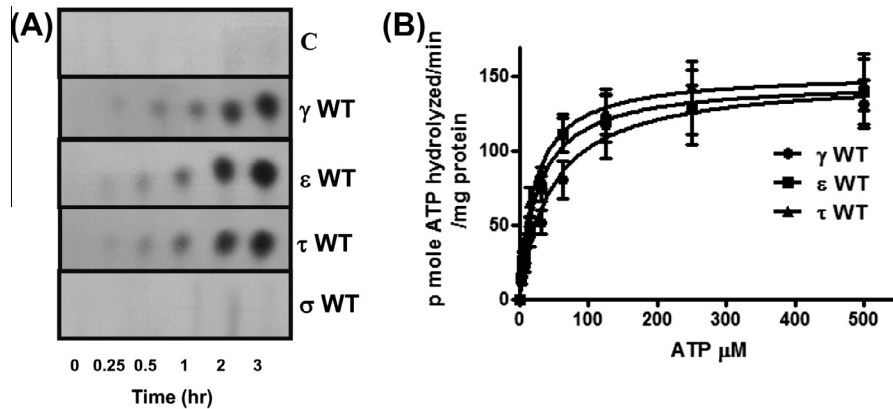
Fig. 4. ATPase activity of other 14-3-3 isoforms (A) Inorganic phosphate (γ-^{32}Pi) released from (γ-^{32}P) ATP hydrolysis by 14-3-3 isoforms at different time points was monitored by PEI-TLC. There is no detectable γ-^{32}P in lanes where ATP was incubated with the sigma isoform. Lane C represents control (γ-^{32}P) ATP without any protein. (B) ATP hydrolysis of active 14-3-3 γ, ε and τ was monitored by ADP-Glo™ max ATPase assay. Two independent experiments in triplicates were conducted. Data are represented as mean ± S.E.M. S.E.M. – standard error of mean.
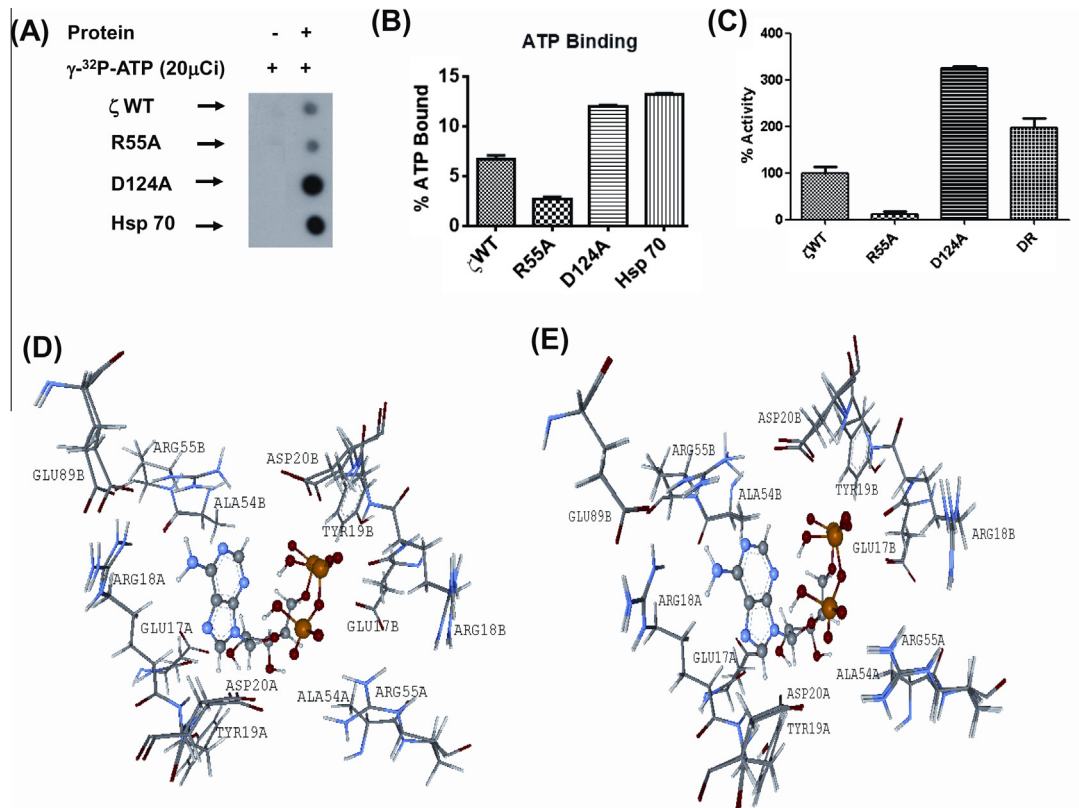
Fig. 5. Effect of mutations on ATP binding (A) ATP bound protein was trapped on nitrocellulose membrane (NC). 14-3-3ζ WT or R55A or D124A mutants or Hsp 70 was incubated with radiolabeled (γ-^{32}P) ATP and spotted on NC. Free ATP was washed away (B) protein bound ATP (γ-^{32}P) was separated using desalting spin column and quantitated using liquid scintillation counter. Data are represented as mean ± S.D. (n = 3). S.D. – standard deviation. (C) 14-3-3ζ WT, R55A, D124A and DR (R55A, D124A) double mutant was subjected for ATPase assay in the presence of 1 mM ATP (Sigma). Pi released was monitored using calorimetry assay. R55A mutation in D124A background resulted in reduction of ATPase activity of D124A mutant. Data are represented as mean ± S.D. (n = 3). S.D. – standard deviation. (D) An overlay of 14-3-3ζ WT and R55A mutant docked poses and (E) is an overlay of D124A mutant and the 14-3-3ζ WT docked poses (only the ligand and interacting residues are shown). D124 is not in view. Bound ATP is represented as a ball and stick model. Residues within 4 Å from ATP are shown and RMSD of superposition (of backbone atoms) is 0.15 Å.

bound protein was isolated from free ATP using a spin column and radioactivity was counted in a liquid scintillation counter. Approximately 6.7% of the total hot ATP added bound to WT protein, 2.66% in R55A and ~12% binding was seen in the D124A mutant (Fig. 5(B)). ~13% of hot ATP was bound to Hsp 70 under the same conditions. These results indicate that the D124 mutant has a better binding affinity for ATP while R55A mutant has less affinity as compared to the WT protein. ~2% binding could be seen with the sigma isoform as well (data not shown).

2.5. Computational analysis of binding energy and experimental constraints converge on one putative binding site

In the absence of high resolution structural information of bound ATP, it is difficult to explain why other amino acid substitutions in the vicinity of bound ATP in either binding pockets failed to show any effect. It is possible that ATP may bind in different orientations or binding may be accompanied by conformational changes that are not captured by docking algorithms. It is also intriguing

that mutation in one pocket resulted in enhancement of activity and in the other a partial loss. To substantiate the effect of these mutations, we engineered R55A mutation in the background of D124A mutant (DR mutant). Compared to the hyper active D124A mutant, DR mutant is only 60% active indicating that R55 near the interface is a key residue in binding/hydrolysis (Fig. 5(C)).

Based on these results we asked whether a single binding pocket can explain the effect of two mutations. We used ligand docking algorithm by VlifeMDS and imposed constraints that would mimic experimental observations in analyzing the docking results. The correct docked pose would be the one in which the D124A mutation results in a more negative binding energy and R55A mutation results in more positive binding energy for ATP. Mutants were engineered in silico using VlifeMDS software [34] and docking was carried out using VlifeMDS tools. Binding energy (BE) for ATP for all proteins was calculated for the same top 10 binding poses (Supplementary Table T2). Although ATP did bind to the same amphipathic pocket in the monomer as seen before (data not shown), no pose on the monomer confirmed to the applied constraints. In contrast a single pose at the dimer interface (pose 4 in Supplementary Table T2) showed (a) better binding of ATP in D124A mutant (BE −0.77 kcal/mol vs 4.04 kcal/mol for the WT protein) and (b) weaker binding in R55A mutant (BE 9.34 kcal/mol). Detailed analysis of this pose indicates that ATP forms two hydrogen bonds with Arg55 in the B chain and also makes charged interactions with Arg55 in the A chain. In addition, Arg55 makes numerous van der Waal (vdW) interactions at the dimer interface (Fig. 5(D)). This docking pose clearly explains the importance of Arg55 in binding interactions (Fig. 5(D)). Mutation of this residue to Ala would result in loss of hydrogen bond interactions as well as the charge interaction between the positively charged guanidine group of arginine and negatively charged phosphate group of ATP, adversely affecting binding energy and therefore catalysis. Increased rate of hydrolysis of D124A is reflected in better binding energy of ATP in this mutant. This could be due to favorable steric interactions between ATP and the mutated protein (Fig. 5(E)) mediated by an increase in the vdW component of the overall binding energy.

2.6. Single turnover studies

To correlate ATP binding and ATP hydrolysis, we performed single turnover ATPase assay. WT 14-3-3ζ, D124A and R55A mutant proteins and 14-3-3σ were independently incubated with radioactive ATP and the bound complex free from ATP was isolated. Protein fraction which has the maximum signal for ATP was chosen and hydrolysis was followed with time (Fig. 6). The data could be

readily fit to a single exponential function and results indicate that 30% of bound ATP is hydrolyzed in 2 h by 14-3-3ζ while D124A hydrolyzes almost 70% of bound ATP by this time (rate constant K = 1.17 ± 0.21). R55A and 14-3-3σ did not show any detectable hydrolysis of ATP under these conditions. Conversion of almost 70% of the bound ATP to product by D124A in a single exponential manner indicates that binding is likely to be stochiometric ruling out the presence of any non-specifically bound ATP that cannot be hydrolyzed. Commensurate with other results 14-3-3ζ WT is slow in hydrolyzing the bound ATP which is very likely due to the faster dissociation of the protein-ATP complex into the free forms.

These results in toto seem to define the pocket near the interface as the most likely binding site for ATP. Nevertheless it is possible that there are indeed two binding pockets for ATP. It is also possible that these mutations have a long range effect on a binding site located elsewhere in the protein or they affect equilibrium distribution between active and inactive conformers.

3. Conclusions

Our study assigns for the first time an ATP hydrolyzing activity to human 14-3-3 ζ γ, ε and τ isoforms. Our mutagenesis results based on prediction tools show that this activity in zeta can be altered resulting in gain or loss of function. While the ultra-structural details of the binding pocket, catalytic residues and more importantly the physiological and functional relevance of this ATP hydrolyzing activity remains to be established, our results are likely to provide the necessary impetus for an in depth investigation of this enzymatic activity and its physiological significance. The ATPase activity in 14-3-3ζ seems to stem from an unconventional binding pocket and could be a moon lighting function. The structure may represent a new fold among atypical ATPases. It remains to be seen whether the enzymatic activity of 14-3-3 proteins is preserved in cellular milieu and whether some of their known functions and perhaps many unknown functions are dependent on this activity. The effect of in vitro mutations may also be mimicked by regulatory mechanisms inside the cell. Notably the sigma isoform which differs from all other isoforms both in sequence, structure and other functions, failed to show any detectable ATPase activity. Whether the same sequence or structure plays a role in other active isoforms remains to be established.

4. Material and methods

Plasmids used in the study, protein purification and characterization by Western blot and nano LC–MS^E analysis [35], ATP binding and single turnover ATPase assay are detailed in Supplemental methods.

4.1. ATPase assay

(A) Calorimetry: 7 μM (calculated for dimeric protein) of protein was incubated with 1 mM of ATP or ATP-γ-S or AMP-PCP (Sigma) at 37 °C in 50 μl reaction buffer (RB) (RB: 20 mM HEPES buffer pH 7.5, 5 mM MgCl$_2$ and 2 mM DTT). Release of inorganic phosphate (Pi) was monitored at different time points using Malachite green assay with minor modifications. 450 μl of assay mixture (3 part of 0.4% malachite green, 1 part 4.2% ammonium molybdate made in 5 N HCl, 0.056% polyvinyl alcohol) was added to 50 μl reaction volume. Mixture was allowed to incubate for 10 min at room temperature and 200 μl of the sample was read at 630 nm (Spectra Max 190, Molecular Devices) with appropriate blank. Amount of phosphate released was estimated with the help of standards generated using KH$_2$PO$_4$.
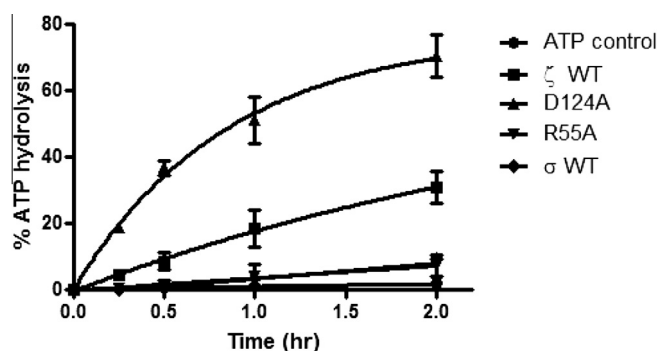

Fig. 6. Single turnover ATPase assay WT 14-3-3ζ, R55A, D124A or WT 14-3-3σ bound-ATP complex was isolated and single turnover ATPase assay was performed. Data represents percentage of ATP hydrolysis with time from two independent experiments. Data are represented as mean ± S.D. S.D. – standard deviation.

(B) *Luminescence assay:* ADP-Glo™ max ATPase assay kit (Promega) was used as per manufacturer's instructions. Luminescence was recorded using multimode microplate reader (Mitras LB 940, Berthold Technologies).

(C) *Radioactive assay:* Trace amounts of (γ-^{32}P) ATP [10 µCi (3000 Ci/mmol), PerkinElmer] in RB (25 µl) containing 100 µM of cold ATP (Sigma) was incubated as before. Reaction was stopped by spotting 2 µl of sample on *poly(ethylene)imine cellulose* thin layer chromatographic (PEI-TLC) plates (Fluka) and developed with 0.75 M KH_2PO_4 (pH 3.5). Plates were dried and exposed to X-ray film (Kodak) to monitor inorganic phosphate (Pi) release. The experiment was repeated at least two times with two independent protein preparations. All radioactive experiments were performed according to standard institutional guidelines.

4.2. Docking of ATP using Schrödinger software and molecular dynamic simulation of the bound complex

ATP was docked to PDB ID: 2C1J which has no structure breakage in between (1–230) [36] using Schrödinger software (for details please see Supplemental methods).

4.3. Computational analysis of binding energy and experimental constraints converge on one putative binding site

ATP was blind docked separately into monomer and dimer structures of 14-3-3ζ (PDB ID: 2C1J) using VlifeMDS software. Top 10 poses based on PLP score were selected (Supplementary Table T2) [37]. Binding energy (kcal/mole) for each pose was calculated using the formula: $E_{bind} = E_{complex} - (E_{protein} + E_{ligand})$. R55A and D124A mutations were created, energy optimized and binding energies were calculated for the same ten docked poses of ATP as seen with the WT protein (Supplementary Table T2).

Author's contributions

M.R. purified all proteins and performed all experiments in this study. P.S. and V.R. were involved in initial studies. A.K. used Schrödinger for docking. A.K.S.G. assisted in radioactive experiments. P.N. purified Hsp 70 protein. S.K. and S.M. performed docking, in silico and binding energy calculations using VLifeMDS software. P.V. designed and directed the project, wrote the manuscript assisted by M.R., S.K. and S.M.

Competing interests

The authors declare that they have no competing interests.

Appendix A. Supplementary data

Supplementary data associated with this article can be found, in the online version, at http://dx.doi.org/10.1016/j.febslet.2013.11.008.

References

[1] Yaffe, M.B., Rittinger, K., Volinia, S., Caron, P.R., Aitken, A., Leffers, H., Gamblin, S.J., Smerdon, S.J. and Cantley, L.C. (1997) The structural basis for 14-3-3: phosphopeptide binding specificity. Cell 91 (7), 961–971.

[2] Zhao, J., Meyerkord, C.L., Du, Y., Khuri, F.R. and Fu, H. (2011) 14-3-3 proteins as potential therapeutic targets. Semin. Cell Dev. Biol. 22 (7), 705–712.

[3] Gardino, A.K. and Yaffe, M.B. (2011) 14-3-3 proteins as signaling integration points for cell cycle control and apoptosis. Semin. Cell Dev. Biol. 22, 688–695.

[4] Ganguly, S., Weller, J.L., Ho, A., Chemineau, P., Malpaux, B. and Klein, D.C. (2005) Melatonin synthesis: 14-3-3-dependent activation and inhibition of arylalkylamine N-acetyltransferase mediated by phosphoserine-205. Proc. Nat. Acad. Sci. U.S.A. 102 (4), 1222–1227.

[5] Dalal, S.N., Yaffe, M.B. and DeCaprio, J.A. (2004) 14-3-3 family members act coordinately to regulate mitotic progression. Cell Cycle 3 (5), 672–677.

[6] Hermeking, H. (2003) The 14-3-3 cancer connection. Nat. Rev. Cancer 3 (12), 931–943.

[7] Hosing, A.S., Kundu, S.T. and Dalal, S.N. (2008) 14-3-3 gamma is required to enforce both the incomplete S phase and G2 DNA damage checkpoints. Cell Cycle 7 (20), 3171–3179.

[8] Telles, E., Hosing, A.S., Kundu, S.T., Venkatraman, P. and Dalal, S.N. (2009) A novel pocket in 14-3-3ε is required to mediate specific complex formation with cdc25C and to inhibit cell cycle progression upon activation of checkpoint pathways. Exp. Cell Res. 315 (8), 1448–1457.

[9] Aitken, A. (2011) Post-translational modification of 14-3-3 isoforms and regulation of cellular function. Semin. Cell Dev. Biol. 22, 673–680.

[10] Muslin, A.J., Tanner, J.W., Allen, P.M. and Shaw, A.S. (1996) Interaction of 14-3-3 with signaling proteins is mediated by the recognition of phosphoserine. Cell 84 (6), 889–897.

[11] Obsil, T., Ghirlando, R., Klein, D.C., Ganguly, S. and Dyda, F. (2001) Crystal structure of the 14-3-3zeta: serotonin N-acetyltransferase complex. A role for scaffolding in enzyme regulation. Cell 105 (2), 257–267.

[12] Gardino, A.K., Smerdon, S.J. and Yaffe, M.B. (2006) Structural determinants of 14-3-3 binding specificities and regulation of subcellular localization of 14-3-3-ligand complexes: a comparison of the X-ray crystal structures of all human 14-3-3 isoforms. Semin. Cancer Biol. 16, 173–182.

[13] Forrest, A. and Gabrielli, B. (2001) Cdc25B activity is regulated by 14-3-3. Oncogene 20 (32), 4393–4401.

[14] Yano, M., Mori, S., Niwa, Y., Inoue, M. and Kido, H. (1997) Intrinsic nucleoside diphosphate kinase-like activity as a novel function of 14-3-3 proteins. FEBS Lett. 419 (2–3), 244–248.

[15] Komiya, T., Hachiya, N., Sakaguchi, M., Omura, T. and Mihara, K. (1994) Recognition of mitochondria-targeting signals by a cytosolic import stimulation factor, MSF. J. Biol. Chem. 269 (49), 30893–30897.

[16] Hachiya, N., Komiya, T., Alam, R., Iwahashi, J., Sakaguchi, M., Omura, T. and Mihara, K. (1994) MSF, a novel cytoplasmic chaperone which functions in precursor targeting to mitochondria. EMBO J. 13 (21), 5146–5154.

[17] Komiya, T. and Mihara, K. (1996) Protein import into mammalian mitochondria. Characterization of the intermediates along the import pathway of the precursor into the matrix. J. Biol. Chem. 271 (36), 22105–22110.

[18] Komiya, T., Sakaguchi, M. and Mihara, K. (1996) Cytoplasmic chaperones determine the targeting pathway of precursor proteins to mitochondria. EMBO J. 15 (2), 399–407.

[19] Yano, M., Nakamuta, S., Wu, X., Okumura, Y. and Kido, H. (2006) A novel function of 14-3-3 protein: 14-3-3zeta is a heat-shock-related molecular chaperone that dissolves thermal-aggregated proteins. Mol. Biol. Cell 17 (11), 4769–4779.

[20] Omi, K., Hachiya, N.S., Tanaka, M., Tokunaga, K. and Kaneko, K. (2008) 14-3-3zeta is indispensable for aggregate formation of polyglutamine-expanded huntingtin protein. Neurosci. Lett. 431 (1), 45–50.

[21] Sluchanko, N.N. and Gusev, N.B. (2011) Probable participation of 14-3-3 in tau protein oligomerization and aggregation. J. Alzheimers Dis. 27 (3), 467–476.

[22] Berg, D., Holzmann, C. and Riess, O. (2003) 14-3-3 proteins in the nervous system. Nat. Rev. Neurosci. 4 (9), 752–762.

[23] Aitken, A. (2006) 14-3-3 proteins: a historic overview. Semin. Cancer Biol. 16 (3), 162–172.

[24] Ames, B.N. (1966) Assay of inorganic phosphate, total phosphate and phosphatase. Methods Enzymol. 8, 115–118.

[25] Chauhan, J.S., Mishra, N.K. and Raghava, G.P.S. (2009) Identification of ATP binding residues of a protein from its primary sequence. BMC Bioinformatics 10 (1), 434.

[26] Liu, D., Bienkowska, J., Petosa, C., Collier, R.J., Fu, H. and Liddington, R. (1995) Crystal structure of the zeta isoform of the 14-3-3 protein. Nature 376, 191–194.

[27] Glide v, Schrödinger, LLC, New York, NY, 2011, Version 5.7; http://www.schrodinger.com.

[28] Jaiswal, H., Conz, C., Otto, H., Wölfle, T., Fitzke, E., Mayer, M.P. and Rospert, S. (2011) The chaperone network connected to human ribosome-associated complex. Mol. Cell. Biol. 31 (6), 1160–1173.

[29] Bimston, D., Song, J., Winchester, D., Takayama, S., Reed, J.C. and Morimoto, R.I. (1998) BAG-1, a negative regulator of Hsp70 chaperone activity, uncouples nucleotide hydrolysis from substrate release. EMBO J. 17 (23), 6871–6878.

[30] Olson, C.L., Nadeau, K.C., Sullivan, M.A., Winquist, A.G., Donelson, J.E., Walsh, C.T. and Engman, D.M. (1994) Molecular and biochemical comparison of the 70-kDa heat shock proteins of *Trypanosoma cruzi*. J. Biol. Chem. 269 (5), 3868–3874.

[31] Owen, B.A., Sullivan, W.P., Felts, S.J. and Toft, D.O. (2002) Regulation of heat shock protein 90 ATPase activity by sequences in the carboxyl terminus. J. Biol. Chem. 277 (9), 7086–7091.

[32] McLaughlin, S.H., Smith, H.W. and Jackson, S.E. (2002) Stimulation of the weak ATPase activity of human hsp90 by a client protein. J. Mol. Biol. 315 (4), 787–798.

[33] Bösl, B., Grimminger, V. and Walter, S. (2006) The molecular chaperone Hsp104-a molecular machine for protein disaggregation. J. Struct. Biol. 156 (1), 139–148.

[34] VLifeMDS V, VLife Sciences Technologies Pvt. Ltd., Pune, India 2012, Version 4.2; http://www.vlifesciences.com.

[35] Silva, J.C., Gorenstein, M.V., Li, G.-Z., Vissers, J.P. and Geromanos, S.J. (2006) Absolute quantification of proteins by LCMSE a virtue of parallel MS acquisition. Mol. Cell. Proteomics 5 (1), 144–156.

[36] Macdonald, N., Welburn, J.P.I., Noble, M.E.M., Nguyen, A., Yaffe, M.B., Clynes, D., Moggs, J.G., Orphanides, G., Thomson, S. and Edmunds, J.W. (2005) Molecular basis for the recognition of phosphorylated and phosphoacetylated histone h3 by 14-3-3. Mol. Cell 20 (2), 199–211.

[37] Gehlhaar, D.K., Verkhivker, G.M., Rejto, P.A., Sherman, C.J., Fogel, D.R., Fogel, L.J. and Freer, S.T. (1995) Molecular recognition of the inhibitor AG-1343 by HIV-1 protease: conformationally flexible docking by evolutionary programming. Chem. Biol. 2 (5), 317–324.

Discovery of multiple interacting partners of gankyrin, a proteasomal chaperone and an oncoprotein—Evidence for a common hot spot site at the interface and its functional relevance

Padma P. Nanaware, Manoj P. Ramteke, Arun K. Somavarapu, and Prasanna Venkatraman*

Advanced Centre for Treatment, Research and Education in Cancer, Navi Mumbai, India

ABSTRACT

Gankyrin, a non-ATPase component of the proteasome and a chaperone of proteasome assembly, is also an oncoprotein. Gankyrin regulates a variety of oncogenic signaling pathways in cancer cells and accelerates degradation of tumor suppressor proteins p53 and Rb. Therefore gankyrin may be a unique hub integrating signaling networks with the degradation pathway. To identify new interactions that may be crucial in consolidating its role as an oncogenic hub, crystal structure of gankyrin-proteasome ATPase complex was used to predict novel interacting partners. EEVD, a four amino acid linear sequence seems a hot spot site at this interface. By searching for EEVD in exposed regions of human proteins in PDB database, we predicted 34 novel interactions. Eight proteins were tested and seven of them were found to interact with gankyrin. Affinity of four interactions is high enough for endogenous detection. Others require gankyrin overexpression in HEK 293 cells or occur endogenously in breast cancer cell line- MDA-MB-435, reflecting lower affinity or presence of a deregulated network. Mutagenesis and peptide inhibition confirm that EEVD is the common hot spot site at these interfaces and therefore a potential polypharmacological drug target. In MDA-MB-231 cells in which the endogenous CLIC1 is silenced, transexpression of Wt protein (CLIC1_EEVD) and not the hot spot site mutant (CLIC1_AAVA) resulted in significant rescue of the migratory potential. Our approach can be extended to identify novel functionally relevant protein-protein interactions, in expansion of oncogenic networks and in identifying potential therapeutic targets.

INTRODUCTION

Protein-protein interactions create complex functional networks in cells and these interaction networks coincide with the signaling networks that regulate cell behavior.[1] Detecting and describing these interaction networks is the goal of many large proteomics and bioinformatics studies.[2–5] Cancer associated proteins especially oncoproteins are identified as hubs in such networks[1] and key interactions within the network represent prime targets for therapeutic interventions.

Gankyrin, an oncoprotein overexpressed in many epithelial cancers[6–12] was initially identified as a non-ATPase subunit of the proteasome. While gankyrin is not considered as a stable component of the 26S proteasome, it is detected in its free form as well as in complex with 19S regulatory particles of the proteasome.[13] Nas6, the homologue of gankyrin acts as chaperone required for the assembly of the 19S regulatory particles.[14,15]

Some of the known functions of gankyrin as an oncoprotein involve its ability to deregulate key signaling networks and/or influence degradation of crucial regulatory molecules by the proteasome. By directly binding to MDM2, gankyrin facilitates degradation of p53.[16] By

directly binding to Rb, gankyrin increases Rb phospho-rylation and degradation by the proteasome[12] resulting in the release of E2F a transcription factor, responsible for cellular proliferation. Gankyrin is also known to interact with CDK4 kinase which may be important for cell cycle regulation.[13,17] Interaction of gankyrin with MAGE-A4 seems to suppress tumor formation in athymic mice overexpressing gankyrin.[18] Gankyrin also binds to ankyrin repeats in NF-κB and inhibits its activity.[19] Gankyrin is also known to bind to NF-κB and suppresses the transcriptional activity by modulating acetylation of SIRT1.[20] Ras mediated oncogenic signaling is dependent on the presence of gankyrin.[7] NIH3T3 cells overexpressing gankyrin when injected into nude mice form tumors.[12] When gankyrin expression is silenced, cells undergo reduced proliferation and reduced colony formation on soft agar assay.[7] When gankyrin silenced pancreatic cancer cells were injected into nude mice, the tumors formed were of reduced size. In contrast, when gankyrin was overexpressed, these cells formed large size tumors.[8]

These findings clearly suggest that gankyrin connects multiple oncogenic pathways and therefore shows characteristics of a key hub protein. Being part of the ubiquitin-proteasome pathway gankyrin is uniquely positioned to link at least some of these pathways to the ubiquitin proteasome network which may play a decisive role in disease progression. As mentioned before, gankyrin is also overexpressed in many cancers. Hub proteins that are overexpressed, are estimated to be at least three times more essential than the non-hub counterparts.[21] They are also potential anti-cancer drug targets.

Challenge in understanding properties of such hub proteins and their utility as therapeutic targets lies in identifying key interactions among the many possible ones. With limited surface available for interactions, the question of how multiple interactions are achieved by a single protein is a matter of considerable debate.[1,22] Although protein-protein interactions may involve large surface areas, bulk of the binding energy is contributed by few key residues at the interaction surface. These when mutated result in either rapid dissociation of the complex or prevent stable association and are called as the 'hot spot' sites.[23,24] Such hot spot sites are conserved across interfaces.[24] A key regulatory molecule therefore may interact with multiple partners through such a common recognition motif.[22]

Our aim to establish protein interaction network of gankyrin are twofold (a) to better understand its role in oncogenesis and (b) in the future to be able to identify vulnerable nodes in the network that are amenable for therapeutic intervention. Since crystal structure of gankyrin in complex with an S6ATPase of the proteasome is known, we began by predicting a probable hot spot site at the S6ATPase interface formed by EEVD a linear short sequence of four amino acid residues. Since hot spot

sites are conserved, it is likely that gankyrin may recognize other proteins which also carry EEVD in an accessible region of the protein. Using a simple bioinformatics tool we identify 34 proteins with EEVD in well exposed region on their surface and experimentally prove interactions with seven out of the eight proteins tested. Three of these interactions occur in HEK 293 cells only when gankyrin is overexpressed but occur in breast cancer cells at endogenous levels. Mutagenesis confirms that these interactions involve predicted residues which form the hot spot sites at the shared interface and could be a potential drug target.

Our strategy may be extended to the identification of novel protein-protein interactions which share linear sequence of amino acids at the interaction sites, to expand functionally relevant interaction networks of key regulatory proteins and perhaps in the identification of therapeutically vulnerable targets.

MATERIALS AND METHODS

Bioinformatic detection of putative interacting partners of gankyrin

Protein sequences from human proteome data was downloaded from the Uniprot website (URL:ftp://ftp.ebi.ac.uk/pub/databases/uniprot; March 21, 2012). This data set contains a total of 81,194 sequences in FASTA format and has two parts, one containing manually annotated data (UniProtKB/Swiss-Prot) and the other a computationally analyzed data awaiting manual annotation (UniProtKB/TrEMBL). Manually annotated 35,961 entries were used for further analysis. Proteins containing EEVD in their primary sequence were extracted using perl scripts. From this list, proteins with three-dimensional structures were short listed and their Uniprot IDs were submitted to the Protein Data Bank (PDB) and structures were downloaded. Solvent Accessible Surface Area (SASA) of the EEVD was calculated in the context of the tetra peptide using Parameter optimized surfaces (POPS) stand alone application.[25]

Clones and constructs

Gankyrin pBluescript II SK (+) construct (kind gift from Dr. Jun Fujita, Kyoto University) was subcloned into mammalian expression vector p3XFLAG-CMV[TM]-10 (Sigma) or in prokaryotic expression vector pRSETA-TEV. Hsp70 in pGEX4T1 vector was received as a kind gift from Dr. Surekha Zingde, ACTREC. CLIC1, NCK2, GRSF1, S6ATPase cDNA were generated by RT-PCR of RNA extracted from HEK 293 cells. CLIC1 was cloned in pGEX4T1 (GE Amersham) and pCDNA 3.1 with HA tag at the N terminus (pCDNA3.1 was received as a kind gift from Dr. Sorab Dalal, ACTREC), while NCK2 and GRSF1 were cloned in pCDNA3.1. Hsp70 was also cloned in

p3XFLAG-CMV^{TM}-10. Mutations in Hsp70 (aa 638EEVD641 to AAVA), CLIC1 (aa 150EEVD153 to AAVA), CLIC1 (aa 152V to aa 152E), NCK2 (aa 167EEVD170 to AAVA), GRSF1 (aa 144EEVD147 to AAVA), S6ATPase (aa 356EEVD359 to AAVA) were generated using PCR based site directed mutagenesis with the help of Phusion high fidelity DNA polymerase (Finnzymes-Thermo Scientific) and were further confirmed by sequencing. Primers used for cloning and site directed mutagenesis are reported in Supporting Information Table S1.

Cell culture, transfection, and generation of stable clones

HEK 293, MDA-MB-231, MDA-MB-435 cells were cultured in DMEM (GIBCO) supplemented with 10% FBS (GIBCO). Cells were maintained in 5% CO_2 incubator at 37°C. HEK 293 cells were transfected with pCMV10-3X-p3XFLAG-CMV^{TM}-10-gankyrin or vector alone using calcium phosphate method. Clonal transformants were selected in presence of 800 µg/mL G418 (Sigma). Lipofectamine 2000 was used to transfect siRNA or gene of interest in MDA-MB-231 and MDA-MB-435 cells.

Characterization of stable clones

Soft agar assay

Gankyrin overexpressing HEK 293 stable clones or vector alone clones obtained by the above method were compared for their ability to exhibit anchorage independent growth using soft agar colony formation assay. 2 × 10^3 cells in each case were overlaid on a thin layer of agar (0.4% over 1% agarose). Colonies formed were counted after 7 days.

MTT assay for proliferation

HEK 293 cells were transiently transfected with gankyrin or vector alone. Forty-eight hours after transfection, 5 × 10^3 cells were seeded in a 96-well plate and 20 µL of (3-[4,5-dimethylthiazol-2-yl]-2,5-diphenyltetrazolium bromide (MTT) (5 mg/mL) (Sigma) was added. After 2 h, 100 µL of 10% SDS in 0.01 N HCl was added and absorbance was read at 550 nm.

Etoposide treatment for apoptosis

Vector alone and gankyrin expressing stable HEK 293 clones were subjected to etoposide (Cipla) treatment; 2 × 10^3 cells were seeded in 96-well and treated with 50 µM etoposide. Cell viability was checked after 72 h using MTT assay as described earlier.

Luciferase assay for NF-κB activity

Stable clones of HEK 293 harboring p3XFLAG-CMV^{TM}-10 or p3XFLAG-CMV^{TM}-10 -gankyrin were transfected with 12 µg of ConA control or 3 kb enhancer ConA luciferase construct (a kind gift from Dr. Neil D. Perkins, UK). After 48 h, cells were treated with 10 ng/mL TNF-α (Invitrogen), lysed and luciferase assay was performed using Promega Luciferase Assay System in triplicates.

Affinity pull down and western blotting

Cells were harvested in NP-40 lysis buffer (20 mM Tris-HCl pH 7.5, 150 mM NaCl, 0.5% NP-40 and 1 mM dithiothreitol (DTT) containing 1× protease inhibitor cocktail (Sigma)). One milligram of total cell lysate was incubated with 10 µL of M2 agarose anti-flag beads (Sigma) for 4 h at 4°C. Beads were washed extensively with the NP-40 lysis buffer containing 300 mM NaCl. In order to increase the stringency in pull down experiments (Figure 3(C-F) and Supporting Information Fig.S2(C)), RIPA buffer (25 mM Tris-HCl pH 7.5, 150 mM NaCl, 1% NP-40, 1% sodium deoxycholate, 0.1% SDS) was used during washes. Samples were boiled in the presence of Laemmli buffer. Proteins were resolved on a 12% SDS PAGE and western blotting was performed using standard protocol. Antibodies used in the analysis were against gankyrin (Sigma), Hsp70 (Abcam), CLIC1 (Abcam), DDAH1 (Sigma), GRSF1 (Sigma), EIF4A3 (Sigma), Hsp90 (Santacruz), MAP2K1 (Sigma), HA (Abcam). Immunoblots were visualized by enhanced chemiluminescence (ECL plus; Amersham). HEK 293 cells and MDA-MB-435 cells overexpressing HA-NCK2 or NCK2_AAVA were treated with 5 µM MG132 for 6 h before cell harvesting.

Immunoprecipitation and western blotting

For immunoprecipitation experiments, cells were harvested in NP-40 lysis buffer. 15 µL of Sepharose G beads were incubated overnight with 3 µg of respective antibody in same buffer. One milligram of precleared lysate was added to the antibody bound beads and incubated for 4 h. These immune complexes were washed thoroughly for four to five times using NP-40 lysis buffer containing 300 mM NaCl. In some cases RIPA buffer (25 mM Tris-HCl pH 7.5, 150 mM NaCl, 1% NP-40, 1% sodium deoxycholate, 0.1% SDS) was used during washes to increase the stringency in immunoprecipitation experiments [Fig. 2(D,E)]. Samples were boiled in the presence of Laemmli buffer. Proteins were resolved on 12% SDS PAGE and western blotting was performed.

Expression and purification of proteins

Recombinant His-gankyrin, GST-fusions of Hsp70, CLIC1 and their corresponding AAVA mutants and EEED mutants were expressed in *Escherichia coli* BL21 DE(3) using 100 µM IPTG at 24°C for 16 h. His-gankyrin was purified using nickel-nitrilotriacetic acid (Ni-NTA) chromatography (Qiagen) as a His-tag protein.

GST and other fusion proteins listed above were purified using glutathione Sepharose (GE Amersham) following manufacturer's protocol. All proteins were dialyzed against 50 mM Tris-HCl pH 7.5 and stored at $-20°$C.

In vitro GST pull down assay

GST-fusion proteins and their mutants in NP-40 lysis buffer were allowed to immobilize on GST beads for 1 h at 4°C. Beads were washed two to three times with the same buffer but containing 300 mM NaCl. His-gankyrin was allowed to bind for 2 h at 4°C. Beads were washed thoroughly (five to six times) and boiled in the presence of Laemmli buffer. Proteins were resolved on a 12% SDS PAGE and western blotting was performed using anti-gankyrin antibody.

Peptide inhibition

His-gankyrin (30 µg) was incubated with different concentrations (1–500 µM) of EEVD peptide. Peptides GRRF and GRRR were included as controls. Preincubated complex were added to 30 µg of purified GST-CLIC1 bound to glutathione beads and incubated for 2 h at 4°C. Beads were washed thoroughly for five to six times with NP-40 lysis buffer and boiled in the presence of Laemmli buffer. Proteins were resolved on a 12% SDS PAGE and western blotting was performed using gankyrin antibody. Band intensities were measured using ImageJ software. To obtain an approximate K_d value of the peptide, we made the following assumptions. We assume that band intensity at zero peptide represents total CLIC1 bound gankyrin. Band intensity in presence of varying concentrations of the peptide is then subtracted from this value. We consider this subtracted value to correspond to peptide bound fraction of gankyrin. These values are then plotted against peptide concentration to obtain $\sim K_d$ of the peptide.

Wound healing assay

Directional cell migration was studied using an *in vitro* wound healing assay.[26] Cells were seeded in six-well plates and allowed to reach 70 to 90% confluence. To monitor the independent role of gankyrin or CLIC1, MDA-MB-231 cells were transfected with 100 nM gankyrin siRNA or CLIC1 siRNA or control siRNA and incubated for 72 h before setting up the wound healing assay. To examine the effect of protein-protein interaction (PPI) on the motility of the cells, HEK 293 and MDA-MB-231 cells were transfected with CLIC1 Wt or CLIC1_AAVA mutant or vector control and incubated for 48 h. These experiments were conducted in the presence of endogenous CLIC1. Parental HEK 293 cells however do not show detectable endogenous CLIC1. To further confirm, the importance of PPI in this functional assay, endogenous CLIC1 in MDA-MB-231 cells were silenced using smartpool of UTR specific siRNA (Dharmacon) and co-transfected with either CLIC1 Wt or CLIC1_AAVA mutant. Control experiments included non-target siRNA with or without the cDNA for CLIC1 Wt or AAVA mutant as the case may be. For transfection in MDA-MB-231 cells, 6 µg DNA and 18 µL of lipofectamine 2000 was used. These transfected cells were grown to 100% confluence and were treated with 10 µg/mL of mitomycin C for 3 h. Cell monolayer was then wounded with a plastic tip, washed with PBS to remove cell debris. Wound healing capacity was monitored for 16 h or 24 h using phase contrast microscopy (Axiovert 200M, Zeiss, Germany). Area under each wound was calculated using Image J software. Percentage of wound healed was calculated using the formula [(initial wound area $-$ final wound area)/initial wound area] $\times$100. The siRNA sequences used are tabulated in Supporting Information Table S1.

In vitro invasion assay

Invasion assay was performed using 24-well transwell culture inserts of 8 µm pore size (BD Biosciences). Matrigel at a concentration 300 µg/mL diluted in 1$\times$ DMEM was added to the inner side of the chamber and allowed to polymerize at 37°C for 1 h. Unpolymerized matrigel was removed and 5×10^4 cells were seeded in 200 µL of DMEM. To the lower chamber complete medium (DMEM + 10% FBS) was added as chemoattractant. Cells were then incubated for 24 h at 37°C in a humidified CO_2 (5%) incubator. After incubation, inserts were removed and the noninvading cells on the upper surface of the insert were scraped. Lower surface of the insert which harbors the invaded cells was fixed using cold methanol and stained using crystal violet. All images were taken at 5$\times$ magnification using a upright microscope (Axio Imager. Z1, Zeiss, Germany).

RESULTS

Overexpression of gankyrin in HEK 293 cells and generation of stable clones

Gankyrin overexpression in NIH3T3 (mouse) cells results in malignant transformation and transfected cells can form colonies on soft agar and seed tumors in nude mice.[12] We replicated this model in HEK 293 cells with the major goal of identifying protein-protein interactions that may be functionally and therapeutically relevant. In addition, by using a model system where gankyrin is transexpressed allows us to establish a causal relationship to gankyrin and attribute the changes in the network to overexpression of gankyrin. Gankyrin was overexpressed as a flag tag fusion protein and stable colonies were selected. Expression levels of gankyrin in the stable clones were tested using qRT-PCR. Total gankyrin (using
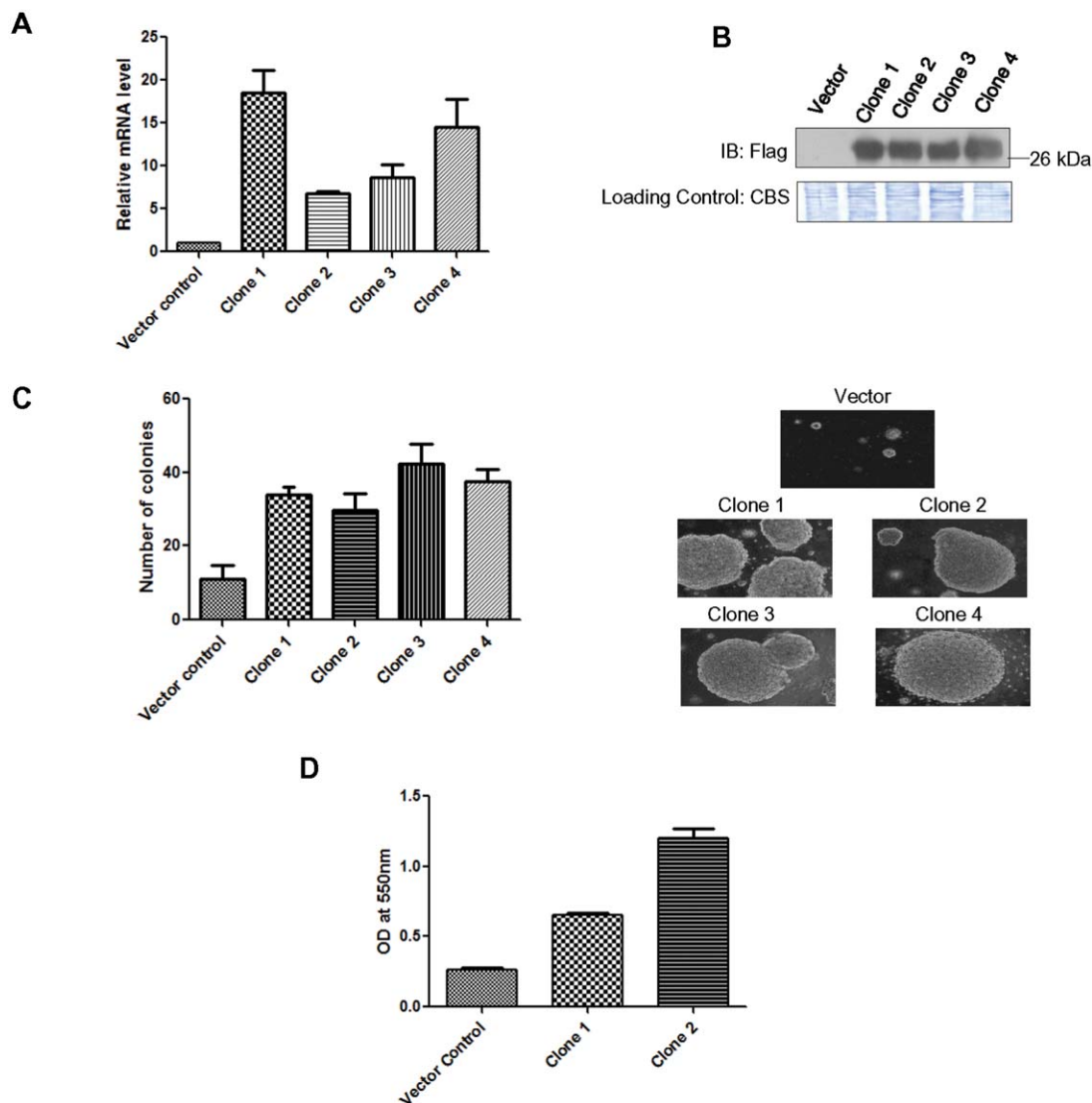
Figure 1

Generation of gankyrin overexpressing stable HEK 293 clones. (**A**) HEK 293 stable clones overexpressing gankyrin were generated. Total levels of gankyrin were quantitated using gankyrin specific primers and real time PCR. HPRT was used as the internal control. Data represent mean ± SD of one experiment done in duplicate; (**B**) Western blot using anti-flag antibody shows overexpression of transfected gankyrin in stable clones. Coomassie brilliant blue stained bots (CBS) indicates equal loading; (**C**) HEK 293 stable clones (four clones) show anchorage independent growth as compared to the vector alone cells; 2×10^3 cells were seeded and number of colonies formed after 7 days are plotted. The data represents mean ± SD of one experiment done in triplicate. Three independent experiments were performed in duplicate to confirm these observations. A representative $10\times$ image of one of the fields from each plate is also shown; (**D**) HEK 293 vector alone and gankyrin over expressing cells were treated with 50 μM etoposide and cell viability was checked after 72 h. Clones overexpressing gankyrin were resistant to apoptosis as compared to the vector alone cells. Data represent mean ± SD of one experiment done in duplicate. [Color figure can be viewed in the online issue, which is available at wileyonlinelibrary.com.]

gankyrin specific primers) is expressed at 5 to 15-fold higher levels in stable clones as compared to the vector alone cells [Fig. 1(A)]. Western blot using anti-flag antibody shows specific expression of flag-gankyrin in transfected cells [Fig. 1(B)]. Some of the reported phenotypic characteristics seen in gankyrin overexpressing cells, like increase in proliferation[27] [Supporting Information Fig. S1(A)] and reduction in NF-κB activity[20] [Supporting Information Fig. S1(B)] were recapitulated. In addition

we found that gankyrin overexpression results in enhanced growth of colonies on soft agar [Fig. 1(C)]. This anchorage independent growth assay is considered as a surrogate assay for *in vivo* tumorigenesis.[28] Since number and size of colonies were much larger upon gankyrin overexpression, additional malignant features are only introduced in these transformed HEK 293 cells in response to gankyrin overexpression. Gankyrin overexpression also resulted in resistance to apoptosis upon

etoposide treatment [Fig. 1(D)]. Thus these HEK 293 stable clones simulate oncogenic properties of gankyrin.

Bioinformatic identification of novel interacting partners of gankyrin

We took advantage of the published crystal structure of mouse gankyrin (m-gankyrin) in complex with human S6ATPase subunit of the proteasome[29] to predict novel interacting partners of human gankyrin. The complex buries 2418 Å^2 of surface area. The human (h) and m-gankyrin share 98% sequence identity and the crystal structure of unliganded h-gankyrin is completely super imposable on the m-gankyrin-S6ATPase structure [Supporting Information Fig. S2(A)]. In this structure, the interface is enriched in polar and charged residues. A linear sequence of four amino acids EEVD (aa 356–359) in S6 ATPase [Supporting Information Fig. S2(B)] makes dominant contribution to the interaction. Residue E356 is hydrogen bonded to Lys116. E357 forms a salt bridge with Arg41 and is also hydrogen bonded to Ser49 and Ser82. Val358 main chain carbonyl group is engaged in a hydrogen bond with Lys116. Asp359 is in polar contact with Ser115. Bridging this contiguous stretch of contact are two arginine residues Arg339 and Arg342 at one end and Lys397 at the other and these interact with residues in gankyrin through hydrogen bonds and salt bridges [Supporting Information Fig. S2(B)].

Complex formation was abolished by any one of the double mutations of E356/E357A or D359/362A, whereas triple mutation of arginine residues, R338/R339/R342A was required to abolish complex formation. Although these results have not been proven in direct interaction assays using purified components, these observations indicate that residues E356, E357 and D359 within EEVD are crucial for interaction. While the Arg residues are present in a helix, E356/E357/D359 residues are present in a loop and E362 is present in a helix. We tested the role of EEVD in complex formation between S6ATPase and gankyrin by overexpressing Flag-S6ATPase Wt and its corresponding AAVA mutant in HEK 293 cells followed by immunoprecipitation. Results indicate that the mutations significantly abrogate interaction [Supporting Information Fig. S2(C)]. Based on these results and evidence cited above, we chose to test the short linear stretch of EEVD present in the loop as a probable hot spot sites at this interface. We hypothesized that other proteins within the human proteome which contain a contiguous stretch of EEVD may also interact with gankyrin. Short sequences such as EEVD are customarily believed to be promiscuous. However, our experience suggest that judicious combination of functionally important short sequences with filters based on structure and other biological properties can reduce false positive identification in proteome wide screening. "Prediction of Natural Substrates from Artificial Substrate of Proteases,"

(PNSAS) an algorithm developed by us for predicting natural substrates of endo proteases uses such principles.[30] Power of the method lies in the use of short sequence motifs coupled with physiologically relevant filters namely, accessibility of the cleavage site in the folded protein and subcellular co-localization to reduce false positive identification.[30] We have validated this algorithm by identifying Dsg-2, a desmosomal protein involved in cell-cell junction as a physiologically relevant novel substrate of a transmembrane protease called matriptase. Ability of matriptase to regulate levels of Dsg-2 at cell surface is likely to play a crucial role in cell invasion and metastasis.[31] In addition, we recently demonstrated that a 13-residue peptide based on the sequence of apomyoglobin can inhibit interaction of the full length protein with the proteasome.[32] Other bioinformatic analysis indicate that sequences of about 3 to 10 residues are signatures of unique biological function.[33] Short linear motifs primarily in disordered regions of the proteins, terminal residues and three amino acid motifs can also assign functions to proteins.[34,35] These motifs have been used to identify novel substrates of kinases harboring SH2-SH3 domains and proteins like 14-3-3 which recognize such short sequences in phosphorylated proteins.[34]

With this background, we decided to test whether proteins from the human proteome which harbor EEVD in the accessible region of the protein can interact with gankyrin. Ability of gankyrin to interact with multiple proteins would lead to a system wide network some of which may dictate cancer specific phenotypes. A total of 264 unique proteins with EEVD in their primary sequence were found (Supporting Information Table S2) and for 34 of them structural information was available using which solvent accessible surface area (SASA) values were calculated. For comparative analysis SASA values were normalized either against EEVD from S6ATPase (considered as 1) or they were obtained from the POPS server. For 4 proteins the corresponding structure did not have any electron density for the peptide sequence and these were verified to be disordered (Table I).

Choice of proteins

To select proteins for experimental validation, we used a stringent cut off for relative solvent accessibility (rSASA). Among the 34 proteins with available crystal structure, we chose proteins with rSASA > 0.5 as determined by POPS server. Among the 11 proteins with rSASA > 0.5, we chose to test NCK2, G-rich RNA sequence binding factor 1 (GRSF1), chloride intracellular channel protein 1 (CLIC1), eukaryotic initiation factor 4A-III (EIF4A3), dimethylarginine dimethylaminohydrolase 1 (DDAH1), and mitogen-activated protein kinase 1 (MAP2K1) as putative interacting partners. We also included two proteins (heat shock protein 70-Hsp70,

Table I
EEVD is Solvent Accessible in Putative Interacting Partners of Gankyrin

| Uniprot ID	Protein Name	PDB ID	rSASA from reference: 2DVW	rSASA from pops program
NCK2_HUMAN	Cytoplasmic protein NCK2	4E6R	1.24	0.8
GRSF1_HUMAN	G-rich sequence factor 1	2LMI	1.18	0.71
BPNT1_HUMAN	3′(2′)5′-bisphosphate nucleo-tidase 1	2WEF	1.15	0.67
DNMT1_HUMAN	DNA (cytosine-5)-methvl-transferase 1	3SWR	1.03	0.62
CLIC1_HUMAN	Chloride intracellular channel protein 1	3UVH	1.02	0.62
PRS6B_HUMAN	26S protease requlatory sub-unit 6B	2DVW	1	0.58
IF4A3_HUMAN	Eukaryotic initiation factor 4A-III	2J0S	0.97	0.56
RIR2B_HUMAN	Ribonucleoside-diphosphate reductase subunit M2 B	4DJN	0.92	0.54
DDAH1_HUMAN	N(G)N(G)-dimethvlarginine dimethylaminohydrolase 1	3I2E	0.92	0.53
MP2K2_HUMAN	Dual specificity mitoqen-activated protein kinase kinase 2	1S9I	0.91	0.54
MP2K1_HUMAN	Dual specificity mitoqen-activated protein kinase kinase 1	3EQC	0.91	0.53
RIR2_HUMAN	Ribonucleoside-diphosphate reductase subunit M2	3OLJ	0.84	0.49
REV1_HUMAN	DNA repair protein REV1	3GQC	0.81	0.47
PPIE_HUMAN	Peptidvl-prolvl cis-trans isomerase E	3MDF	0.80	0.46
CALM_HUMAN	Calmodulin	2LL6	0.79	0.46
HLTF_HUMAN	Helicase-like transcription factor	2L1I	0.78	0.45
HECW2_HUMAN	E3 ubiquitin-protein liqase HECW2	2LFE	0.77	0.44
SYT1_HUMAN	Svnaptotaqmin-1	2R83	0.69	0.40
CALL3_HUMAN	Calmodulin-like protein 3	1GGZ	0.66	0.38
FBXL5_HUMAN	F-box/LRR-repeat protein 5	3U9J	0.66	0.38
DYN1_HUMAN	Dynamin-1	3SNH	0.65	0.38
SIR5_HUMAN	NAD-dependent protein deacylase sirtuin-5	3RIY	0.60	0.35
LMNA_HUMAN	Prelamin-A/C	1IVT	0.59	0.35
SCO1_HUMAN	Protein SCO1 homolog	2HRN	0.57	0.34
SETB1_HUMAN	Histone-lysine N-methyltransferase SETDB1	3DLM	0.54	0.32
R0A1_HUMAN	Heterogeneous nuclear ribo-nucleoprotein A1	1U1P	0.53	0.31
PZRN3_HUMAN	E3 ubiquitin-protein liqase PDZRN3	1WH1	0.52	0.31
SH3L2_HUMAN	SH3 domain-bindinq qlutamic acid-rich-like protein 2	2CT6	0.42	0.25
OTC_HUMAN	Ornithine carbamoyltransferase	1OTH	0.42	0.25
AIMP1_HUMAN	Aminoacyl tRNA synthase complex-interacting multi-functional protein 1	1FL0	0.28	0.17
HS90A_HUMAN	Heat shock protein HSP 90-alpha	3Q6M	Disordered	
SLD5_HUMAN	DNA replication complex GINS protein SLD5	2E9X	Disordered	
HSP71_HUMAN	Heat shock 70 kDa protein 1 A/1 B	3LOF	Disordered	
TB22A_HUMAN	TBC1 domain family member 22A	2QFZ	Disordered	

Solvent accessible surface area values for EEVD in each sequence was calculated using the POPS program. Values were normalized (relative SASA or rSASA) using the SASA values for EEVD in the gankyrin-S6 ATPase complex. The values calculated from POPS program are also tabulated. The value for S6 ATPase was obtained in its uncomplexed form.
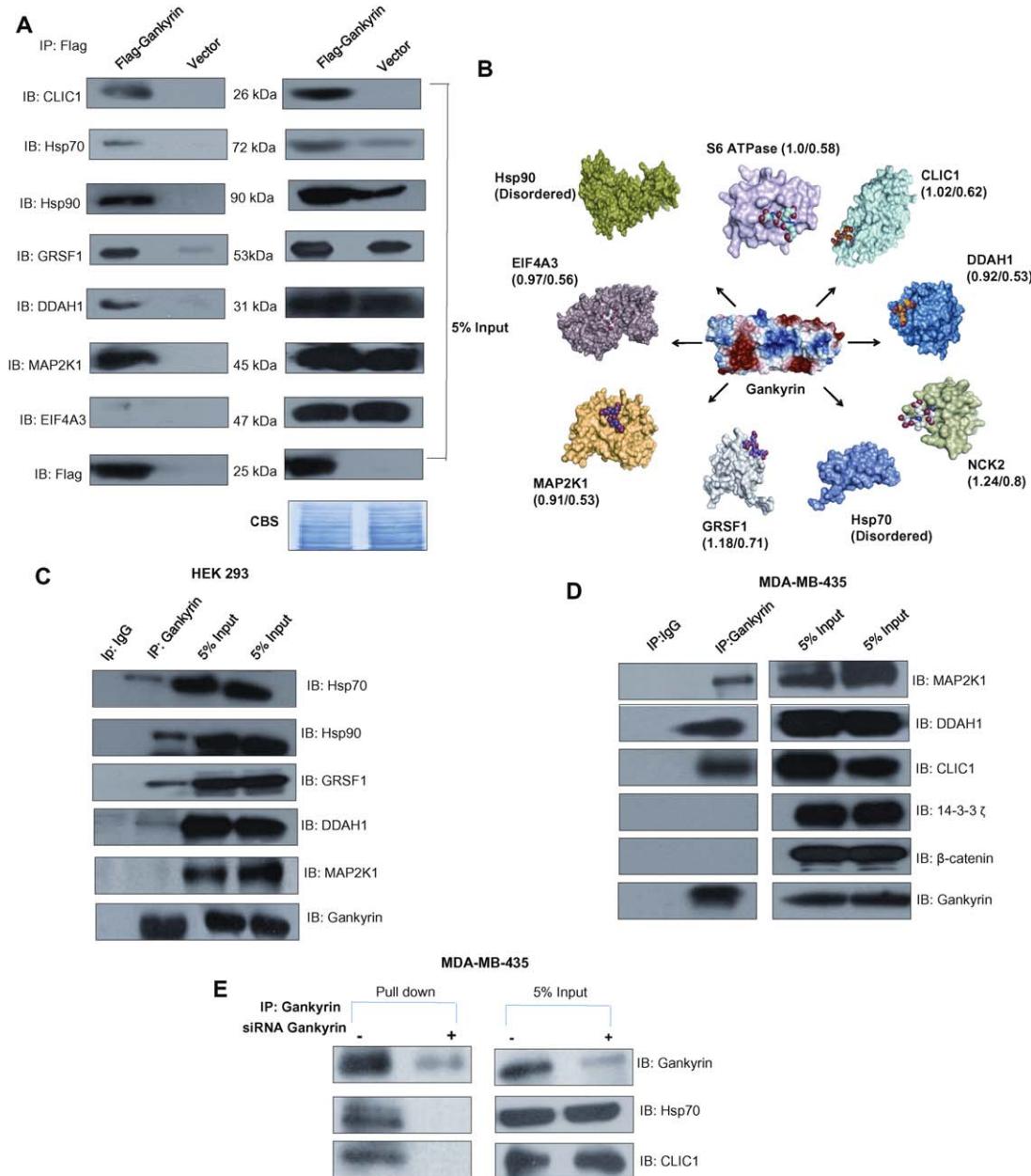
Figure 2

Within the cellular milieu, gankyrin interacts with CLIC1, Hsp70, Hsp90, GRSF1, DDAH1, MAP2K1, and does not interact with EIF4A3. (**A**) Lysate of HEK 293 cells expressing flag-gankyrin or flag alone (vector) were immobilized on M2 agarose anti-flag beads followed by immunoblotting with anti-Hsp70, anti-Hsp90, anti-GRSF1, anti-DDAH1, anti-CLIC1, anti-MAP2K1, anti-EIF4A3 antibody; 5% input represents loading control. CBS indicates equal loading. Note that some proteins are upregulated upon gankyrin overexpression; (**B**) Gankyrin (centre) is represented using surface electrostatic potential and interacting partners with rSASA value >0.5 are represented as protein surfaces. 'Hot spot' site of interaction EEVD is represented in spheres. We believe that gankyrin is the hub protein and the putative interacting partners harbouring the hot spot site EEVD act as potential nodes to create a system wide network; (**C**) Lysate of HEK 293 cells were added to gankyrin bound and IgG bound Sepharose G beads followed by immunoblotting with anti-Hsp70, anti-Hsp90, anti-GRSF1, anti-DDAH1, anti-MAP2K1 and anti-gankyrin antibody. MAP2K1 does not interact with gankyrin at endogenous levels; (**D**) Lysate of MDA-MB-435 cells were added to gankyrin bound or IgG bound Sepharose G beads followed by immunoblotting with anti-MAP2K1, anti-DDAH1, anti-CLIC1, anti-14-3-3 zeta, anti-β-catenin and anti-gankyrin antibody; (**E**) Lysate of MDA-MB-435 cells expressing siRNA against gankyrin and MDA-MB-435 cells were added to gankyrin bound Sepharose G beads followed by immunoblotting with anti-Hsp70, anti-CLIC1 and anti-gankyrin antibody.

heat shock protein90-Hsp90) out of four where EEVD was present in the disordered region. All these proteins are expressed in the cytoplasm or both in cytoplasm and nucleus. Gankyrin is a nuclear cytoplasmic shuttling protein.[20] Hsp70 and Hsp90 proteins carrying a putative signature motif for gankyrin binding intrigued us and it
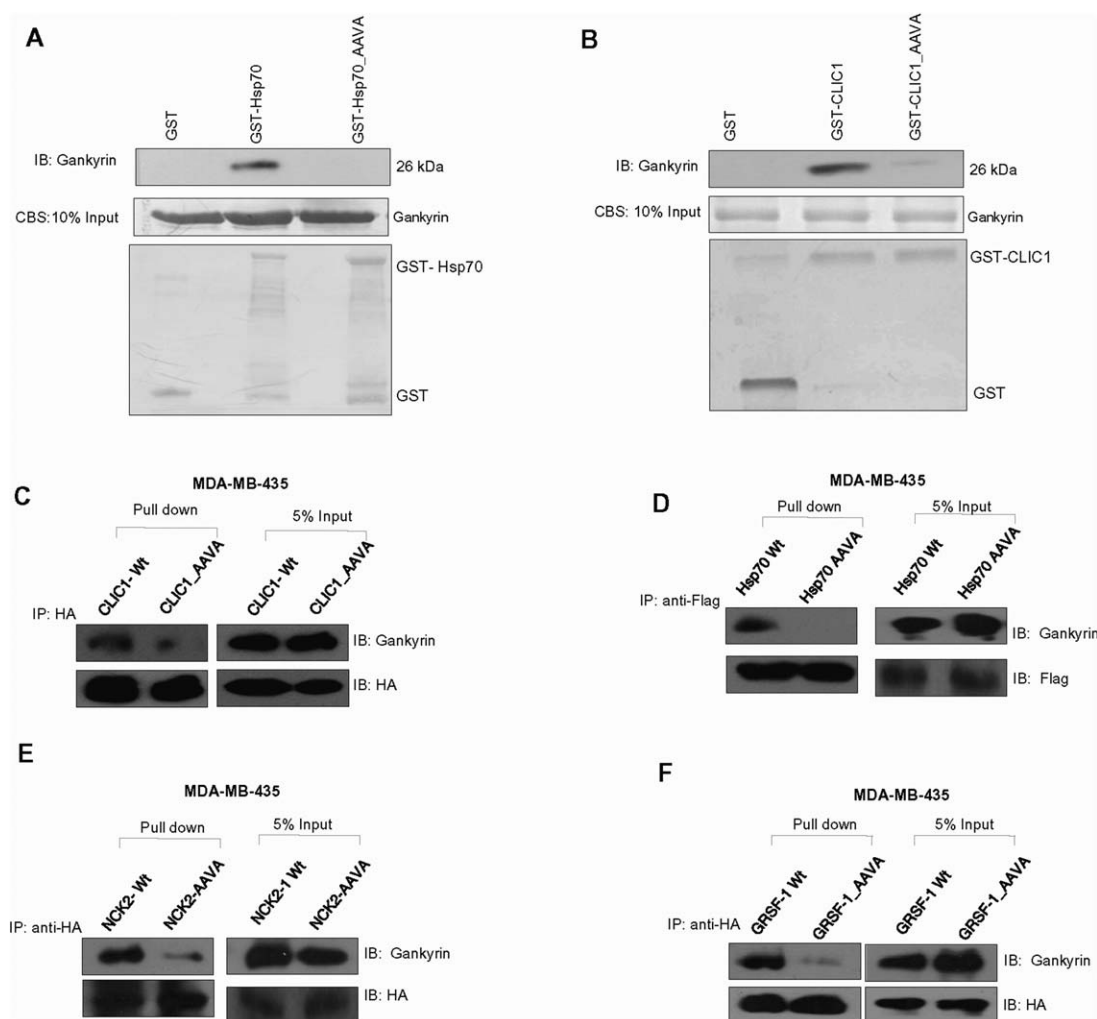
Figure 3

Gankyrin binds to Hsp70, CLIC1, NCK2 and GRSF1 through E, E and D residues. (**A** and **B**) Purified GST-Hsp70, GST-CLIC1 and their respective AAVA mutants were independently immobilized on glutathione-Sepharose 4B and incubated with 6×His tagged gankyrin. Bound His-gankyrin was detected using anti-gankyrin antibody. Wt proteins interact with His-gankyrin while the mutants are unable to do so. GST alone does not interact with gankyrin. The input for gankyrin and GST-fusion proteins are shown; (**C**) Lysate of MDA-MB-435 cells expressing HA-CLIC1 Wt or CLI-C1_AAVA; (**D**) Flag-Hsp70 Wt or Hsp70_AAVA; (**E**) HA-NCK2 Wt or NCK2_AAVA; (**F**) HA-GRSF1 Wt or GRSF1_AAVA were independently added to anti-HA antibody bound to Sepharose G beads followed by immunoblotting with anti-gankyrin antibody. Gankyrin interacts with CLIC1 Wt, Hsp70 Wt, NCK2 Wt, GRSF1 Wt but not with the corresponding AAVA mutants.

seemed important to ask if native gankyrin would actually bind these chaperones which may directly influence their function. Interestingly, Hsp90 plays a role in the assembly of 26S proteasome.[36] Functions of these proteins were discerned from Panther data base[37] and their association with cancer was verified using the classic eight hall mark properties of cancer.[38] Six out of eight proteins that we chose carried hall mark cancer properties (Supporting Information Table S3). Apart from their role as conventional chaperones, Hsp70 and Hsp90 in cancer cells are very important in conferring resistant to cell death, in malignant transformation and in generation of antigenic peptides.[39] While their well characterized role seems to be in binding to unfolded proteins via degenerate but specific sequence motifs these chaperones also recognize native or near native proteins under unique circumstances.[40,41] These chaperones also bind to kinases.[39] Geldanamycin, a known anti-cancer agent targets Hsp90 in cancer cells. CLIC1, a chloride intracellular channel protein is involved in metastasis and invasion.[42,43] In many cancer cells, voltage gated channels show this property and are considered attractive targets for cancer therapy.[44] NCK2 binds to growth factor receptors or their substrates and modulates gene expression in response to Kras signaling.[45,46] Gankyrin is a key regulator of Ras mediated activation and seems to specifically activate PI3K/Akt pathway. Evidence suggests that gankyrin is highly expressed in human lung cancer

having Kras mutations which results in Akt activation.[7] MAP kinase pathway is involved in sustained proliferation.[47] DDAH1 is a positive regulator of angiogenesis.[48] EIF4A3 is an abundant DEAD-box RNA helicase and a member of the eukaryotic initiation factor-4A (eIF4A) family of translation initiation factors.[49] Presence of EEVD in a well accessible region and the functions of these proteins make them good candidates to test our presumptions. Structure of these proteins with EEVD in the accessible region (where applicable) along with their rSASA values are shown in Figure 2(B).

Experimental validation of predicted interactions

For experimental validation of predicted interactions we used affinity pull down of gankyrin expressed as a flag tagged fusion in HEK 293 cells. Six proteins Hsp70, Hsp90, CLIC1, GRSF1, DDAH1 and MAP2K1 were present in the pull down complex indicating that the predicted sequence EEVD may be involved in the interaction between each of these client proteins and gankyrin [Fig. 2(A)]. However EIF4A3 was not found in the pull down complex. NCK2 antibody failed to detect protein from cell lysate even when used at lower dilutions than recommended. Owing to the important role of this protein in cancer we expressed this protein in mammalian cells and show that interaction is mediated through EEVD (see below).

Due to similar subcellular localization of gankyrin and the client proteins it is possible that some of these interactions may occur constitutively and at endogenous levels. It is also possible that some of these interactions may occur in response to gankyrin overexpression and therefore may be unique to malignant phenotype. To test these possibilities we used anti-gankyrin antibody immobilized on protein G Sepharose beads to pull down the endogenous complexes in HEK 293 cells. Three proteins (Hsp70, Hsp90 and GRSF1) were found in the immune complex while DDAH1 was barely detectable [Fig. 2(C)]. MAP2K1 did not interact with gankyrin [Fig. 2(C)]. CLIC1 was hardly detectable in lysate of HEK 293 cells but was several fold overexpressed in HEK 293 stable clones [Fig. 2(A); input]. Levels of MAP2K1 and DDAH1 were not very different between vector control and gankyrin overexpressing HEK 293 cells. Enough evidence exists in literature to demonstrate the role of heat shock proteins in non chaperone function which may go beyond their ability to recognize mis-folded proteins. Chaperones also interact with their co-chaperones through specific interactions between native proteins to execute their function.[39] It is interesting to note that the EEVD in Hsp70 and Hsp90 is involved in interaction with other proteins.[40]

To test if interactions seen in response to gankyrin overexpression in HEK 293 also occur in cancer cells where gankyrin is known to play a role in the deregulated phenotype, we used a breast cancer cell line. Endogenous levels of gankyrin mRNA reportedly is less in normal and other tumor tissues as compared to breast cancer tissues.[6] Therefore we used MDA-MB-435, a breast tumor derived cell line to check if the interactions observed upon gankyrin overexpression in HEK 293 cells are also seen in this cell line. MAP2K1, DDAH1, and CLIC1 were found to interact with gankyrin at endogenous levels in MDA-MB-435 cells [Fig. 2(D)]. Proteins which do not have EEVD like 14-3-3ζ or β-catenin which carries a variant EEED do not interact with gankyrin under the same conditions [Fig. 2(D)]. Interestingly we found that β-catenin levels increase in HEK 293 cells upon gankyrin overexpression but this protein as in MDA-MB-435 cells does not interact with gankyrin (data not shown). Specificity of interaction between gankyrin and EEVD containing proteins CLIC1 and Hsp70 in MDA-MB-435 cells was further confirmed by repeating IP upon gankyrin knock down using specific siRNA [Fig. 2(E)]. Normal cellular homeostasis requires turnover of proteins and spatiotemporal regulation of protein interactions. By stabilizing existing networks or creating new networks gankyrin may induce deregulated phenotype that may be partly responsible for malignancy.

Direct interactions of client proteins and evidence for EEVD as the hot spot site of interaction

When methods used to identify protein-protein interactions are compared, techniques which demonstrate physical association seem to be more faithful representatives of functionally relevant interactions; 90 to 95% interactions established by direct/indirect immune precipitation studies and 80% of *in vitro* biochemical studies correlate with the cellular role.[50]

We followed affinity pull down assays with *in vitro* biochemical experiments to demonstrate direct interactions between gankyrin and the client proteins identified in this study. Recombinant form of gankyrin was expressed as a his-tagged fusion protein while the client proteins Hsp70 and CLIC1 were expressed as GST-fusions. Gankyrin was present only in fractions containing GST-fusion proteins and not in GST alone control [Fig. 3(A,B)]. To confirm that these direct interactions are mediated through residues E, E and D in each case, the sequence EEVD was mutated to AAVA and GST pull down assay was repeated. Mutations abolished interaction of each of these proteins with gankyrin [Fig. 3(A,B)]. To verify whether the *in vitro* direct interaction between recombinant proteins is also sensitive to mutations within EEVD within the cellular milieu, HA-CLIC1, Flag-Hsp70, HA-NCK2 and HA-GRSF1 and their corresponding AAVA mutant were cloned and expressed in MDA-MB-435 cells. While all the Wt proteins showed

definitive interaction with endogenous gankyrin [Fig. 3(C–F)], as expected the corresponding mutant proteins failed to interact. Interaction of endogenous gankyrin with Wt NCK2 and Wt GRSF1 and not the corresponding AAVA mutant were also detected in HEK 293 cells [Supporting Information Fig. S3(A,B)]. These results establish that observed interactions within the cells are direct and EEVD is the shared hot spot site at the interface.

To further illustrate our point, we tested the ability of naked short peptide sequence EEVD to inhibit binding of CLIC1 (used as a representative example) to gankyrin. In the *in vitro* pull down assay, peptide EEVD prevented complex formation between the two proteins in a concentration dependent manner [Fig. 4]. Control peptides that do not interact with gankyrin but interact with another subunit of the proteasome (unpublished work) did not prevent interaction even at 0.5 mM, the highest concentration tested for EEVD. Using a semiquantitative approach, peptide concentration required for 50% inhibition in binding was estimated to be approximately 50 μM (Supporting Information Fig. S4). This value for a short peptide lies within the range reported for other peptides used to inhibit protein-protein interactions[51] (Supporting Information Table S4). These results provide unequivocal evidence for the presence of a hot spot motif shared by proteins in the gankyrin hub network.

Interaction between Gankyrin and CLIC1 is important for cell migration and invasion in MDA-MB-231 and HEK 293 cells

In order to evaluate the functional relevance of the interaction between gankyrin and proteins containing EEVD, we chose to study function of gankyrin-CLIC1 interaction because of the following reasons: (a) CLIC1 was barely detectable in HEK 293 Wt cells and levels increase in response to gankyrin overexpression; (b) Chloride intracellular channel proteins are well known for their role in invasion and metastasis.[42–44] We initially tested the independent role of gankyrin and CLIC1 in the metastatic potential of MDA-MB-231 by performing surrogate wound healing and invasion assays. Knock down of either of the two proteins decreased the ability of these cells to migrate and close the wound. CLIC1 seems to be more effective than gankyrin in healing the wound (Fig. 5). These results were recapitulated in the invasion assay using Boyden Chamber [Supporting Information Fig. S5(A)]. These results confirmed the role of these two proteins in migration and invasion.

To check if the interaction is important for driving this phenotype CLIC1 Wt or the AAVA mutant of CLIC1 were overexpressed in MDA-MB-231 cells as well as in HEK 293 cells and their ability to migrate and close the wound was monitored. In MDA-MB-231 cells, over expression of CLIC1 Wt protein resulted in an increase
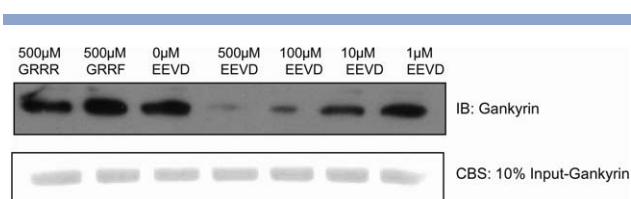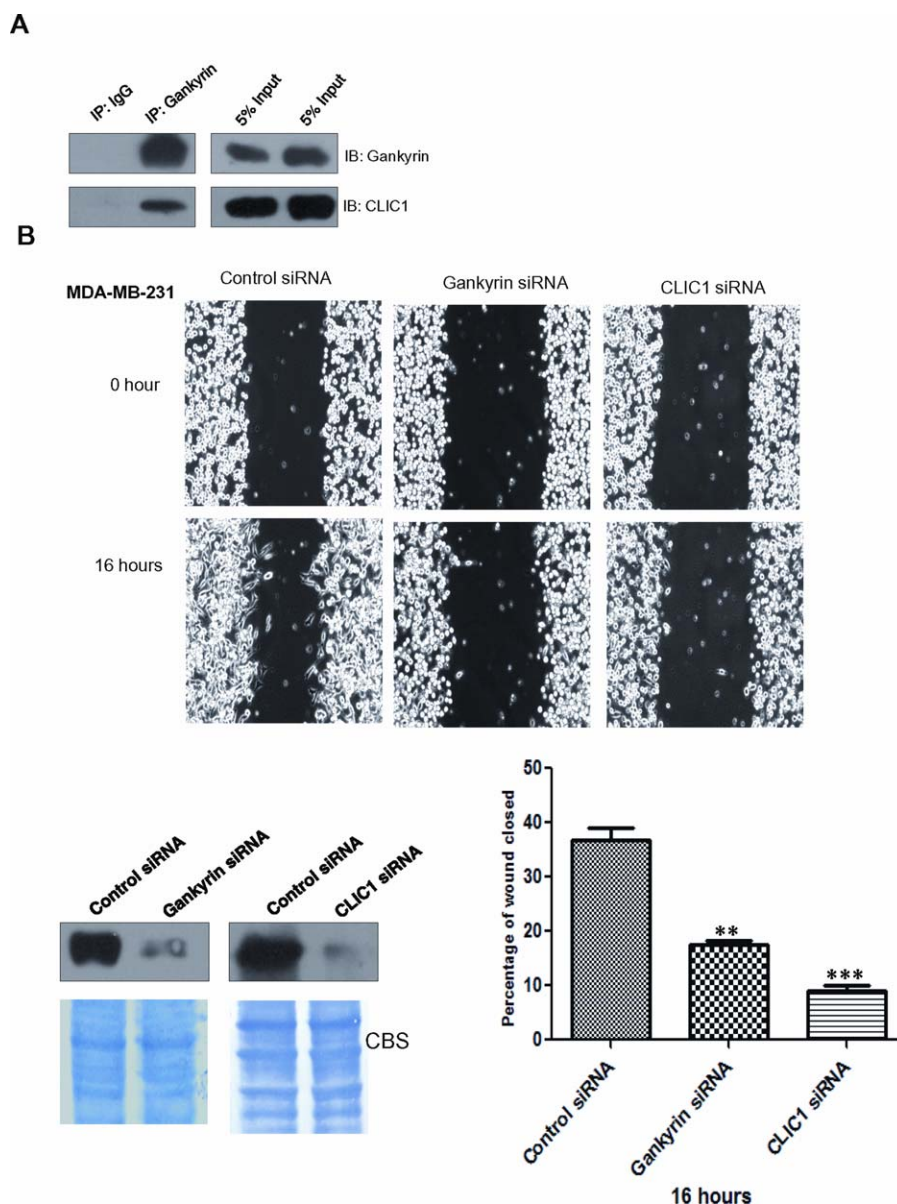

Figure 4

Interface peptide EEVD inhibits interaction of full length protein with gankyrin. His-Gankyrin was incubated with different concentrations of EEVD peptide. Peptides GRRF and GRRR were used as controls. These preincubated complexes were added to the GST-CLIC1 bound GST beads. EEVD peptide and the two control peptides inhibited binding of His-Gankyrin to GST-CLIC1 in a concentration dependent manner.

in the percentage of wound closed (48%) as compared to vector control (31%) while the mutant cells (27%) behaved like those of the vector control cells (Fig. 6). HEK 293 cells overexpressing CLIC1 Wt showed ∼98% wound closure as compared to vector control cells (42%) and cells overexpressing CLIC1_AAVA mutant showed 27% wound closure. MDA-MB-231 cells overexpressing CLIC1 Wt showed increase in their invasive potential as compared to vector control and CLIC1_AAVA overexpressing cells [Supporting Information Fig. S5(B)] behaved like the vector control cells. We further confirmed these observations by specifically silencing endogenous CLIC1 using smart pool of UTR specific siRNA and demonstrating that only Wt CLIC1 and not the mutant protein can rescue the "phenotype" in MDA-MB-231 cells (Fig. 7). These results taken together indicate that interaction of CLIC1 with gankyrin through EEVD enhances the migratory potential of CLIC1 in this *ex vivo* model.

DISCUSSION

Protein-protein interactions are central to cellular communication.[1] These interactions are stabilized or new interactions created in abnormal conditions like cancer.[1] Therefore identifying system wide interactions of a key regulatory protein like an oncoprotein or a tumor suppressor protein is crucial for understanding the deregulated phenotype. Many studies aimed at characterizing network of interactions show that oncoproteins act as hubs. Perturbation of key interactions of such hubs with other proteins in the node would render the network unstable.[22] Therefore these interactions are vulnerable for therapeutic intervention.

In the present study we illustrate one method to identify multiple interacting partners of a hub protein. We use residue level knowledge of a known protein interface of gankyrin-S6ATPase complex to predict unknown complexes of gankyrin.[1,52–54] We asked whether some of the basic principles common to protein-protein interactions identified by independent investigators can be used
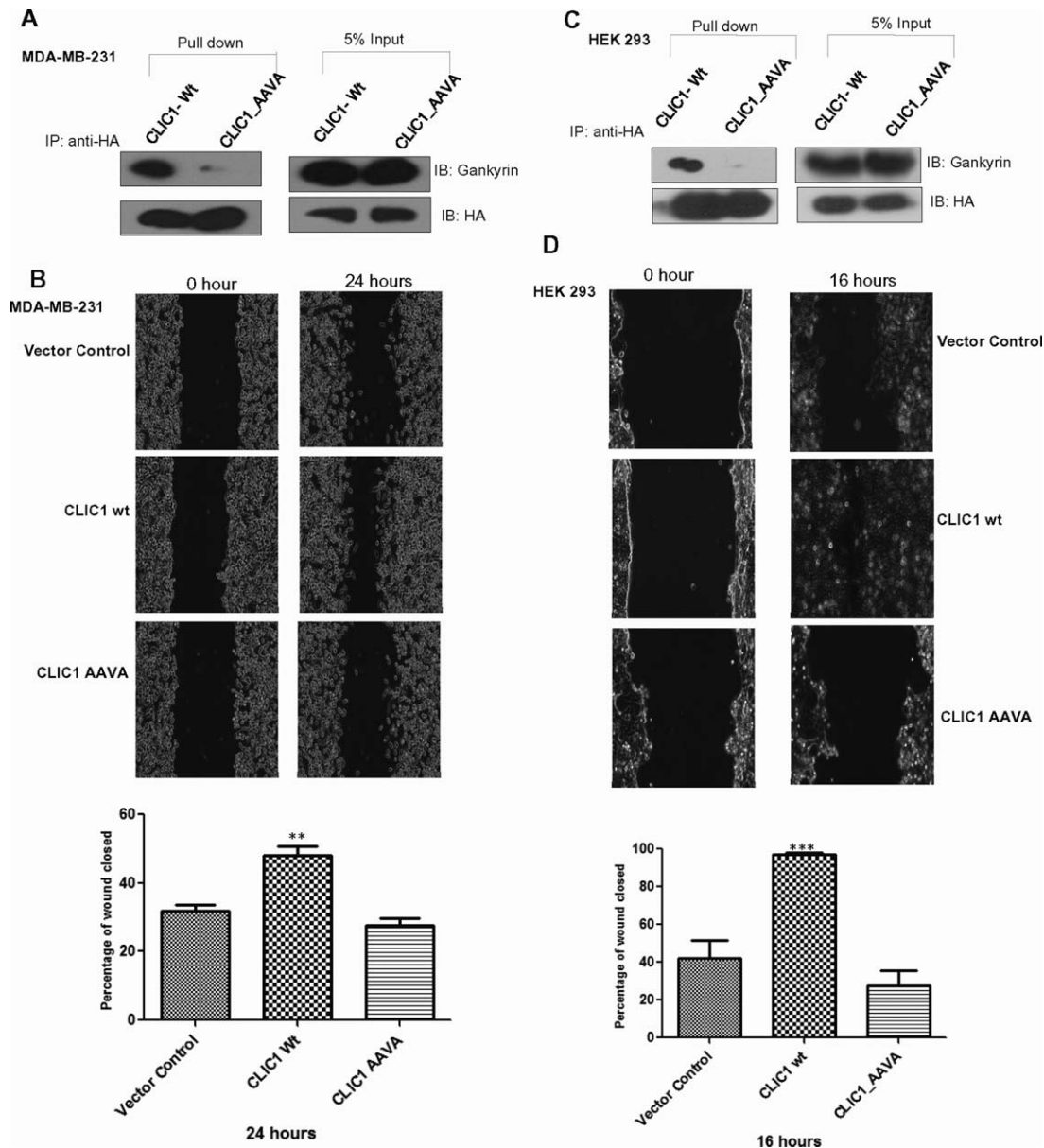
Figure 5

Silencing of gankyrin and CLIC1 affects migration in MDA-MB-231 cells. (**A**) Lysate of MDA-MB-231 cells were added to gankyrin bound or IgG bound Sepharose G beads followed by immunoblotting with anti-CLIC1 and anti-gankyrin antibody; (**B**) MDA-MB-231 cells were treated with 100 nM of gankyrin specific siRNA or CLIC1 siRNA or control siRNA. After 72 h, cells at 90% confluence were treated with 10 μg/mL of mitomycin C for 3 h, wounded and healing monitored for 16 h. Percentage wound healed at the end of 16 h were calculated and the data are represented as mean ± SEM of three experiments. Statistical analysis is done using unpaired t-test (**$P = 0.0013$, ***$P = 0.0004$). Western blot confirms down regulation of gankyrin and CLIC1 in the respective experiments. CBS shows equal loading. [Color figure can be viewed in the online issue, which is available at wileyonlinelibrary.com.]

to predict large number of novel interactions? Basic assumptions of our method are the following: (a) interactions of a protein with multiple partners may involve a common recognition motif (b) this recognition motif may be independent of sequence homology among the client proteins (c) hub protein like gankyrin whose deregulated functions are dependent on overexpression are likely to recognize such common motifs in non-homologous proteins. This may explain their ability to alter multiple pathways and drive the oncogenic phenotype (d) since hot spot sites are conserved across interfaces and represent very few residues, they may also be vulnerable for interventions.

Protein interfaces are determined by shape complementarity, enriched in patches of buried salt bridges and pairing of hydrophobic and hydrophilic hot spots which

Figure 6

Overexpression of CLIC1 and CLIC1_AAVA affects migration of MDA-MB-231 cells. (**A**) Lysate of MDA-MB-231 cells expressing HA-CLIC1 Wt and CLIC1_AAVA were independently added to anti-HA antibody bound to Sepharose G beads followed by immunoblotting with anti-gankyrin antibody. Gankyrin interacts with CLIC1 Wt but not with its corresponding mutant; (**B**) MDA-MB-231 cells transiently overexpressing CLIC1 Wt or CLIC1_AAVA were treated with 10 μg/mL of mitomycin C for 3 h, wounded and healing monitored for 24 h. Percentage of wound healed was calculated and the data are represented as mean ± SEM of three independent experiments (**$P = 0.0059$); (**C**) Lysate of HEK 293 cells expressing HA-tagged CLIC1 Wt and CLIC1_AAVA were independently added to anti-HA antibody bound to Sepharose G beads followed by immunoblotting with anti-gankyrin antibody. Gankyrin interacts with CLIC1 Wt but not with its corresponding mutant; (**D**) HEK 293 cells transiently overexpressing CLIC1 Wt and CLIC1_AAVA were treated with 10 μg/mL of mitomycin C for 3 h, wounded and healing monitored for 16 h. Data were processed as above (***$P = 0.0002$).

are juxtaposed on the opposite sides of the interface.[55] As described above, gankyrin-S6 interface is enriched in charged residues at the interface and buries a large surface area upon complex formation. Residues like tryptophan, glycine, proline, cysteine, tyrosine, and glutamate are apparently more conserved at hot spot sites.[55] Aspar-

tate is also considered as a relatively common hot spot site residue.[24] Besides as described above, we found that in mammalian cells mutation of EEVD to AAVA in S6ATPase prevents interaction with gankyrin [Supporting Information Fig. S2(C)]. Based on the strength of these observations using a linear stretch of a four amino acid
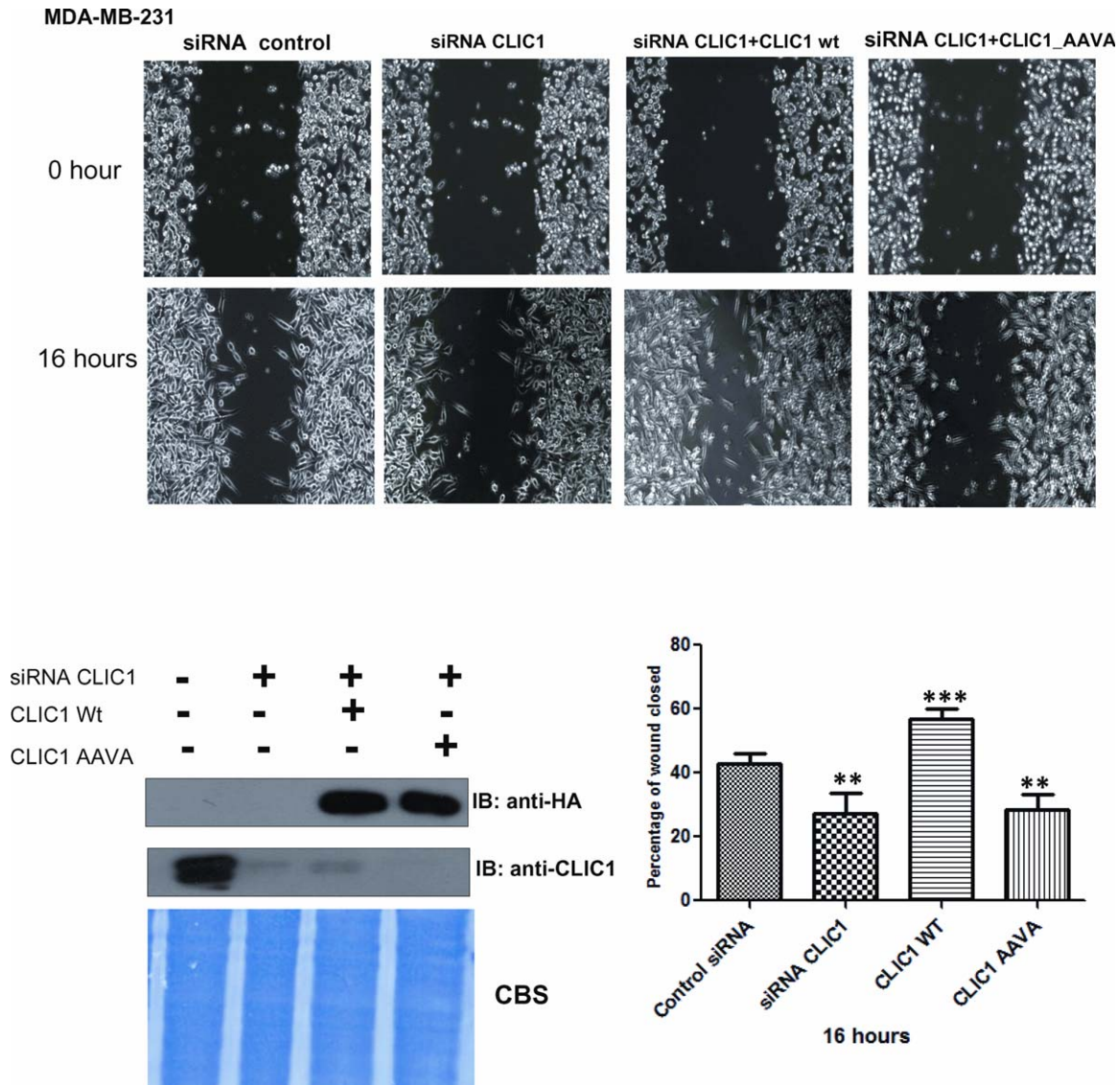
Figure 7

Interaction of gankyrin with CLIC1 enhances migration. MDA-MB-231 cells were transfected with control siRNA or CLIC1 siRNA (UTR region) or CLIC1 siRNA + cDNA for CLIC1 Wt or CLIC1 siRNA + cDNA for CLIC1_AAVA. After 72 h these cells were treated with 10 μg/mL of mitomycin C for 3 h, wounded and healing monitored for 16 h. Data from two independent experiments were processed as described in Figure 5 (**$P = 0.0042$, ***$P = 0.0006$, **$P = 0.0020$). Cells transfected with CLIC1 Wt show significant increase in the percentage of wound healed as compared with that of CLIC1_AAVA transfected cells which behave like the vector control cells. [Color figure can be viewed in the online issue, which is available at wileyonlinelibrary.com.]

sequence EEVD at the S6ATPase gankyrin interface, 34 novel interacting partners from the PDB data of human proteins were predicted. Stringent cut offs were used for testing our hypothesis. Proteins in which EEVD was present in an accessible region (with rSASA values >0.5) were chosen. Interactions within the cell would be dictated by factors other than sequence specificity viz. subcellular distribution, post translational modifications and signaling cues.[30] Proteins present in the cytoplasm like gankyrin were short listed. Some of these may also be resident in other subcellular compartments like nuclei as well.

Among the eight proteins tested, seven interactions were seen in at least two stable clones and in three independent experiments. Four of these interactions occur at endogenous levels indicating that these are of sufficient affinity to be detected whereas three are unique to gankyrin overexpression either in stable clones or in breast cancer cells. These are probably of lower affinity or occur in response to oncogene induced signaling. Not all proteins containing EEVD in an accessible region interact with gankyrin as seen by the failure of EIF4A3 to be detected in the pull down complex [Fig. 2(A)]. This is

not surprising since there are additional levels of regulation that govern PPI. Interaction between recombinant proteins and failure of AAVA mutants to interact establishes that, observed interactions are in fact through predicted EE and D residues. Ability of EEVD peptide to compete with full length protein for interaction further substantiates that bulk of the binding energy indeed comes from this short sequence motif. Therefore this motif is a conserved hot spot site interaction shared among the client proteins. Although it is unclear if interacting residues in gankyrin are the same in all cases, interaction interfaces of the same protein, mediating different interactions are more likely to cause distinct interruptions in the overall interactome. This has different biological consequences leading to pleiotropic effects.[56] We believe that one of the major reasons for the observed oncogenic property of gankyrin in multiple cell types is its ability to interact with different partners through the conserved hot spot sites on the client proteins. There are many more EEVD containing proteins in the human proteome that remain to be tested. Moreover based on our mutagenesis experiments valine at the EEVD hot spot site does not seem to have a major contribution to binding affinity. It seems therefore that other sequence variants of EEVD such as EEXD (X is any residue) may also interact with gankyrin. This is supported by the fact that when Val is mutated to Glu in CLIC1 the mutant protein still binds to gankyrin [Supporting Information Fig. S3(C)]. On the other hand β-catenin which carries EEED does not interact with gankyrin which is not surprising because interactions are not dictated by sequence or accessibility alone. Subcellular localization and other regulatory mechanisms are well known to play a role in determining interactions.

Among the proteins that were reported to interact with gankyrin such as Rb, CDK4, MDM2, MAGE-A4, p65 (RelA) of NF-kB and FIH-1,[57] EEND is present in MDM2 and Rb carries the tetrapeptide motif EEPD (Supporting Information Table S5). While there is no structural information available for MDM2 in this region, in RB EEPD forms the N-terminus of the solved crystal structure (aa 53EEPD56). Whether these residues are actually involved in interaction with gankyrin however remains to be tested. But it is interesting to note two key proteins known to interact with gankyrin carry the EEXD motif.

How does identification of these novel interactions help in better understanding of the role of gankyrin in oncogenesis and as a key hub protein?

Based on its role in Rb, p53 degradation, involvement of gankyrin in cell proliferation seems understandable. However, its role in other oncogenic properties like can-

cer metastasis is still unclear. A very recently study show that gankyrin is involved in tumor metastasis.[6]

Two novel interacting proteins CLIC1 and DDAH1 identified here are important in metastasis and angiogenesis.[48,58] DDAH1 is involved in vascular permeability and in NO synthesis.[59,60] It is especially involved in inflammation induced cancer. Increased DDAH1 expression has direct consequence on vascularization and tumor growth.[48] DDAH1 is also predicted to methylate arginine residues in proteins which are likely to affect protein turnover. Here is another example wherein gankyrin via interaction with DDAH1 may cross talk with the proteasome pathway.

CLIC1 protein levels are more when gankyrin is overexpressed. This protein is seen in complex with gankyrin in breast cancer cells [Fig. 2(D)]. Voltage gated channels such as CLIC1 induce metastatic phenotype.[58] Overexpression of CLIC1 is a potential prognostic marker for colorectal carcinoma,[58] gallbladder carcinoma,[61] gastric cancer,[42] lung adenocarcinoma[62] and glioma.[63] Both DDAH1 and CLIC1 play a universal role in metastasis and angiogenesis in many cancer types. In this context it will be interesting to note that these interactions with gankyrin are conserved in both glioma cells and in DAOY medulloblastoma cells (data not shown). These results implicate a more universal role for gankyrin as an important hub in protein-protein interaction network in several different cancer types and therefore a potentially vulnerable target for therapeutic intervention.

What would be the consequence of interaction of gankyrin with these proteins?

Gankyrin may deregulate normal cellular homoeostasis by stabilizing the basal network. It may rewire the network by introducing new players and shift the nodes and edges of the functional networks. Establishing this concept through experimentation is a difficult but an important and mandatory task. We have initiated these studies and in this report we clearly demonstrate that interaction of CLIC1 with gankyrin is mandatory for the ability of MDA-MB-231 cells to migrate/invade as demonstrated by the wound healing assay. Since this property is dependent on the motility of the cells, we believe that this interaction is likely to be crucial in the invasive properties of these metastatic cells in breast cancer.

How does the approach used here compare with similar or different approaches used in the identification of protein-protein interactions?

Several methods like yeast two hybrid, phage display or mass spectrometry based high throughput detection of affinity enriched complexes are used to identify unknown protein-protein interactions.[2,3,64,65] While first two methods suffer from accuracy, MS based

approaches tend to be more accurate. Experimental strategies like proteome peptide scanning and whole interactome scanning experiments (WISE) which rely on short peptide sequences within proteins (Short Linear Motifs or SliM) have been used to identify new interactions. However, identifying functionally relevant SliMs from random occurrences in eukaryotes is not straightforward.[4,34,66–69] This is because many such SliMs seem to be part of unstructured or disordered regions in proteins with large variability in sequence making it difficult to accurately predict or use this information. Experimental proof from a wide variety of examples such as ours will help in enhancing the reliability and accuracy of these predictions.

All such studies can be reliable and accurate if residue-level structural information on protein-protein interfaces is incorporated in prediction programs or other detection algorithms. However, high-resolution structural information, especially of protein complexes, grows at a much lower pace and therefore there is paucity of information that can be readily extended to large scale identifications. Nevertheless ability to do so will go a long way to better understand deregulated physical and functional networks mediated by oncoproteins in diseases such as cancer. Recently published article makes a bold attempt in predicting novel interactions by modelling structures of unknown complexes.[5]

Some of the well-known interactions with information on hot spot sites are derived from single complex analysis driven by investigator driven interest. These have been deposited in different data bases.[23,24] In addition there are many examples in literature where peptides and small molecules are used as inhibitors of protein-protein interaction emphasizing again the importance of structural information in the success of such approaches.[51,70–85] Supporting information Table S4 lists examples of protein complexes with known interface and peptides/small molecules to inhibit such interactions. It is in this context that the approach presented here gains importance. Our study integrates various key important principles described above for accurately identifying novel protein-protein interactions. We use the concept of (a) SLiM across secondary structural elements including disordered regions in proteins, (b) the concept of sequence conservation at protein interfaces and (c) presence of hot spot sites to identify novel interactions of a hub protein. Judging by the functional annotations of the proteins identified it seems that this network of interactions is likely to bridge at least six of the eight hall mark properties of cancer. Our ability to inhibit these interactions implies that this network of interactions can be perturbed. Disruption of interaction between gankyrin and CLIC1 by mutating the hot spot site inhibits the ability of the cancer cell line MDA-MB-231 cells to migrate or invade thus validating functional relevance of these interactions. Taken together the concept of short linear

sequence motifs at protein interfaces can be used to identify novel functionally relevant protein complexes formed by key hub proteins.

REFERENCES

1. Kar G, Gursoy A, Keskin O. Human cancer protein-protein interaction network: a structural perspective. PLoS Comput Biol 2009;5: e1000601.
2. Vasilescu J, Figeys D. Mapping protein-protein interactions by mass spectrometry. Curr Opin Biotechnol 2006;17:394–399.
3. Vermeulen M, Hubner NC, Mann M. High confidence determination of specific protein-protein interactions using quantitative mass spectrometry. Curr Opin Biotechnol 2008;19:331–337.
4. Weatheritt RJ, Luck K, Petsalaki E, Davey NE, Gibson TJ. The identification of short linear motif-mediated interfaces within the human interactome. Bioinformatics 2012;28:976–982.
5. Zhang QC, Petrey D, Deng L, Qiang L, Shi Y, Thu CA, Bisikirska B, Lefebvre C, Accili D, Hunter T, Maniatis T, Califano A, Honig B. Structure-based prediction of protein-protein interactions on a genome-wide scale. Nature 2012;490:556–560.
6. Zhen C, Chen L, Zhao Q, Liang B, Gu YX, Bai ZF, Wang K, Xu X, Han QY, Fang DF, Wang SX, Zhou T, Xia Q, Gong WL, Wang N, Li HY, Jin BF, Man JH. Gankyrin promotes breast cancer cell metastasis by regulating Rac1 activity. Oncogene 2013;32:3452–3460.
7. Man JH, Liang B, Gu YX, Zhou T, Li AL, Li T, Jin BF, Bai B, Zhang HY, Zhang WN, Li WH, Gong WL, Li HY, Zhang XM. Gankyrin plays an essential role in Ras-induced tumorigenesis through regulation of the RhoA/ROCK pathway in mammalian cells. J Clin Invest 2010;120:2829–2841.
8. Meng Y, He L, Guo X, Tang S, Zhao X, Du R, Jin J, Bi Q, Li H, Nie Y, Liu J, Fan D. Gankyrin promotes the proliferation of human pancreatic cancer. Cancer Lett 2010;297:9–17.
9. Fu XY, Wang HY, Tan L, Liu SQ, Cao HF, Wu MC. Overexpression of p28/gankyrin in human hepatocellular carcinoma and its clinical significance. World J Gastroenterol 2002;8:638–643.
10. Li J, Knobloch TJ, Kresty LA, Zhang Z, Lang JC, Schuller DE, Weghorst CM. Gankyrin, a biomarker for epithelial carcinogenesis, is overexpressed in human oral cancer. Anticancer Res 2011;31: 2683–2692.
11. Tang S, Yang G, Meng Y, Du R, Li X, Fan R, Zhao L, Bi Q, Jin J, Gao L, Zhang L, Li H, Fan M, Wang Y, Wu K, Liu J, Fan D. Overexpression of a novel gene gankyrin correlates with the malignant phenotype of colorectal cancer. Cancer Biol Ther 2010;9:88–95.
12. Higashitsuji H, Itoh K, Nagao T, Dawson S, Nonoguchi K, Kido T, Mayer RJ, Arii S, Fujita J. Reduced stability of retinoblastoma protein by gankyrin, an oncogenic ankyrin-repeat protein overexpressed in hepatomas. Nat Med 2000;6:96–99.
13. Dawson S, Apcher S, Mee M, Higashitsuji H, Baker R, Uhle S, Dubiel W, Fujita J, Mayer RJ. Gankyrin is an ankyrin-repeat oncoprotein that interacts with CDK4 kinase and the S6 ATPase of the 26 S proteasome. J Biol Chem 2002;277:10893–10902.
14. Bedford L, Paine S, Sheppard PW, Mayer RJ, Roelofs J. Assembly, structure, and function of the 26S proteasome. Trends Cell Biol 2010;20:391–401.
15. Roelofs J, Park S, Haas W, Tian G, McAllister FE, Huo Y, Lee BH, Zhang F, Shi Y, Gygi SP, Finley D. Chaperone-mediated pathway of proteasome regulatory particle assembly. Nature 2009;459:861–865.
16. Higashitsuji H, Higashitsuji H, Itoh K, Sakurai T, Nagao T, Sumitomo Y, Masuda T, Dawson S, Shimada Y, Mayer RJ, Fujita J.

The oncoprotein gankyrin binds to MDM2/HDM2, enhancing ubiquitylation and degradation of p53. Cancer Cell 2005;8:75–87.

17. Krzywda S, Brzozowski AM, Higashitsuji H, Fujita J, Welchman R, Dawson S, Mayer RJ, Wilkinson AJ. The crystal structure of gankyrin, an oncoprotein found in complexes with cyclin-dependent kinase 4, a 19 S proteasomal ATPase regulator, and the tumor suppressors Rb and p53. J Biol Chem 2004;279:1541–1545.

18. Nagao T, Higashitsuji H, Nonoguchi K, Sakurai T, Dawson S, Mayer RJ, Itoh K, Fujita J. MAGE-A4 interacts with the liver oncoprotein gankyrin and suppresses its tumorigenic activity. J Biol Chem 2003; 278:10668–10674.

19. Chen Y, Li HH, Fu J, Wang XF, Ren YB, Dong LW, Tang SH, Liu SQ, Wu MC, Wang HY. Oncoprotein p28 GANK binds to RelA and retains NF-kappaB in the cytoplasm through nuclear export. Cell Res 2007;17:1020–1029.

20. Higashitsuji H, Higashitsuji H, Liu Y, Masuda T, Fujita T, Abdel-Aziz HI, Kongkham S, Dawson S, John Mayer R, Itoh Y, Sakurai T, Itoh K, Fujita J. The oncoprotein gankyrin interacts with RelA and suppresses NF-kappaB activity. Biochem Biophys Res Commun 2007;363:879–884.

21. Ekman D, Light S, Björklund ÅK, Elofsson A. What properties characterize the hub proteins of the protein-protein interaction network of *Saccharomyces cerevisiae*? Genome Biol 2006;7:R45.

22. Tsai C-J, Buyong M, Nussinov R. Protein-protein interaction networks: how can a hub protein bind so many different partners? Trends Biochem Sci 2009;34:594–600.

23. Kortemme T, Baker D. A simple physical model for binding energy hot spots in protein-protein complexes. Proc Natl Acad Sci USA 2002;99:14116–14121.

24. Bogan AA, Thorn KS. Anatomy of hot spots in protein interfaces. J Mol Biol 1998;280:1–9.

25. Fraternali F, Cavallo L. Parameter optimized surfaces (POPS): analysis of key interactions and conformational changes in the ribosome. Nucleic Acids Res 2002;30:2950–2960.

26. Rodriguez LG, Wu X, Guan JL. Wound-healing assay. Methods Mol Biol 2005;294:23–29.

27. Kim SY, Hur W, Choi JE, Kim D, Wang JS, Yoon HY, Piao LS, Yoon SK. Functional characterization of human oncoprotein gankyrin in Zebrafish. Exp Mol Med 2009;41:8–16.

28. Mani SA, Guo W, Liao MJ, Eaton EN, Ayyanan A, Zhou AY, Brooks M, Reinhard F, Zhang CC, Shipitsin M, Campbell LL, Polyak K, Brisken C, Yang J, Weinberg RA. The epithelial-mesenchymal transition generates cells with properties of stem cells. Cell 2008;133:704–715.

29. Nakamura Y, Nakano K, Umehara T, Kimura M, Hayashizaki Y, Tanaka A, Horikoshi M, Padmanabhan B, Yokoyama S. Structure of the oncoprotein gankyrin in complex with S6 ATPase of the 26S proteasome. Structure 2007;15:179–189.

30. Venkatraman P, Balakrishnan S, Rao S, Hooda Y, Pol S. A sequence and structure based method to predict putative substrates, functions and regulatory networks of endo proteases. PLoS One 2009;4:e5700.

31. Wadhawan V, Kolhe YA, Sangith N, Gautam AK, Venkatraman P. From prediction to experimental validation: desmoglein 2 is a functionally relevant substrate of matriptase in epithelial cells and their reciprocal relationship is important for cell adhesion. Biochem J 2012;447:61–70.

32. Singh Gautam AK, Balakrishnan S, Venkatraman P. Direct ubiquitin independent recognition and degradation of a folded protein by the eukaryotic proteasomes-origin of intrinsic degradation signals. PLoS One 2012;7:e34864.

33. Jacob E, Unger R. A tale of two tails: why are terminal residues of proteins exposed? Bioinformatics 2007;23:e225–e230.

34. Edwards RJ, Davey NE, Shields DC. SLiMFinder: a probabilistic method for identifying over-represented, convergently evolved, short linear motifs in proteins. PLoS One 2007;2:e967.

35. Dror T, Ivet B. Recruitment of rare 3-grams at functional sites: is this a mechanism for increasing enzyme specificity? BMC Bioinformatics 2007;8:226.

36. Imai J, Maruya M, Yashiroda H, Yahara I, Tanaka K. The molecular chaperone Hsp90 plays a role in the assembly and maintenance of the 26S proteasome. EMBO J 2003;22:3557–3567.

37. Thomas PD, Kejariwal A, Campbell MJ, Mi H, Diemer K, Guo N, Ladunga I, Ulitsky-Lazareva B, Muruganujan A, Rabkin S, Vandergriff JA, Doremieux O. PANTHER: a browsable database of gene products organized by biological function, using curated protein family and subfamily classification. Nucleic Acids Res 2003;31: 334–341.

38. Hanahan D, Weinberg RA. Hallmarks of cancer: the next generation. Cell 2011;144:646–674.

39. Jolly C, Morimoto RI. Role of the heat shock response and molecular chaperones in oncogenesis and cell death. J Natl Cancer Inst 2000;92:1564–1572.

40. Carrello A, Allan RK, Morgan SL, Owen BA, Mok D, Ward BK, Minchin RF, Toft DO, Ratajczak T. Interaction of the Hsp90 cochaperone cyclophilin 40 with Hsc70. Cell Stress Chaperones 2004;9: 167–181.

41. Pang Q, Keeble W, Christianson TA, Faulkner GR, Bagby GC. FANCC interacts with Hsp70 to protect hematopoietic cells from IFN-gamma/TNF-alpha-mediated cytotoxicity. EMBO J 2001;20: 4478–4489.

42. Chen CD, Wang CS, Huang YH, Chien KY, Liang Y, Chen WJ, Lin KH. Overexpression of CLIC1 in human gastric carcinoma and its clinicopathological significance. Proteomics 2007;7:155–167.

43. Petrova DT, Asif AR, Armstrong VW, Dimova I, Toshev S, Yaramov N, Oellerich M, Toncheva D. Expression of chloride intracellular channel protein 1 (CLIC1) and tumor protein D52 (TPD52) as potential biomarkers for colorectal cancer. Clin Biochem 2008;41: 1224–1236.

44. Le Guennec JY, Ouadid-Ahidouch H, Soriani O, Besson P, Ahidouch A, Vandier C. Voltage-gated ion channels, new targets in anti-cancer research. Recent Pat Anticancer Drug Discov 2007;2: 189–202.

45. Braverman LE, Quilliam LA. Identification of Grb4/Nckβ, a src homology 2 and 3 domain-containing adapter protein having similar binding and biological properties to Nck. J Biol Chem 1999;274: 5542–5549.

46. Latreille M, Larose L. Nck in a complex containing the catalytic subunit of protein phosphatase 1 regulates eukaryotic initiation factor 2α signaling and cell survival to endoplasmic reticulum stress. J Biol Chem 2006;281:26633–26644.

47. Liu X, Yan S, Zhou T, Terada Y, Erikson RL. The MAP kinase pathway is required for entry into mitosis and cell survival. Oncogene 2004;23:763–776.

48. Kostourou V, Troy H, Murray JF, Cullis ER, Whitley GS, Griffiths JR, Robinson SP. Overexpression of dimethylarginine dimethylaminohydrolase enhances tumor hypoxia: an insight into the relationship of hypoxia and angiogenesis in vivo. Neoplasia 2004;6:401–411.

49. Chan CC, Dostie J, Diem MD, Feng W, Mann M, Rappsilber J, Dreyfuss G. eIF4A3 is a novel component of the exon junction complex. RNA 2004;10:200–209.

50. Sprinzak E, Sattath S, Margalit H. How reliable are experimental protein-protein interaction data? J Mol Biol 2003;327:919–923.

51. Koch WJ, Inglese J, Stone WC, Lefkowitz RJ. The binding site for the beta gamma subunits of heterotrimeric G proteins on the beta-adrenergic receptor kinase. J Biol Chem 1993;268:8256–8260.

52. Ogmen U, Keskin O, Aytuna AS, Nussinov R, Gursoy A. PRISM: protein interactions by structural matching. Nucleic Acids Res 2005; 33(Suppl 2):W331–W336.

53. Tuncbag N, Gursoy A, Nussinov R, Keskin O. Predicting protein-protein interactions on a proteome scale by matching evolutionary and structural similarities at interfaces using PRISM. Nat Protoc 2011;6:1341–1354.

54. Guney E, Tuncbag N, Keskin O, Gursoy A. HotSprint: database of computational hot spots in protein interfaces. Nucleic Acids Res 2008;36(Database issue):D662–D666.

55. Ma B, Elkayam T, Wolfson H, Nussinov R. Protein–protein interactions: structurally conserved residues distinguish between binding sites and exposed protein surfaces. Proc Natl Acad Sci USA 2003;100:5772–5777.

56. Wang X, Wei X, Thijssen B, Das J, Lipkin SM, Yu H. Three-dimensional reconstruction of protein networks provides insight into human genetic disease. Nat Biotechnol 2012;30:159–164.

57. Liu Y, Higashitsuji H, Higashitsuji H, Itoh K, Sakurai T, Koike K, Hirota K, Fukumoto M, Fujita J. Overexpression of gankyrin in mouse hepatocytes induces hemangioma by suppressing factor inhibiting hypoxia-inducible factor-1 (FIH-1) and activating hypoxia-inducible factor-1. Biochem Biophys Res Commun 2013;432:22–27.

58. Wang P, Zhang C, Yu P, Tang B, Liu T, Cui H, Xu J. Regulation of colon cancer cell migration and invasion by CLIC1-mediated RVD. Mol Cell Biochem 2012;365:313–321.

59. MacAllister RJ, Parry H, Kimoto M, Ogawa T, Russell RJ, Hodson H, Whitley GS, Vallance P. Regulation of nitric oxide synthesis by dimethylarginine dimethylaminohydrolase. Br J Pharmacol 1996;119:1533–1540.

60. Leiper J, Nandi M, Torondel B, Murray-Rust J, Malaki M, O'Hara B, Rossiter S, Anthony S, Madhani M, Selwood D, Smith C, Wojciak-Stothard B, Rudiger A, Stidwill R, McDonald NQ, Vallance P. Disruption of methylarginine metabolism impairs vascular homeostasis. Nat Med 2007;13:198–203.

61. Wang J-W, Peng S-Y, Li J-T, Wang Y, Zhang Z-P, Cheng Y, Cheng D-Q, Weng W-H, Wu X-S, Fei X-Z. Identification of metastasis-associated proteins involved in gallbladder carcinoma metastasis by proteomic analysis and functional exploration of chloride intracellular channel 1. Cancer Lett 2009;281:71–81.

62. Wang W, Xu X, Wang W, Shao W, Li L, Yin W, Xiu L, Mo M, Zhao J, He Q. The expression and clinical significance of CLIC1 and HSP27 in lung adenocarcinoma. Tumor Biol 2011;32:1199–1208.

63. Wang L, He S, Tu Y, Ji P, Zong J, Zhang J, Feng F, Zhao J, Zhang Y, Gao G. Elevated expression of chloride intracellular channel 1 is correlated with poor prognosis in human gliomas. J Exp Clin Cancer Res 2012;31:1–7.

64. Dengjel J, Hoyer-Hansen M, Nielsen MO, Eisenberg T, Harder LM, Schandorff S, Farkas T, Kirkegaard T, Becker AC, Schroeder S, Vanselow K, Lundberg E, Nielsen MM, Kristensen AR, Akimov V, Bunkenborg J, Madeo F, Jǎǎttelǎ M, Andersen JS. Identification of autophagosome-associated proteins and regulators by quantitative proteomic analysis and genetic screens. Mol Cell Proteomics 2012;11:M111014035.

65. Rodi DJ, Makowski L, Kay BK. One from column A and two from column B: the benefits of phage display in molecular-recognition studies. Curr Opin Chem Biol 2002;6:92–96.

66. Neduva V, Russell RB. Peptides mediating interaction networks: new leads at last. Curr Opin Biotechnol 2006;17:465–471.

67. Ceol A, Chatr-aryamontri A, Santonico E, Sacco R, Castagnoli L, Cesareni G. DOMINO: a database of domain-peptide interactions. Nucleic Acids Res 2007;35(Database issue):D557–D560.

68. Kuzuoglu-Ozturk D, Huntzinger E, Schmidt S, Izaurralde E. The *Caenorhabditis elegans* GW182 protein AIN-1 interacts with PAB-1 and subunits of the PAN2-PAN3 and CCR4-NOT deadenylase complexes. Nucleic Acids Res 2012;40:5651–5665.

69. Landgraf C, Panni S, Montecchi-Palazzi L, Castagnoli L, Schneider-Mergener J, Volkmer-Engert R, Cesareni G. Protein interaction networks by proteome peptide scanning. PLoS Biol 2004;2:E14.

70. Kritzer JA, Stephens OM, Guarracino DA, Reznik SK, Schepartz A. β-Peptides as inhibitors of protein–protein interactions. Bioorg Med Chem 2005;13:11–16.

71. London N, Raveh B, Movshovitz Attias D, Schueler Furman O. Can self inhibitory peptides be derived from the interfaces of globular protein–protein interactions? Proteins 2010;78:3140–3149.

72. Mochly-Rosen D, Khaner H, Lopez J, Smith BL. Intracellular receptors for activated protein kinase C. Identification of a binding site for the enzyme. J Biol Chem 1991;266:14866–14868.

73. Mochly-Rosen D, Qvit N. Peptide inhibitors of protein-protein interactions. Trends Endocrinol Metab 2009;20:25–33.

74. Stebbins EG, Mochly-Rosen D. Binding specificity for RACK1 resides in the V5 region of beta II protein kinase C. J Biol Chem 2001;276:29644–29650.

75. Emerson SD, Palermo R, Liu CM, Tilley JW, Chen L, Danho W, Madison VS, Greeley DN, Ju G, Fry DC. NMR characterization of interleukin-2 in complexes with the IL-2Ralpha receptor component, and with low molecular weight compounds that inhibit the IL-2/IL-Ralpha interaction. Protein Sci 2003;12:811–822.

76. Sauve K, Nachman M, Spence C, Bailon P, Campbell E, Tsien WH, Kondas JA, Hakimi J, Ju G. Localization in human interleukin 2 of the binding site to the alpha chain (p55) of the interleukin 2 receptor. Proc Natl Acad Sci USA 1991;88:4636–4640.

77. Zurawski SM, Vega F, Jr., Doyle EL, Huyghe B, Flaherty K, McKay DB, Zurawski G. Definition and spatial location of mouse interleukin-2 residues that interact with its heterotrimeric receptor. EMBO J 1993;12:5113–5119.

78. Arkin MR, Randal M, DeLano WL, Hyde J, Luong TN, Oslob JD, Raphael DR, Taylor L, Wang J, McDowell RS, Wells JA, Braisted AC. Binding of small molecules to an adaptive protein-protein interface. Proc Natl Acad Sci USA 2003;100:1603–1608.

79. Arkin MR, Wells JA. Small-molecule inhibitors of protein-protein interactions: progressing towards the dream. Nat Rev Drug Discov 2004;3:301–317.

80. Clackson T, Wells JA. A hot spot of binding energy in a hormone-receptor interface. Science 1995;267:383–386.

81. Erbe DV, Wang S, Xing Y, Tobin JF. Small molecule ligands define a binding site on the immune regulatory protein B7.1. J Biol Chem 2002;277:7363–7368.

82. Green NJ, Xiang J, Chen J, Chen L, Davies AM, Erbe D, Tam S, Tobin JF. Structure-activity studies of a series of dipyrazolo[3,4-b:3′,4′-d]pyridin-3-ones binding to the immune regulatory protein B7.1. Bioorg Med Chem 2003;11:2991–3013.

83. Sattler M, Liang H, Nettesheim D, Meadows RP, Harlan JE, Eberstadt M, Yoon HS, Shuker SB, Chang BS, Minn AJ, Thompson CB, Fesik SW. Structure of Bcl-xL-Bak peptide complex: recognition between regulators of apoptosis. Science 1997;275:983–986.

84. Prasanna V, Bhattacharjya S, Balaram P. Synthetic interface peptides as inactivators of multimeric enzymes: inhibitory and conformational properties of three fragments from *Lactobacillus casei* thymidylate synthase. Biochemistry 1998;37:6883–6893.

85. Cardinale D, Guaitoli G, Tondi D, Luciani R, Henrich S, Salo-Ahen OM, Ferrari S, Marverti G, Guerrieri D, Ligabue A, Frassineti C, Pozzi C, Mangani S, Fessas D, Guerrini R, Ponterini G, Wade RC, Costi MP. Protein-protein interface-binding peptides inhibit the cancer therapy target human thymidylate synthase. Proc Natl Acad Sci USA 2011;108:E542–E549.

A novel role for the proteasomal chaperone PSMD9 and hnRNPA1 in enhancing IκBα degradation and NF-κB activation – functional relevance of predicted PDZ domain–motif interaction

Indrajit Sahu, Nikhil Sangith, Manoj Ramteke, Rucha Gadre and Prasanna Venkatraman

Advanced Center for Treatment, Research and Education in Cancer, Tata Memorial Centre, Kharghar, Navi Mumbai, India

PSMD9 is a PDZ domain containing chaperone of proteasome assembly. Based on the ability of PDZ-like domains to recognize C-terminal residues in their interactors, we recently predicted and identified heterogeneous nuclear ribonucleoprotein A1 (hnRNPA1) as one of the novel interacting partners of PSMD9. Contingent on the reported role of hnRNPA1 in nuclear factor κB (NF-κB) activation, we tested the role of human PSMD9 and hnRNPA1 in NF-κB signaling. We demonstrated in human embryonic kidney 293 cells that PSMD9 influences both basal and tumor necrosis factor α (TNF-α) mediated NF-κB activation through inhibitor of nuclear factor κB α (IκBα) proteasomal degradation. PSMD9 mediates IκBα degradation through a specific domain–motif interaction involving its PDZ domain and a short linear sequence motif in the C-terminus of hnRNPA1. Point mutations in the PDZ domain or deletion of C-terminal residues in hnRNPA1 disrupt interaction between the two proteins which has a direct influence on NF-κB activity. hnRNPA1 interacts with IκBα directly, whereas PSMD9 interacts only through hnRNPA1. Furthermore, hnRNPA1 shows increased association with the proteasome upon TNF-α treatment which has no such effect in the absence of PSMD9. On the other hand endogenous and trans-expressed PSMD9 are found associated with the proteasome complex. This association is unaffected by PDZ mutations or TNF-α treatment. Collectively, these interactions between IκBα, hnRNPA1 and proteasome bound PSMD9 illustrate a potential mechanism by which ubiquitinated IκBα is recruited on the proteasome for degradation. In this process, hnRNPA1 may act as a shuttle receptor and PSMD9 as a subunit acceptor. The interaction sites of PSMD9 and hnRNPA1 may emerge as a vulnerable drug target in cancer cells which require consistent NF-κB activity for survival.

Introduction

Mammalian PSMD9 is known to form a stable subcomplex with PSMC3 and PSMC6, two of the AAA-ATPases, assisting in the assembly of the 20S and 19S particles to form the holo complex [1,2]. Structurally PSMD9 contains an 88 amino acid long (108–195) PDZ-like domain [3]. Many PDZ domain containing

proteins act as scaffolds to form supramolecular assemblies which allow them to function in signaling, mediating adhesive properties of cells, and in ion transport [4,5]. Bridge-1, the PSMD9 homolog in rats, has been shown to act as a coactivator of insulin gene transcription through interaction of its PDZ-like domain with transcription factors E12 and histone acetyl transferase, p300 [3,6]. In ovarian cells, changes in the levels of PSMD9 are known to alter activin signaling [7]. Overexpression of Bridge-1 increases pancreatic apoptosis with a reduction in the number of insulin-expressing β-cells leading to insulin deficiency and diabetes [8].

Based on the classical property of some PDZ domains to recognize 4–7 C-terminal residues or short linear sequence motifs (SLIMs) in proteins, we recently identified several novel interacting partners of PSMD9 (FEBS Open Bio, submitted). Such SLIMs have been identified as functionally relevant recognition motifs in SH2, SH3 domain containing proteins [9]. We recently showed that a 13 residue A-helix acts as an anchor while a floppy F-helix acts as an initiator of ubiquitin independent degradation of apomyoglobin by the proteasome [10]. We also identified novel interacting partners of gankyrin, a chaperone of the proteasome and an oncoprotein, by recognizing proteins which share EEVD, a conserved SLIM seen at the interface of gankyrin-S6 ATPase complex [11]. In addition we predicted the structure of the PDZ domain of PSMD9 and identified residues at the PDZ interface which are important for recognizing the C-terminal residues of four novel interacting partners (FEBS Open Bio, submitted). Heterogeneous nuclear ribonucleoprotein A1 (hnRNPA1), an RNA binding protein involved in mRNA export, splicing and protein translation, was one of the novel interacting partners. This protein in the mouse CB3 cells was reported to be responsible for inhibitor of nuclear factor κB α (IκBα) degradation by an unknown mechanism leading to transcriptional activation of nuclear factor κB (NF-κB) [12]. This observation formed the premise of this work which aims to establish the functional relevance of the newly found PSMD9–hnRNPA1 interaction.

NF-κB is a family of transcription factors that regulate expression of various genes involved in inflammatory, anti-apoptotic and immune responses [13,14]. The NF-κB family or the Rel family of proteins includes p50 (p105), p52 (p100), p65 (RelA), c-Rel and Rel-B [15,16]. If cells are not stimulated, heterodimeric NF-κB complexes remain in the cytoplasm, where they are associated with an inhibitory molecule of the IκB family [17]. In mammalian species, six structural homologs of IκB have been identified: IκBα, IκBβ, IκBε, IκBγ, Bcl-3 and IκBζ [18]. Among these, IκBα, the prototypical member of the IκB family, has been

extensively studied. The canonical NF-κB p65/p50 heterodimer is largely, although not exclusively, found in complex with its inhibitor IκBα in cytoplasm. In response to stimulation by various agents such as phorbol esters (e.g. phorbol 12-myristate 13-acetate), pervanadate, tumor necrosis factor α (TNF-α), interleukin-1a (IL-1a), γ-radiation and lipopolysaccharide, IκBα undergoes phosphorylation by the IKK complex at Ser32, Ser36 and/or Tyr42 followed by polyubiquitination at Lys21 and Lys22 [19–22]. This leads to proteasomal degradation of the phosphorylated and ubiquitinated IκBα and nuclear translocation of free p50/p65, resulting in NF-κB transcription activity [13,19,23,24]. Apart from proteasomal degradation some reports suggest that in uninduced cells IκBα undergoes non-proteasomal, calcium dependent proteolysis resulting in high and consistent NF-κB activity [25–28]. Among the other IκB proteins, IκBβ, IκBε, p100 (precursors of p52) and p105 (precursors of p50) also undergo proteasomal degradation/endoproteolytic processing under induced and uninduced conditions [29–33]. Although the upstream processes of IκBα degradation are extensively deciphered, the detailed mechanism of proteasomal degradation is still not clear.

It is with this background that we were intrigued by the reports of Hay et al., who demonstrated interaction between ankyrin repeats of IκBα and hnRNPA1 which somehow seemed necessary for IκBα degradation and NF-κB transcriptional activity [12]. But the identity of the protease involved and the role of proteasome in this process were not established. Since the bigger and fundamental question of how IκBα is recruited to the proteasome for degradation remains largely unaddressed, it would be interesting to investigate whether hnRNPA1, well known for its role in mRNA processing and transport [34], cross-talks with the proteasomal degradation pathway in human cells. The mechanism by which ubiquitinated proteins are recruited to proteasome remains an active area of research. Based on our finding that PSMD9 interacts with hnRNPA1 in vitro (FEBS Open Bio, submitted) and the reported role of hnRNPA1 in IκBα degradation and NF-κB activity, we hypothesized that PSMD9 may have a role in the degradation of IκBα by the proteasome and influence NF-κB activity in human cells. Here we provide evidence that in human embryonic kidney 293 (HEK293) cells, PSMD9 through its PDZ domain interacts with the C-terminus of hnRNPA1 and this tripartite interaction subjects ubiquitinated IκBα to proteasomal degradation enhancing both basal and signal mediated NF-κB activity. By a series of experiments we identify a novel role for hnRNPA1 as a shuttle receptor that recruits IκBα for degradation and

recognizes PSMD9 as a novel subunit receptor on the proteasome. Our results demonstrate an atypical function of hnRNPA1 which seems to integrate into the ubiquitin proteasome pathway through a specific interaction with proteasome bound PSMD9. We speculate about the general role of this interaction and the utility of the PDZ domain interface as a potential drug target.

Results

PSMD9 interacts with the C-terminus of hnRNPA1

Using a bioinformatics approach (*FEBS Open Bio*, submitted) and the knowledge that some PDZ domains interact with C-terminal regions of proteins [5], we predicted putative interacting partners of PSMD9, from the human proteome. This prediction was validated by screening C-terminal peptides for their ability to bind to pure recombinant PSMD9. Using this strategy we identified hnRNPA1 as a novel interacting partner of PSMD9 and further proved that this interaction is mediated by the C-terminal residues of hnRNPA1 (*FEBS Open Bio*, submitted). To test if PSMD9 and hnRNPA1 interact endogenously, as this would be physiologically and functionally relevant, we used PSMD9 antibody to immunoprecipitate PSMD9 from HEK293 cell lysates and probed for the presence of hnRNPA1 using hnRNPA1 antibody. As expected, hnRNPA1 was found in the immunoprecipitation (IP) complex (Fig. 1A). We further validated this endogenous interaction by performing a reverse IP where hnRNPA1 antibody was used for IP and the complex was probed with PSMD9 antibody (Fig. 1B). We reconfirmed our earlier observation that only wild type (wt) hnRNPA1 and not the C-terminal mutant can interact with PSMD9 (Fig. 1C).

Overexpression of PSMD9 enhances basal and TNF-α mediated NF-κB activity

In CB3 cells, hnRNPA1 reportedly interacts with IκBα and overexpression of hnRNPA1 in these cells enhances NF-κB transcriptional activity [12]. No such role has been reported for hnRNPA1 in human cells. Since we found that PSMD9 interacts with hnRNPA1 *ex vivo* and hnRNPA1 reportedly influences NF-κB activity, we asked if PSMD9 was involved in this pathway. If so, changes in the levels of PSMD9 must influence NF-κB activity. PSMD9 was overexpressed under doxycycline inducible conditions in three different stable clones (Fig. 2A), and NF-κB transcriptional activity was measured by luciferase reporter assay. In all three inducible
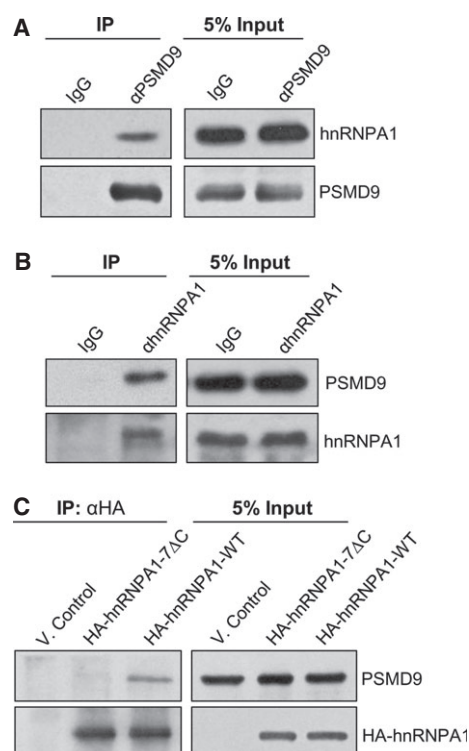
Fig. 1. PSMD9 interacts with wt-hnRNPA1 but not with the 7ΔC mutant of hnRNPA1 *ex vivo*. (A) HEK293 cell lysates were incubated either with PSMD9 antibody-bound Protein-G Sepharose beads or mouse IgG (isotype control) bound Protein-G Sepharose beads. Pull-down complexes were probed with hnRNPA1 and PSMD9 antibodies. (B) HEK293 cell lysates were incubated with either hnRNPA1 antibody-bound Protein-G Sepharose beads or mouse IgG isotype bound Protein-G Sepharose (isotype control). Then pull-down complexes were probed with PSMD9 and hnRNPA1 antibodies and analyzed by WB. (C) HA-wt-hnRNPA1 or 7ΔC mutant HA-hnRNPA1 was transiently overexpressed in HEK293 cells and cell lysates were incubated with HA antibody-bound Protein-G Sepharose beads. Pull-down complexes were probed with PSMD9 antibodies and analyzed by WB.

clones, NF-κB activity was found to be 3–4-fold higher than that of the uninduced control cells (Fig. 2B). In addition, we regulated the expression of PSMD9 using an inducible system in HEK293 cells (Fig. 2C) and found that doxycycline induced the expression of PSMD9 in a concentration dependent manner, which led to a corresponding increase in NF-κB transcriptional activity monitored using the luciferase reporter assay (Fig. 2D).

The influence of PSMD9 overexpression on NF-κB activity was further validated by demonstrating nuclear translocation of NF-κB (p65) and by electrophoretic mobility shift assay (EMSA). In PSMD9 overexpressing HEK293 cells, there was a significant increase in nuclear p65 in comparison with control cells (Fig. 2E). Upon
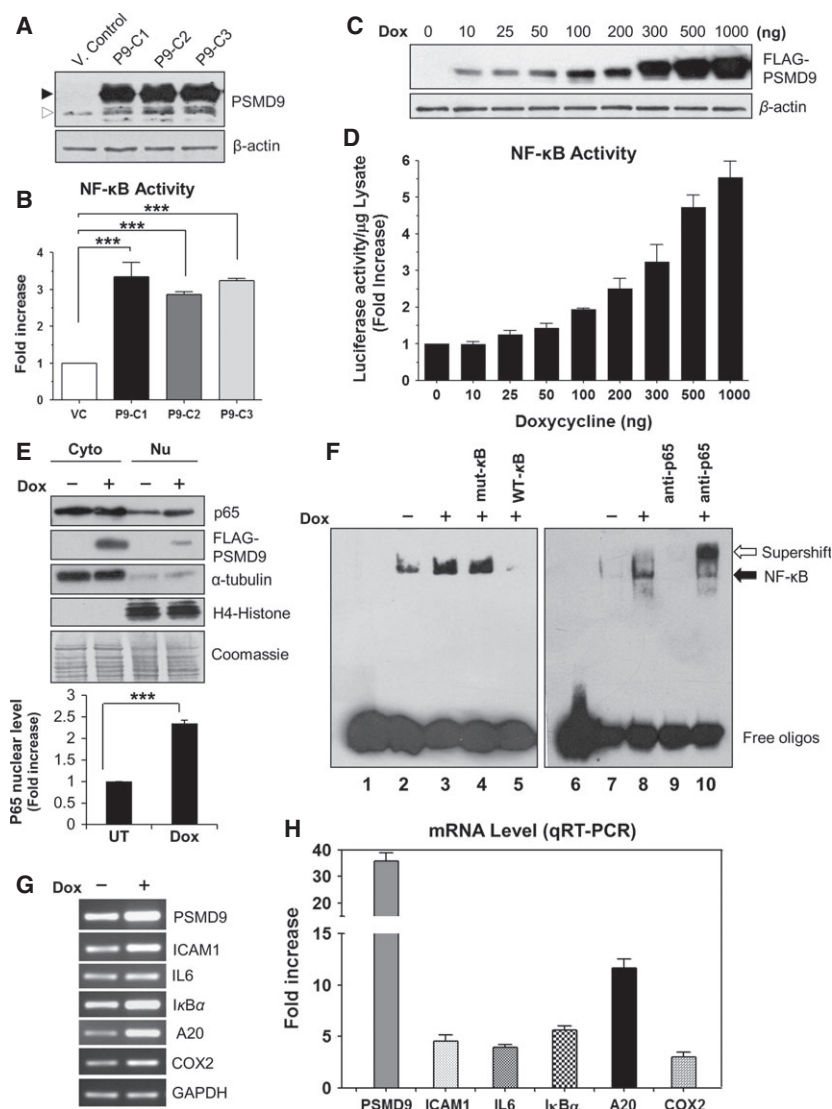
PSMD9 overexpression binding of NF-κB to the κB enhancer element was increased. This binding was competed out by unlabeled wt κB-oligos but not by mutant κB-oligos (Fig. 2F, lanes 4 and 5) [35]. Furthermore when the reaction mixture was incubated with p65 antibody, a supershift band was obtained which confirms the presence of p65 and its DNA binding activity (Fig. 2F, lane 10). In addition, five of the NF-κB target genes, namely intercellular adhesion molecule 1 (ICAM-1), IL-6, IκBα, A20 and cyclooxygenase-2 (COX-2) [36], were several-fold upregulated in PSMD9 overexpression cells compared with vector control cells (Fig. 2G,H). When doxycycline induced or uninduced cells were treated with TNF-α, a potent signal for NF-κB activation [37], both NF-κB DNA binding capacity and its transcriptional activity were increased. This increase was more pronounced in PSMD9 overexpress-

ing cells (Fig. 3A,B, lane 5). These results suggest that PSMD9 is involved in both basal and the signal mediated NF-κB pathway.

PSMD9 overexpression increases NF-κB activity by enhancing degradation of IκBα by proteasome

In the classical NF-κB pathway, upon signal induction, NF-κB bound IκBα is degraded by the 26S proteasome. Since NF-κB activity increased with increase in the levels of PSMD9 in HEK293 cells (current study), we hypothesized that PSMD9 may accelerate the degradation of IκBα by the proteasome. Accordingly when PSMD9 expression was induced by doxycycline there was a visible decrease in IκBα protein after 4–6 h of cycloheximide (CHX) treatment, whereas in uninduced cells reduction in the levels of IκBα was

seen only after 18–24 h of treatment (Fig. 4A). Similarly signal mediated IκBα degradation was considerably enhanced 10 min post TNF-α treatment in cells induced to overexpress PSMD9 (Fig. 4B). These results indicate that PSMD9 is involved in modulating IκBα levels presumably through proteasomal degradation in both basal as well as the signal mediated NF-κB signaling pathway.

To determine the role of proteasome in PSMD9 mediated degradation of IκBα, we treated PSMD9 overexpressing HEK293 cells with proteasome inhibitors. Treatment with MG132 or Velcade significantly inhibited both basal and TNF-α mediated IκBα degradation in cells overexpressing PSMD9 (Fig. 4C,D). In further support of proteasomal degradation, ubiquitinated IκBα was also seen to accumulate when PSMD9 overexpressing cells were treated with the proteasomal inhibitors (Fig. 4C). It is well established that degradation of IκBα by the proteasome, upon signal induction, requires phosphorylation at sites S32 and S36 [13]. To determine whether the processing of IκBα occurs through the same way in the case of PSMD9 mediated degradation, we overexpressed IκBα super-repressor (S32A–S36A) in control cells as well as in PSMD9 overexpressing cells. After 30 min of TNF-α induction, super-repressor IκBα was not degraded even under PSMD9 overexpression conditions whereas endogenous IκBα got degraded significantly (Fig. 4E). In accordance with this, NF-κB activity is decreased significantly in the cells upon overexpression of the super-repressor irrespective of PSMD9 overexpression (Fig. 4F). These results indicate that the phosphorylation at S32 and S36 residues is necessary for the PSMD9 mediated IκBα degradation by the proteasome.

Endogenous PSMD9 is involved in basal and signal mediated activation of NF-κB and IκBα degradation

In order to demonstrate the role of endogenous PSMD9 in NF-κB activation, we knocked down PSMD9 in HEK293 cells using small hairpin RNA (shRNA) under inducible conditions. Upon knockdown of PSMD9, IκBα levels were found to be stable even after 24 h of CHX treatment (Fig. 5A). In the same cells, a reduction in TNF-α induced IκBα degradation was observed whereas in control cells IκBα degradation was already apparent after 20 min of TNF-α treatment (Fig. 5B). Concomitantly a decrease in NF-κB DNA binding activity was observed by EMSA both in TNF-α treated and untreated PSMD9 knockdown cells (Fig. 5C). This was further confirmed by semi-quantitative RT-PCR and real-time PCR of five different NF-κB target genes, namely ICAM-1, IL-6, IκBα, A20 and COX-2, the levels of which decreased in PSMD9 knockdown cells compared with control cells (Fig. 5D,E). These results indicate that endogenous PSMD9 is indeed responsible for the basal and signal induced degradation of IκBα and subsequent increase in NF-κB activity.

Fig. 2. Basal NF-κB activity increases upon PSMD9 overexpression in HEK293 cells. (A) Three clones of HEK293 cells inducibly expressing FLAG-PSMD9 were either treated with doxycycline or left untreated, and the cell lysates were analyzed by WB. (B) The above clones were transfected with 3x κB ConA luc vector or ConA luc control vector and induced with doxycycline (1 μg·mL^{-1} of medium). After 48 h of induction NF-κB activity was checked by measuring luciferase activity using dual luciferase substrate. Luciferase activity from firefly luciferase was normalized with renilla luciferase used as a transfection control. Data represent mean luciferase activity per microgram of protein ± SEM of two independent experiments done in triplicate. (C) HEK293 cells inducibly expressing FLAG-PSMD9 were transfected with 3x κB ConA luc vector or ConA luc control vector. Cells were induced with different concentrations (0–1000 ng·mL^{-1} of medium) of doxycycline. After 48 h of induction, levels of FLAG-PSMD9 were analyzed by WB. (D) NF-κB activity was checked by measuring luciferase activity of the above described (in C) cell lysates, using dual luciferase substrate. Luciferase activity from firefly luciferase was normalized with renilla luciferase used as a transfection control. Data represent mean luciferase activity per microgram of protein ± SEM of two independent experiments done in triplicate. (E) HEK293 cells inducibly expressing FLAG-PSMD9 were either treated with doxycycline (1 μg·mL^{-1} of medium for 48 h) or left untreated. Nuclear fractions were prepared as described in Materials and methods and analyzed by WB. The graph represents the mean fold increase of p65 nuclear translocation ± SEM of two independent experiments in three different stable clones. (F) HEK293 inducible FLAG-PSMD9 stable clones were either treated with doxycycline (1 μg·mL^{-1} of medium for 48 h) or left untreated. The nuclear fractions were subjected to EMSA (following the protocol described in Materials and methods). Lane 1 indicates biotinylated oligos only. The black arrow indicates NF-κB DNA binding activity in doxycycline untreated (lanes 2 and 7) and treated (lanes 3 and 8) cells. NF-κB DNA binding specificity is shown by competing it with 200× unlabeled mutant oligos (lane 4) or wt oligos (lane 5). In lanes 9 and 10 p65 antibody was incubated with the binding reaction mix (with/without lysate) and the white arrow indicates the resulting supershift band. (G) HEK293 inducible FLAG-PSMD9 stable clones either treated with doxycycline for 48 h or left untreated. RNA was isolated and semi-quantitative RT-PCR was performed for five different target genes; the PCR products were run in a 2% agarose gel. (H) Real-time PCR was performed for the same five different target genes. The graph represents glyceraldehyde-3-phosphate dehydrogenase (GAPDH) normalized mean fold increase in mRNA level of the genes ± SEM for three independent experiments done in duplicate.
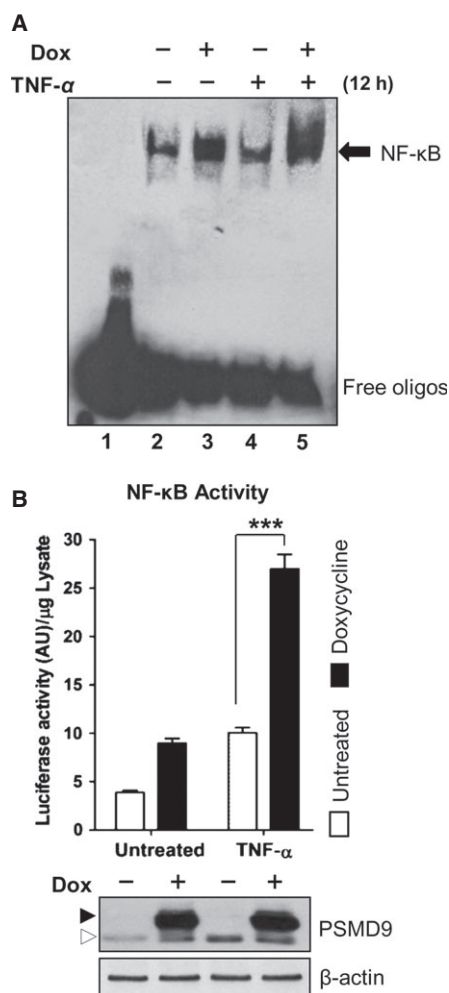
Fig. 3. TNF-α mediated NF-κB activity increases upon PSMD9 overexpression in HEK293 cells. (A) HEK293 inducible FLAG-PSMD9 stable clones were treated with doxycycline (1 μg·mL^{-1} of medium for 48 h) and/or with TNF-α (20 ng·mL^{-1} of medium for 12 h) or left untreated. The nuclear fractions were subjected to EMSA (following the protocol described in Materials and methods). Lane 1 indicates biotinylated oligos only. The black arrow indicates NF-κB DNA binding activity in doxycycline untreated (lanes 2 and 4) and treated (lanes 3 and 5) cells. Upon TNF-α treatment NF-κB DNA binding activity increased, shown by the thick gel shift band (in lanes 4 and 5). (B) HEK293 cells inducibly expressing FLAG-PSMD9 were transfected with 3x κB ConA luc vector or ConA luc control vector. Transfected cells were treated with doxycycline (1 μg·mL^{-1} of medium for 48 h) and/or with TNF-α for 12 h or left untreated. NF-κB activity was measured as described in Fig. 2B. Data represent mean luciferase activity per microgram of protein ± SEM of two independent experiments done in triplicate. WB shows the level of PSMD9 expression in these cell lysates. Symbol ▶ corresponds to trans-expressed FLAG-PSMD9 and ▷ symbol corresponds to the endogenous PSMD9.

PSMD9 does not affect the IκBα ubiquitination and proteasomal activity

Given its role as an assembly chaperone, PSMD9 expression may influence proteasomal activity which in turn may dictate the overall IκBα levels. We tested the activity of proteasome upon overexpression of PSMD9 and upon silencing the endogenous PSMD9. Proteasomal activity was unaltered in these cells and remained uninfluenced by TNF-α treatment (Fig. 6A). Our observation that PSMD9 does not influence proteasomal activity is in line with a previous report by Shim *et al.* [38]. Here similar to our method the authors used total cell lysates for monitoring proteasomal activity. In another study Keneko *et al.* showed that knocking down PSMD9 results in reduced proteasomal activity [1]. Here, in contrast to our method and those by Shim *et al.*, cell lysates were fractionated by glycerol gradient centrifugation and the fractions were monitored for proteasomal activity. Increase in proteasomal activity is seen in the presence of p27 modulator complex in reconstitution experiments involving subcomplexes of the proteasome [39]. The role of this modulator seems to involve rescue of improperly assembled or damaged 19S particles to ensure correct orientation of the ATPase rings [40].

Due to the importance of ubiquitination in IκBα degradation by the proteasome, we checked the requirement of PSMD9 in this process. We treated both doxycycline induced and uninduced cells with MG132 for 2 h followed by CHX treatment for 6, 12 and 24 h. The initial 2 h of MG132 treatment resulted in a 75% decrease in proteasomal activity. To ensure that after removal of MG132 and during the CHX treatment (used to follow degradation of ubiquitinated IκBα) proteasomes were functional, activity was monitored at every assay point. Then, 12 h following removal of MG132, proteasomal activity was restored almost completely both in PSMD9 knockdown cells and in control cells. Coincident with the time period of CHX treatment and upon PSMD9 gene silencing, levels of ubiquitinated IκBα did not change significantly. Rather an increased accumulation of ubiquitinated IκBα was seen in these PSMD9 knockdown cells. In control cells there was a clear decrease in levels of ubiquitinated IκBα (Fig. 6B). These results indicate that PSMD9 does not affect ubiquitination of IκBα and confirm that cells fail to degrade ubiquitinated IκBα efficiently not because of impaired proteasomal activity but due to the absence of PSMD9.
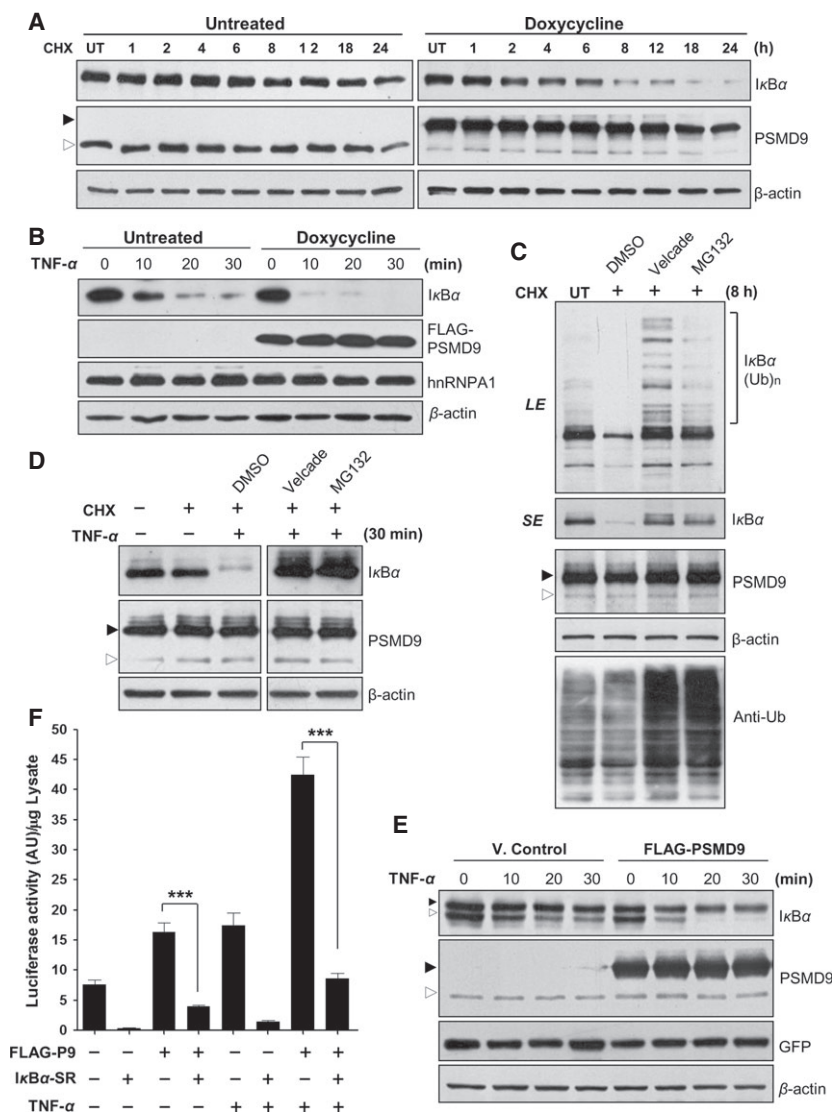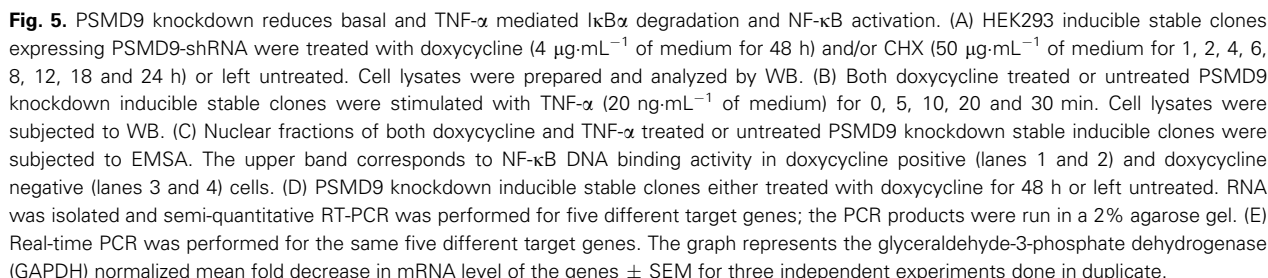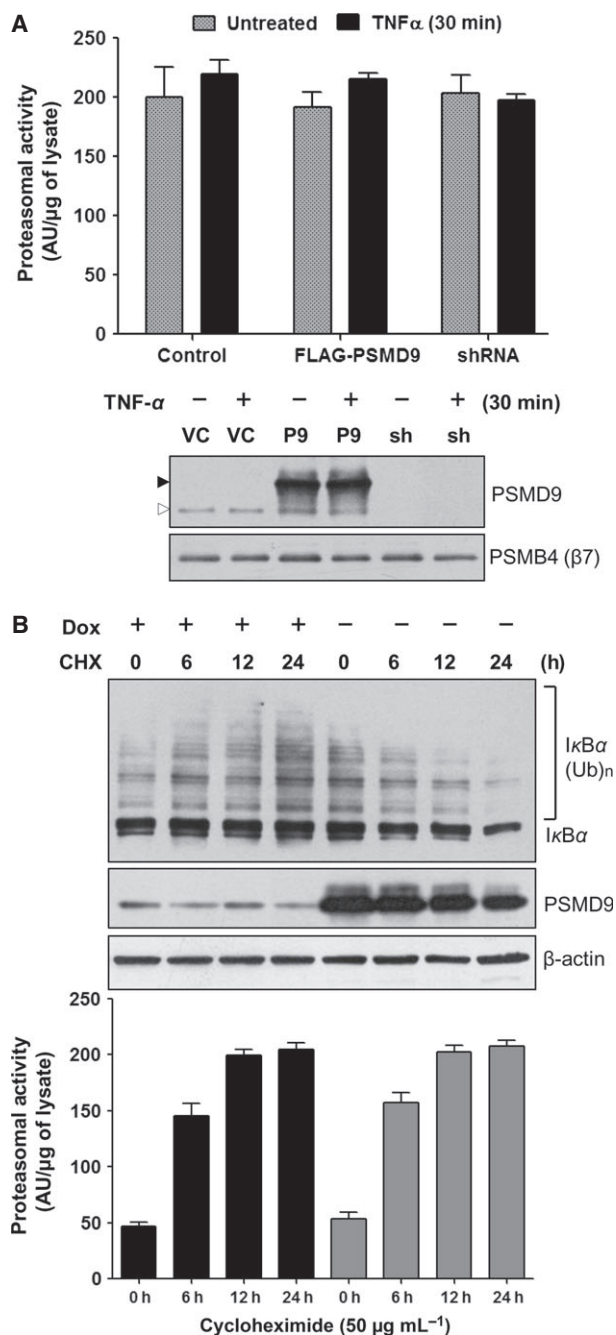
Fig. 4. PSMD9 overexpression accelerates basal and TNF-α mediated IκBα degradation. (A) HEK293 inducible FLAG-PSMD9 stable clones were treated with doxycycline (1 μg·mL^{-1} of medium for 48 h) and/or CHX (50 μg·mL^{-1} of medium for 1, 2, 4, 6, 8, 12, 18 and 24 h) or left untreated. Cell lysates were prepared and analyzed by WB. (B) Both doxycycline treated or untreated HEK293 inducible FLAG-PSMD9 stable clones were stimulated with TNF-α (20 ng·mL^{-1} of medium) for 0, 10, 20 and 30 min. Cell lysates were subjected to WB. (C) The above doxycycline induced stable clones were treated with CHX (50 μg·mL^{-1} of medium for 8 h) (where indicated) and with MG132 (10 μM), Velcade (10 μg·mL^{-1} of medium) or 0.1% dimethylsulfoxide for 6 h and analyzed by WB. LE, long exposure; SE, short exposure. At LE accumulation of polyubiquitinated IκBα is observed in the case of Velcade and MG132 treatment. (D) Cells were treated as described in (C) and either stimulated with TNF-α (20 ng·mL^{-1} of medium) for 30 min or left unstimulated and the lysates were analyzed by WB. Cropped image blots for each antibody are of the same exposure and from the same experiment, represented in a convenient manner. Symbol ► corresponds to trans-expressed FLAG-PSMD9 and symbol △ corresponds to the endogenous PSMD9. (E) HEK293 FLAG-PSMD9 stable clones and pCMV-10 empty vector stable clones were transiently co-transfected with pTRIPZ-IκBα-SR and pEGFPN3 vector. Cells were induced with doxycycline (1 μg·mL^{-1} of medium) for 48 h and treated with TNF-α (20 ng·mL^{-1} of medium) for 0, 10, 20 and 30 min. Cell lysates were prepared and analyzed by WB. Symbol ► corresponds to trans-expressed FLAG-IκBα-SR or FLAG-PSMD9 and symbol ▷ corresponds to the endogenous IκBα or PSMD9. (F) HEK293 FLAG-PSMD9 stable clones and pCMV-10 empty vector stable clones were co-transfected with pTRIPZ-IκBα-SR and 3x κB ConA luc vector or ConA luc control vector and induced with doxycycline (1 μg·mL^{-1} of medium). After 36 h of induction cells were treated with TNF-α (20 ng·mL^{-1} of medium) for 12 h. Cell lysates were prepared and NF-κB activity was measured as described in Fig. 2B. Data represent mean luciferase activity per microgram of protein ± SEM of two independent experiments done in duplicate.

Fig. 5. PSMD9 knockdown reduces basal and TNF-α mediated IκBα degradation and NF-κB activation. (A) HEK293 inducible stable clones expressing PSMD9-shRNA were treated with doxycycline (4 μg·mL^{-1} of medium for 48 h) and/or CHX (50 μg·mL^{-1} of medium for 1, 2, 4, 6, 8, 12, 18 and 24 h) or left untreated. Cell lysates were prepared and analyzed by WB. (B) Both doxycycline treated or untreated PSMD9 knockdown inducible stable clones were stimulated with TNF-α (20 ng·mL^{-1} of medium) for 0, 5, 10, 20 and 30 min. Cell lysates were subjected to WB. (C) Nuclear fractions of both doxycycline and TNF-α treated or untreated PSMD9 knockdown stable inducible clones were subjected to EMSA. The upper band corresponds to NF-κB DNA binding activity in doxycycline positive (lanes 1 and 2) and doxycycline negative (lanes 3 and 4) cells. (D) PSMD9 knockdown inducible stable clones either treated with doxycycline for 48 h or left untreated. RNA was isolated and semi-quantitative RT-PCR was performed for five different target genes; the PCR products were run in a 2% agarose gel. (E) Real-time PCR was performed for the same five different target genes. The graph represents the glyceraldehyde-3-phosphate dehydrogenase (GAPDH) normalized mean fold decrease in mRNA level of the genes ± SEM for three independent experiments done in duplicate.

The PDZ domain of PSMD9 interacts with hnRNPA1

Point mutations in the PDZ domain of PSMD9 inhibit *in vitro* binding of hnRNPA1 (*FEBS Open Bio*, submitted). Since hnRNPA1 interacts with PSMD9 through its C-terminal residues, this interaction represents a typical PDZ domain–motif interface. We checked if this domain–motif recognition is also a key determinant of interaction inside the cells. We recently showed that Q181G and the β2 L124G/Q126G/E128G triple mutant (all in the PDZ domain) abolished interaction with PSMD9 while L173G (also in the PDZ domain) did not affect binding (*FEBS Open Bio*, submitted). To check the functional

relevance of these mutations, we overexpressed FLAG-tagged wt-PSMD9, Q181G-PSMD9, L173G-PSMD9 or the β2 L124G/Q126G/E128G triple mutant in HEK293 cells. Endogenous hnRNPA1 was immuno-precipitated from each cell lysate and probed with FLAG antibody. In accordance with the *in vitro* pull-down assays, wt-PSMD9 and L173G-PSMD9 were detected in the IP complexes. However, neither the Q181G mutant nor the triple mutant of PSMD9 could be detected in these IP complexes (Fig. 7A).

Presence of IκBα was tested in the IP complex from cell lysates of HEK293 cells overexpressing wt-PSMD9, Q181G or the β2 L124G/Q126G/E128G triple mutant. IκBα was detected only in the wt-PSMD9–hnRNPA1

A

B

Fig. 6. PSMD9 does not affect proteasomal activity and IκBα ubiquitination. (A) Both the overexpression (FLAG-PSMD9) and knockdown (shRNA) HEK293 inducible stable clones of PSMD9 were treated with doxycycline for 48 h and/or with TNF-α (20 μg·mL⁻¹ of medium) for 30 min or left untreated. Cell lysates were prepared with ATP buffer as described in Materials and methods. Proteasomal activity was measured as described in Materials and methods. The Control panel in the graph represents the average value of doxycycline untreated control cells of both the stable clones. Data represent Suc-LLVY-AMC proteasomal activity in arbitrary units (AU·μg⁻¹ of lysate) ± SEM of two independent experiments done in duplicate. The WB shows the level expression of PSMD9 in the above cell lysates and PSMB4 is taken as the loading control. Symbol ► corresponds to trans-expressed FLAG-PSMD9 and symbol ▷ corresponds to the endogenous PSMD9. (B) HEK293 inducible stable clones expressing PSMD9-shRNA were either treated with doxycycline (4 μg·mL⁻¹ of medium for 48 h) or left untreated. In addition cells were treated with MG132 (5 μM) for 2 h followed by treatment with CHX (50 μg·mL⁻¹ of medium) for 0, 6, 12 and 24 h. Cell lysates were prepared and analyzed by WB. The graph represents the proteasomal activity, measured as described in Materials and methods, of cells for the above experimental conditions.

mutant were similar to those of wt-PSMD9 and cells expressing this mutant showed faster IκBα degradation and enhanced NF-κB activation (Fig. 7E,F). These results confirm that specific residues on the PDZ domain of PSMD9 form the interface for binding hnRNPA1 and this domain–motif interaction plays an important role in the NF-κB activation pathway.

PSMD9 is linked to IκBα via hnRNPA1

hnRNPA1 was previously shown to interact with IκBα through its RNA binding domain [12]. We demonstrated that PSMD9 interacted with hnRNPA1 through its C-terminus. And the PDZ mutation analysis indicates that the interaction between PSMD9 and IκBα is probably through hnRNPA1. To determine the structural hierarchy of this tripartite interaction between PSMD9, hnRNPA1 and IκBα, we performed both *ex vivo* and *in vitro* interaction studies. We first verified whether interaction of hnRNPA1 with PSMD9 and IκBα is mutually exclusive or not. When HA-tagged wt-hnRNPA1 and CΔ7hnRNPA1 mutant were pulled down, IκBα was detected in both the pull-down complexes (Fig. 8A) suggesting that C-terminus deletion of hnRNPA1 does not affect its interaction with IκBα. In contrast, PSMD9 was found only in the wt-hnRNPA1–IκBα complex. As inferred from the failure of PDZ mutants to interact with IκBα in the absence of hnRNPA1, these results suggest that wt-PSMD9 and IκBα interaction is indirect and is through hnRNPA1. To further validate these

complex but not in PDZ Q181G and β2 L124G/Q126G/E128G triple mutant IP complexes (Fig. 7B) suggesting that PSMD9 is probably linked to IκBα through hnRNPA1. Unlike cells overexpressing wt-PSMD9, in cells overexpressing PDZ mutants (Q181G and the β2 triple mutant) IκBα was not efficiently degraded even after TNF-α treatment (Fig. 7C) nor was there a significant change in NF-κB activity (Fig. 7D). In addition, properties of L173G PSMD9
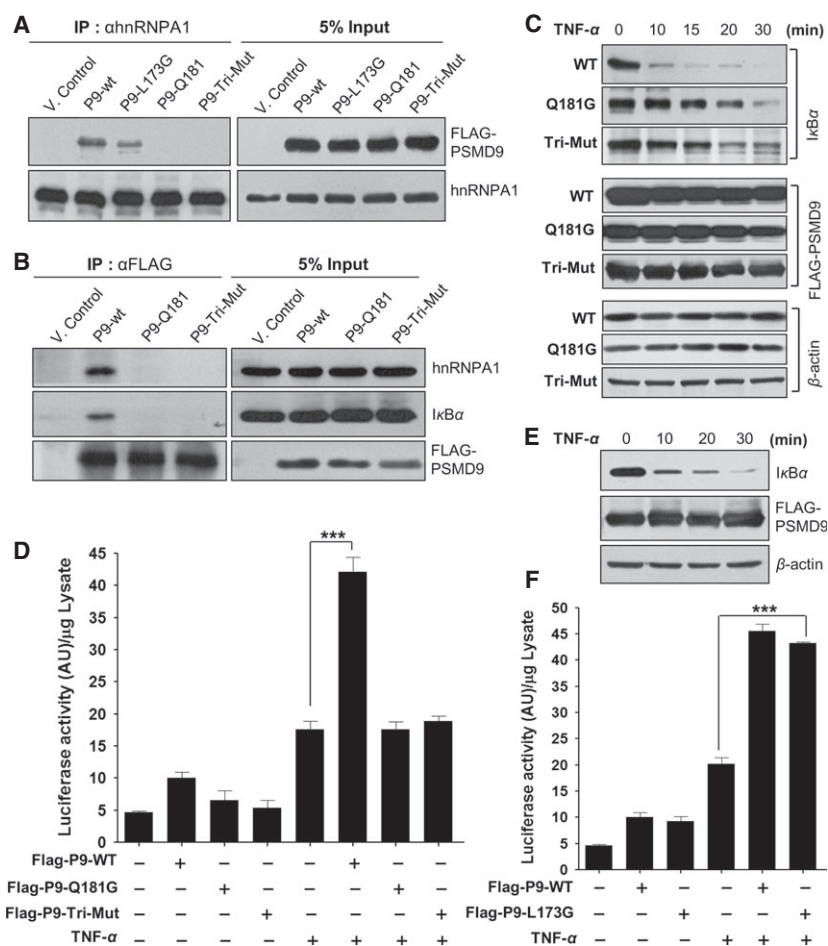
Fig. 7. The PDZ domain of PSMD9 is important for NF-κB activation and IκBα degradation. (A) HEK293 cells were transiently transfected with p3xFLAG-CMV-10-PSMD9, p3xFLAG-CMV-10-PSMD9(L173G), p3xFLAG-CMV-10-PSMD9(triple mutant) or p3xFLAG-CMV-10-PSMD9 (Q181G). Endogenous hnRNPA1 was immunoprecipitated from the cell lysates of the above transfected cells, probed with FLAG antibody and analyzed by WB. (B) HEK293 cells were transiently transfected with p3xFLAG-CMV-10 empty vector/p3xFLAG-CMV-10-wt-PSMD9/ p3xFLAG-CMV-10-PSMD9(Q181G)/p3xFLAG-CMV-10-PSMD9(triple mutant). Cell lysates were incubated with anti-FLAG M2 agarose beads and pull complexes were probed with hnRNPA1, IκBα, FLAG antibodies and analyzed by WB. (C) HEK293 cells were transiently transfected with p3xFLAG-CMV-10-PSMD9/p3xFLAG-CMV-10-PSMD9(Q181G)/p3xFLAG-CMV-10-PSMD9 (triple mutant). After 48 h of transfection cells were treated with TNF-α (20 ng·mL^{-1} of medium) for 10, 15, 20, 30 min or left untreated. Cell lysates were prepared and analyzed by WB. (D) HEK293 cells were co-transfected with p3xFLAG-CMV-10 empty vector or p3xFLAG-CMV-10-PSMD9 (wt, Q181G, triple mutant) and 3x κB ConA luc vector or ConA luc control vector. After 36 h cells were either treated with TNF-α (20 ng·mL^{-1} of medium) for 12 h or left untreated. Cell lysates were prepared and NF-κB activity was measured as described in Fig. 2B. Data represent mean luciferase activity per microgram of protein ± SEM of two independent experiments done in duplicate. (E) HEK293 cells were transiently transfected with p3xFLAG-CMV-10-PSMD9(L173G). After 24 h of transfection cells were treated with TNF-α (20 ng·mL^{-1} of medium) for 12 h or left untreated. Cell lysates were prepared and analyzed by WB. (F) HEK293 cells were co-transfected with p3xFLAG-CMV-10 empty vector or p3xFLAG-CMV-10-PSMD9 (wt or L173G) and 3x κB ConA luc vector or ConA luc control vector. After 36 h cells were either treated with TNF-α (20 ng·mL^{-1} of medium) for 12 h or left untreated. Cell lysates were prepared and NF-κB activity was measured as described in Fig. 2B. Data represent mean luciferase activity per microgram of protein ± SEM of two independent experiments done in duplicate.

observations we overexpressed both the FLAG-tagged wt-IκBα and C-terminal deleted IκBα (amino acids 253–372) in HEK293 cells. As discussed above, C-terminal residues in the ankyrin repeats of murine IκBα are necessary for interaction with hnRNPA1 [12].

When we pulled down the overexpressed FLAG-tagged IκBα, PSMD9 was found in the pull-down complex of wt protein where hnRNPA1 was present and not in the mutant IκBα (which does not interact with hnRNPA1) complex (Fig. 8B). This suggests that
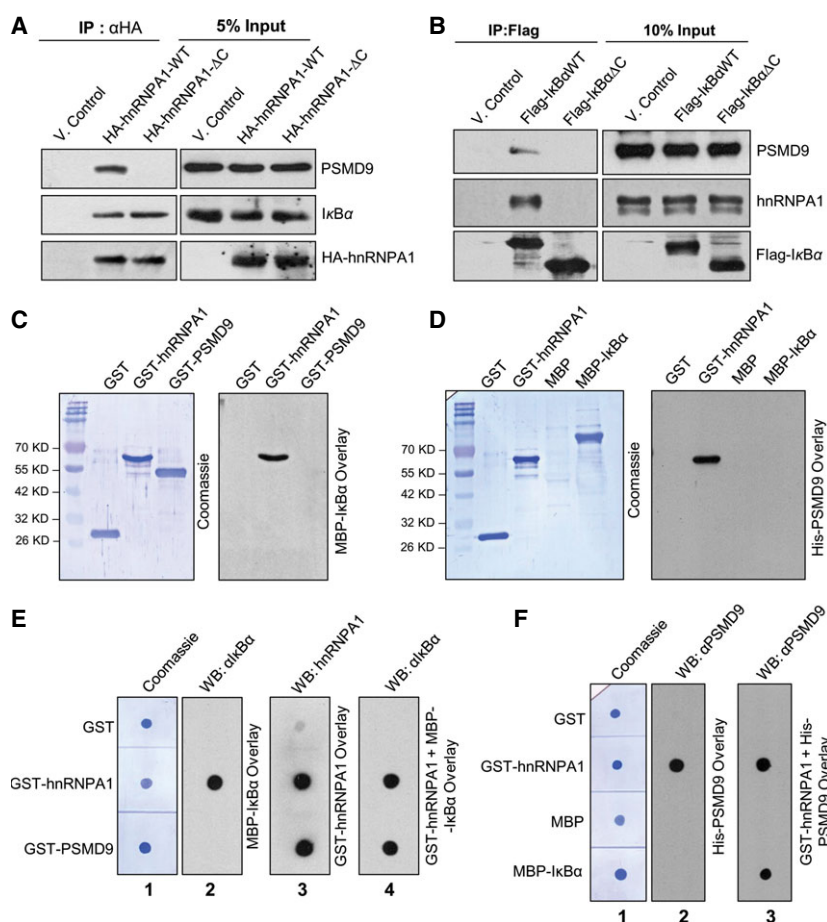
Fig. 8. PSMD9 is linked to IκBα via hnRNPA1. (A) HA-wt-hnRNPA1 and 7ΔC mutant HA-hnRNPA1 were transiently overexpressed in HEK293 cells and cell lysates were incubated with HA antibody-bound Protein-G Sepharose beads. Pull-down complexes were probed with PSMD9 and IκBα antibodies and analyzed by WB. (B) HEK293 cells were transfected with p3xFLAG-CMV-10-wt-IκBα p3xFLAG-CMV-10-ΔCIκBα and cell lysates were incubated with anti-FLAG M2 agarose beads. The pull-down complexes were probed with PSMD9, hnRNPA1 and IκBα antibodies and analyzed by WB. (C) 2 μg of recombinant GST, GST-hnRNPA1 and GST-PSMD9 proteins were run on SDS/PAGE, transferred onto a PVDF membrane and the proteins on the membrane were denatured/renatured using guanidine-HCl AP buffer. Then the membrane was overlaid with recombinant MBP-IκBα (100 nM), probed with IκBα antibody and analyzed by WB. (D) 2 μg of recombinant GST, GST-hnRNPA1 MBP and MBP-IκBα proteins were run on SDS/PAGE, transferred onto a PVDF membrane and the proteins were denatured/renatured on the membrane using guanidine-HCl AP buffer. Then the membrane was overlaid with recombinant His-PSMD9 (100 nM), probed with PSMD9 antibody and analyzed by WB. (E) 1 μg of recombinant GST, GST-hnRNPA1 and GST-PSMD9 proteins were spotted on equilibrated PVDF membrane, blocked with 3% BSA-TBST. The membranes were overlaid with recombinant MBP-IκBα (100 nM) and probed with IκBα antibody (panel 2); overlaid with GST-hnRNPA1 (100 nM) and probed with hnRNPA1 antibody (panel 3); overlaid with both GST-hnRNPA1 (100 nM) and MBP-IκBα (100 nM) and probed with IκBα antibody (panel 4). Panel 1 corresponds to the respective Coomassie stained protein spots on the membrane. (F) 1 μg of recombinant GST, GST-hnRNPA1 MBP and MBP-IκBα proteins were spotted on equilibrated PVDF membrane, blocked with 3% BSA-TBST. The membranes were overlaid with recombinant His-PSMD9 (100 nM) (panel 2) or with both GST-hnRNPA1 (100 nM) and His-PSMD9 (100 nM) (panel 3). Panel 1 corresponds to the respective Coomassie stained protein spots on the membrane.

the interaction between IκBα and PSMD9 is mediated by hnRNPA1.

We performed a series of far western or overlay experiments to substantiate these observations. Recombinant glutathione *S*-transferase (GST) PSMD9 and GST-hnRNPA1 were immobilized on a poly (vinylidene difluoride) (PVDF) membrane followed by

overlay of recombinant maltose binding protein (MBP)-IκBα protein and were then probed with IκBα antibody. No IκBα was detected in the GST-PSMD9 lane but it was clearly visible in the GST-hnRNPA1 lane (Fig. 8C). Furthermore, when MBP-IκBα and GST-hnRNPA1 were immobilized on a PVDF membrane, overlaid with His-PSMD9 followed by probing

with PSMD9 antibody, PSMD9 was clearly detected in the GST-hnRNPA1 lane but not in the MBP-IκBα lane (Fig. 8D). In a sandwich dot blot assay, we immobilized GST-PSMD9 on the membrane, followed by overlay with GST or GST-hnRNPA1 and then with MBP-IκBα. When this sandwich was probed with IκBα antibody, MBP-IκBα was found to interact with GST-PSMD9 only when hnRNPA1 was sandwiched in between these two proteins (Fig. 8E). Furthermore, this indirect interaction was validated by reversing the sandwich, i.e. by immobilizing MBP-IκBα and overlay of GST or GST-hnRNPA1 followed by GST-PSMD9 (Fig. 8F). These results altogether confirmed that there is no direct interaction between PSMD9 and IκBα and they can only interact through hnRNPA1, which uses different structural regions for these interactions that are not mutually exclusive.

Interaction between C-terminus of hnRNPA1 and PSMD9 is required for degradation of IκBα as well as NF-κB activity

The involvement of hnRNPA1 in IκBα degradation was shown previously [12]. We have demonstrated here a novel role of PSMD9 and a specific interaction between the PDZ domain of PSMD9 and a SLIM at the C-terminus of hnRNPA1. We asked if hnRNPA1 has any role to play in IκBα degradation/NF-κB activation when interaction with PSMD9 is lost or in the absence of PSMD9. When HA-wt-hnRNPA1 was trans-expressed in HEK293 cells, degradation of IκBα was considerably enhanced after 10 min of TNF-α treatment (Fig. 9A). HA-7ΔChnRNPA1 mutant, on the other hand, had no influence on the degradation of IκBα. Correspondingly, only the HA-wt-hnRNPA1
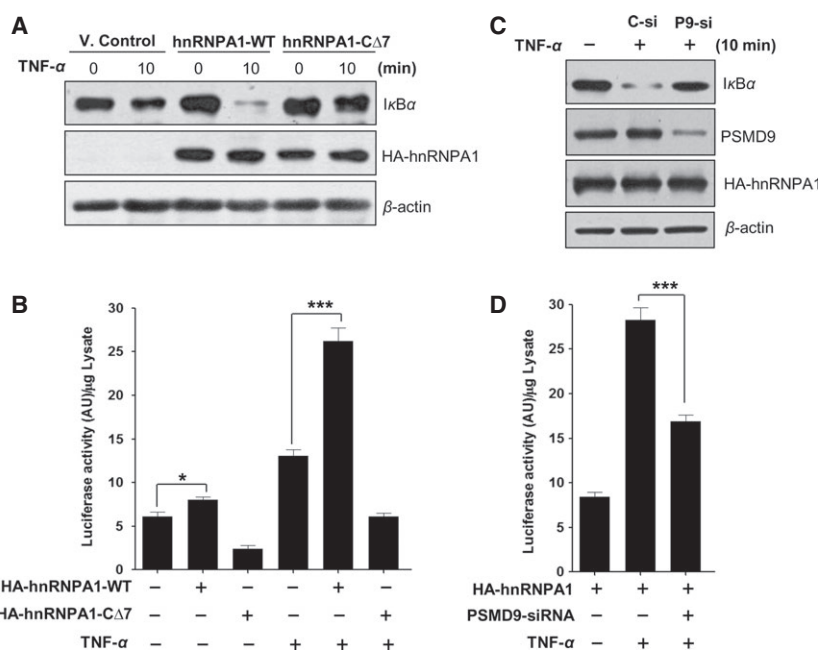

Fig. 9. C-terminus deleted hnRNPA1 mutant fails to enhance TNF-α mediated IκBα degradation and NF-κB activation. (A) HA-wt-hnRNPA1 and 7ΔC mutant HA-hnRNPA1 were transiently overexpressed in HEK293 cells and after 48 h cells were treated with TNF-α (20 ng·mL^{-1} of medium) for 10 min or left untreated. Cell lysates were prepared along with vector control and subjected to WB analysis. (B) HEK293 cells were co-transfected with pCDNA3.1-HA-empty vector or pCDNA3.1-HA-hnRNPA1 (wt or 7ΔC mutant) and 3x κB ConA luc vector or ConA luc control vector. After 36 h cells were either treated with TNF-α (20 ng·mL^{-1} of medium) for 12 h or left untreated. Cell lysates were prepared and NF-κB activity was measured as described in Fig. 2B. Data represent mean luciferase activity per microgram of protein ± SEM of three independent experiments done in duplicate. (C) HEK293 cells were transfected with PSMD9-siRNA/control-siRNA (100 μM) and after 48 h cells were again transfected with pCDNA3.1-HA-wt-hnRNPA1. After 72 h of siRNA transfection cells were either treated with TNF-α (20 ng·mL^{-1} of medium) for 20 min or left untreated. Cell lysates were prepared and analyzed by WB. (D) HEK293 cells were transfected with PSMD9-siRNA/control-siRNA (100 μM) and after 48 h cells were again transfected with pCDNA3.1-HA-wt-hnRNPA1 and 3x κB ConA luc vector or ConA luc control vector. After 60 h of siRNA transfection cells were either treated with TNF-α (20 ng·mL^{-1} of medium) for 12 h or left untreated. Cell lysates were prepared and NF-κB activity was measured as described in Fig. 2B. Data represent mean luciferase activity per microgram of protein ± SEM of two independent experiments done in duplicate.

transfected cells showed a significant increase in NF-κB activity after TNF-α treatment (Fig. 9B). In contrast, cells expressing HA-7ΔChnRNPA1 mutant showed a lower NF-κB activity compared with the control cells. Furthermore, when we silenced PSMD9 and overexpressed HA-wt-hnRNPA1, TNF-α mediated IκBα degradation was significantly reduced (Fig. 9C). In addition, a considerable decrease (up to 40%) in NF-κB activity was also observed in these cells (Fig. 9D). These results suggest that both PSMD9 and hnRNPA1 are in the same pathway and further support the role of PSMD9–hnRNPA1interaction in IκBα degradation and NF-κB activation.

PSMD9 anchors hnRNPA1–IκBα complex on 26S proteasome which facilitates proteasomal degradation of IκBα

PSMD9 is known to be a chaperone of proteasome assembly and is reported to dissociate before the mature complex [1,2,41]. Nas2, the yeast homolog, was not found in any of the cryo EM studies of the proteasome [42–44]. Like other classical chaperones, PSMD9 or its homologs may only be transiently associated with the assembled proteasome. We hypothesized that PSMD9, by virtue of its interaction with the proteasome on one hand and its interaction with hnRNPA1 on the other, would recruit IκBα to the proteasome for degradation. We first asked if endogenous or trans-expressed FLAG-PSMD9 could be located in the proteasome complex. We pulled down the whole 26S proteasomal complex using β7-subunit antibody. When probed for PSMD9 antibody we found both endogenous and FLAG-tagged PSMD9 in the complex. To ensure that PSMD9 is associated with the intact 26S mature complex, we probed the complex for the presence of ATPase subunit (Rpt6), a marker for the base subcomplex, and α5-subunit, a marker of 20S core particle. The results showed that β7-subunit antibody pulls down the intact 26S complex and PSMD9 is indeed associated with the mature proteasome (PSMD9 is not shown to interact with Rpt6). TNF-α treatment did not alter the levels of either endogenous or overexpressed PSMD9 in stable clones. But there was a definite increase in the levels of proteasome bound hnRNPA1 in PSMD9 overexpressing cells which were further enhanced upon TNF-α treatment (Fig. 10A). In contrast, when PSMD9 was silenced, no hnRNPA1 was found in the proteasome pull-down complex even after TNF-α treatment. These results together indicate that recruitment of hnRNPA1 to the proteasome requires the presence of PSMD9.

To enable the degradation of IκBα by the proteasome, PSMD9 not only has to interact with hnRNPA1 but should also interact with the proteasome as demonstrated above. However, based on current evidence PSMD9 seems to harbor only the PDZ-like domain for protein–protein interaction. Therefore it was important to test whether the PDZ mutations affect association of PSMD9 with the proteasome. Affinity pull-down of the 26S proteasome in cells overexpressing PDZ mutant Q181G indicated that this association was unimpaired (Fig. 10B). Proteasomal activity was also unaffected by this mutant (Fig. 10C). Probably there are other regions in PSMD9 that can interact with the proteasome. Although PSMD9 mutants cannot bind to hnRNPA1 because of the endogenous PSMD9, some hnRNPA1 could still be detected in the pull-down complex (Fig. 10B). These results further validate the role of the PDZ domain in proteasomal degradation of IκBα through interaction of PSMD9 with hnRNPA1. In addition these results indicate that PSMD9 functions as an anchor rather than a chaperone and bridges IκBα bound hnRNPA1 to the proteasome. This interaction enables regulated degradation of IκBα and modulates NF-κB activity.

While there is no clear evidence for the presence of PSMD9 on mature proteasomes or for the role of PDZ domains in interaction with ATPase subunits in mammalian cells, the lack of any detectable effect of PDZ domain mutations on the association of PSMD9 with intact 26S proteasomes requires further explanation. To address this we analysed the primary sequence of PSMC6 (Rpt4) and PSMC3 (Rpt5). GRRF was present in PSMC6. Intrigued we co-expressed wt-PSMD9 or PSMD9-Q181G mutant with wt-PSMC6 and performed co-immunoprecipitation studies. The results showed that the Q181G mutation which inhibits binding of PSMD9 to hnRNPA1 does not affect PSMD9 binding to PSMC6 (Fig. 10D). This result in conjunction with the observation that the PDZ mutations do not affect PSMD9 association with proteasome indicates that the interaction with the mature proteasome may not involve Rpt5. Moreover Rpt5 C-terminus is known to play a key role in interaction with the 20S α-subunit necessary for gate opening and activation of the proteasome. Therefore, Rpt5 on mature proteasome is unlikely to interact with PSMD9.

Since we found increased IκBα degradation upon hnRNPA1 overexpression with TNF-α treatment, we wanted to check the recruitment of overexpressed hnRNPA1 on 26S proteasome. HA-hnRNPA1 was overexpressed in HEK293 cells and treated with TNF-α (20 ng for 30 min). Cell lysates were prepared in ATP buffer and 26S proteasome was pulled down
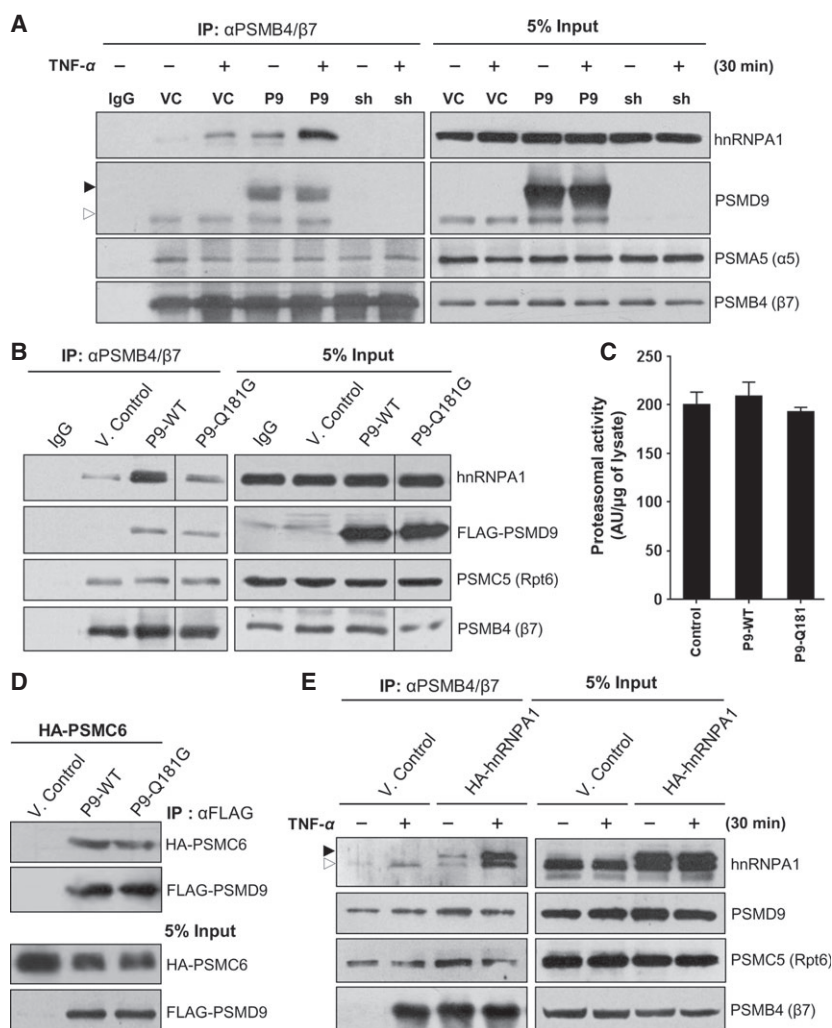
Fig. 10. PSMD9 is crucial for the recruitment of hnRNPA1-IκBα complex on 26S proteasome. (A) Both the overexpression (P9) and knockdown (sh) HEK293 inducible stable clones of PSMD9 were treated with doxycycline for 48 h and/or with TNF-α (20 ng·mL^{-1} of medium) for the next 30 min or left untreated. Cell lysates were prepared with ATP buffer as described in Materials and methods. Whole 26S proteasome was pulled down from the above cell lysates using β7 antibody and probed with different antibodies and analyzed by WB. Symbol ► corresponds to trans-expressed FLAG-PSMD9 and symbol ▷ corresponds to the endogenous PSMD9. (B) HEK293 cells were transiently transfected with pCMV-10 empty vector or pCMV-10-PSMD9 (wt or mutants D157P/Q181G) and cell lysates were prepared in ATP buffer as in Materials and methods. 26S proteasome was pulled down from the above cell lysates using β7 antibody and probed with different antibodies as indicated and analyzed by WB. (C) Proteasomal activity of the above mentioned (in B) cell lysates was measured as described in Materials and methods. Data represent Suc-LLVY-AMC proteasomal activity in arbitrary units (AU·μg^{-1} of lysate) ± SEM of two independent experiments done in duplicate. The WB shows the expression of FLAG-PSMD9 in the above cell lysates and PSMB4 is taken as the loading control. (D) HEK293 cells were co-transfected with pCDNA3.1-PSMC6 and p3X-FLAG-CMV-10, p3X-FLAG-CMV-10-wt-PSMD9 or p3X-FLAG-CMV-10-Q181G-PSMD9. After 48 h of transfection cell lysates were used for pull-down with anti-FLAG-M2 agarose beads and analyzed by WB. (E) HEK293 cells were transfected with pCDNA3.1 empty vector or pCDNA3.1-HA-wt-hnRNPA1 and after 48 h of transfection cells were treated with TNF-α for 30 min. Cell lysates were prepared in ATP buffer (as described in Materials and methods); 26S proteasome was pulled down using β7 antibody and analyzed by WB. Symbol ► corresponds to trans-expressed HA-hnRNPA1 and symbol ▷ corresponds to the endogenous hnRNPA1.

using β7 antibody. When the pull-down complexes were probed with hnRNPA1 antibody, both endogenous and trans-expressed hnRNPA1 levels were found to be increased upon TNF-α treatment, which correlates with the IκBα degradation (Fig. 10E). Furthermore levels of hnRNPA1 remain unaltered upon PSMD9 overexpression (Fig. 4B) or downregulation (Fig. 5B) or after TNF-α treatment. These results are strongly suggestive of a mechanism which involves recruitment of hnRNPA1 to the proteasome complex

during TNF-α signaling that would result in more and more IκBα degradation by the proteasome. Our attempts to substantiate this by capturing IκBα on 26S proteasome with/without TNF-α treatment under hnRNPA1 or PSMD9 overexpressing conditions failed perhaps due to its rapid degradation by the proteasome. Hence all these results suggest that hnRNPA1 either recruits or presents IκBα to the proteasome and this shuttle receptor hnRNPA1 is anchored by PSMD9 on the proteasome. While ubiquitinated IκBα is degraded, hnRNPA1 in all probability is released intact. It is possible that the PSMD9–hnRNPA1 interaction shortens the distance between the substrate and the proteasomal ATPases or ensures that IκBα is not prematurely released from the proteasome.

Discussion

Protein–protein interactions are seminal to signal transduction. They are involved in spatiotemporal regulation of cellular functions. Therefore, identification of novel interactions can help in deciphering unknown functions of a protein. We have established bioinformatics methods for identification of unknown interacting partners of 19S subunits of the proteasome (*FEBS Open Bio*, submitted). Using one such method we identified hnRNPA1, an RNA binding protein involved in RNA metabolism and transport [34], as a novel interacting partner of PSMD9, a PDZ domain containing a subunit of the proteasome. To test whether this interaction is physiologically relevant and to identify functions associated with the interaction, we searched for

the reported functions of hnRNPA1. The N-terminal of hnRNPA1 binds to ankyrin repeats in IκBα and this interaction somehow influences the processing of IκBα, the nature or mechanism of which is unclear [12]. Here we demonstrate that PSMD9 through its PDZ domain interacts with hnRNPA1 C-terminus and this domain–motif interaction is necessary for the proteasomal degradation of IκBα. Overexpression of PSMD9 accelerates both basal and TNF-α mediated proteasomal degradation of IκBα. This results in increased NF-κB activation and expression of its target genes. We establish a new role for hnRNPA1 as a shuttle receptor for the degradation of IκBα in HEK293 cells. PSMD9, contrary to its expected role as a chaperone, acts as a part of the 19S recognition module to facilitate delivery of ubiquitinated IκBα to the proteasome via hnRNPA1, as depicted in the model (Fig. 11).

Although the degradation of IκBα by the proteasome has long been established, the mechanism of how it is recruited to the proteasome is not well defined. Here we show how ubiquitinated IκBα is targeted to the proteasome for degradation. This is important because how ubiquitinated substrates in general are recruited to the proteasome is an active area of research. So far two modes of substrate recognition have been well defined. In the direct mode, substrates are recognized by the ubiquitin binding motifs in 19S subunits like Rpn10 containing the UIM domain, or via motifs like pleckstrin in Rpn13 [45,46]. In the indirect mode of recognition, Rad23, Dsk2 and Ddi1 proteins called 'shuttle receptors' bind proteasome
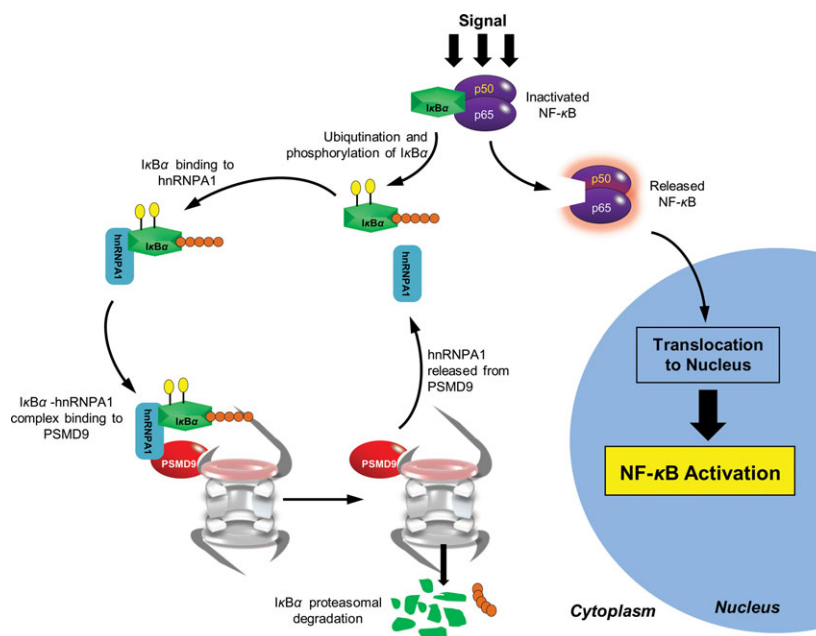

Fig. 11. Model for the mechanism of IκBα presentation and degradation by 26S proteasome. Signal activated and modified IκBα binds to hnRNPA1 and this complex interacts with PSMD9 on 26S proteasome. IκBα gets degraded through proteasomal activity hnRNPA1 shuttles back to bind with free IκBα and the cycle repeats.

through their UBL domains present at the N-terminus while their C-terminal ubiquitin association domain (UBA) binds to ubiquitin chains on the substrates [47,48]. These shuttle receptors bind to the Rpn1 subunit of the proteasome in non-stoichiometric amounts and apparently dissociate with fast kinetics. In an in-depth study, Deshaies group showed that Ddi1 is a proteasomal shuttle receptor that binds to the LRR1 domain of Rpn1 [49] and facilitates the degradation of Ufo1, a Ddi1 substrate. A UBA domain containing protein, p62, interacts with K63 ubiquitin chains of ubiquitinated tau and facilitates its proteasomal degradation by interacting with Rpt1 through its N-terminal PB1 domain [50]. HSP27 may also act as a shuttle receptor that recruits ubiquitinated IκBα to the proteasome for degradation in cancer cells in response to stress signals [51]. In this report HSP27 was shown to bind ubiquitinated IκBα and to the 19S regulatory particle of the proteasome to mediate this degradation. HSP27 recognizes covalently linked ubiquitin on IκBα but how it interacts with the proteasome is unclear. Recently we have demonstrated that non-ubiquitinated proteins can be directly recognized and degraded by 26S proteasome [10].

We describe our findings in the context of these reported mechanisms of substrate recognition and highlight unique features that are an outcome of our study. PSMD9 unlike HSP27 does not directly bind to ubiquitinated IκBα. This interaction is mediated by hnRNPA1 and, therefore, Ub-IκBα is targeted to the proteasome through the indirect pathway. Since the hnRNPA1 level does not change under any conditions tested here, we argue that it acts as a shuttle receptor that brings in Ub-IκBα. Since hnRNPA1 lacks a UBL-like domain, it does not bind to the proteasome in a classical manner like other shuttle receptors. Instead this function is mediated by a C-terminal region of the protein which acts as a recognition signal for the PDZ domain of PSMD9 bound to the proteasome. PDZ domains can recognize native sequences in proteins typically through the C-terminal residues. Such a classical domain–motif interaction for PSMD9–hnRNPA1 is established by our study. Nevertheless, the exact mechanism of hnRNPA1 release, the mode of binding of PSMD9 to the proteasome and the molecular basis of this recognition remain to be investigated.

While our studies show how PSMD9 directly affects the degradation of IκBα by the proteasome which helps in NF-κB activation, there are several upstream steps that process IκBα for degradation. A possible role of PSMD9 in these processes has been somewhat addressed in this study. Since in the absence of any external stimuli PSMD9 overexpression results in increased basal activity of NF-κB, it remains to be seen whether PSMD9 acts as an internal signal for NF-κB activation. This may be dependent or independent of its interaction with hnRNPA1. Previously it was reported that in cells lacking hnRNPA1 (mouse leukemic cells) NF-κB, activity is reduced [12]. Likewise in the current study we show that in cells lacking PSMD9 NF-κB, activity is reduced. Taken together, these studies suggest that PSMD9 and hnRNPA1 are probably not mutually exclusive in the context of the NF-κB signaling pathway which may be explained by their ability to interact with each other.

It will be important to see whether the mechanism of IκBα degradation and NF-κB activity is general to other cell types. While hnRNPA1 is a ubiquitous protein, PSMD9 may be expressed in a cell or tissue specific manner [3]. Although PSMD9 deletion is not lethal in yeast [52], loss of PSMD9 expression may have phenotypic consequences in mammalian cells due to inhibition of NF-κB activity. We have demonstrated that the PDZ domain mutants do not bind to hnRNPA1 and therefore their overexpression does not affect NF-κB activity. Thus small molecules that can target the interaction sites on the PDZ domain of PSMD9 are likely to act as inhibitors of NF-κB activity. Such molecules may be useful in targeting cancer cells that are dependent on a consistently high NF-κB activity for their survival [53,54]. The first step in this direction, however, is to establish the role of the PSMD9–hnRNPA1 interaction in this pathway in such cancer cells.

Based on our findings on the molecular details of the interaction between the PDZ domain of PSMD9 and hnRNPA1, we speculate about a general role for PSMD9 in substrate recognition by the proteasome. For example IκBα may be one of the many examples of how substrates may converge on the proteasome through the PDZ domain of PSMD9. It is possible that other substrates are brought to the proteasome by a similar mechanism through either hnRNPA1 or other shuttle receptors that may carry a similar recognition motif. In addition, by virtue of its binding to ATPase subunits, PSMD9 on the surface of the 19S regulatory particles may be uniquely positioned to ensure rapid unfolding, prevention of premature release of the substrates and translocation of the unfolded protein through the central channel that lines the ATPase ring. Another aspect of our finding is the nature and origin of the components involved in IκBα degradation – a chaperone from the proteasome pathway and an RNA binding protein. Thus it is speculated that there may be other functions mediated by this domain–motif interaction between PSMD9 and

hnRNPA1 relevant to their respective network and/or the crosstalk between different functional modules.

Two important points reported in the literature regarding the association of PSMD9 with proteasomes merit special attention: (a) chaperones such as PSMD9 and PSMD10 have not been found as part of the mature proteasome structure [43,44] and (b) Nas-2, the yeast homolog of PSMD9, has been shown to interact with Rpt5 through C-terminal residues implying a role for the PDZ domain in interaction. We believe PSMD9 or PSMD10 may transiently associate with the mature proteasome. It is likely that only few of the mature 26S proteasomes bind these chaperones at any given moment and they can be washed away under very stringent conditions during IPs or affinity purifications. It is interesting to note that reports on the interaction of shuttle receptors such as Ddi1 in yeast with the proteasome have been controversial. Ddi1 belongs to the UBA-UBL domain containing proteins that bind polyubiquitin chains in substrate proteins. Ddi1 is reported by some to physically interact with the intact proteasome while others question this finding. It is argued by Deshaies group, who find that Ddi1 does indeed interact with the proteasome in a specific and functionally relevant manner, that such discrepancies may be due to the qualitative nature of IP experiments and the rapid dynamics of UBL binding to and dissociation from the proteasome. The same could be true for the proteasomal chaperones such as PSMD9 or PSMD10.

Regarding the involvement of the PDZ domain in the interaction with the ATPase subunits, we find that mutations in the PDZ domain of PSMD9 that affect hnRNPA1 binding do not affect the association with the proteasome. While we do not find any literature evidence for the role of PDZ domains in interaction with the ATPases in mammalian cells, Nas2 in yeast has been shown to interact with Rpt5 or PSMC3 via the C-terminal residues [55]. Although we have not tested the interaction of PSMD9 with PSMC3, interaction of PSMD9 with PSMC6 is unaffected by the PDZ mutations (current study). It is possible that the association of PSMD9 with the mature proteasome is different from its interaction with the ATPase subunits in the modular structure. It is obvious that we are far from a clear understanding of the role of PSMD9 in the functioning of holo 26S proteasome and its interaction with the different subunits. More studies with detailed molecular characterization as reported in this current study will be necessary to clarify the complexity associated with these supramolecular structures.

In summary, we have established that PSMD9 through its PDZ domain interacts with the C-terminus of hnRNPA1, a novel interacting partner, and this interaction regulates degradation of IκBα and, therefore, NF-κB activity in HEK293 cells. hnRNPA1 acts as a shuttle receptor while PSMD9 is the docking site on the 19S regulatory particle. IκBα may be one of the many examples of how ubiquitinated substrates may be recruited on the proteasome through the PDZ domain of PSMD9. It is possible that features of the C-terminal sequence found in hnRNPA1 may be conserved in other shuttle receptors. Our study opens up new areas of investigation on the role of PSMD9 in cellular homeostasis. The generality of this interaction between hnRNPA1 and PSMD9 may propose the interface as a potential drug target in tumor cells relying on high NF-κB activity. Moreover, the interaction between hnRNPA1, a protein well known for mRNA transport and splicing, and PSMD9, a subunit chaperone of the proteasome, is intriguing. Although speculative, whether this interaction influences these well known functions of hnRNPA1 and whether there is crosstalk between the degradation pathway and the RNA metabolism remains to be seen.

Materials and methods

Plasmids

PSMD9 was amplified from PSMD9 cDNA (Origene Technologies) and cloned within *Hin*dIII and *Eco*RI in p3xFLAG-CMV-10 mammalian expression vector (Sigma, USA). For bacterial expression vector pRSETA, *Bam*HI and *Xho*I sites are used for cloning PSMD9. The PSMD9 (L173G), PSMD9(Q181G) and PSMD9(triple mutant L124G-Q126G-E128G) mutants were generated in p3xFLAG-CMV-10-PSMD9 construct by site directed mutagenesis. 3xFLAG-tagged PSMD9 was amplified from p3xFLAG-CMV-10-PSMD9 construct using the primers Fw 5′-AC-CGGTCGCCACCATGGACTACAAAGACCATG-3′ and Rv 5′-GAATTCGACAATCATCTTTGCAGAGG-3′ cloned between *Age*I and *Eco*RI into doxycycline inducible vector pTRIPZ (a gift from S. Dalal, Advanced Center for Treatment, Research and Education in Cancer, Navi Mumbai, India). mir30 based shRNA of PSMD9 was PCR amplified using the primers Fw 3′-GGCTCGAGGAAGGTATATT GCTGTTGACAGTGAGCG<u>GCAGATCAAGGCCAACT ATGA</u>TAGTGAAGCCACAGATGT-3′ and Rv 5′-GCGA ATTCCCGAGGCAGTAGGCA<u>GCAGATCAAGGCCAA CTATGA</u>TACA TCTGTGGCTTCACTATCATAG-3′. The PCR product was digested with *Xho*I and *Eco*RI and inserted into doxycycline inducible vector pTRIPZ. hnRNPA1 was PCR amplified from HEK293 cDNA library generated by RT-PCR of RNA from HEK293 cells and cloned within *Bam*HI and *Xho*I in HA-pCDNA3.1 mammalian expression vector (gift from S. Dalal, Advanced Center for

Treatment, Research and Education in Cancer, Navi Mumbai, India). For bacterial expression vector pGEX-4T-1, *Bam*HI and *Eco*RI sites were used for cloning hnRNPA1. The hnRNPA1(Δ7C) mutant was generated by deleting seven amino acids from the C-terminus. wt IκBα and ΔC mutant (1–252 amino acids) IκBα were amplified from HEK293 cDNA and were cloned into mammalian expression vector p3xFLAG-CMV-10 vector using *Hin*dIII and *Eco*RI sites. wt IκBα was cloned into bacterial expression vector pMALc5X within *Bam*HI and *Eco*RI sites. PSMC6 was PCR amplified from the HEK293 cDNA library generated by RT-PCR of RNA from HEK293 cells and cloned within *Bam*HI and *Xho*I in HA-pCDNA3.1 mammalian expression vector (gift from S. Dalal, Advanced Center for Treatment, Research and Education in Cancer, Navi Mumbai, India). The phospho-mutant pTRIPZ- IκBαSR (S32A–S36A) vector (gift from N. Shirsat, Advanced Center for Treatment, Research and Education in Cancer, Navi Mumbai, India, and D. C. Guttridge, Ohio State University, USA), pEGFPN3 vector and pBSK3 vectors were used for mammalian cell transfection. 3x κB ConA luc vector and ConA luc control vector (gift from N. D. Perkins, Newcastle University, UK) were used for the luciferase reporter assay.

Expression, purification of recombinant proteins

Recombinant His-PSMD9, GST-PSMD9, GST-hnRNPA1 and MBP-IκBα were expressed in *Escherichia coli* BL21 DE(3) using 100 μM isopropyl thio-β-D-galactoside at 18 °C for 18 h. His-PSMD9 and its mutant were purified by Ni-nitrilotriacetic acid column chromatography (Qiagen, Hilden, Germany) using 250 mM imidazole buffer; GST, GST-PSMD9 and GST-hnRNPA1 were purified using glutathione Sepharose beads (GE Healthcare Life Sciences, Amersham, UK) and MBP, MBP-IκBα were purified using amylose beads (NEB, UK) and 10 mM maltose buffer, according to the manufacturer's protocol. His-PSMD9 was FPLC purified using a Superdex-200 column (Amersham, GE Healthcare Life Science).

Far western blot and dot blot

Recombinant GST-PSMD9, GST-hnRNPA1 and MBP-IκBα proteins (2 μg each) were SDS denatured, run on an SDS/PAGE and transferred onto a PVDF membrane. The transferred proteins were denatured/renatured on the membrane using guanidine-HCl AC buffer with the protocol described in Yuliang Wu *et al.* [56]. For dot blot 1 μg of recombinant proteins (GST, GST-hnRNPA1, GST-PSMD9, MBP and MBP-IκBα) were spotted on a methanol equilibrated PVDF membrane. The spotted membranes were blocked in 3% BSA-TBST and overlaid with either His-PSMD9 or MBP-IκBα (100 nM in 1% BSA-TBST) for 1 h. Anti-PSMD9 (mouse monoclonal; Sigma) in 1 : 4000

dilution, anti-hnRNPA1 (mouse monoclonal; Sigma) in 1 : 4000 dilution and anti-IκBα (rabbit polyclonal; Sigma) in 1 : 4000 dilution were used for probing the overlaid proteins.

Cell culture, transfection and reagents

HEK293 cells were cultured in DMEM (Gibco, USA) supplemented with 10% fetal bovine serum (Gibco), 100 IU·mL^{-1} penicillin (Sigma) and 100 μg·mL^{-1} streptomycin (Sigma). For transfection Lipofectamine 2000 (Invitrogen, Carlsbad, CA, USA) or the calcium phosphate method were used according to the manufacturer's protocol. 100 μM of PSMD9 small interfering RNA (siRNA) (Dharmacon; Thermo Scientific, Waltham, MA, USA) or scrambled siRNA (Dharmacon; Thermo Scientific) with Lipofectamine 2000 was used for transfection. Doxycycline (Sigma) 1–4 μg·mL^{-1} of medium, CHX (Sigma) 50 μg·mL^{-1} of medium, TNF-α (Peprotech, Rocky Hill, NJ, USA) 20 ng·mL^{-1} of medium, MG132 (Sigma) 10 μM·mL^{-1} of medium and Velcade (Johnson & Johnson, NJ, USA) 10 μg·mL^{-1} of medium were used for different experiments.

Establishment of stable cell line

HEK293 cells were transfected with p3xFLAG-CMV-10 and p3xFLAG-CMV-10-PSMD9 constructs using Lipofectamine 2000 (Invitrogen) to generate PSMD9 overexpressing stable clones. After 24 h, transfected cells were subcultured and kept under selection in DMEM supplemented with 10% fetal bovine serum and 800 μg·mL^{-1} of G418 (Sigma). After 2–4 weeks G418 resistant single colonies were picked up and grown in DMEM supplemented with 10% fetal bovine serum and 400 μg·mL^{-1} of G418. Three different clones with high FLAG-PSMD9 expression were selected for further studies. For generating doxycycline inducible stable clones, HEK293 cells were transfected with pTRIPZ, pTRIPZ-3xFLAG-PSMD9, pTRIPZ-shRNA-PSMD9 using Lipofectamine 2000. After 24 h transfected cells were subcultured and kept under selection in DMEM supplemented with 10% fetal bovine serum and 800 ng·mL^{-1} puromycin (Sigma). After 5–7 days puromycin resistant single colonies were picked up and grown in DMEM supplemented with 10% fetal bovine serum and 400 ng·mL^{-1} puromycin. Three clones with high FLAG-PSMD9 expression and three clones with maximum PSMD9 knockdown upon doxycycline induction were selected for further studies.

Immunoprecipitation

Cells were pelleted, washed twice with NaCl/P$_i$ and lysed in NP-40 lysis buffer [50 mM Tris pH 7.6, 150 mM NaCl, 0.5% NP-40 detergent, 10 mM NaF, 1 mM Na$_2$VO$_5$, 10 mM β-glycerophosphate and 1× protease inhibitor cocktail (Sigma,

P2714)]. For proteasomal pull-down, buffer containing 50 mM Tris (pH 7.6), 5 mM MgCl₂, 1 mM ATP, 10% glycerol and 1× protease inhibitor cocktail (Sigma) was used. Briefly, monoclonal antibodies (1 : 1000 vol/vol of antibody : cell lysate) were bound overnight to Protein-G Sepharose beads (GE Amersham) and pre-cleared cell extracts were incubated with antibody-bound Sepharose beads or anti-FLAG M2 agarose (Sigma) for 3 h at 4 °C. After extensive washing with washing buffer [50 mM Tris, pH 7.6, 150–450 mM NaCl, 10 mM NaF, 1 mM Na₂VO₅, 10 mM β-glycerophosphate and 1× protease inhibitor cocktail (Sigma, P2714)], immune complexes were separated by SDS/PAGE and analyzed by western blotting, following standard protocols.

Luciferase reporter assay

Stable clones of HEK293 harboring FLAG-PSMD9 and HEK293 cells transiently transfected with p3xFLAG-CMV-10/p3xFLAG-CMV-10-PSMD9/p3xFLAG-CMV-10-PSMD9(D157P)/p3xFLAG-CMV-10-PSMD9(Q181G)/pcDNA3.1-HA-hnRNPA1/pcDNA3.1-HA-hnRNPA1(CΔ7) were co-transfected with ConA luc control or 3x κB ConA luc vectors by the calcium phosphate method. After 48 h, cells were lysed and luciferase assays were performed using the Luciferase Assay System (Promega, Fitchburg, WI, USA) in triplicate. In inducible stable clones of control pTRIPZ and pTRIPZ-3xFLAG-PSMD9 after 48 h of doxycycline addition luciferase assays were performed as explained.

Western blotting and antibodies

Cell lysates were prepared with NP-40 lysis buffer and separated on 12–15% SDS/PAGE gels, and western blot (WB) was performed following standard protocols. Antibodies anti-PSMD9 in 1 : 1000 (mouse monoclonal; Sigma, and rabbit polyclonal; Abcam, Cambridge, UK), anti-FLAG in 1 : 8000 (mouse monoclonal; Sigma), anti-hnRNPA1 in 1 : 1000 (mouse monoclonal; Sigma, and rabbit polyclonal; Abcam), anti-HA in 1 : 1000 (rabbit polyclonal; Abcam), anti-IκBα in 1 : 1000 (rabbit polyclonal; Sigma), anti-β-actin in 1 : 2000 (mouse monoclonal; Sigma), anti-α-tubulin in 1 : 2000 (mouse monoclonal; Sigma), anti-acetyl histone H4 K12 in 1 : 1000 (rabbit polyclonal; Cell Signaling, Danvers, MA, USA), anti-β7 in 1000 (mouse monoclonal), anti-α5 in 1 : 1000 (mouse monoclonal), anti-ubiquitin in 1 : 1000 (mouse polyclonal, Sigma) and anti-p65 in 1 : 1000 (rabbit polyclonal, Abcam) were used for western blotting experiments.

RT-PCR and real-time PCR

Total RNA was isolated from HEK293 cells, PSMD9 overexpression and knockdown clone by TRIzol® Reagent (Invitrogen) following the manufacturer's protocol. cDNA

was prepared using SuperScript® III Reverse Transcriptase kit (Life Technologies, Invitrogen). Real-time PCR was performed using SYBR Green based Kappa-Biosystems kit (Woburn, MA, USA) and gene specific primers (Table S1).

Electrophoretic mobility shift assay

Nuclear fractions were extracted from HEK293 FLAG-PSMD9 stable clones, HEK293 inducible FLAG-PSMD9 stable clones and HEK293 inducible PSMD9-shRNA stable clones using N-XTRACT kit (Sigma) following the manufacturer's protocol. wt κB-oligo 5′-AGTTGA-GGGGACTTTCCCAGGC-3′ and mutant κB-oligo 5′-AGTTGAGCTCACTTTCC CAGGC-3′ [35] were purchased from Sigma and biotin labeled at the 3′ end of the oligos using the Biotin 3′ End DNA Labeling Kit (Thermo Scientific) following the manufacturer's protocol. Both biotinylated complementary oligos were annealed at 65 °C for 10 min followed by incubation at room temperature for 30 min. Then 3–5 μg of nuclear extract was incubated with the biotinylated oligos and poly dI-dC for 20 min at room temperature. This binding reaction was carried out using LightShift® Chemiluminescent EMSA Kit (Thermo Scientific) following the manufacturer's protocol. Reactions were separated on 6% native PAGE, transferred onto positively charged nylon membrane and UV crosslinked for 30 min at 256 nm at 1 cm distance. The membrane was developed onto an X-ray film using Chemiluminescent Nucleic Acid Detection Module (Thermo Scientific) following the manufacturer's protocol.

Proteasomal activity assay

Cells were pelleted, washed twice with NaCl/P$_i$ and resuspended in buffer containing 50 mM Tris (pH 7.6), 5 mM MgCl₂, 1 mM ATP, 10% glycerol and 1× protease inhibitor cocktail (Sigma). Cell suspensions were ultrasonicated for four cycles of 20 s each (with 1 s break after each 2 s) at 30 kHz on ice. Proteasomal activity was measured using 25 nM Suc-LLVY-7-amino-4-methyl coumarin substrate and fluorescence readings were taken at excitation 355 nm/emission 460 nm.

Densitometric and statistical analysis

Densitometric quantitation of scanned images was performed using MAC BIOPHOTONICS IMAGEJ. Statistical analysis was performed using GRAPH PAD PRISM 5. To evaluate the significance of the values obtained, an unpaired Student's *t* test was performed. $P < 0.05$ and $P > 0.05$ are considered as significant and non-significant data respectively. In graphs the symbol *** represents P value < 0.001.

Acknowledgements

Author contributions

Indrajit Sahu: planned, performed, analyzed experiments and assisted in manuscript writing. Nikhil Sangith: planned, performed initial NF-κB activity experiments, some *in vitro* interactions and designed PDZ and C-terminal mutations. Manoj Ramteke: initial establishment of stable cell lines and transfection. Rucha Gadre: performed some cloning and *in vitro* interaction experiments. Prasanna Venkatraman: conceived, directed the project and wrote the manuscript.

References

1 Kaneko T, Hamazaki J, Iemura S, Sasaki K, Furuyama K, Natsume T, Tanaka K & Murata S (2009) Assembly pathway of the mammalian proteasome base subcomplex is mediated by multiple specific chaperones. *Cell* **137**, 914–925.

2 da Fonseca PC, He J & Morris EP (2012) Molecular model of the human 26S proteasome. *Mol Cell* **46**, 54–66.

3 Thomas MK, Yao KM, Tenser MS, Wong GG & Habener JF (1999) Bridge-1, a novel PDZ-domain coactivator of E2A-mediated regulation of insulin gene transcription. *Mol Cell Biol* **19**, 8492–8504.

4 Jelen F, Oleksy A, Smietana K & Otlewski J (2003) PDZ domains − common players in the cell signaling. *Acta Biochim Pol* **50**, 985–1017.

5 Lee HJ & Zheng JJ (2010) PDZ domains and their binding partners: structure, specificity, and modification. *Cell Commun Signal* **8**, 8.

6 Lee JH, Volinic JL, Banz C, Yao KM & Thomas MK (2005) Interactions with p300 enhance transcriptional activation by the PDZ-domain coactivator Bridge-1. *J Endocrinol* **187**, 283–292.

7 Banz C, Munchow B & Diedrich K (2010) Bridge-1 is expressed in human granulosa cells and is involved in the activin A signaling cascade. *Fertil Steril* **93**, 1349–1352.

8 Volinic JL, Lee JH, Eto K, Kaur V & Thomas MK (2006) Overexpression of the coactivator bridge-1 results in insulin deficiency and diabetes. *Mol Endocrinol* **20**, 167–182.

9 Ren S, Uversky VN, Chen Z, Dunker AK & Obradovic Z (2008) Short linear motifs recognized by SH2, SH3 and Ser/Thr kinase domains are conserved in disordered protein regions. *BMC Genomics* **9** (Suppl 2), S26.

10 Singh Gautam AK, Balakrishnan S & Venkatraman P (2012) Direct ubiquitin independent recognition and degradation of a folded protein by the eukaryotic proteasomes − origin of intrinsic degradation signals. *PLoS One* **7**, e34864.

11 Nanaware PP, Ramteke MP, Somavarapu AK & Venkatraman P (2013) Discovery of multiple interacting partners of gankyrin, a proteasomal chaperone and an oncoprotein − evidence for a common hot spot site at the interface and its functional relevance. *Proteins*. doi: 10.1002/prot.24494.

12 Hay DC, Kemp GD, Dargemont C & Hay RT (2001) Interaction between hnRNPA1 and IkappaBalpha is required for maximal activation of NF-kappaB-dependent transcription. *Mol Cell Biol* **21**, 3482–3490.

13 Hayden MS & Ghosh S (2008) Shared principles in NF-kappaB signaling. *Cell* **132**, 344–362.

14 Li H & Lin X (2008) Positive and negative signaling components involved in TNFalpha-induced NF-kappaB activation. *Cytokine* **41**, 1–8.

15 Grilli M, Chiu JJ & Lenardo MJ (1993) NF-kappa B and Rel: participants in a multiform transcriptional regulatory system. *Int Rev Cytol* **143**, 1–62.

16 Ghosh S, May MJ & Kopp EB (1998) NF-kappa B and Rel proteins: evolutionarily conserved mediators of immune responses. *Annu Rev Immunol* **16**, 225–260.

17 Baeuerle PA & Baltimore D (1988) I kappa B: a specific inhibitor of the NF-kappa B transcription factor. *Science* **242**, 540–546.

18 Beg AA & Baldwin AS Jr (1993) The I kappa B proteins: multifunctional regulators of Rel/NF-kappa B transcription factors. *Genes Dev* **7**, 2064–2070.

19 Chen Z, Hagler J, Palombella VJ, Melandri F, Scherer D, Ballard D & Maniatis T (1995) Signal-induced site-specific phosphorylation targets I kappa B alpha to the ubiquitin−proteasome pathway. *Genes Dev* **9**, 1586–1597.

20 Li N & Karin M (1998) Ionizing radiation and short wavelength UV activate NF-kappaB through two distinct mechanisms. *Proc Natl Acad Sci USA* **95**, 13012–13017.

21 Mukhopadhyay A, Manna SK & Aggarwal BB (2000) Pervanadate-induced nuclear factor-kappaB activation requires tyrosine phosphorylation and degradation of IkappaBalpha. Comparison with tumor necrosis factor-alpha. *J Biol Chem* **275**, 8549–8555.

22 Hayden MS & Ghosh S (2004) Signaling to NF-kappaB. *Genes Dev* **18**, 2195–2224.

23 Alkalay I, Yaron A, Hatzubai A, Orian A, Ciechanover A & Ben-Neriah Y (1995) Stimulation-dependent I kappa B alpha phosphorylation marks the NF-kappa B inhibitor for degradation via the ubiquitin−proteasome pathway. *Proc Natl Acad Sci USA* **92**, 10599–10603.

24 Tanaka K, Kawakami T, Tateishi K, Yashiroda H & Chiba T (2001) Control of IkappaBalpha proteolysis by the ubiquitin−proteasome pathway. *Biochimie* **83**, 351–356.

25 Miyamoto S, Seufzer BJ & Shumway SD (1998) Novel IkappaB alpha proteolytic pathway in WEHI231 immature B cells. *Mol Cell Biol* **18**, 19–29.

26 Shumway SD, Berchtold CM, Gould MN & Miyamoto S (2002) Evidence for unique calmodulin-dependent nuclear factor-kappaB regulation in WEHI-231 B cells. *Mol Pharmacol* **61**, 177–185.

27 Shumway SD & Miyamoto S (2004) A mechanistic insight into a proteasome-independent constitutive inhibitor kappaBalpha (IkappaBalpha) degradation and nuclear factor kappaB (NF-kappaB) activation pathway in WEHI-231 B-cells. *Biochem J* **380**, 173–180.

28 Ponnappan S, Cullen SJ & Ponnappan U (2005) Constitutive degradation of IkappaBalpha in human T lymphocytes is mediated by calpain. *Immun Ageing* **2**, 15.

29 Palombella VJ, Rando OJ, Goldberg AL & Maniatis T (1994) The ubiquitin−proteasome pathway is required for processing the NF-kappa B1 precursor protein and the activation of NF-kappa B. *Cell* **78**, 773–785.

30 Hoffmann A, Levchenko A, Scott ML & Baltimore D (2002) The IkappaB-NF-kappaB signaling module: temporal control and selective gene activation. *Science* **298**, 1241–1245.

31 Cohen S, Achbert-Weiner H & Ciechanover A (2004) Dual effects of IkappaB kinase beta-mediated phosphorylation on p105 Fate: SCF(beta-TrCP)-dependent degradation and SCF(beta-TrCP)-independent processing. *Mol Cell Biol* **24**, 475–486.

32 Liang C, Zhang M & Sun SC (2006) beta-TrCP binding and processing of NF-kappaB2/p100 involve its phosphorylation at serines 866 and 870. *Cell Signal* **18**, 1309–1317.

33 Moorthy AK, Savinova OV, Ho JQ, Wang VY, Vu D & Ghosh G (2006) The 20S proteasome processes NF-kappaB1 p105 into p50 in a translation-independent manner. *EMBO J* **25**, 1945–1956.

34 Dreyfuss G, Matunis MJ, Pinol-Roma S & Burd CG (1993) hnRNP proteins and the biogenesis of mRNA. *Annu Rev Biochem* **62**, 289–321.

35 Reigstad CS, Lunden GO, Felin J & Backhed F (2009) Regulation of serum amyloid A3 (SAA3) in mouse colonic epithelium and adipose tissue by the intestinal microbiota. *PLoS One* **4**, e5842.

36 Zhou A, Scoggin S, Gaynor RB & Williams NS (2003) Identification of NF-kappa B-regulated genes induced by TNFalpha utilizing expression profiling and RNA interference. *Oncogene* **22**, 2054–2064.

37 Miyamoto S, Maki M, Schmitt MJ, Hatanaka M & Verma IM (1994) Tumor necrosis factor alpha-induced phosphorylation of I kappa B alpha is a signal for its degradation but not dissociation from NF-kappa B. *Proc Natl Acad Sci USA* **91**, 12740–12744.

38 Shim SM, Lee WJ, Kim Y, Chang JW, Song S & Jung YK (2012) Role of S5b/PSMD5 in proteasome inhibition caused by TNF-alpha/NFkappaB in higher eukaryotes. *Cell Rep* **2**, 603–615.

39 DeMartino GN, Proske RJ, Moomaw CR, Strong AA, Song X, Hisamatsu H, Tanaka K & Slaughter CA (1996) Identification, purification, and characterization of a PA700-dependent activator of the proteasome. *J Biol Chem* **271**, 3112–3118.

40 Ferrell K, Wilkinson CR, Dubiel W & Gordon C (2000) Regulatory subunit interactions of the 26S proteasome, a complex problem. *Trends Biochem Sci* **25**, 83–88.

41 Chen C, Huang C, Chen S, Liang J, Lin W, Ke G, Zhang H, Wang B, Huang J, Han Z *et al.* (2008) Subunit−subunit interactions in the human 26S proteasome. *Proteomics* **8**, 508–520.

42 Bohn S, Beck F, Sakata E, Walzthoeni T, Beck M, Aebersold R, Forster F, Baumeister W & Nickell S (2010) Structure of the 26S proteasome from *Schizosaccharomyces pombe* at subnanometer resolution. *Proc Natl Acad Sci USA* **107**, 20992–20997.

43 Lander GC, Estrin E, Matyskiela ME, Bashore C, Nogales E & Martin A (2012) Complete subunit architecture of the proteasome regulatory particle. *Nature* **482**, 186–191.

44 Lasker K, Forster F, Bohn S, Walzthoeni T, Villa E, Unverdorben P, Beck F, Aebersold R, Sali A & Baumeister W (2012) Molecular architecture of the 26S proteasome holocomplex determined by an integrative approach. *Proc Natl Acad Sci USA* **109**, 1380–1387.

45 Deveraux Q, Ustrell V, Pickart C & Rechsteiner M (1994) A 26S protease subunit that binds ubiquitin conjugates. *J Biol Chem* **269**, 7059–7061.

46 Husnjak K, Elsasser S, Zhang N, Chen X, Randles L, Shi Y, Hofmann K, Walters KJ, Finley D & Dikic I (2008) Proteasome subunit Rpn13 is a novel ubiquitin receptor. *Nature* **453**, 481–488.

47 Su V & Lau AF (2009) Ubiquitin-like and ubiquitin-associated domain proteins: significance in proteasomal degradation. *Cell Mol Life Sci* **66**, 2819–2833.

48 Chen L & Madura K (2002) Rad23 promotes the targeting of proteolytic substrates to the proteasome. *Mol Cell Biol* **22**, 4902–4913.

49 Gomez TA, Kolawa N, Gee M, Sweredoski MJ & Deshaies RJ (2011) Identification of a functional docking site in the Rpn1 LRR domain for the UBA-UBL domain protein Ddi1. *BMC Biol* **9**, 33.

50 Babu JR, Geetha T & Wooten MW (2005) Sequestosome 1/p62 shuttles polyubiquitinated tau for proteasomal degradation. *J Neurochem* **94**, 192–203.

51 Parcellier A, Schmitt E, Gurbuxani S, Seigneurin-Berny D, Pance A, Chantome A, Plenchette S, Khochbin S, Solary E & Garrido C (2003) HSP27 is a ubiquitin-binding protein involved in I-kappaBalpha proteasomal degradation. *Mol Cell Biol* **23**, 5790–5802.

52 Watanabe TK, Saito A, Suzuki M, Fujiwara T, Takahashi E, Slaughter CA, DeMartino GN, Hendil KB, Chung CH, Tanahashi N *et al.* (1998) cDNA cloning and characterization of a human proteasomal modulator subunit, p27 (PSMD9). *Genomics* **50**, 241–250.

53 Dolcet X, Llobet D, Pallares J & Matias-Guiu X (2005) NF-kB in development and progression of human cancer. *Virchows Arch* **446**, 475–482.

54 Ravi R & Bedi A (2004) NF-kappaB in cancer − a friend turned foe. *Drug Resist Updat* **7**, 53–67.

55 Lee SY, De la Mota-Peynado A & Roelofs J (2011) Loss of Rpt5 protein interactions with the core particle and Nas2 protein causes the formation of faulty proteasomes that are inhibited by Ecm29 protein. *J Biol Chem* **286**, 36641–36651.

56 Wu Y, Li Q & Chen XZ (2007) Detecting protein–protein interactions by far western blotting. *Nature protocol* **2**, 3278–3284.

Supporting information

Additional supporting information may be found in the online version of this article at the publisher's web site:

Table S1. List of qRT-PCR primers.